THEORETICAL MODELS OF THERMO-MECHANICAL DUCTILE SHEAR ZONE DEFORMATION IN ROCKS

Jeremy Mark Lockett

A thesis presented for the degree of
Doctor of Philosophy at the
University of Keele

September 1982

ACKNOWLEDGEMENTS

I would like to thank Dr. Nick Kusznir and Dr. Graham Park for their support over the past three years. The former has provided supervision, inspiration, and when dealing with finite elements, divine guidance. The latter introduced me to real shear zones in the field. I would also like to thank the staff and users of the Computer Centre for their assistance with programming problems, and Christine Owen for typing the thesis.

This work was financed by the Natural Environment Research Council with a little help from my parents and brother.

Abstract

Thermo-mechanical models of ductile shear zones have been constructed for both viscous and viscoelastic materials. The viscous model has been applied to both shear zones and ductile thrusts for constant velocity and constant shear stress boundary conditions. For the constant velocity boundary condition the viscous shear zone model provides an explanation for a number of geological structures. Constant velocity shears broaden with time and have a large temperature anomaly. The temperatures increase slowly with time but are insufficient for melting. The shears can be shown to broaden with increase in ambient temperature with depth. A minimum separation distance between pairs of shears is required for them to remain discrete. Constant velocity viscous shears have a near singularity in the shear stress at time t=o.

The viscoelastic model shows a more realistic initial stress evolution; with a zero initial stress. The viscoelastic constant velocity model predicts the occurrence of viscoelastic rebounds, under certain conditions, in which very large instantaneous shear velocities are developed. In viscoelastic rebounds large amounts of stored elastic stress are relaxed catastrophically in a localized region by viscous deformation. The rapid velocities generate large amounts of shear heating and give rise to localized thermal runaway and melting. The high temperatures generated rapidly decay to lower levels. With time the temperature and stress field solutions of the viscous and viscoelastic models converge.

For constant stress boundary conditions the viscous and viscoelastic models are identical except for the initial elastic strains in the viscoelastic model. At low values of temperature and stress, very small, geologically insignificant strains are developed. Higher temperatures and stresses give rise to thermal runaways and melting.

Thermo-mechanical stabilization using a dislocation creep process explains many of the features seen in ductile shear zones. At lower ambient temperatures the models produce high stresses which would be limited by brittle failure.

Contents

Chapter 8

Discussion and Conclusions

CHAPTER 1

The Geological Structure of Shear Zones

1.1 Introduction

In some deformed rocks high strain zones are localized within approximately planar zones termed shear zones or shear belts. These shear zones vary from fractions of a centimetre to tens of kilometres in width. The shear zone is a high strain zone separating two relatively undeformed regions which have undergone relative motion. The displacement across a shear zone is usually of the same order of magnitude as the width of the shear zone. The deformation in the high strain zone can be brittle shear or more commonly ductile shear, or a combination of the two.

Ductile shear zones are characterised by rotation of earlier structures such as gneissose foliation into a direction which is sub-parallel to the shear zone. The shear zone fabric can be related to the state of finite strain of the shear. The variation of strain across shear zones was investigated by Ramsay and Graham (1970). The strain profile across a shear zone is often symmetrical, the strain increasing to a maximum in the central part of the zone. There may also be some small variation in strain profile along the length of the shear zone but this is relatively minor. Figure 1.1.1 shows a schematic diagram of a rectangular block which has been sheared. The edge of the block shows how the angular shear strain varies across the shear zone. Shear zones are regions of plane strain deformation. The plane of the shear zone is related to the state of stress. The shear plane is parallel to the intermediate principal stress direction and forms an acute angle with the maximum principal

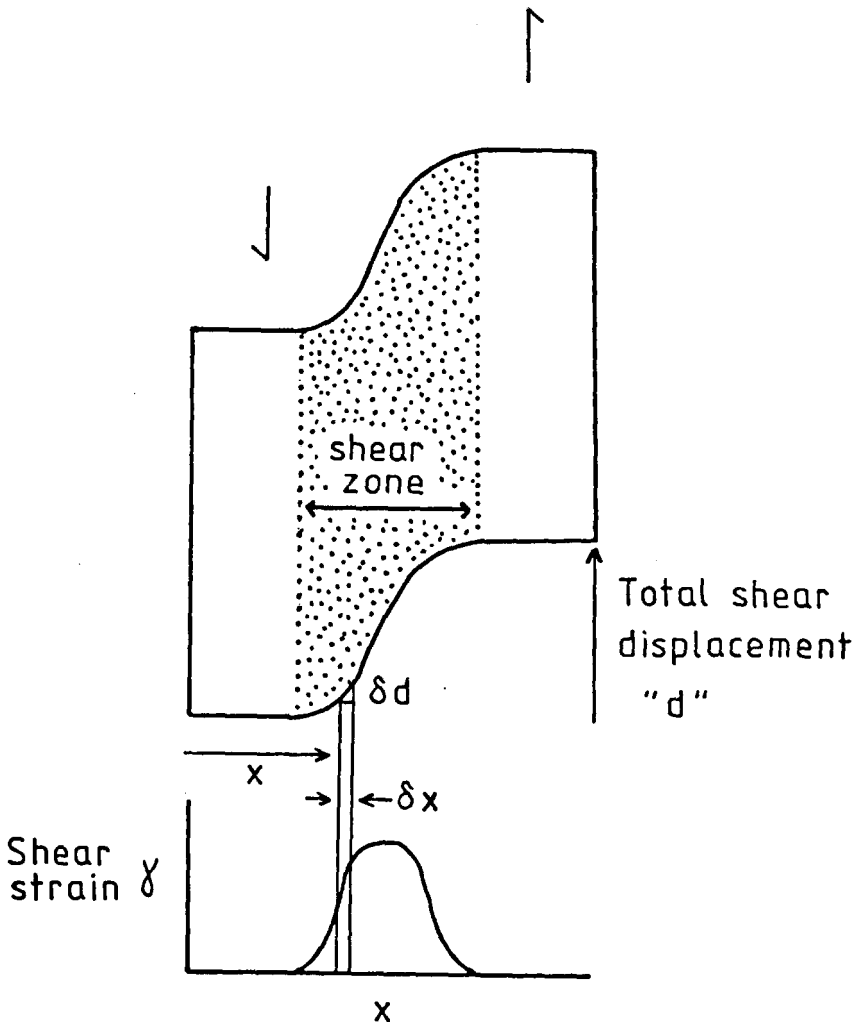

Figure 1.1.1. Variation of shear strain through a shear zone with heterogeneous strain. The total displacement "d" is derived by summation of all small elements δd. Redrawn after Ramsay and Graham 1970.

stress direction. Figure 1.1.2 shows a map of the strains and strain profiles for a typical small shear zone.

The role of the ductile shear in rock deformation was recognised early in the history of geological science. Although the results of ductile shearing are readily observable and measurable in the field, little is known about the process itself. Deformation can be controlled by variations in strength of the rocks within the shear zone, and syn-kinematic metasomatism can also affect the deformation. Little is known, however, about the physical conditions under which shear deformation takes place. Parameters such as the state of stress and the strain rate cannot be deduced from direct observations on the rocks alone. As a result mathematical models must be constructed to determine the relationship between the physical conditions and processes involved in ductile shearing and the structures produced.

In this thesis mathematical models are presented for ductile shear deformation in both viscous and viscoelastic rock materials. Ductile shear zones are modelled in an attempt to determine their stress and strain histories. The temperature and displacement profiles produced by shearing are also studied. The variation in physical and material properties are investigated and related to observed structures. Both strike-slip and thrust shear zones are investigated.

The mathematical and numerical formulations are described in chapters 2 and 3. Shear zone models can be divided into viscous and viscoelastic types. Viscous models and their applications are studied in chapters 4 and 5 and the simple viscous model has been extended in chapter 6 to include thrust type shear zones. The viscoelastic models are described in chapters 7 and 8 and are compared with viscous models.

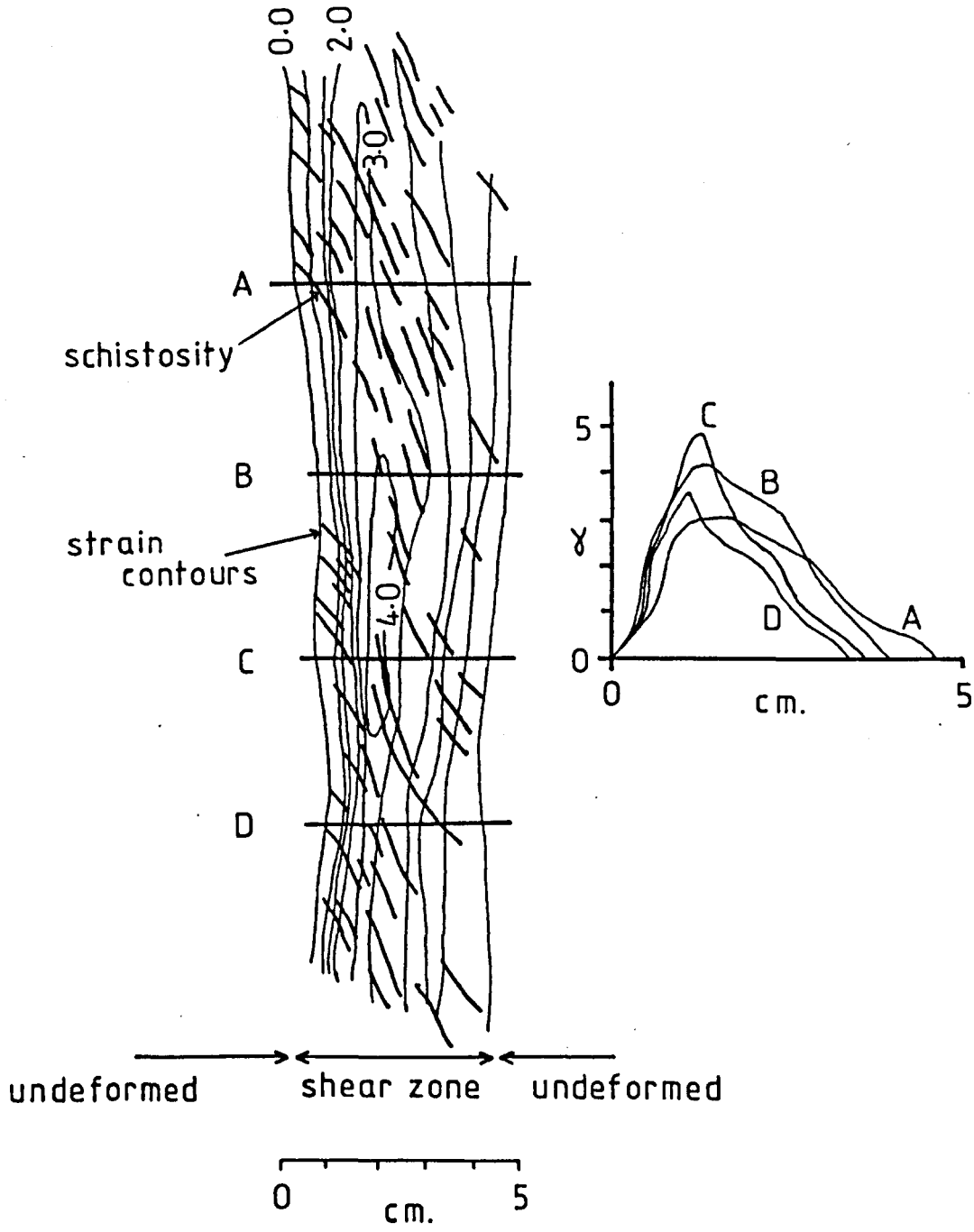

Figure 1.1.2. Map showing the variation in schistosity and values of strain computed from the angle between the schistosity and the shear zone. The graph shows the variation of strain profile along the shear zone. Shear zone is in metagabbro, Castell Odair, N.Uist(after Ramsay and Graham 1970).

1.2 The structure of ductile shear zones

Although shearing was recognised early in geological research, detailed study has only come with recent advances in the study of Pre-Cambrian geology. The majority of the shear zones described to date are found in Proterozoic rocks, although this may be partly due to the present levels of erosion. Shear zones of Proterozoic age are particularly well developed in the north Atlantic region (Sutton and Watson 1974, Davies and Windley 1976). Some of these shear zones are very large and form major tectonic structures. Amongst the best described examples are those of western Greenland (Bak et al. 1975).

Large shear zones generally have a steep dip and may be up to 40 km in width. The length of the shear zones can be hundreds of kilometres, the largest structures having a length of 2500 km as inferred from aeromagnetic evidence (Watson 1973). Broadening of shear zones with depth has been inferred on theoretical grounds (Aoki 1973) and interpreted from field evidence in the case of Nordre Strømfjord, western Greenland (Bak et al. 1975).

Proterozoic shear belts are broadly contemporaneous with "hairpin" bends in the polar wander paths for North America and Africa and may be related to major changes in the Proterozoic continental masses (Windley 1978). Sutton and Watson (1974) suggested that the transcurrent displacements were produced by rotation of a supercontinent. The continental plate interiors were not entirely rigid but were undergoing ductile strain along a number of discrete zones.

Evidence exists that some of the Proterozoic shear belts are superimposed on earlier lineaments of Archaean origin (Davies 1975). Some larger shear zones have undergone progressive shearing for long periods of time. The Laxford Shear Zone may have been active for a duration of more than 100 Myr. commencing around 2800 Myr. During this

time the total displacement has amounted to some 35 km produced by a series of distinct movement phases (fig. 1.2.1, Davies, 1978).

The location of shear zones can often be related to initial structural weaknesses in rocks (Coward 1973). Detailed study of the strain profiles across major shear zones shows that the total strain is accommodated on a large number of smaller high strain zones (fig. 1.2.2, Grocott and Watterson 1980). In an area where a group of shear zones of the same age exist, it is possible in some cases to relate the bulk strain of the area to movement on the shear zones. This provides an estimate of the amount of the total strain which is accommodated by ductile shear within an area (Park 1981).

Estimates of stress and strains for shear zones are fairly limited. The range of shear stress values based on palaeopiezometers is from 20-150 MPa (Kohlstedt and Weathers 1980, Scholz 1980). However different palaeopiezometers often give different values of stress for the same shear zone. Strain profiles are easier to measure than stresses. Strains vary widely in value and shape of profile; the profiles being generally symmetrical, however exceptions do exist. The sharpness of the peak of the strain profile also varies (fig. 1.2.3) but the maximum value of strain in any profile does not seem to exceed 10. A summary of shear zone parameters is given in Table 1.2.

The interaction of shear heating produced by deformation and synkinematic metasomatic activity has been studied by Beach (1976). Chemical alteration of the rocks in the Lewisian shear zones generally consists of the addition of H_2O, K and Na and the loss of Fe, Ca and Mg. These reactions are considered to have resulted from the interaction between large volumes of water and the rocks of the shear zone along which the fluid travelled. Adiabatic transport of water upwards through the crust may increase the geothermal gradient within the shear zone.

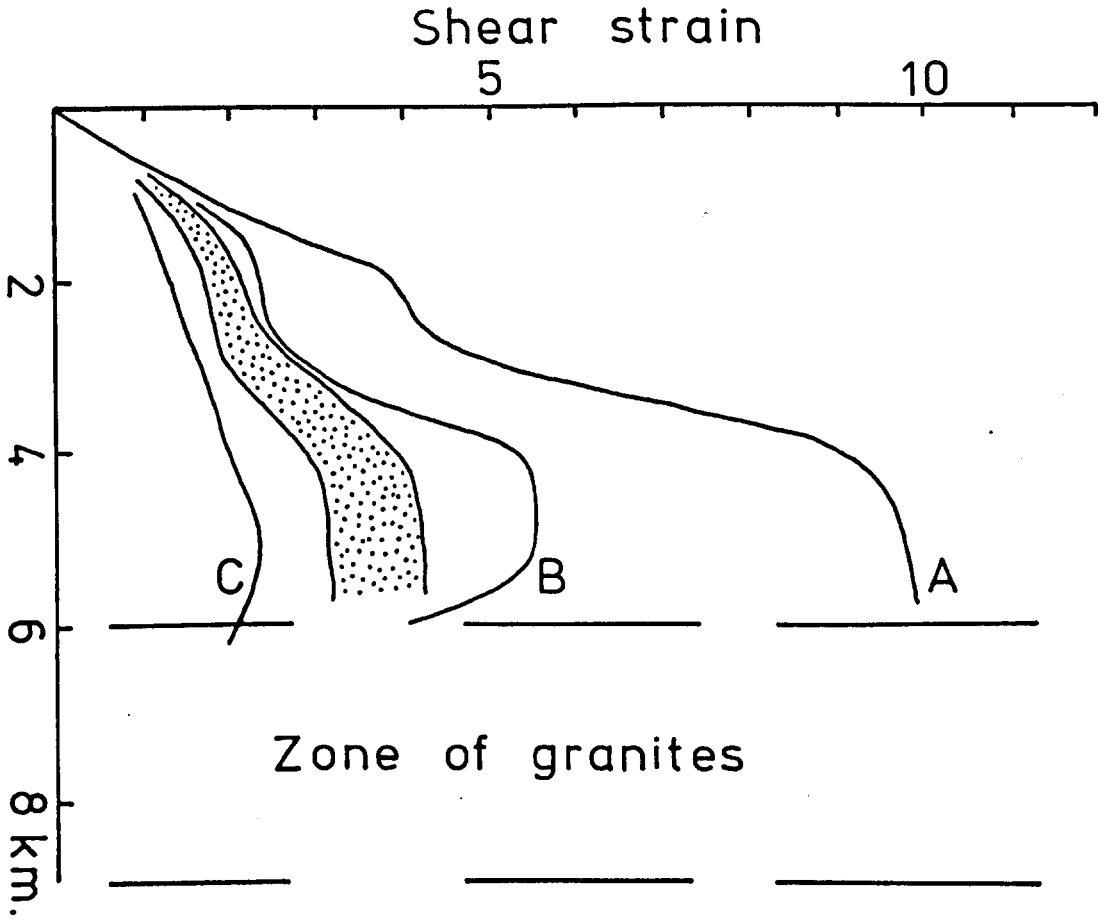

Figure 1.2.1. Dextral shear strain profiles from the southern margin of the Laxford shear zone, the graph showing progressive shearing. Profile A; shear strain from early Scourian; B shear strain from late Scourian; dashed zone ,Laxfordian shears and; C shear strain determined by rotation of Scourie dykes (after Davies 1978).

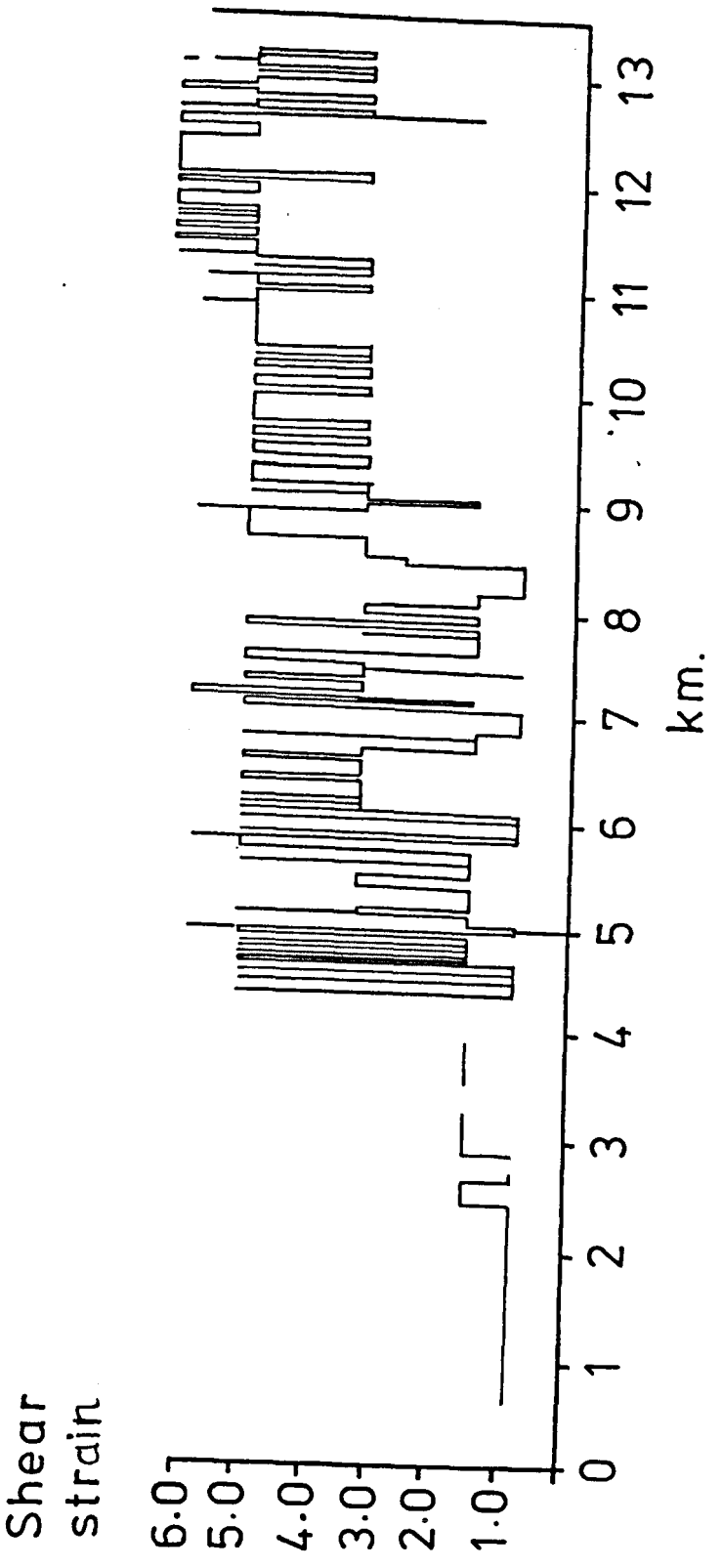

Figure 1.2.2. Quantitative strain profile across a boundary within the Ikertoq shear belt, western Greenland. The ordinate is calibrated using the interlimb fold angle of the sheared rocks(after Grocott and Watterson 1980).

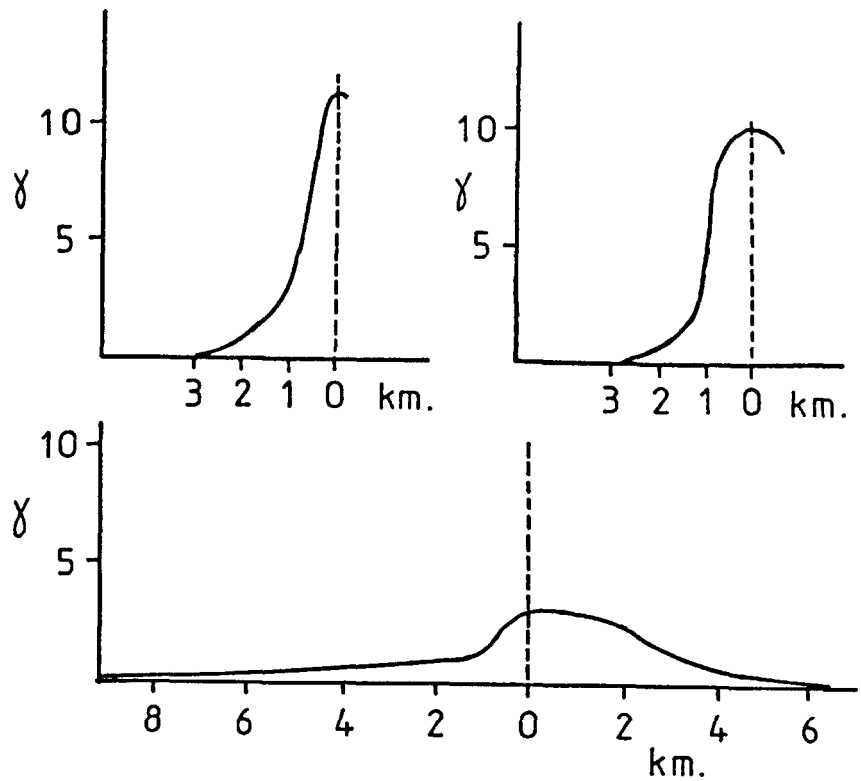

Figure 1.2.3. Example of strain profiles across shear zones in the western Superior Province, Canada showing variation in shape of the strain profile (after Park 1981).

The water will also lower the melting temperature and apparent viscosity of the rock.

Ductile deformation will only occur where the ambient temperatures are sufficiently high. The nature of the transitions between brittle and ductile deformation has been studied by Sibson (1977). This transition may occur over a fairly wide region in which both brittle and ductile processes occur. For example ductile shear fabrics may also contain pseudotachylites produced by brittle failure within the transitional region. In quartzo-felspathic crust the transition is estimated to occur at the 350^{o}C geotherm which will correspond to a depth of 10-15 km depending upon the geothermal gradient.

Shear zones may be thermo-mechanically stabilized. This mechanism relies upon the high temperature dependence of the viscosity of rocks. The shear heating produced by deformation raises the temperature of the shear zone and decreases the apparent viscosity of the rocks. As a result any further deformation will be localized in the softer hotter shear zone. This mechanism, whereby the shear heating serves to localize the deformation, is termed thermo-mechanical and is studied in this thesis. Any present day observations of heat flow and strain rates are useful in understanding the mechanism.

If modern day analogues of Proterozoic shear zones exist, they may be represented at the present level of erosion as intracontinental transform faults (Badham 1976, Grocott 1977). Ductile deformation is assumed to be occurring beneath present day transform faults. The San Andreas fault is the best studied example. The strain rate across the San Andreas fault has been measured as 3×10^{-14} s^{-1}, but no thermal anomaly exists over the zone (Lachenbruch and Sass 1980). The shear heating must be too small to produce any measurable change in heat flow at the surface. Seismicity on the San Andreas fault (Eaton, Lee and

Pakiser 1970) and on oceanic fracture zones (Reid and MacDonald 1973) is limited to the upper 10-15 km of the crust. At these shallow levels the deformation is dominated by brittle deformation processes. Frictional heating may modify the temperature field at these levels.

Models of shear zones must be constrained by these geological observations of the nature of processes occurring in the ductile deformation regions.

1.3 The structure of ductile thrusts

The mechanism of overthrust faulting and the role of fluids is well understood (Hubbert and Rubey 1959, Hsu 1969). The mechanism proposed by Hubbert and Rubey however, can only be applied to gravity slide overthrusting in porous rocks. Where large thicknesses of non-porous crystalline material are transported by thrusts a different mechanism exists. If the slab of crustal material is sufficiently thick then an inversion of the geotherm may occur. Frictional heating along the thrust plane and, if the temperature is sufficiently high, shear heating, may produce a thermal anomaly on the thrust plane and thus localize any further shear movement. Thermal stabilization of a ductile thrust is dependent upon the maintainance of the inversion of the geotherm by shear heating.

Thin-skinned thrust tectonics where décollement occurs along a basal weak layer has been investigated by many authors (Elliot 1976, Chapple 1978) and is not considered in this thesis. All the models presented here are thermo-mechanically stabilized by the geotherm inversion.

Oxburgh and Turcotte (1974) showed how the instantaneous overthrusting of a slab of rock 15 km thick in the Alps could produce an inversion of the geotherm. Calculations of the relaxation of the

inverted geotherm showed a low temperature, high pressure area to exist below that thrust, and this was suggested as a source of blueschist facies metamorphism.

The simple conduction model of Oxburgh and Turcotte has been refined to include the effects of frictional heating along the thrust (Graham and England 1976, England 1978). Observations of the inversion of metamorphic zonation around overthrust faults were used to constrain the degree of shear heating within the model.

A most sophisticated model of thrust faulting proposed by Brewer (1981) calculates the shear stress at the level of the thrust and determines the frictional heating for a given rate of movement. The frictional heating is sufficient to generate an inversion of the geotherm for faster thrusting rates. Temperatures predicted by the model are sufficiently high to enable ductile processes to take place.

No clear trends can be deduced from stress and strain levels for thrusts. It appears that a number of mechanisms may operate during the development of a single thrust and that different thrusts may develop by different processes. Table 1.3 presents a summary of some thrust characteristics from the literature.

1.4 Previous models of shear zone deformation

The majority of models of shear deformation to date are not directly concerned with vertical crustal shear zones. Viscous deformation processes in subduction zones and asthenosphere flow are the best studied.

The earliest model was presented by Turcotte and Oxburgh (1968). Their model treated a subduction zone as a viscous shear. A Newtonian rheology was assumed and a one-dimensional model of the velocity and temperature was constructed. Both the boundary velocity and the shear stress were assumed, and the temperature and velocity profiles then cal-

culated. The model related the shear velocity to the maximum temperature reached within the shear zone, in the form

$$U_o = k(CTm)^{\frac{1}{2}}$$

where U_o is shear velocity, Tm is the maximum temperature in the shear zone and k and C are constants depending upon the material.

The stability of steady state flow in Newtonian materials has been especially well studied. For a steady state viscous flow, heat flow within the model is balanced by shear heating. For a single dimension y,

$$k\frac{\partial^2 T}{\partial y^2} + \tau\frac{\partial u}{\partial y} = 0$$

where k is thermal conductivity, τ is shear stress and T is temperature. Most solutions of this use rheological properties described by the Arrhenius equation, such that,

$$k\frac{\partial^2 T}{\partial y^2} + \tau^{n+1}(2B/T)\exp(-H/RT) = 0$$

(see chapter 2 for full discussion).

Yuen and Schubert (1977) and Schubert and Yuen (1978) have used this equation to model asthenosphere shear flow. They showed that for a given value of stress two possible strain rates existed (fig. 1.4.1). The behaviour can be divided into a subcritical branch marked C in the diagram and a supercritical branch marked I. At low shear rates (subcritical flow), the rate of shear strain increases monotonically with stress, according to the stress exponent, n. The heat produced within the slab is negligible. At higher shear rates the shear heating is more

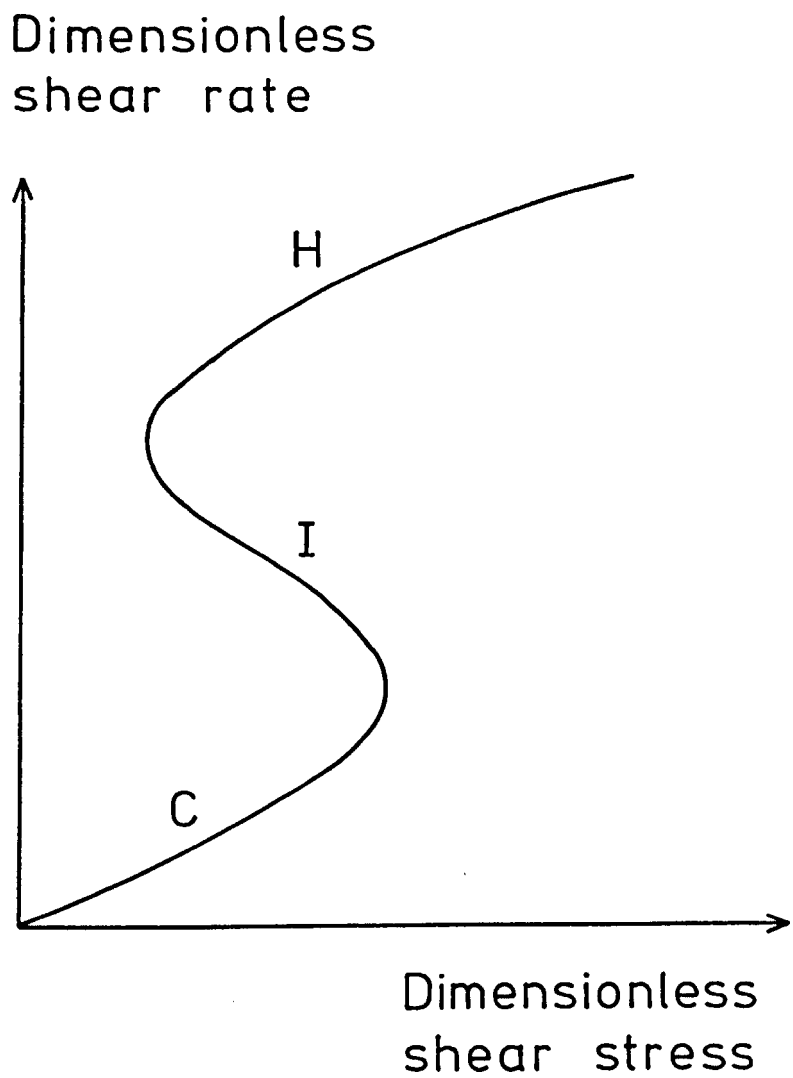

Figure 1.4.1. Sketch of the steady state solution for shear in a Newtonian slab with the Arrhenius factor. H-hot branch; I-intermediate or supercritical branch; C-Cold or subcritical branch. (see text for explaination).

significant. The strain rate still increases with stress, although thermal softening has an effect. Above a critical rate, heat is produced faster than it can be conducted out of the system, the material becomes softer and the stress drops as the strain rate is increased (section I on the diagram). Yuen and Schubert (1979) have also shown the existence of a third or hot branch marked H in the diagram. At high shear rates, shear heating causes large temperature rises, and the Arrhenius factor then tends towards a limiting value. The thermal factor is then almost negligible and stress once again increases with strain rate.

The possibility of supercritical flow (Gruntfest 1963) occurring within the earth presented the possibility of steady state shears being unstable. This instability has been observed experimentally in viscous flows (Sukanek and Laurence 1974).

The stability of steady state flows have been studied for both infinitesimal and finite perturbations. Infinitesimal perturbations are easier to solve mathematically due to the linear nature of the equations but finite perturbations may have a larger destabilizing effect. Melosh (1976) has previously argued that one dimensional supercritical flows are unstable in the presence of infinitesimal perturbations with a constant stress boundary condition. Yuen and Schubert (1977) and Schubert and Yuen (1978) showed that supercritical flow was stable for infinitesimal perturbations under constant velocity conditions.

A two dimensional asthenosphere shear model for a power law rheology was presented by Yuen and Schubert (1979). They showed that all basic states are stable to infinitesimal perturbations and argued that a three dimensional perturbation would decay even faster. Finite perturbations if large enough could produce instabilities, especially if this perturbation is a stress change. This agrees well with one

dimensional experimental evidence (Clark et al. 1977). Yuen and Schubert also showed the existence of a third or hot branch solution of strain rate for a given stress value (fig. 1.4.1).

Shallow return flow in the asthenosphere has been investigated using a two dimensional boundary layer solution (Schubert et al. 1978). Using a temperature and pressure dependent power law rheology the stresses were calculated to be a few tens of bars depending upon the amount of shallow return flow. Yuen, Tovish et al. (1978) calculated the effects of using local similarity in the previous model and found the approximations valid.

Yuen et al. (1978) produced the first model of viscous deformation on a vertical shear zone. The heat flow and inertial equations governing the system were solved in a one dimensional model with a Newtonian rheology. Using a similarity transformation, they produced a model which solved the shear stress for a given velocity boundary condition. The initial velocity profile across the model was assumed to be a Heaviside funtion. For a steady state solution they showed like Turcotte and Oxburgh (1968) that the maximum temperature in the shear zone was dependent upon the velocity of shearing. The shear stress for the model was shown to decrease almost linearly with increasing ambient temperature. Shear stress also decreases with the square root of shearing time.

The model also studies shearing between two half spaces of different materials. According to Yuen et al. partial melting under constant velocity conditions can only occur within a shear between a hard and a soft material. The shear heating produced by the harder material causes the softer material to melt.

Fleitout and Froidevaux (1980) extended the model of Yuen et al. The main difference between the two models is Fleitout and Froidevaux's assumption of constant shear stress across the shear zone at a given

time (i.e. the inertial terms of the equations are negligible). This simplifies the mathematical solution which no longer requires the use of a similarity transformation, the velocity profile being given by a simple integral equation.

Fleitout and Froidevaux distinguish two types of boundary condition for the model, a constant shear velocity condition and a constant shear stress condition. Their constant velocity solution agrees closely with that of Yuen et al. whereas the constant stress condition shows the possibility of thermal feedback instabilities melting the rocks.

Lockett and Kusznir (1982) have extended the work of the previous authors, expanding the mathematical formulation and showing that the Heaviside funtion starting condition is inapplicable. The work described in this paper forms part of this thesis (see chapters 2, 4 and 5).

All of the shear zone models published to date have assumed that thermo-mechanical processes have softened the rock and localized the shearing. Other possible mechanisms do exist. Conditions under which shear heating is effective (Poirier et al. 1979, Brun and Cobbold 1980) have been reviewed, along with other processes such as strain softening and metamorphic reaction, by Poirier (1980). Mechanisms by which shear localization could occur include geometric and structural softening, strain softening and hardening as well as thermo-mechanical localization.

Table 1.2 Shear Zone Characteristics from the Literature

Shear Zone	Maximum metamorphic grade	Width km	Total slip km	Shear Stress MPa	Strain	References
Lanvaux-Angers, France	biotite gneiss ∿600°C	6		100	2.3-6.2	Nicolas et al. 1977
Montague Noire, France	sillimanite migmatite ∗650°C	<20		100		Nicolas et al. 1977
Maydan, Afghanistan	migmatite ∿700°C	8-10		100	∿10	Nicolas et al. 1977
Linquine-Ofqui Fault, Chile	Ar-depletion	40				Herve et al. 1979
Alpine Fault, New Zealand	amphibolite, Ar depletion ∿600°C	24	480	100-150		Scholz et al. 1979
Lachlan Fold Belt, Australia	mylonitised granite			60-150(A)		Etheridge and Wilkie 1979
Massif Central, France	granodiorite 7.5 km deep 300-400°C			50(C) 25-150(B)		Burg and Laurent 1978
Idaho Springs, Colorado	10-15 km deep 500-600°C			95(A) 90(B) 110(C)		Kohlstedt and Weathers 1980
Ikertoq, Greenland	granodiorite gneiss 15-30 km deep 600-800°C	40	150+	20-40(A) 20-40(B) 50-110(C)	>6	Kohlstedt et al. 1979

Vasterland, Greenland	15-30 km deep 600-800°C	10		>6	Bak et al. 1975
Nordre Stromfjord, Greenland	15-30 km deep 600-800°C	15	100+	6	Bak et al. 1975
Laxford Front, Scotland	retrograde amphibolite 600°C 6kbar	10	35+	∿3.5	Davies 1978
Karmoy ophiolite, Norway	upper/middle greenschist 450-500°C	0.1	0.7	6-7	Thon 1980
South Harris, Scotland	granulite amphibolite 700°C	2	14		Graham 1980
South Amorican, France	greenschist >400°C <600°C	0.4			Jégouzo 1980
Superior Province, Canada	greenschist 450-600°C 10 km deep				Park 1981

Palaeopiezometer: (A) dynamically recrystallized
(B) subgrain size
(C) free dislocation density

Table 1.3 Thrust Characteristics from the Literature

Thrust Zone	Maximum metamorphic grade	Width of thrust km	Total slip km	Shear Stress MPa	Thickness of slab km	References
Olympus thrust, Greece	400°C	6	>15	30-100		Barton and England 1979
Coast Range, California	blueschist 400°C >7kbar	6				Blake et al. 1967
Blue Ridge Thrust, N. Carolina						Bryant 1967
Glarus, Switzerland	400°C		30	1-100	5-6	Schmid 1975 Schmid et al. 1977 Briegel and Goetze 1978 Hsu 1969
Subduction zones, western Pacific	Heat flow			100-300		Oxburgh and Turcotte 1970 Turcotte and Schubert 1973 Jischke 1975
Median tectonic line, Japan	sillimanite >650°C	80				Miyashiro 1961 Suwa 1961
Main central thrust, Himalayas	sillimanite in granite >650°C	10	230	20-200		LeFort 1975 Bird 1978
Unterostalpin, eastern Alps	amphibolite 550°C	20				Oxburgh and Turcotte 1974 Bickle et al. 1975
Franciscan thrusts, California	amphibolite 650°C	2		50-100		Williams and Smyth 1973 Nicolas 1979 Nicolas and Le Pichon 1980

Table 1.3 continued

Bay of Islands, Newfoundland	amphibolite 650°C	0.6	50-100		Williams and Smyth 1973 Nicolas 1979 Nicolas and Le Pichon 1980
San Gabriel Mts. California	mylonite		130-190		Twiss 1977
Arltunga Nappe, Australia	mylonite		30-130		Twiss 1977
Moine Thrust, Scotland	4-10 km deep. <450°C		85-110 100-150 200		Weathers et al. 1979
Woodruffe thrust, Australia	mylonite		30-130 60-150		Twiss 1977 Etheridge and Wilkie 1979
Lewis thrust, Canada		32.5		1.4	Hubbert and Rubey 1959
Muddy thrust, Navada		24		7.6	Hubbert and Rubey 1959
McConnell thrust, Canada					Elliott 1976
Valley and Range, Appalachians				10-22.5	Chappel 1978

CHAPTER 2

The Mathematical Formulation of Shear Zone Models

2.1 Introduction

In the simplest form the shear zone model consists of two identical half spaces of rock sliding horizontally past one another (fig. 2.1.1). The two half spaces are separated by a vertical surface. The mechanism where shear heat reduces the viscosity and localizes further deformation forms the basis of thermo-mechanical shear zones. The underlying assumption of thermo-mechanical models is the high temperature dependence of the apparent viscosity of rocks.

Development of a localized shear zone can only occur where there is some initial heterogeneity in the model. A shear heat maxima between the two slabs requires a higher shear velocity gradient at this point. This is usually achieved by using an initial small positive temperature anomaly in the centre of the model. The slightly lower viscosity gives rise to a shear heat maximum at the centre. The higher shear heating produces a positive temperature anomaly and decreases the viscosity further. The low viscosities in the centre of the shear zone localize any further deformation. In this thesis the deformation is assumed to be controlled by a highly temperature dependent non-Newtonian rheology.

To construct a mathematical model consideration must be given to the following parameters,

(i) the differential velocity U_o to be applied across the model and the width of the model over which it is applied. If a velocity boundary condition is not applied then the shear stress τ, across the model must be specified.

(ii) the mechanical properties of the rocks shearing, such as elasticity and apparent viscosity and its temperature dependence.

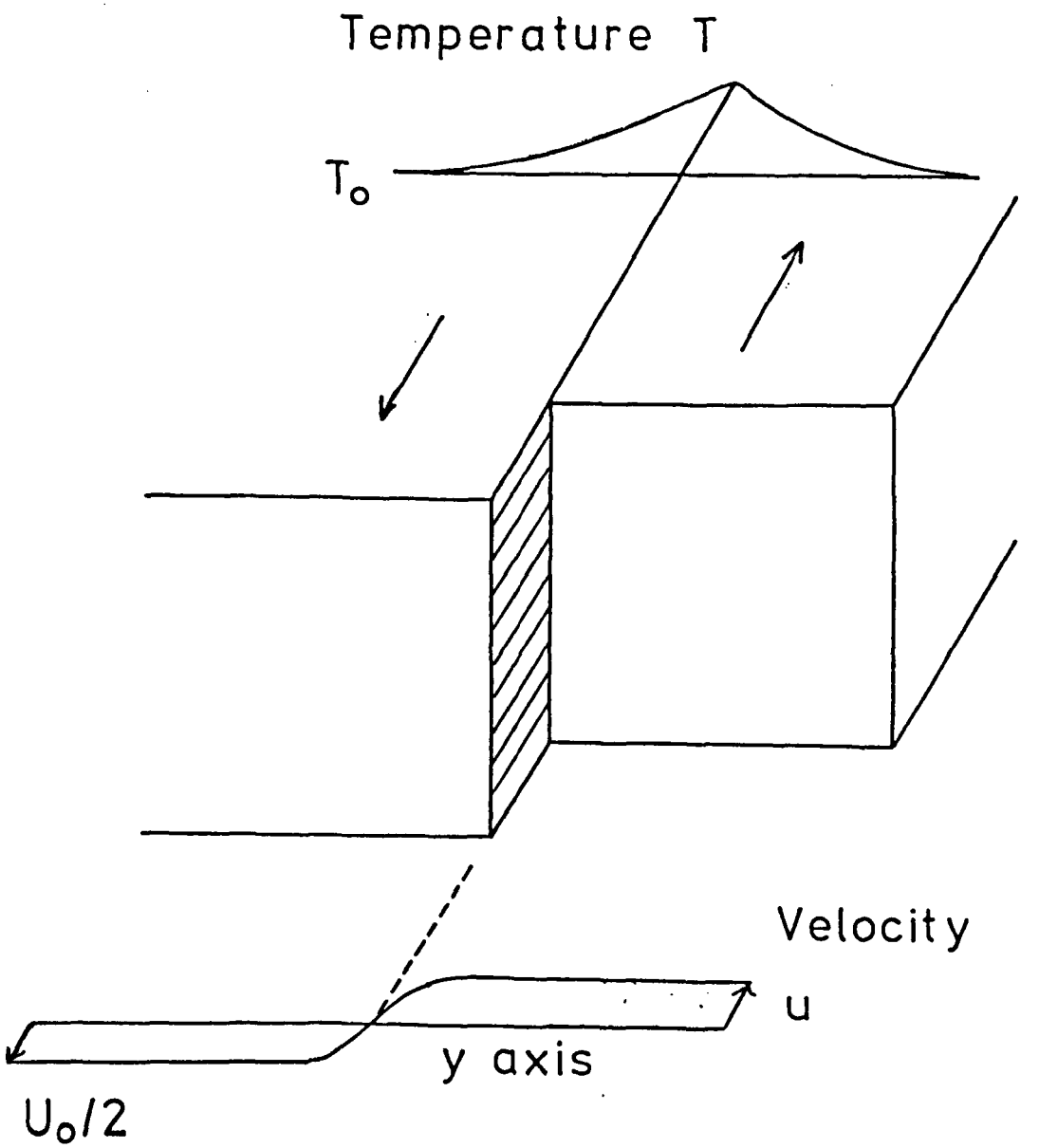

Figure 2.1.1. Diagrammatic representation of shear zone model showing velocity and temperature profiles(after Yuen et al. 1978).

(iii) the initial temperature profile across the model and the thermal properties of the rocks.

The models presented in this thesis include both viscous and viscoelastic shear zone models. The fundamental properties of elastic continua have been described by many authors (Sokolnikoff 1956, Fung 1965, Jaeger and Cook 1969).

The elastic strain of a simple Hookean body is given by

$$\varepsilon_E = k\sigma$$

where σ is stress, and k is the elastic modulus. This deformation takes place instantaneously on application of the stress. Viscous deformation is however time dependent, the longer the stress is applied the greater the deformation. Viscous strain rate is given by

$$\dot{\varepsilon}_v = S\sigma^n$$

where S is a function of viscosity and n is a constant. S is highly temperature dependent. Values of n>1 result in the deformation being non-Newtonian power law creep. This relationship is used in the viscous model.

The viscoelastic model combines both a Hookean elasticity and a non-Newtonian rheology resulting in a Maxwell body whose strain rate is given by

$$\dot{\varepsilon} = k\dot{\sigma} + S\sigma^n.$$

This may be rewritten as

$$\dot{\varepsilon} = k\dot{\sigma} + \sigma/\eta$$

where η is the apparent viscosity.

The apparent viscosity of rock is highly dependent upon the physical conditions under which deformation is taking place and depends on

temperature, stress and possibly strain. Stocker and Ashby (1973) described 13 different creep processes that occured in rocks under differing conditions. The majority of these can be divided into diffusion creep and dislocation creep processes.

Diffusion creep processes include mechanisms such as Coble creep and Nabarro-Herring creep. The strain rate is controlled by grain boundary diffusivity and is given by (Weertman 1970)

$$\dot{\varepsilon} = f(\sigma) Do \exp(-\frac{Q}{RT})$$

where Do is the diffusion coefficient, T is temperature, R is the gas constant and Q is the activation energy. The activation energy term can be replaced giving an equation of the form

$$\dot{\varepsilon} = f(\sigma) Do \exp(-g\ Tm/T)$$

where Tm is the melting temperature and g is a constant (Weertman 1970).

Stocker and Ashby (1973) concluded that dislocation creep was the dominant deformation mechanism in rocks under lower crust and mantle conditions. Goetze (1978), however, has suggested that this is not always the case. The general form of a dislocation creep expression is

$$\dot{\varepsilon} = \frac{\tau^n}{A \exp(BTm/T)}$$

where A, B and n are constants.

Dislocation creep is used throughout this thesis and is discussed in more detail in section 2.4.

2.2 The viscous model

The simple viscous model consists of two identical half spaces of rock sliding past each other (fig. 2.1.1). The temperature field of the continuum is given by

$$\frac{dT}{dt} = \frac{k}{\rho Cp} \nabla^2 T + H'$$

where

$$H' = \sigma_{ij} \frac{du_i}{dx_j} \Big/ \rho C_p$$

T is temperature, σ is stress, ρ is density, Cp is specific heat, k is conductivity, u is displacement, t is time and H' represents shear heating. The force equilibrium of the continuum is given by

$$F_i = \rho \ddot{u}_i + \frac{d\sigma_{ji}}{dx_j}$$

where F is force.

In the absence of internally derived forces, $F_i = 0$ and the inertial equation for the simple shear zone model then becomes

$$\rho \frac{\partial u}{\partial t} = \frac{\partial \tau}{\partial y} \qquad (2.2.1)$$

where τ is shear stress and the corresponding temperature field is given by

$$\frac{\partial T}{\partial t} = \frac{k}{\rho Cp} \frac{\partial^2 T}{\partial y^2} + \tau \frac{\partial u}{\partial y} \Big/ \rho C_p \qquad (2.2.2)$$

Equations 2.2.1 and 2.2.2 have been used previously by Yuen et al. (1978) and Fleitout and Froidevaux (1980) as the basis for their shear zone models.

To solve the two coupled partial differential equations a rheology expression is required. The Navier-Stokes equation defines the strain rates as

$$\{\dot{\varepsilon}^{v}\} = [G]\{\sigma\}$$

the components being

$$\{\dot{\varepsilon}^{v}_{x}\} = \tfrac{1}{2}\eta(\sigma_x - \sigma_{av})$$

$$\{\dot{\varepsilon}^{v}_{y}\} = \tfrac{1}{2}\eta(\sigma_y - \sigma_{av})$$

$$\{\dot{\varepsilon}^{v}_{xy}\} = \eta(\sigma_{xy})$$

$$\{\dot{\varepsilon}^{v}_{z}\} = \tfrac{1}{2}\eta(\sigma_z - \sigma_{av})$$

where $\sigma_{av} = {}^{1}/_{3}(\sigma_x + \sigma_y + \sigma_z)$ and η is apparent viscosity. For one dimension the equation reduces to

$$\dot{\varepsilon}^{v}_{xy} = \tau_{xy}/2\eta$$

Assuming a dislocation creep process the following expression can be used (Neugebauer and Breitmayer 1975, Woodward 1976)

$$\frac{\partial u}{\partial y} = \frac{\tau^{n}}{A \exp(BTm/T)} \qquad (2.2.3)$$

where A, B and n are constants.

Rewriting equation 2.2.1 as

$$\frac{\partial u}{\partial t} = {}^{1}/_{\rho}\,\frac{\partial \tau}{\partial y} \qquad (2.2.4)$$

and combining with the rheology equation 2.2.3 the following equation can be obtained

$$\frac{\partial u}{\partial t} = {}^{1}/_{\rho} \frac{\partial}{\partial y} \left[\left\{ A \exp(BT_m/T) \frac{\partial u}{\partial y} \right\}^{1/n} \right] \qquad (2.2.5)$$

To solve for temperature, equation 2.2.2 is rewritten as

$$\frac{\partial T}{\partial t} = \frac{k}{\rho Cp} \frac{\partial^2 T}{\partial y^2} + H' \qquad (2.2.6)$$

where H' represents the viscous shear heating. H' itself can be written as

$$H' = \frac{\tau \frac{\partial u}{\partial y}}{\rho Cp} = \frac{\left(A \exp(BTm/T) \frac{\partial u}{\partial y} \right)^{1/n} \frac{\partial u}{\partial y}}{\rho Cp} \qquad (2.2.7)$$

or

$$H' = \frac{\tau^{n+1}}{\rho Cp \; A \exp(BTm/T)} \qquad (2.2.8)$$

Simultaneous solution of equations 2.2.5 and 2.2.6 with 2.2.8 provides a description of the shear deformation.

The temperature anomaly of the shear zone is symmetrical about the centre and the velocity profile is anti-symmetrical. As a result only one half space need be considered for modelling.

The boundary conditions applied to the temperature solution are

$$T(y = \infty) = T_o$$

where T_o is the ambient temperature and

$$\frac{\partial T}{\partial y} (y = o) = 0$$

since T is symmetrical about the shear zone. Assuming a constant velocity

boundary condition then

$$u(y = o) = 0$$

$$u(y = \infty) = U_o/2$$

where U_o is the relative slip velocity of the two adjacent blocks.

Following Yuen et al. (1978) a possible initial velocity distribution may take the form of a Heaviside function (fig. 2.2.1) such that

$$u(y>0,\ t = 0) = U_o/2 \qquad (2.2.9)$$

The above equations were solved by the finite difference technique using the Yuen et al. starting boundary conditions.

Very small time iteration increments were required for the numerical solution with time increments typically representing 10^{-24} yr. in length. The initial step profile is rapidly smoothed out to give a uniform velocity gradient. This requires a total time of about 10^{-20} yr. In such a short time there was no modification of the temperature profile. If an initial constant gradient velocity profile is used it remains unchanged.

From equation 2.2.1 if $\partial u/\partial t$ is small then $\partial \tau/\partial y$ is small tending to zero. For any physically significant time span the shear stress τ, does not vary with y. A constant gradient velocity profile is the preferred starting condition and is used throughout this thesis.

This casts doubt on the applicability of the results of Yuen et al. since they use a Heaviside function starting condition which is invalid. They also use a similarity transform in their analytical solution which mathematically "blurs" the solution at and near time zero.

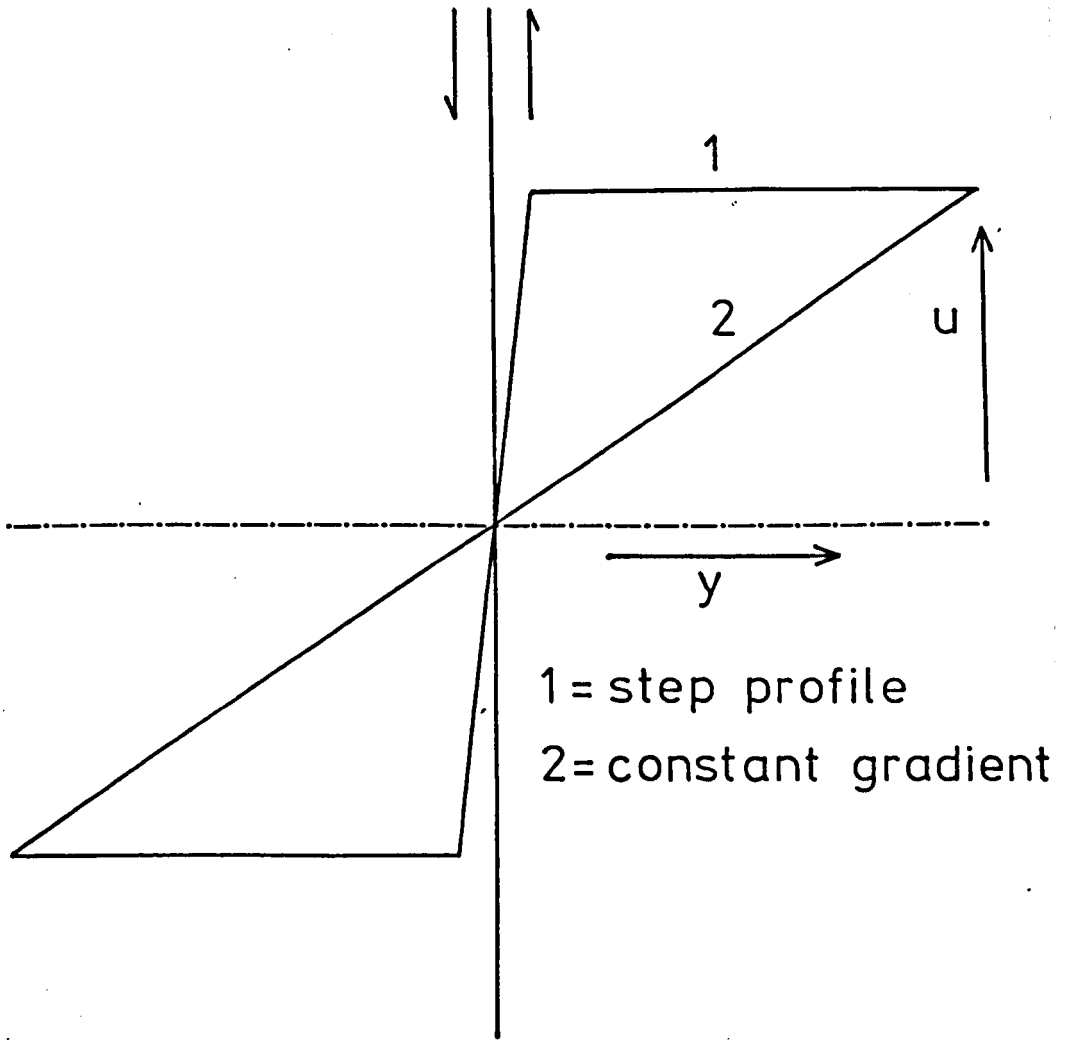

Figure 2.2.1. Initial velocity profiles for the initiation of shearing :(1) the step profile(Heaviside function); (2) a constant gradient profile.

Fleitout and Froidevaux (1980) have presented an analytical solution which assumes that $\partial\tau/\partial y = 0$. The solution does not use a similarity transformation.

Since τ is independent of y, equation 2.2.3 can be used to obtain a velocity function u' such that

$$u'(y) = \tau^n \int_o^y 1/\left[A \exp(BTm/T)\right].dy' \qquad (2.2.10)$$

For the constant velocity boundary condition $u'(y = \infty) = U_o/2$. It therefore follows that

$$\tau^n = U_o/2 \Big/ \left\{ \int_o^{y=\infty} 1/\left[A \exp(BT_m/T)\right].dy' \right\} \qquad (2.2.11)$$

Consequently velocity as a function of y is given by

$$u(y) = U_o/2 \frac{\int_o^y 1/\exp(BTm/T).dy'}{\int_o^\infty 1/\exp(BTm/T).dy'} \qquad (2.2.12)$$

For a constant shear stress boundary condition

$$u(y) = \tau^n \int_o^y 1/\left[A \exp(BTm/T)\right].dy' \qquad (2.2.13)$$

The model can now be constructed for both constant velocity and constant shear stress boundary conditions. Simultaneous solution of equations 2.2.12 and 2.2.6 provides the constant velocity model while equations 2.2.13 and 2.2.6 give constant shear stress conditions.

Equations 2.2.12 and 2.2.13 are both formulated for dislocation creep. Similar integrals can be derived using diffusion creep expressions, only the power of the stress and the constants in the integral change.

2.3 The viscoelastic model

The viscoelastic model assumes that the body behaves as a Maxwell substance, the strain rate being the sum of both elastic and viscous strains. The total strain in the x direction is given by

$$\varepsilon_x = {}^1/_E\,\sigma_x - {}^V/_E\,\sigma_y - {}^V/_E\,\sigma_z + \varepsilon_x^v \qquad (2.3.1)$$

where σ_x and ε_x^v are stress and viscous strain in the x direction. E is Young's modulus and V is Poisson's ratio. The total strains in the y and z directions are given by similar equations. The creep strain rate is given by the Navier-Stokes equation

$$\{\dot{\varepsilon}\} = [G]\{\sigma\}$$

the total creep rate in the x direction $\dot{\varepsilon}_x^v$ is given by

$$\dot{\varepsilon}_x^v = \frac{(2\sigma_x - \sigma_y - \sigma_z)}{6\eta}$$

Referring back to equation 2.2.3 we can see that the apparent viscosity is highly dependent upon temperature. Solution of the equations must involve the simultaneous solution of shear heating and its inclusion in the temperature field equation.

The temperature field is given by

$$\frac{\partial T}{\partial t} = K\nabla^2 T + H'$$

where K is thermal diffusivity and H' is the shear heating. For a viscoelastic material the shear heating is given by

$$H = (\sigma_x \dot{\varepsilon}_x + \sigma_y \dot{\varepsilon}_y + \sigma_z \dot{\varepsilon}_z)$$

where x, y and z are the principal components.

The mechanical structure of the shear zone can be described in terms of the force equilibrium equation for a continuum.

$$F_i = \ddot{u}_i + \frac{d\sigma_{ji}}{dx_j}$$

The thermal and mechanical equations can be solved in two ways;

(i) by using an integral equation for the velocity profile in an analogous way to equations 2.2.12 and 2.2.13 and solving this simultaneously with the temperature field equation or

(ii) using the finite element technique for viscoelastic continuum analysis and using the finite element nodes as points for a finite difference temperature field solution.

The latter method has been used in this thesis.

For both viscous and viscoelastic models two boundary conditions can be envisaged,

(i) constant boundary velocity conditions

(ii) constant shear stress conditions.

In both viscous and viscoelastic models the two boundary conditions are investigated assuming that the viscous creep is a dislocation process. The effect of using diffusional creep is discussed later in the thesis.

2.4 Apparent viscosity and other material properties

To model shear zone processes it is essential to have a good estimate of the physical properties of the rock. Both mechanical properties such as Youngs modulus and apparent viscosity as well as thermal effects must be investigated. Clark (1966) has documented physical properties for a large number of rock types. For the majority of models the following values were used,

Youngs modulus 10^{11} Nm^{-2}

Poissons ratio 0.25

Rock density: dolerite/granodiorite 2.7 gm/cm^3

olivine rocks 3 gm/cm^3

Specific heat capacity 0.27 cal/gm ^oK

Any differing values used are specified with the model in question. Apparent viscosity and thermal conducitvity show marked variations with temperature and require more detailed consideration.

(i) Apparent viscosity

For detailed modelling a flow law is essential. These flow laws are often empirical simplifications of the theoretical relationship due to the large number of parameters controlling the strain rate and the difficulty of their measurement.

Weertman (1970) produced the empirical relationship

$$\dot{\varepsilon}^v = Af(\tau)D_o \exp(-Q/RT)$$

where $f(\tau)$ is a funtion of τ and is usually a power law $f(\tau) = \tau^n$ and D_o is a diffusion constant dependent upon the activation energy and temperature. The value of D_o varies slightly with temperature conditions but these variations are small compared with the range of estimates for the other parameters.

Stocker and Ashby (1973) summarised the processes of steady state deformation of crystalline materials. The deformation maps they produced divided the stress-temperature field into various regions dominated by various creep processes (fig. 2.4.1). Diffusional creep processes such as Nabarro-Herring and Coble creep do not produce sufficiently high strain rates; dislocation (power law) creep being the dominant mechanism in upper mantle deformation (Stocker and Ashby 1973). From these maps the temperatures involved in shear zones, >400°C will result in dislocation creeps dominating the deformation. Recent work by Goetæ (1978) has shown that under high stress conditions lithosphere deformation is dominated by Coble creep once dynamic recrystallization commences. Goetzeproposes a Dorn law for shear stresses above 2 kbar of the form,

$$\dot{\varepsilon} = 5.7 \times 10'' \exp\left[\frac{-128 \text{ kcal/mol}}{RT}\left(1-\frac{\tau}{85000}\right)^2\right].$$

Kohlstedt and Goetæ (1974) derived a flow law of the form

$$\dot{\varepsilon} = f(\sigma) \exp(-Q/RT)$$

for dislocation creep and derived constants for dry olivine rock applicable over a wide temperature and stress range. The function $f(\sigma)$ is an empirical funtion and not simply a power law σ^n. Neugebauer and Breitmayer (1975) showed that by using power laws of n=3 and n=5, depending upon the shear stress, good approximations to dry olivine flow data can be obtained. The values are for dry olivine rock in S.I. units are (Woodward 1976) using Q = 40.0.

$$\dot{\varepsilon} = 1.6 \times 10^{-15} \exp(-40.0\ Tm/T)\tau^3 : \tau<1.0 \times 10^8\ Nm^{-2}$$

$$\dot{\varepsilon} = 1.6 \times 10^{-32} \exp(-40.0\ Tm/T)\tau^5 : \tau>1.0 \times 10^8\ Nm^{-2}$$

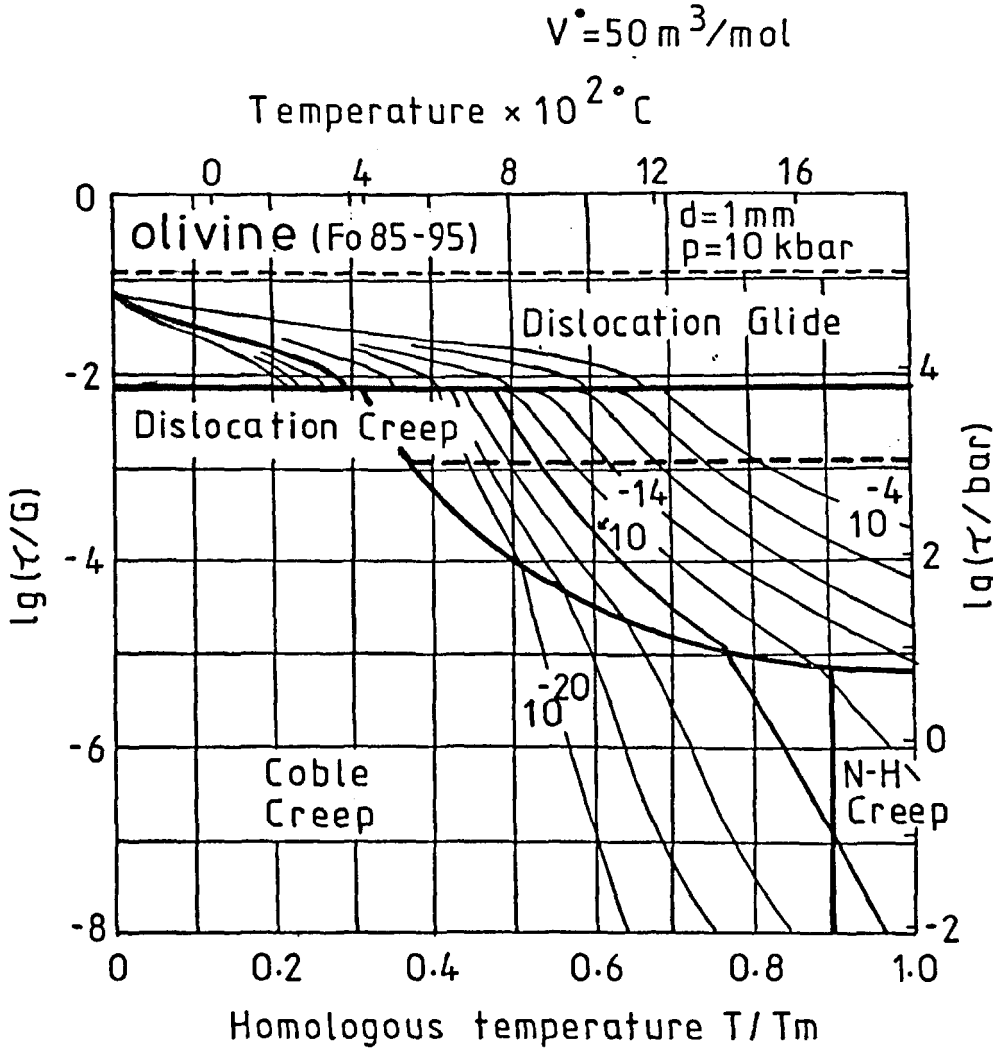

Figure 2.4.1. Deformation map of olivine predicting the stress developed at each temperature as a function of strain rate. Redrawn from Stocker and Ashby(1973).

At low stresses linear diffusional creep may occur. The maximum stresses for significant diffusional creep is estimated at

1.5×10^5 Nm^{-2} (Weertman 1970)

0.7×10^5 Nm^{-2} (Stocker and Ashby 1973) .

The amount of flow at these stresses is very small compared to higher stress regimes.

Woodward (1976) reformulated the equations of Neugebauer and Breitmayer to give the following based on Kohlstedt and Goetæs' data

$$\eta = 2.1 \times 10^{14} \exp(40.0\ Tm/T)\tau^{-2}: \quad \tau < 2.18 \times 10^8\ Nm^{-2}$$

$$\eta = 1.0 \times 10^{31} \exp(40.0\ Tm/T)\tau^{-4}: \quad \tau > 2.18 \times 10^8\ Nm^{-2}$$

Murrell and Chakravarty (1973) produced values for dolerite and granodiorite rocks based on the assumption of Andrade creep ($\varepsilon = \beta.t^m$, where $m \sim 0.5$, t = time and $\beta = f(\tau,T)$). Woodward reformulated these values to give

$$\eta = 1.5 \exp(53\ Tm/T)\tau^{-1.5} \qquad \text{dolerite}$$

$$\eta = 6.0 \exp(42\ Tm/T)\tau^{-1.5} \qquad \text{granodiorite}$$

Woodwards formulations for dry olivine, dolerite and granodiorite rheologies are used in this thesis. The effects of using a Coble creep mechanism under the conditions described by Goetæ (1978) are described later in this thesis.

(ii) Thermal conductivity

Values of thermal conductivity have been determined for many rock types (Clark 1966). The majority of the models presented use a value of 0.006 $cal/cm^2sec\ ^oC$. In models where the thermal conductivity may be critical a number of values have been used ranging from 0.004-0.01 $cal/cm^2sec\ ^oC$.

Modification of the value of the thermal conductivity may be necessary at higher temperatures to account for radiative heat transfer. Clark and Ringwood (1964) presented values of thermal conductivity which show an increase at 800°C.

Schatz and Simmons (1972) have determined both the thermal conductivity and radiative conductivity of dunite rock for various temperatures. Using their data an effective conductivity has been determined to incorporate both thermal (phonon) and radiative conductivities as below

$$k_{eff.} = 0.0109 - (4.5 \times 10^{-6}.T) \text{ cal/cm}^2\text{sec } ^{o}\text{C}$$

where T is in °K.

This expression does not show the marked increase in conductivity at higher temperatures predicted by earlier workers. More recent experimental work by Cull (1975) agrees closely with that of Schatz and Simmons. The above expression was used to determine the total conductivities in some models. Detailed description of its effects are included with the actual model.

CHAPTER 3

Numerical Techniques Used in Shear Zone Modelling

3.1 Introduction

All the geodynamic models of shear zones presented in this thesis assume that the rocks behave as a mechanical continuum. While the fundamental properties of an elastic continuum have been studied by a number of workers (Sokolnikoff 1956, Fung 1965, Jaeger and Cook 1969) and analytical solutions for various simple geometric bodies have been produced, all but the most simple geological models involve sharp discontinuities and complex spatial distributions of material properties and boundary conditions. The resulting differential equations for the continuum are often mathematically intractable or involve so many simplifying assumptions as to limit the model's value.

To overcome this the continuum may be discretized into a finite number of units each having its own properties and the equations solved by numerical methods. Using finite difference and finite element techniques elaborate numerical models can be constructed, their size and complexity often being limited by the amount of computational power available. The models in this thesis have used both finite difference and finite element techniques.

3.2 Finite Difference Methods

The finite difference method solves differential equations by dividing the region to be analysed into a finite number of discrete points. The method replaces the differential equation by a difference equation which approximates to the precise mathematical solution. The difference equation calculates the derivative of any parameter at a point by using the values from adjacent points. The derivative is then

used in the calculation of the new value for the parameter.

Finite difference problems can be formulated either implicitly or explicitly. An implicit formulation involves the solution of a set of simultaneous equations for unknown quantities, whereas in an explicit formulation the quantities at each point are directly calculated at small successive increments of time.

An example of an explicit formulation may be applied to the one dimensional partial differential equation for the temperature field,

$$\frac{\partial T}{\partial t} = K \frac{\partial^2 T}{\partial x^2} \qquad (3.2.1)$$

where K is thermal difussivity.

The temperature gradient at a point N is calculated using the values at adjacent points N - 1 and N + 1 in the x direction. If the difference points are equally spaced a distance 'a', apart then equation 3.2.1 can be replaced by the difference expression (see fig. 3.2.1)

$$\frac{\partial T}{\partial t} = K \left(\frac{T_{N+1} + T_{N-1} - 2T_N}{a^2} \right) . \qquad (3.2.2)$$

Replacing the time derivative by a difference expression we get

$$\frac{\partial T}{\partial t} = \frac{\Delta T}{\Delta t} . \qquad (3.2.3)$$

For a given time interval Δt the temperature change at point N becomes,

$$\Delta T_N = K \Delta t \left\{ T_{N+1} + T_{N-1} - 2T_N \right\} / a^2 . \qquad (3.2.4)$$

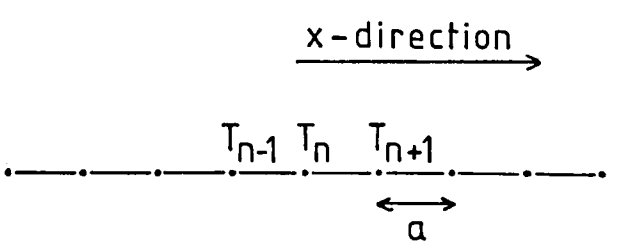

$$\frac{dT}{dt} = K \frac{d^2T}{dx^2}$$

$$\Delta T_n = K \Delta t \left[\frac{T_{n-1} + T_{n+1} - 2T_n}{a^2} \right]$$

Figure 3.2.1. Finite difference formulation for an explicit one dimensional temperature solution.

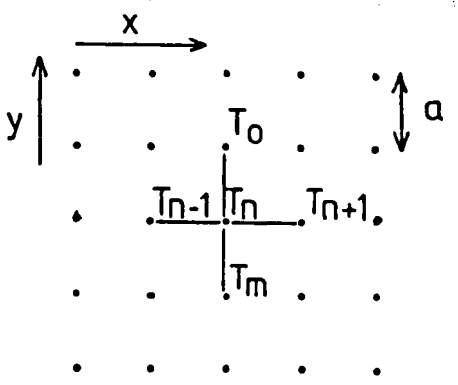

$$\Delta T_n = K \Delta t \left[(T_o + T_m + T_{n-1} + T_{n+1} - 4T_n) / a^2 \right]$$

Figure 3.2.2. Finite difference formulation for an explicit two dimensional temperature solution.

The temperature field over the region to be analysed can be determined by using this equation on each point in turn and then repeating the process iteratively for each time step. To maintain the stability of this numerical process the length of a time increment must not exceed (Carslaw and Jaeger 1959)

$$\Delta t = \tfrac{1}{2}a^2/K . \qquad (3.2.5)$$

The solution can easily be extended to two dimensions. The temperature field differential equation becomes

$$\frac{\partial T}{\partial t} = K \frac{\partial^2 T}{\partial x^2} + \frac{\partial^2 T}{\partial y^2} \qquad (3.2.6)$$

and the difference equation is

$$\Delta T_N = K\Delta t \, (T_{N+1} + T_{N-1} + T_M + T_O - 4T_N)/a^2 \qquad (3.2.7)$$

where T_M and T_O are the adjacent temperature values in the y-direction (see fig. 3.2.2).

An initial starting condition and boundary conditions must be applied to the finite difference solution. The value of temperature at each point is set to an initial value T_o. A boundary condition is applied to the edge of the region to be analysed. To prevent heat flowing out from the edge of the model, the end nodes are constrained such that the temperature gradient is zero or fixed.

$$\frac{\partial T}{\partial n} = 0$$

The explicit finite difference formulation is used in this thesis for solving the temperature field.

3.3 Finite element methods

The finite element technique is used in this thesis for the determination of the stress and displacement fields of a viscoelastic continuum. The method of finite element analysis of elastic and viscoelastic continua will be described together with its specific application. Matrix notation will be used throughout this section. For a comprehensive treatment of finite element techniques the reader is referred to Zienkiewicz (1977), from which the following description is derived.

For analysis the two dimensional elastic continua is divided into a number of subdomains or "finite elements". The simplest finite element is a constant strain triangular element. Each element has its own mechanical properties and is linked to the adjacent elements by the vertices or "nodes". The element properties can be represented by behaviour of the nodes, the nodes being used directly in the finite element calculation. The edges of each element must remain coincident with those of its neighbours to ensure continuity within the elastic continua. Solution of the problem is achieved by calculating the nodal forces involved for each individual element and then assembling the entire structure to determine the force equilibrium as a whole.

Considering a single element (see fig. 3.3.1) the displacements $\{d\}$ at any point can be defined in terms of the nodal displacements $\{u\}$ by a shape function $\left[N\right]$ whose parameters are spatialy dependent.

$$\{d\} = \left[N\right] \{u\} \quad . \tag{3.3.1}$$

The shape function $\left[N\right]$ is defined as

$$\left[N\right] = \left[IN_i + IN_j + IN_k\right]$$

where $\left[I\right]$ is the identity matrix and

$$\left[N_i\right] = (a_i + b_i x_i + c_i y_i)/2\Delta \quad .$$

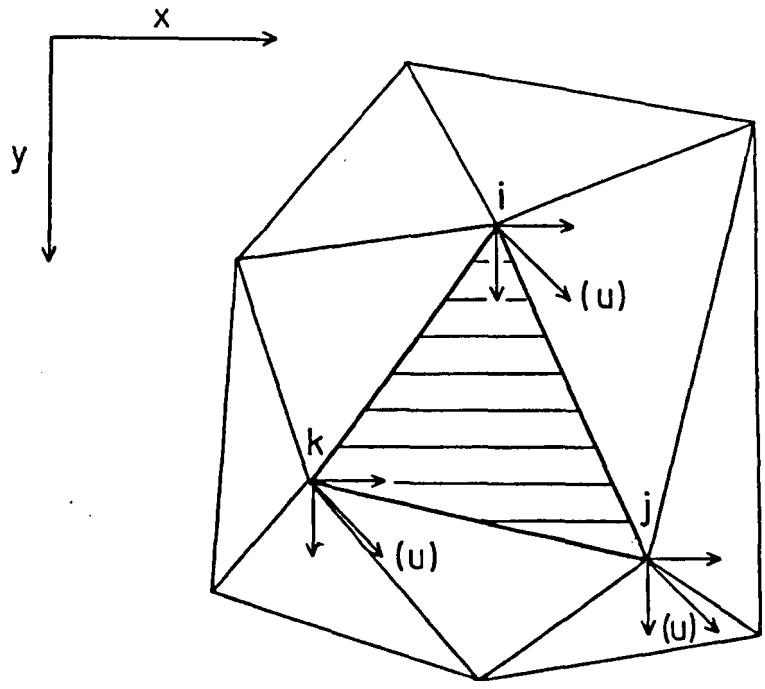

Figure 3.3.1. A plane strain region divided into finite elements showing the nodal displacements (u) for one element.

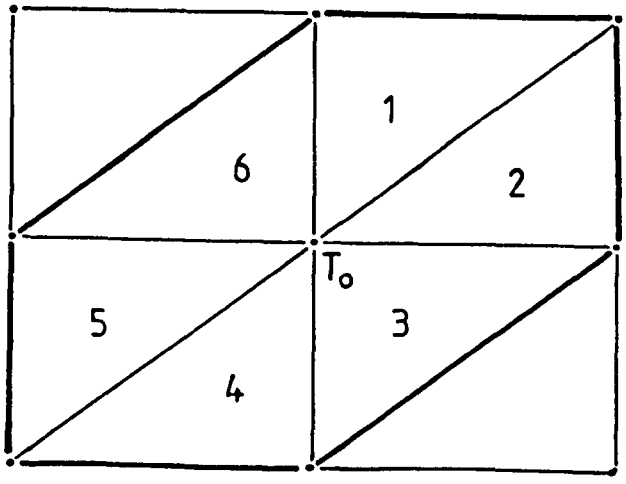

Figure 3.5.1. Diagrammatic representation of the six adjacent finite elements used to calculate the average shear heating at node T_o.

Δ is the area of the element

$$= \tfrac{1}{2} \det \begin{vmatrix} 1 & x_i & y_i \\ 1 & x_j & y_j \\ 1 & x_k & y_k \end{vmatrix}$$

$$a_i = x_j y_k - x_k y_j$$
$$b_i = y_j - y_k$$
$$c_i = x_k - x_j .$$

Strain can be derived from the displacements

$$\{\varepsilon\} = \begin{Bmatrix} du/dx \\ dv/dy \\ dv/dy + du/dx \end{Bmatrix} = \begin{Bmatrix} \varepsilon_{xx} \\ \varepsilon_{yy} \\ \varepsilon_{xy} \end{Bmatrix} \qquad (3.3.2)$$

and can also be described in terms of the nodal displacements such that

$$\{\varepsilon\} = [B]\{u\} . \qquad (3.3.3)$$

Matrix $[B]$ is termed the strain shape function and has the form

$$[B] = \tfrac{1}{2\Delta} \begin{bmatrix} b_i & 0 & b_j & 0 & b_k & 0 \\ 0 & c_i & 0 & c_j & 0 & c_k \\ c_i & b_i & c_j & b_j & c_k & b_k \end{bmatrix} . \qquad (3.3.4)$$

Hence $[B] = [L][N]$ (3.3.5)

where $[L]$ is a strain operator.

The next step is to obtain the internal stresses of the element from the nodal displacements. If we assume a linear elastic behaviour then we can define the stress as

$$\{\sigma\} = [D](\{\varepsilon\} - \{\varepsilon_o\}) + \{\sigma_o\} \qquad (3.3.6)$$

where $\{\varepsilon_o\}$ represents any initial strains and $\{\sigma_o\}$ represents initial stress. $\{\varepsilon\}$ is the total strain. For conditions of plane strain or stress in the z direction the stress tensor $\{\sigma\}$ becomes

$$\{\sigma\} = \begin{Bmatrix} \sigma_x \\ \sigma_y \\ \tau_{xy} \end{Bmatrix} .$$

$[D]$ is an elasticity matrix which for plane strain in the z direction is

$$[D] = \frac{E(1-v)}{(1+v)(1-2v)} \begin{bmatrix} 1 & v/(1-v) & 0 \\ v/(1-v) & 1 & 0 \\ 0 & 0 & (1-2v)/2(1-v) \end{bmatrix} \qquad (3.3.7)$$

and for plane stress is

$$[D] = \frac{E}{(1-v^2)} \begin{bmatrix} 1 & v & 0 \\ v & 1 & 0 \\ 0 & 0 & (1-v)/2 \end{bmatrix} \qquad (3.3.8)$$

where E is Young's modulus and v = Poisson's ratio.

Any external stresses acting on the body are incorporated as an equivalent set of nodal forces $\{F\}$. The resulting nodal displacements must be distributed around the finite element grid in such a way as to minimise their total strain energy. The total internal strain energy of the system U, can be described as

$$U = \tfrac{1}{2} \int \{\varepsilon\}^T \{\sigma\} \, d(vol) \quad . \qquad (3.3.9)$$

T represents the transpose of matrix $\{\epsilon\}$.

The total potential energy is given by

$$W = -\{u\}\{R\} - \int \{d\}^T \{P\}\, d(\text{vol}) - \int \{d\}^T \{f\}\, d(\text{area}) \qquad (3.3.10)$$

where $\{R\}$ is the external nodal forces, $\{P\}$ is the matrix of body forces and $\{f\}$ is the external loading.

The total elastic energy X is given by

$$X = U + W \qquad (3.3.11)$$

To solve the differential equation for the elastic continua it is necessary to minimise the total energy of the system. The finite element process seeks such a minimum within the constraint of an assumed displacement pattern, i.e.

$$\frac{\delta X}{\delta \{u\}} = 0 \qquad (3.3.12)$$

By substituting 3.3.4 and 3.3.6 into 3.3.11 the following can be obtained

$$X = \tfrac{1}{2}\int [B]^T \{u\}^T [D][B]\{u\}\, d(\text{vol}) + \int [B]^T \{u\}^T \{\sigma_0\}\, d(\text{vol}) - \int [B]^T \{u\}^T [D]\{\epsilon_0\}\, d(\text{vol})$$

$$- \{u\}^T \{R\} - \int [N]^T \{u\}\{P\}\, d(\text{vol}) - \int [N]^T \{u\}\{f\}\, d(\text{area}) \qquad (3.3.13)$$

From 3.3.12 we get on differentiating with respect to $\{u\}$

$$\int [B]^T [D][B]\, d(\text{vol}) + \int [B]^T \{\sigma_0\}\, d(\text{vol}) - \int [B]^T [D]\{\epsilon_0\}\, d(\text{vol}) - \{R\}$$

$$- \int [N]^T \{P\}\, d(\text{vol}) - \int [N]^T \{f\}\, d(\text{area}) = 0 \qquad (3.3.14)$$

By defining a stiffness matrix $[K]$ such that

$$[K] = \int [B]^T [D][B]\, d(\text{vol}) \qquad (3.3.15)$$

an equation may be derived showing the nature of the nodal displacements.

$$[K]\{u\} + \{F\}_f + \{F\}_p + \{F\}_{\varepsilon_o} + \{F\}_{\sigma_o} - \{R\} = 0 \qquad (3.3.16)$$

where $\{F\}_f$ = external applied forces

$\{F\}_p$ = body forces

$\{F\}_{\varepsilon_o}$ = forces due to initial strain

$\{F\}_{\sigma_o}$ = forces due to initial stress .

Force boundary conditions can be applied directly using the vector $\{F\}_f$. Displacement boundary conditions can be affected by multiplication of the element within the $[K]$ matrix corresponding to the node, by a large number ($\simeq 10^{12}$) (pers comm., Payne and Irons to Zienkiewicz, 1963). Simultaneously the corresponding force vector is replaced by the prescribed displacement multiplied by the new element of the $[K]$ matrix.

Solution of the viscoelastic problem by finite elements is accomplished by using the concept of initial strain (Zienkiewicz 1977). From equation 3.3.16 we can get

$$[K]\{u\} = \{R\} - \{F\}_{\varepsilon_o}$$

where $\{R\}$ is the nodal forces and

$$-\{F\}_{\varepsilon_o} = \int [B]^T [D]\{\varepsilon o\}\, d(\text{vol}) \quad . \qquad (3.3.17)$$

Creep is then incorporated in the calculation as an initial strain. The stress at any time is given by

$$\{\sigma\} = [D](\{\varepsilon\} - \{\varepsilon o\}) \quad . \qquad (3.3.18)$$

The viscous creep is calculated using the Navier-Stokes equation. The components being

$$\begin{aligned}
\{\dot{\varepsilon}_x^v\} &= \tfrac{1}{2}\eta(\sigma_x - \sigma_{av}) \\
\{\dot{\varepsilon}_y^v\} &= \tfrac{1}{2}\eta(\sigma_y - \sigma_{av}) \\
\{\dot{\varepsilon}_{xy}^v\} &= \eta(\tau_{xy}) \\
\{\dot{\varepsilon}_z^v\} &= \tfrac{1}{2}\eta(\sigma_z - \sigma_{av})
\end{aligned} \qquad (3.3.19)$$

where $\sigma_{av} = \frac{1}{3}(\sigma_x + \sigma_y + \sigma_z)$ and η is the apparent viscosity.

For viscoelastic analysis the finite element model must be first solved for elastic conditions. Propagation through time is achieved by an iterative finite difference algorithm. The steps of the algorithm are as follows:-

(i) The first estimate of the creep rate for the time step is calculated from the stress values at the end of the previous time step.

(ii) The creep rate is integrated over the time step and this is added to the creep of the previous time steps.

(iii) The total creep is incorporated in the initial stress vector.

(iv) A solution is obtained for the displacements, strains and stresses at the end of the time increment.

(v) The values of stress are used to give a better estimate of the average value for the time increment.

(vi) The sequence then repeats until there is no difference in the value of stress at the end of the increment.

(vii) The next time increment can then be commenced.

The maximum time increment for this numerical solution to remain stable is

$$\Delta t = 2\eta/E \quad . \tag{3.3.20}$$

For plain stress in an isotropic material, the total strains, ε_T are given by

$$\varepsilon_x^T = \sigma_x/E - V\sigma_y/E + \varepsilon_x^V$$

$$\varepsilon_y^T = -V\sigma_x/E + \sigma_y/E + \varepsilon_y^V$$

$$\gamma_{xy}^T = 2(1 + V)\tau_{xy}/E + \varepsilon_{xy}^V$$

where ε^V represents the viscous strains.

For plain strain we have a stress component σ_z. Also the total strain in the z direction is zero, i.e.

$$\varepsilon_z^T = 0 = -V\sigma_x/E - V\sigma_y/E + \sigma_z/E + \varepsilon_z^V \quad . \tag{3.3.21}$$

The viscous creep is non zero and is equal and opposite to the elastic strain. As a result the $[D]$ matrix as used in equation 3.3.7 must be amended for the strains in the z direction. The initial force vector is still given by equation 3.3.16, except now

$$\{\varepsilon_o\} = \begin{Bmatrix} \varepsilon_{xo} \\ \varepsilon_{yo} \\ \varepsilon_{zo} \\ \varepsilon_{xyo} \end{Bmatrix} \tag{3.3.22}$$

and the $[D]$ matrix becomes

$$[D] = \frac{E(1-V)}{(1+V)(1-2V)} \begin{bmatrix} 1 & V/(1-V) & V/(1-V) & 0 \\ V/(1-V) & 1 & V/(1-V) & 0 \\ 0 & 0 & 0 & (1-2V)/2(1-V) \end{bmatrix} . \tag{3.3.23}$$

3.4 Solution of the viscous and simple viscoelastic model.

The mathematical formulation of the viscous model has already been described. The model can be reduced to a pair of equations to be solved simultaneously. For constant shear velocity boundary conditions these are (from Chapter 2),

$$\frac{\partial T}{\partial t} = \frac{k}{\rho Cp} \frac{\partial^2 T}{\partial y^2} + \tau \frac{\partial u}{\partial y} \Big/ \rho C_p \tag{3.4.1}$$

and

$$u(y) = Uo/2 \frac{\int_o^y 1/\exp(BTm/T)dy'}{\int_o^\infty 1/\exp(BTm/T)dy'} . \tag{3.4.2}$$

For constant shear stress conditions the temperature field expression 3.4.1 must be solved with

$$u(y) = \tau^n \int_o^y 1/\left\{ A\exp(BTm/T) \right\} dy' . \tag{3.4.3}$$

Equation 3.4.1 was solved using an explicit central difference finite difference routine. The initial temperature was set at an ambient value T_o across the model. To produce shear localization within the model a small temperature perturbation A is introduced such that

$$T(y=o) = T_o + A \quad .$$

The perturbation A is rapidly swamped by the shear heating of the model. Various values of A have been tested over a range up to 50^oC without significantly changing the behaviour of the model. A value of 10^oC is used throughout the thesis.

A boundary condition must also be applied to the temperature solution such that the temperature at the edge of the model remains at the initial value.

$$T(y = \infty) = T_o$$

Solution of the velocity profile is achieved by integration of the velocity derivative across the width of the model. The velocity derivative is calculated using a backward difference formula.

The constant boundary velocity condition has been shown to have a constant gradient initial velocity profile (see section 2.2). The boundary conditions applied to the model are

$$u(y = o) = 0$$
$$u(y = \infty) = U_o/2 \quad .$$

The model was tested for various half widths of shear zone to determine the effect of the distance of the boundary velocity $U_o/2$ from the shear zone centre. The constant velocity model gives a very steep localized shear zone and is unaffected by the models width. A half width of

100 km is used in most models to ensure the temperature boundary condition $T(y = \infty) = T_o$ was remote from the shear zone.

Constant shear stress boundary condition models behave differently. The velocity profiles produced often have constant gradients. Under these conditions the half width of the model becomes important since the total differential velocity across the shear zone depends upon the width of the model. However as the behaviour of a constant shear stress model is fairly uniform across the model, the half width need only be sufficient to maintain the temperature boundary condition.

An algorithm for a viscous shear zone model is listed in Appendix 1. The program calculates the optimum time increments for solution and is numerically stable even under unrealistic conditions.

A one dimensional viscoelastic model can also be solved in a similar way, the viscous equation being replaced by a viscoelastic term. The strain rate is given by

$$\frac{\partial u}{\partial y} = \frac{2(1+\nu)}{E}\dot{\tau}_{xy} + \frac{\tau_{xy}^{n}}{A\exp(BTm/T)} \qquad (3.4.4)$$

or

$$\frac{\partial u}{\partial y} = \dot{\tau}f' + \tau^{n}f'' \qquad (3.4.5)$$

where f' is a function of elasticity and f'' a function of temperature. The equation for velocity is

$$u(y) = \dot{\tau}\int_{o}^{y} f'\,dy' + \tau^{n}\int_{o}^{y} f''\,dy' \quad . \qquad (3.4.6)$$

The integrals in equation 3.4.6 can be solved by integration of the velocity and stress derivatives (N.J. Kusznir, pers. comm. 1982).

3.5 Solution of viscoelastic models by coupled finite element and finite difference techniques.

The viscoelastic model presented in this thesis utilizes a coupled finite element and finite difference technique. Velocity and displacement fields are determined using the nodal displacements obtained by finite element analysis, while the temperature field is calculated by the finite difference method using the finite element nodes.

The viscosity of a given element is calculated using the element average temperature. Finite element analysis gives the state of stress, strain and strain rate for each element. From this information the shear heating energy for each element can be calculated using the equation (Jaeger and Cook 1969).

$$H = (\sigma_x \dot{\varepsilon}^v_x + \sigma_y \dot{\varepsilon}^v_y + \sigma_z \dot{\varepsilon}^v_z)$$

where x, y and z represent the principalised directions.

The temperature field of the model is calculated using a two dimensional, central finite difference formulation. As the finite element nodes are used as points for the temperature field calculation it is necessary to map the element average shear heating onto the element nodes. In a rectangular grid each node is shared by six surrounding elements. The shear heat applied to each node is calculated as a weighted average of the six adjacent element values (fig. 3.5.1).

The finite difference temperature field solution used the formulation described in section 3.2. The time periods necessary for the stability of iterations for the finite element and finite difference techniques

are not the same. The model calculates the optimum time step and provides for a number of iterations of the finite difference temperature solution for each finite element iteration, ensuring the numerical process remains stable.

The initial temperature conditions are such that all nodes are given an ambient value T_o with the exception of nodes at y = o which have an initial positive perturbation above this value. Boundary conditions are applied to the model such that all the edges of the rectangular grid have zero temperature gradient across them i.e.

$$\frac{\partial T}{\partial n} = 0$$

where n is the direction perpendicular to the edge of the grid. However, the edge of the grid where y = w, w being the half width of the model, has the boundary condition $T = T_o$ at all values of t (fig. 3.5.2).

Mechanical boundary conditions must also be applied to the model. For constant boundary velocity conditions the nodes at y = w are constrained to move in the x direction at a fixed displacement rate. The nodes at the centre of the shear zone at y = o are fixed in both the x and y directions. The other two edges of the grid have their nodes constrained to move in the x direction only. Nodes in the interior of the grid are unconstrained.

For constant shear stress conditions the displacement rate condition is replaced by a force applied to the edge nodes acting in the x direction. The force is applied to all the nodes along the edges of the grid that are perpendicular to the direction of shear. The force per unit length is calculated for a given stress level, the force is then distributed between the edge nodes.

Unlike viscous models the effect of varying the half width of the model w and the value of the initial temperature perturbation can have significant effects on viscoelastic models. These effects are studied later in the thesis.

Appendix 2 contains a set of algorithms for viscoelastic analysis of shear zones. The finite difference heat flow and the finite element stress analysis have been tested and are included as Appendices 3 and 4.

CHAPTER 4

Viscous Shear Zone Models

4.1 Introduction

The general viscous model and its mathematical formulation have been described in the previous chapters. The models can be divided into two types having either constant shear velocity or constant shear stress boundary conditions. The behaviour of these two types of boundary condition will be described separately for the general case of a dry olivine rheology. The behaviour of models with other rheologies will be mentioned where appropriate.

4.2 The constant shear velocity model

The constant shear velocity model consists of two identical half spaces of rock sliding past each other with a constant slip velocity U_o across the shear zone (see Chapter 2). The initial velocity profile for this model is a constant gradient profile from zero velocity at the centre of the shear zone to the chosen boundary value at the models edge. The initial temperature is uniform across the model except for a $10^{o}C$ destabilizing perturbation at the models centre.

After initiation the constant gradient velocity profile rapidly changes with time to produce a very narrow, localized shear zone with a steep velocity gradient. Figure 4.2.1 shows how the initial constant gradient profile persists for the first 2500 yr or so and then rapidly changes to a step like profile. This step like profile accommodates most of the deformation in a narrow central zone which broadens slowly with time. The shear zone is very narrow for the first million years or so.

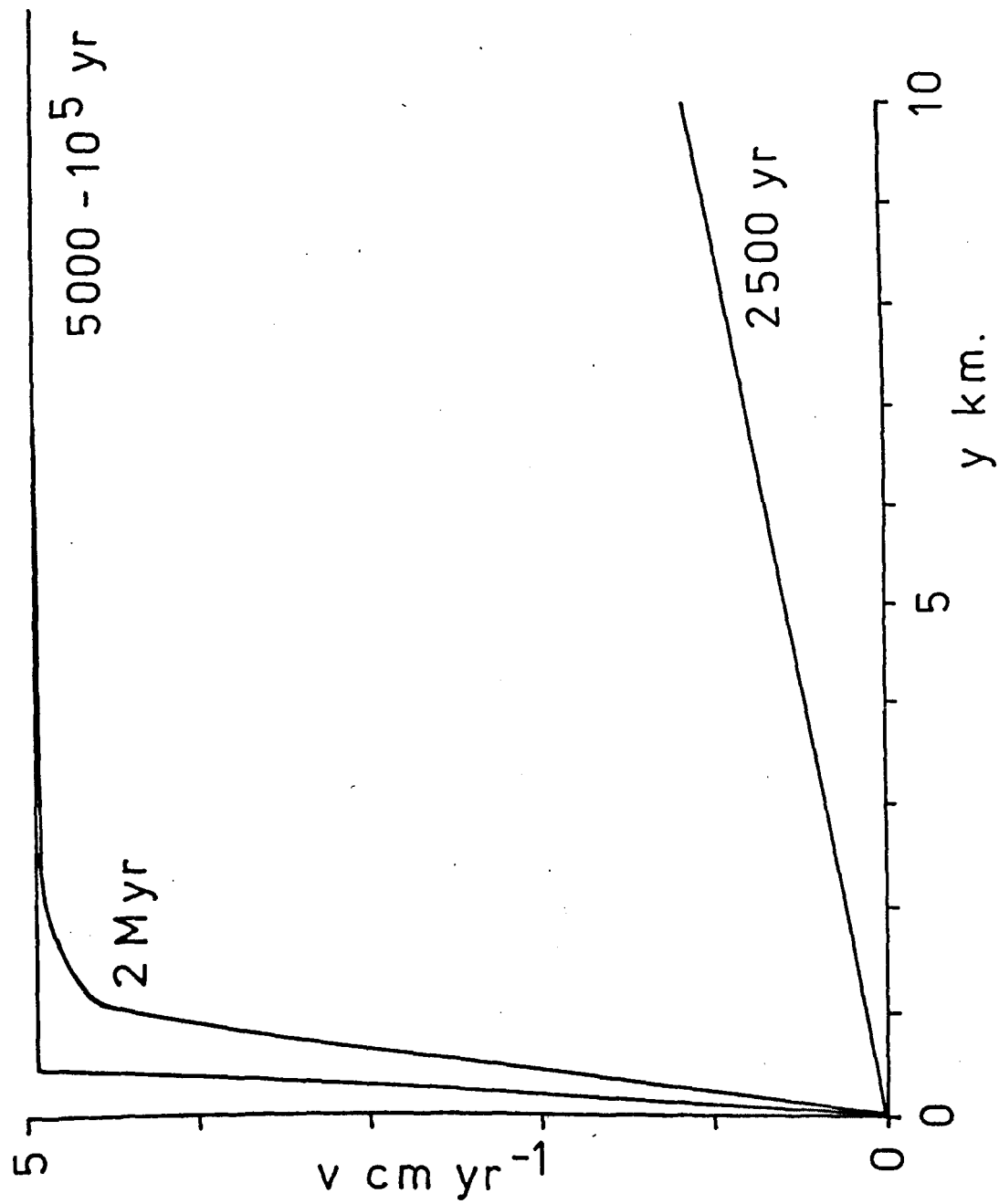

Figure 4.2.1. The velocity profiles of a shear zone 50km. wide in dry olivine. T_o=600°C, $U_o/2$=5 cm yr^{-1}.

The width of the narrow high velocity gradient shear zone increases with time. Figure 4.2.2 shows the velocity and temperature profiles for a shear zone in a dry olivine material at an ambient temperature of 600°C and a half velocity of 5 cm yr^{-1}. Temperatures in the centre of the shear zone increase with time and the shear heat diffuses outwards broadening the thermal anomaly. The velocity profile also shows a broadening of the zone of mechanical deformation. At all times the width of the thermal anomaly is approximately an order of magnitude greater than the zone of mechanical deformation. The temperature in the centre of the shear zone is still increasing at a time of 30 Myr although the rate of increase is very slow. The temperatures produced in the centre of the shear zone are always insufficient for partial melting.

The viscosity in the centre of the shear zone drops to a value around 10^{19} Pa.s. As the shear zone develops and widens the deformation is accommodated by an increase in the width of the low viscosity zone rather than a further decrease in viscosity at the centre of the shear zone (fig. 4.2.3). The strain rates associated with constant velocity models vary from 10^{-14} s^{-1} in the centre to 10^{-18} s^{-1} at the edges.

Higher boundary velocities should result in more shear heating being produced. Figure 4.2.4 shows the temperature profiles for various half velocities. Faster velocities generate higher central temperatures in the shear zone but even 10 cm yr^{-1} produces insufficient shear heat for melting. Slow shear velocities will produce low strain rates and little shear heating. If the velocity is small enough the shear heating will be insufficient to maintain a large temperature anomaly. As a result no localized shear zone forms and the velocity profile remains a constant gradient. Figure 4.2.5 shows the velocity profiles for slow shear velocities applied to a model with a half width of 1 km. Half

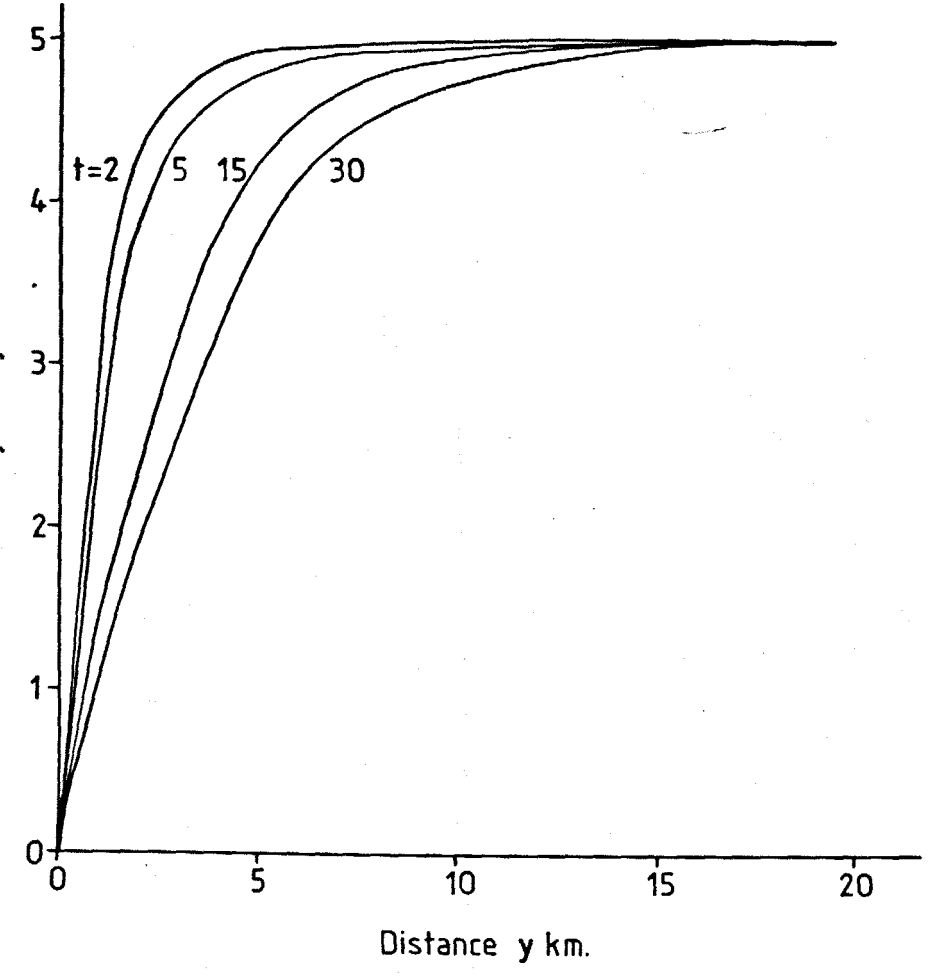

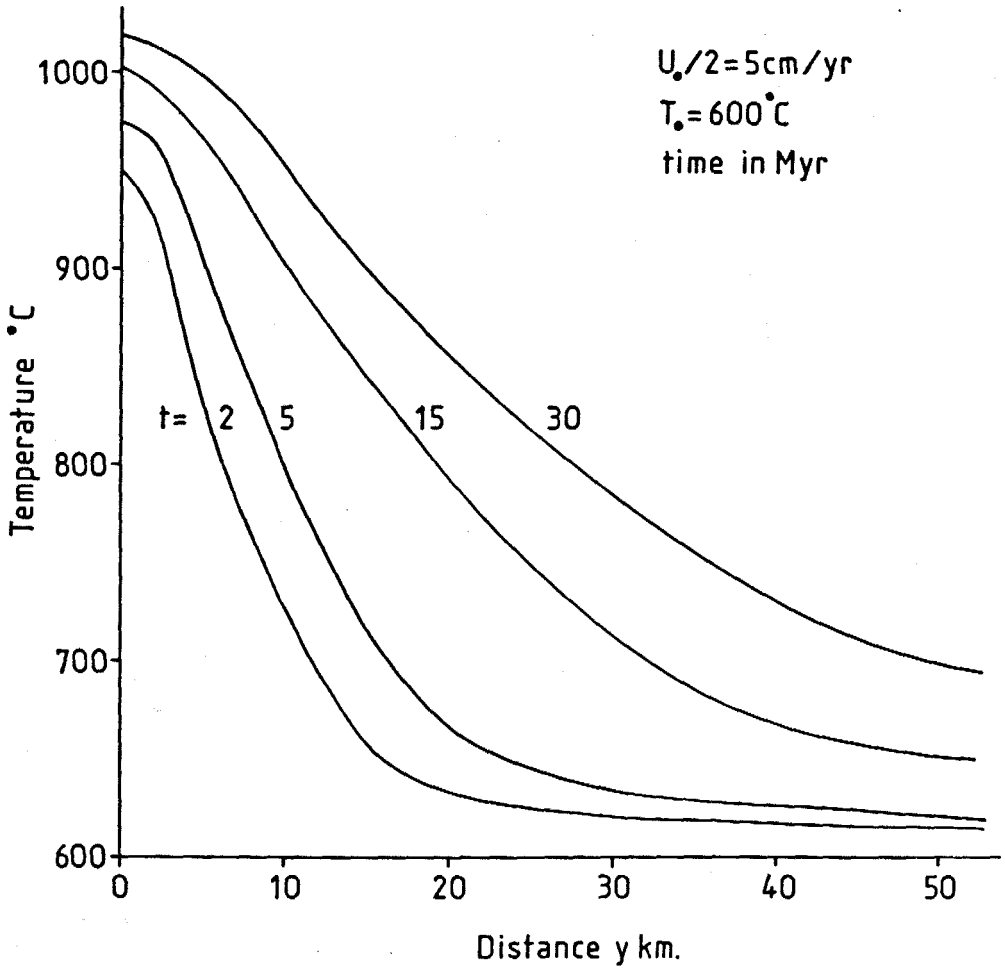

Figure 4.2.2. The velocity and temperature profiles for a dry olivine rheology at various times. T_o=600°C, $U_o/2$=5 cm yr^{-1}.

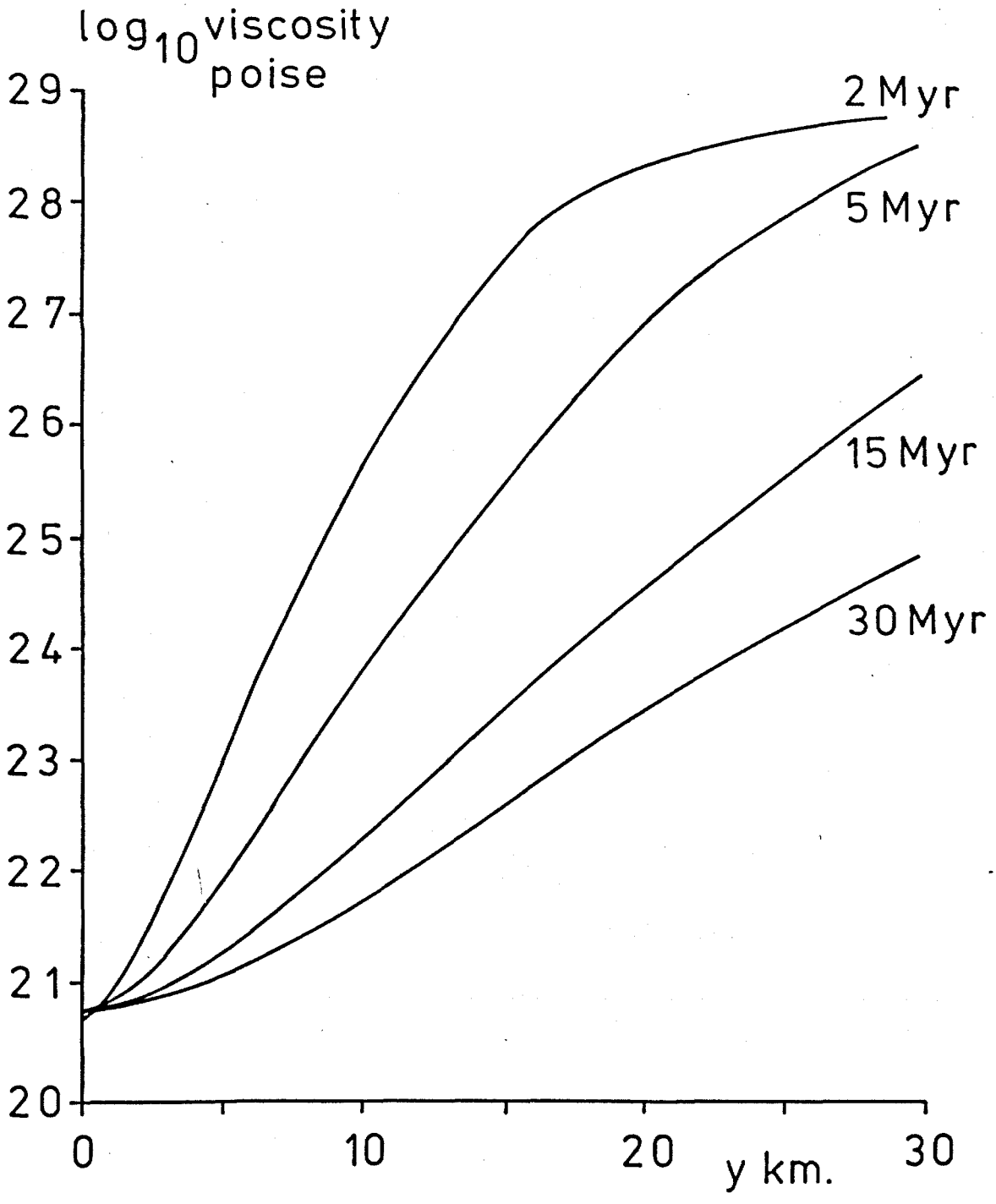

Figure 4.2.3. The viscosity profiles for a dry olivine rheology for various times. T_o=600°C, $U_o/2$=5 cm yr^{-1}.

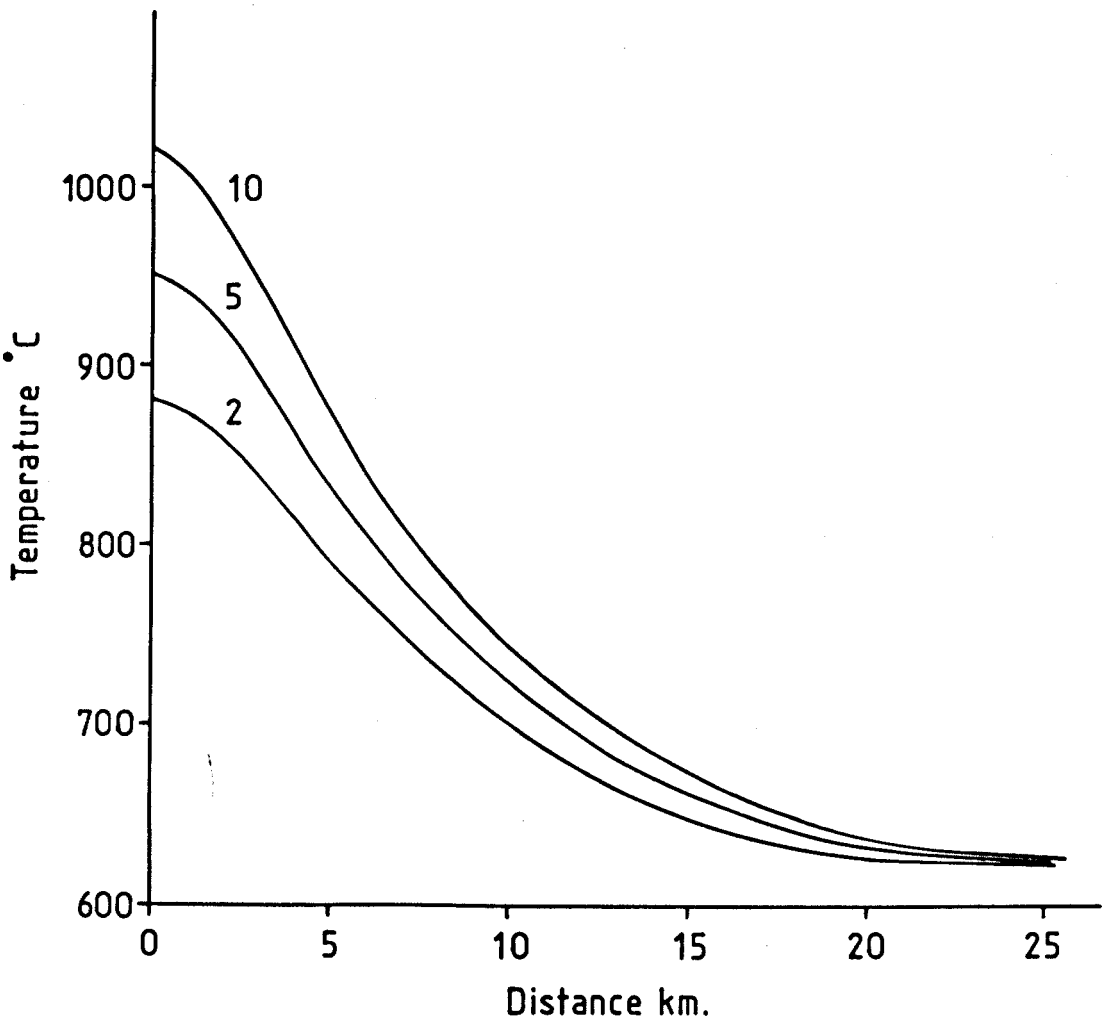

Figure 4.2.4. The temperature profiles for various half shearing velocities, at 2Myr. T_o=600°C.

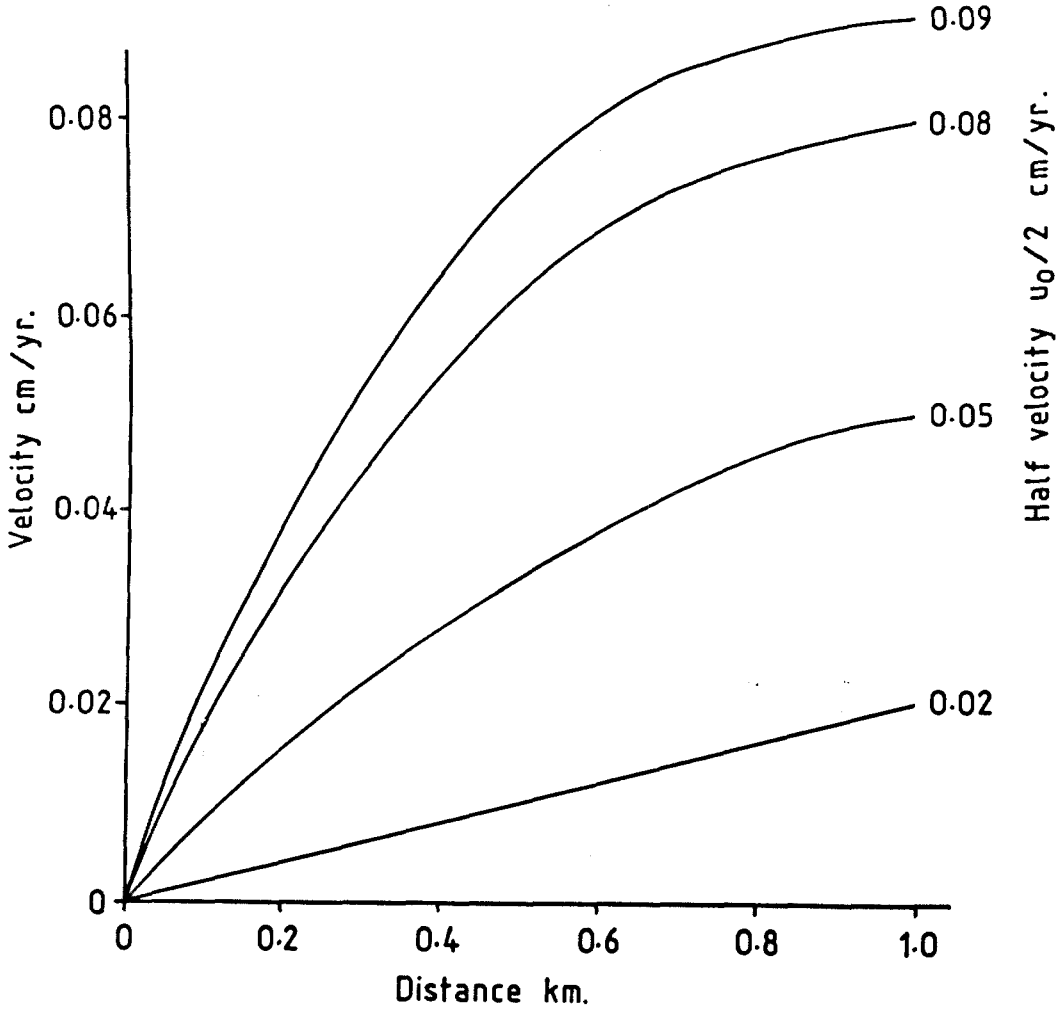

Figure 4.2.5. The velocity profiles for slow shear velocities for a model half width of 1km. T_o=600°C, t=2Myr.

velocities in the order of 0.02 cm yr^{-1} produce no significant temperature anomalies and do not develop localized shear zones.

It would at first appear that the width of the model over which the boundary velocity is imposed would be important since the steeper the initial velocity gradient the higher the initial shear heating. However as constant velocity shears form narrow localized zones very rapidly, the width of the model has very little effect providing the narrow shear zone is within the width of the model. The width of the model does have some effect on the temperature profile during the first 10,000 yr or so after initiation, but it is insufficient to affect the subsequent evolution of the shear zone.

For a given width of shear zone there is a shear velocity below which no localization occurs. From figure 4.2.5 we can see that this velocity is very slow for a model with a 1 km half width. If the half width is reduced to 100 metres the critical velocity is very high. Narrow shear zones lose the shear heat through the sides of the model very rapidly. Shear velocities of 5 or 10 cm yr^{-1} fail to produce enough shear heat for localization a linear velocity gradient remaining. Small shear zones do not give a localized central zone at reasonable shear rates.

The velocity profile of a shear zone is very strongly dependent upon the ambient temperature. Lower temperatures produce narrower shear zones for any given shear velocity. Figure 4.2.6 shows the velocity and temperature profiles for various ambient temperatures for a comparable time and half velocity. The velocity profiles show a change from narrow

Figure 4.2.6. The velocity and temperature profiles for various ambient temperatures at 2Myr. $U_o/2$=5 cm yr^{-1}.

intense shear zones for lower ambient temperatures to wider more diffuse zones for ambient temperatures in excess of 700°C. The nature of the temperature profiles also show a marked dependence on the ambient temperature. At lower ambient temperatures, the temperature profiles show a high central anomaly. Higher ambient temperatures produce much smoother temperature profiles with significant shear heating across the total width of the shear zone. Above an ambient temperature of 700°C the character of the temperature profile changes from having a large central peak at 700°C to a profile with even shear heating across the model and no central peak at 800°C. The velocity profiles also change at this ambient temperature; the viscous deformation being no longer confined to a narrow zone but occurring over a much broader zone. The geological significance of this is investigated in the next chapter.

The stresses associated with constant velocity shearing are very high soon after initiation but decay rapidly to a kilobar or so in a million years (fig. 4.2.7). The higher the boundary velocity the lower the value of shear stress. Higher boundary velocities produce more shear heating and the stresses can decay faster. Figure 4.2.7 also shows the stress curves for various ambient temperatures for a fixed rate of shearing. The highest ambient temperature does not necessarily give the lowest stresses. The level of stress is governed by the maximum temperature reached in the shear zones. Lower ambient temperatures produce thermal anomalies with a hot central peak whereas higher ambient temperatures produce thermal anomalies with an even temperature rise of a few degrees across the entire shear zone (see fig. 4.2.6). The highest peak temperature and hence the lowest stress is not necessarily going to occur at the highest ambient temperature for a given time and shear velocity.

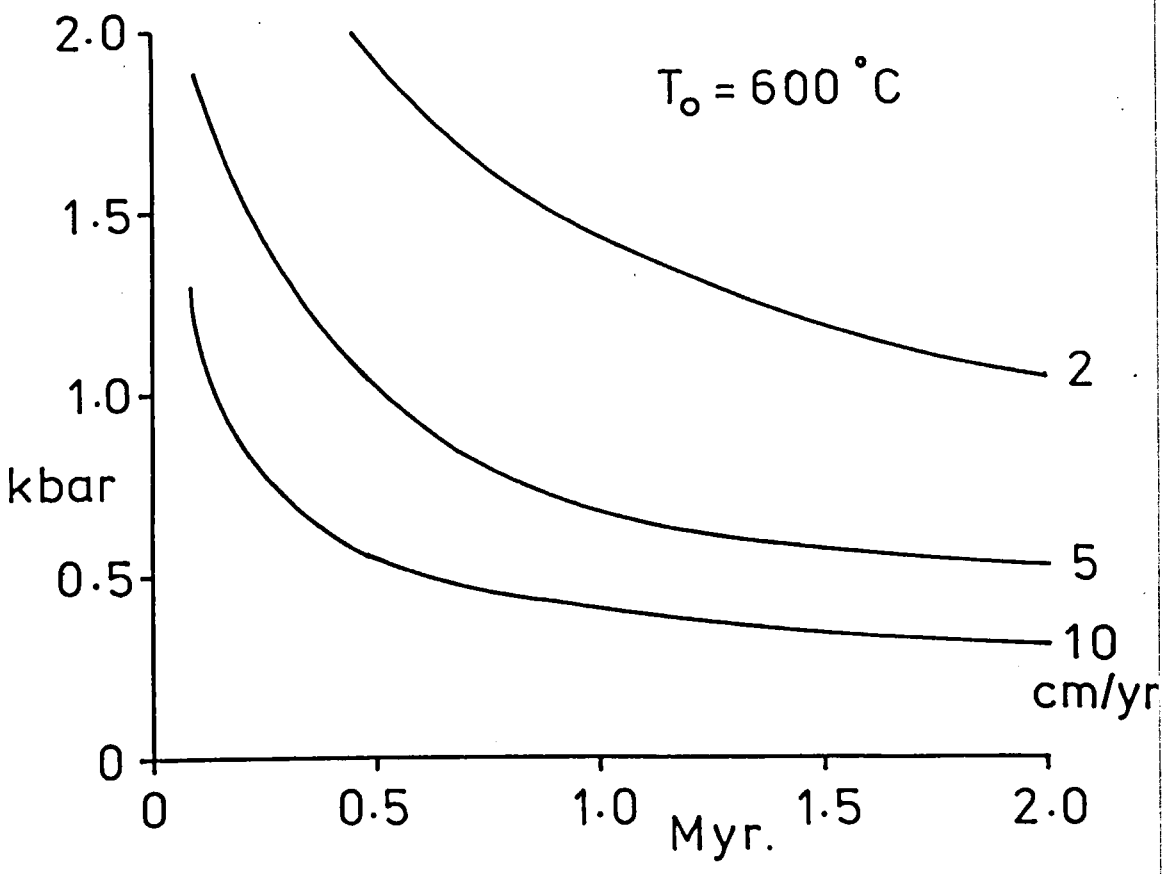

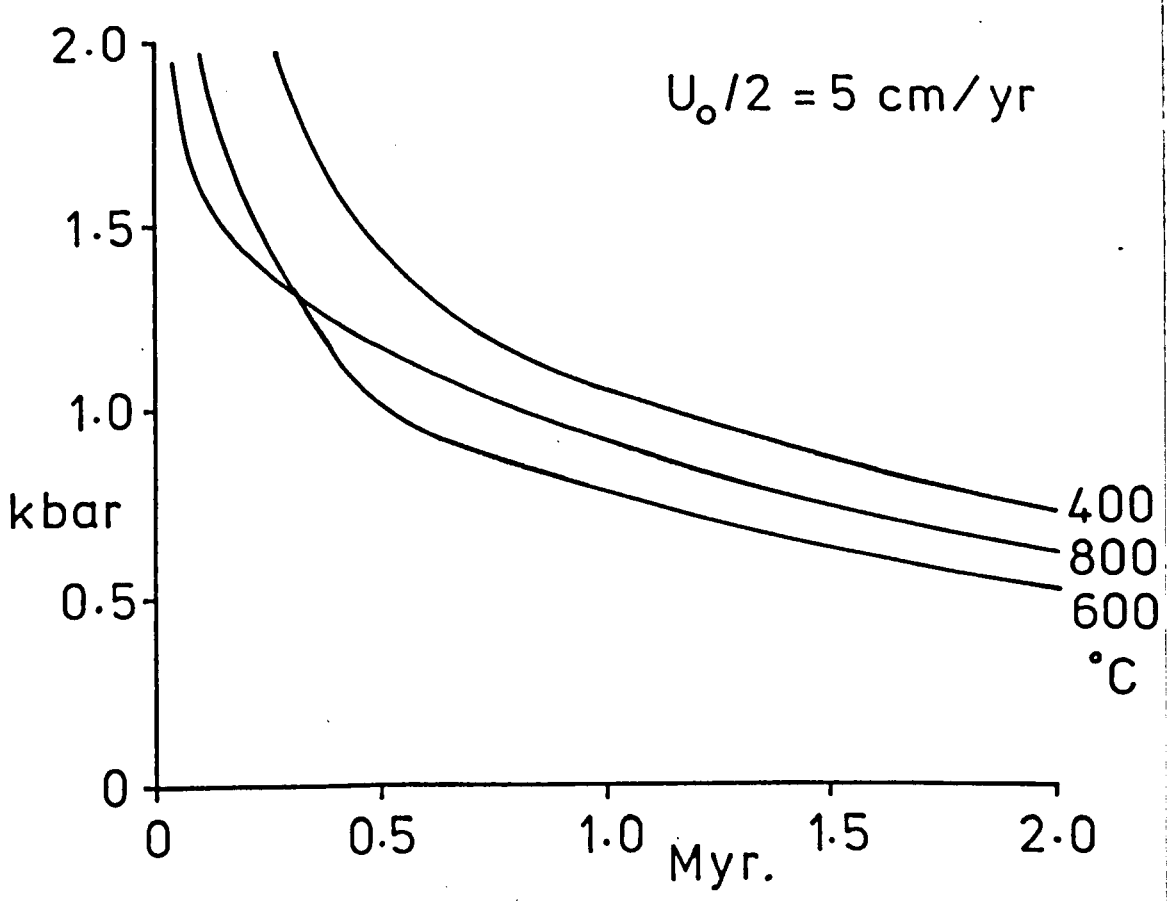

Figure 4.2.7. The variation of stress with time. (Top) for various half velocities at an ambient temperature of 600°C and, (Bottom) for various ambient temperatures for a shear rate of 5 cm yr^{-1}.

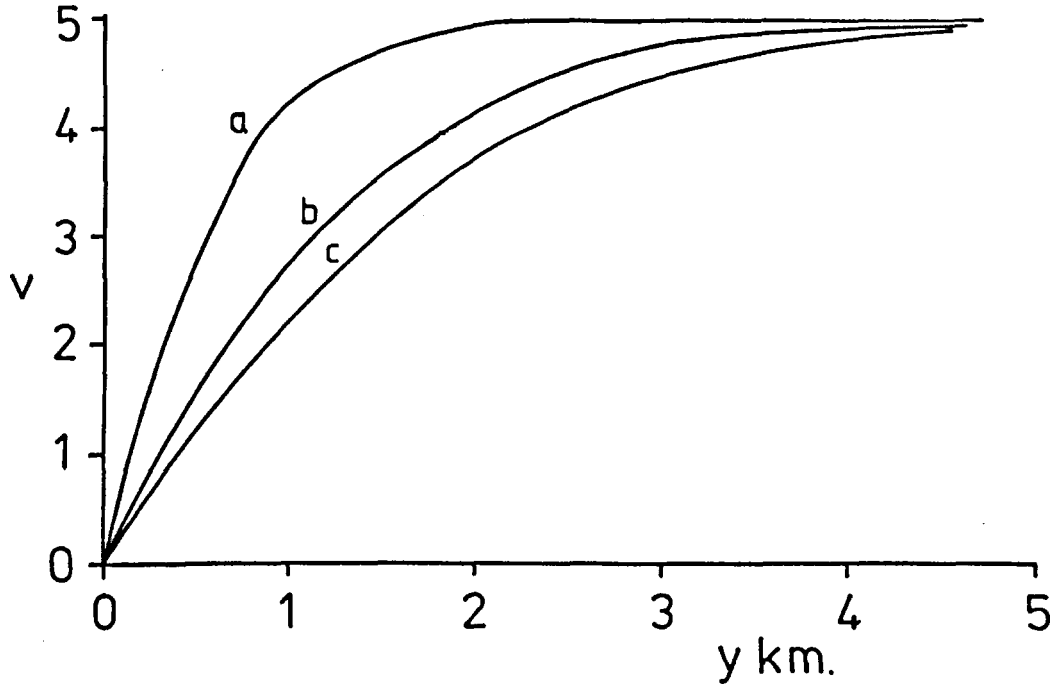

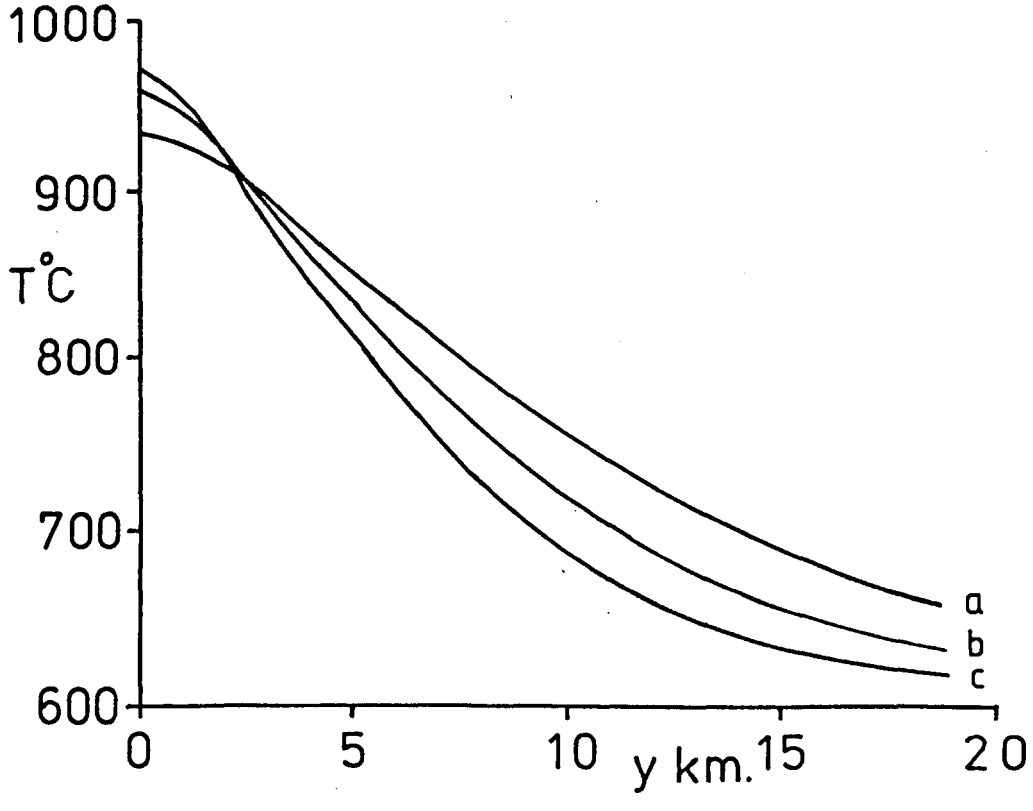

Figure 4.2.8. The velocity and temperature profiles for various thermal conductivities. t=2Myr., $U_o/2$=5 cm yr^{-1}, T_o=600°C. Profiles: a=0.01, b=0.006, c=0.004 cal cm^2 sec °C.

Characteristic of all the stress profiles is the very high initial stress values. These stresses have values of hundreds of kilobars at t=0 and represent a near singularity in the shear stress at the initiation of shearing.

Variation in the thermal conductivity of the shearing rocks will have an effect upon the shear zone evolution. The thermal conductivity of rocks ranges from 4.0×10^{-3} to 1.0×10^{-2} cal/cm^2 sec^oC (Clark 1966). A value of 6.0×10^{-3} cal/cm^2 sec^oC has been used for the dry olivine models. Thermal conductivity is very important when considering the thermal structure of shear zones. Figure 4.2.8 shows a set of velocity and temperature profiles for various conductivities for a given ambient temperature and shear rate. Higher thermal conductivities produce wider thermal anomalies with lower central temperatures. Variation in thermal conductivity also affects the velocity profiles, lower thermal conductivities produce narrower and hotter shear zones.

Comparison of dry olivine rheology with dolerite and granodiorite rheologies shows significant differences. Figure 4.2.9 shows the velocity and temperature profiles for all three rheologies. Dolerite and granodiorite deform more easily than dry olivine producing smaller temperature anomalies and wider, less intense, shear zones for the same ambient temperature. Each rock type produces its own peak temperature value. Constant velocity shears do not reach temperatures sufficient for melting irrespective of the media being sheared.

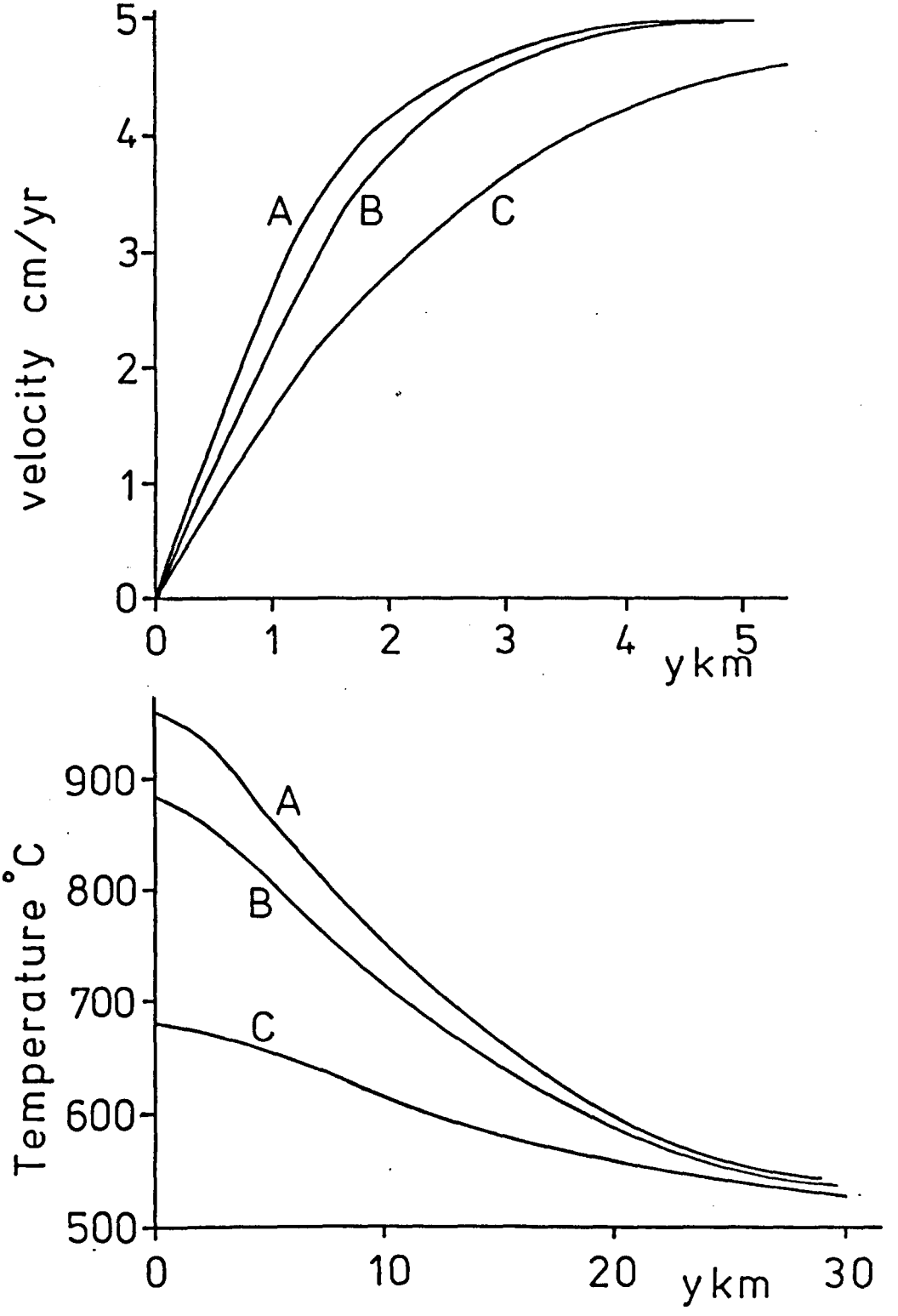

Figure 4.2.9 The velocity and temperture profiles for various rheologies . T_o=500°C, t=5 Myr., $U_o/2$=5 cm yr^{-1}. Profiles : A=dolerite ,B=dry olivine, C=granodiorite.

4.3 The constant shear stress model

The constant stress model has a shear stress boundary condition. The velocity profile across the model is calculated using equation 2.2.13,

$$u(y) = \tau^n \int_o^y 1/\left[A \exp(BTm/T)\right].dy'.$$

Since stress is constant across the model in both space and time any variation in viscosity will be due to variations in temperature. The half width of the model, W must be wide enough to ensure no edge effects from the temperature boundary condition

$$T(y = W) = T_o \quad .$$

The velocity at the edge of the model is dependent upon the width of the model, with wider models having higher velocities at the edge.

The temporal development of a shear zone with constant stress is shown in fig. 4.3.1. The velocity profiles are nearly linear except at the very centre of the model. Since the velocity profiles are constant gradient except at the very centre, the width of the model is determined by the width necessary for the temperature boundary condition to remain remote from the centre of the model. The width of the model has no other physical significance.

The gradient of the velocity profile gradually increases until a steep shear zone rapidly develops. The corresponding temperature profiles show an increase in temperature across the shear zone before the sudden development of a central peak. This background increase in temperature is a result of the constant gradient velocity profiles; the constant strain producing an even shear heating across the zone. When the steep shear zone develops, the strain becomes high enough to produce intense shear heating in the centre of the zone. Temperatures

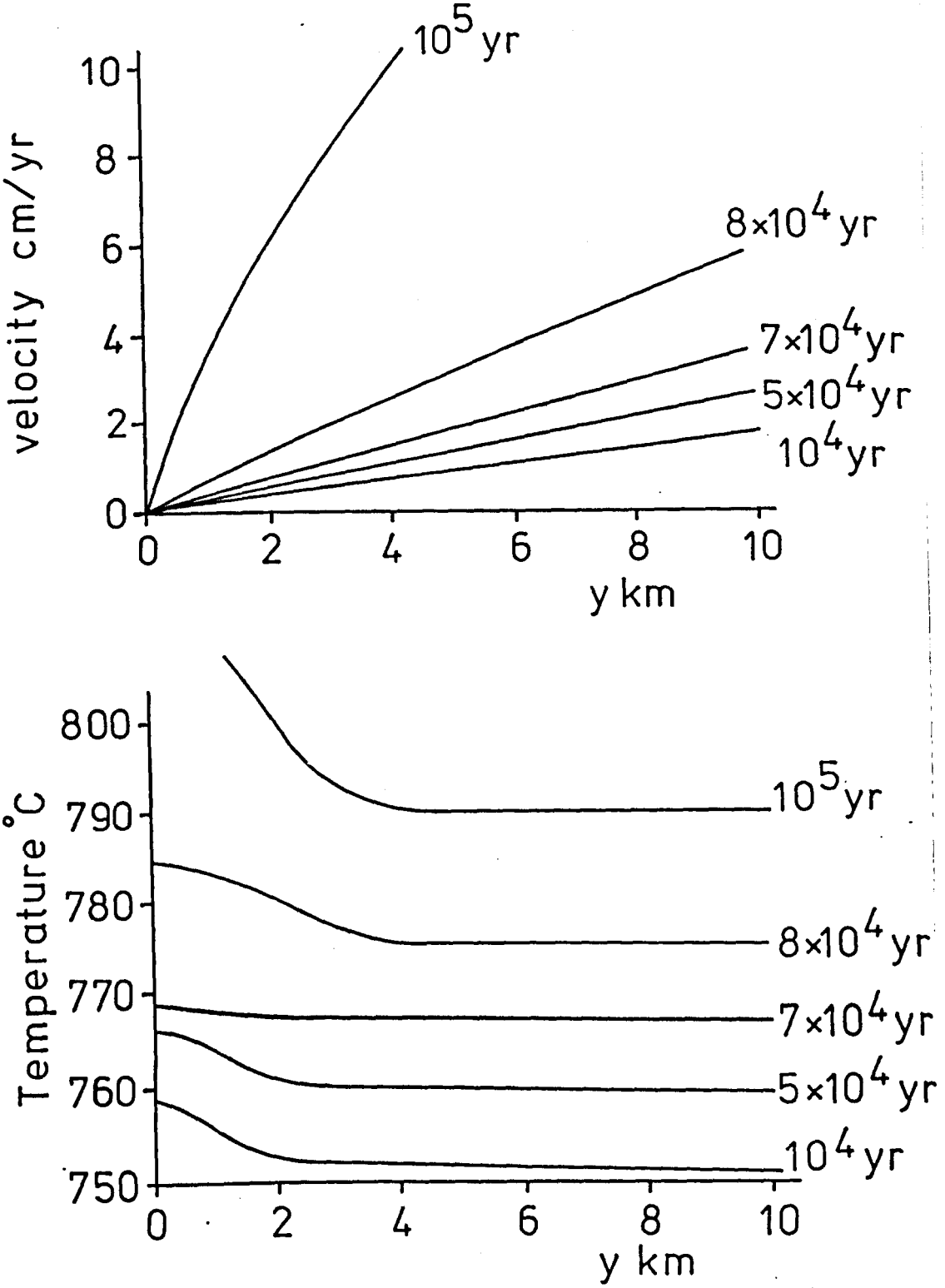

Figure 4.3.1. The temporal development of a shear zone at constant stress and temperature. T_o=750°C, stress=3.5kbar.

in the centre rise and the shear velocity becomes so high that the shear heating produces melting. Once this "thermal runaway" (Gruntfest 1963) takes place the model loses its physical significance and can no longer be used to describe shear zone behaviour.

At low levels of stress and ambient temperature the constant stress model will produce low shearing velocities (10^{-3} cm yr^{-1} for a shear width of 100 km. at $T_o = 400^{o}C$ and $\tau = 2$ kbar) which are geologically insignificant. The strains generated even over long periods of geological time, will be unobservable in the field.

Ambient temperature once again has a strong effect on the behaviour of the shear zone. Figure 4.3.2 shows the variation of velocity and temperature profiles with ambient temperature. The velocity profiles show a marked increase in gradient above an ambient temperature of $785^{o}C$. Temperature profiles show that the change in velocity gradient corresponds to a rapid increase in shear heating and the approach of thermal runaway.

The effect of variation in shear stress at a fixed time and ambient temperature is shown in fig. 4.3.3. There exists a critical value above which an increase in stress results in rapid modification of the velocity and temperature profiles followed by thermal runaway.

Both the temperature and stress results can be combined to produce the temperature-stress field for thermal runaway. The value of stress and temperature required for runaway are time dependent; higher values bringing about runaway in shorter times. Figure 4.3.4 shows the temperature-stress field for runaway within a time of 10^{5} yr. Figure 4.3.5 is a similar diagram showing the runaway curve for various times and also

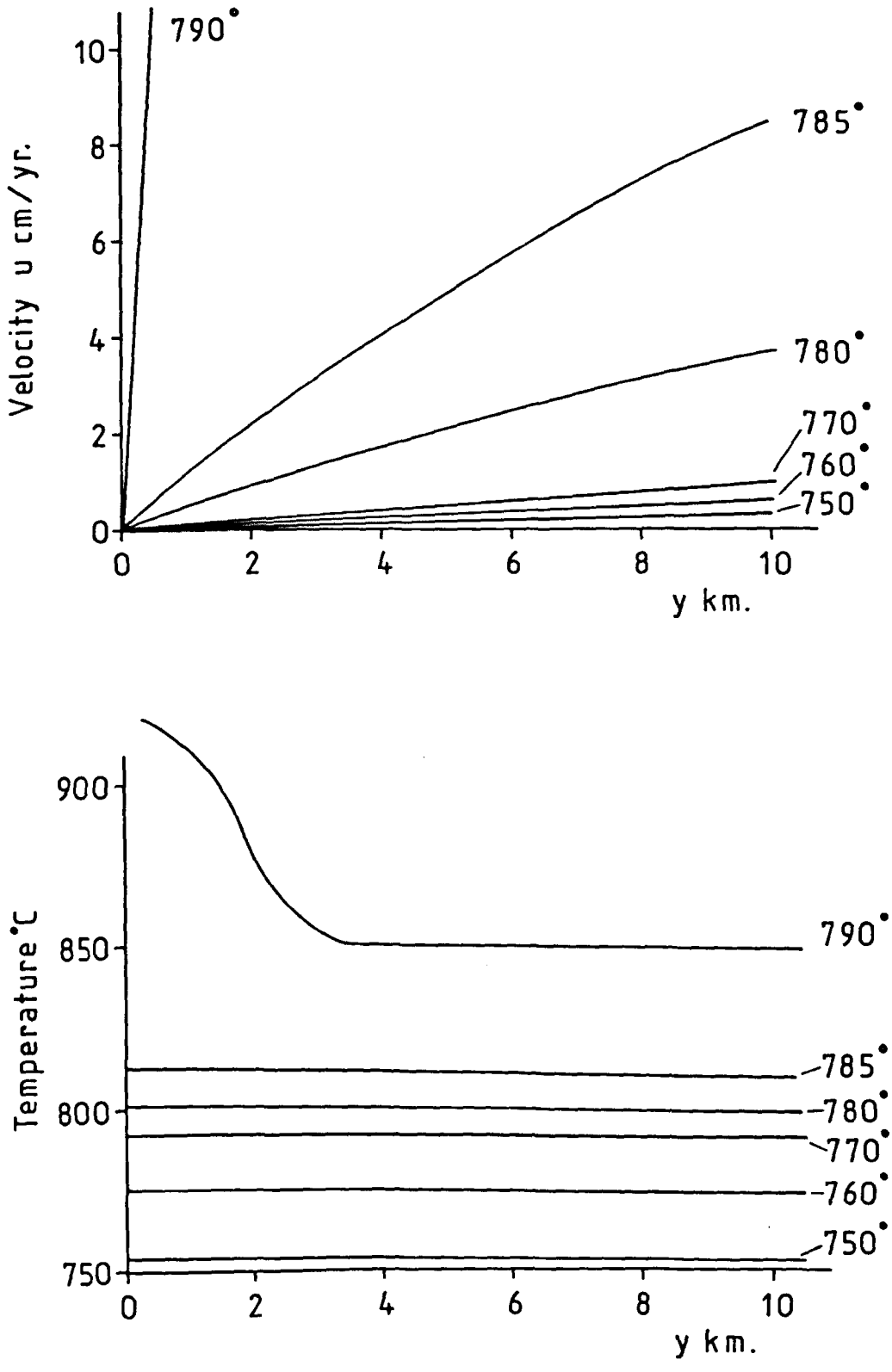

Figure 4.3.2. The velocity and temperature profiles at constant stress for various ambient temperatures. $t=10^5$ yr., stress=2.5kbar.

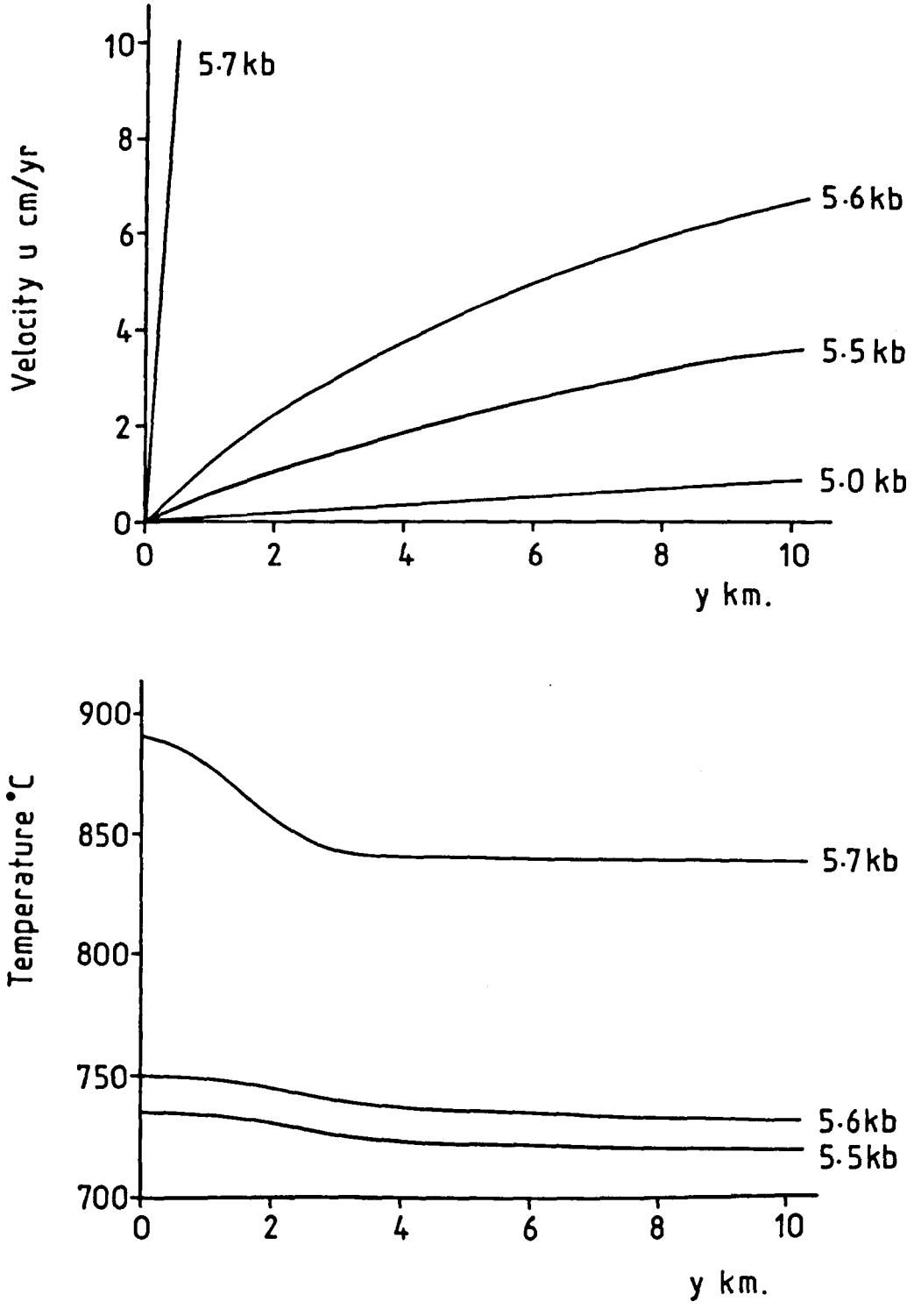

Figure 4.3.3. The velocity and temperature profiles for various stresses at a fixed time. $t=10^5$yr., $T_o=700^oC$.

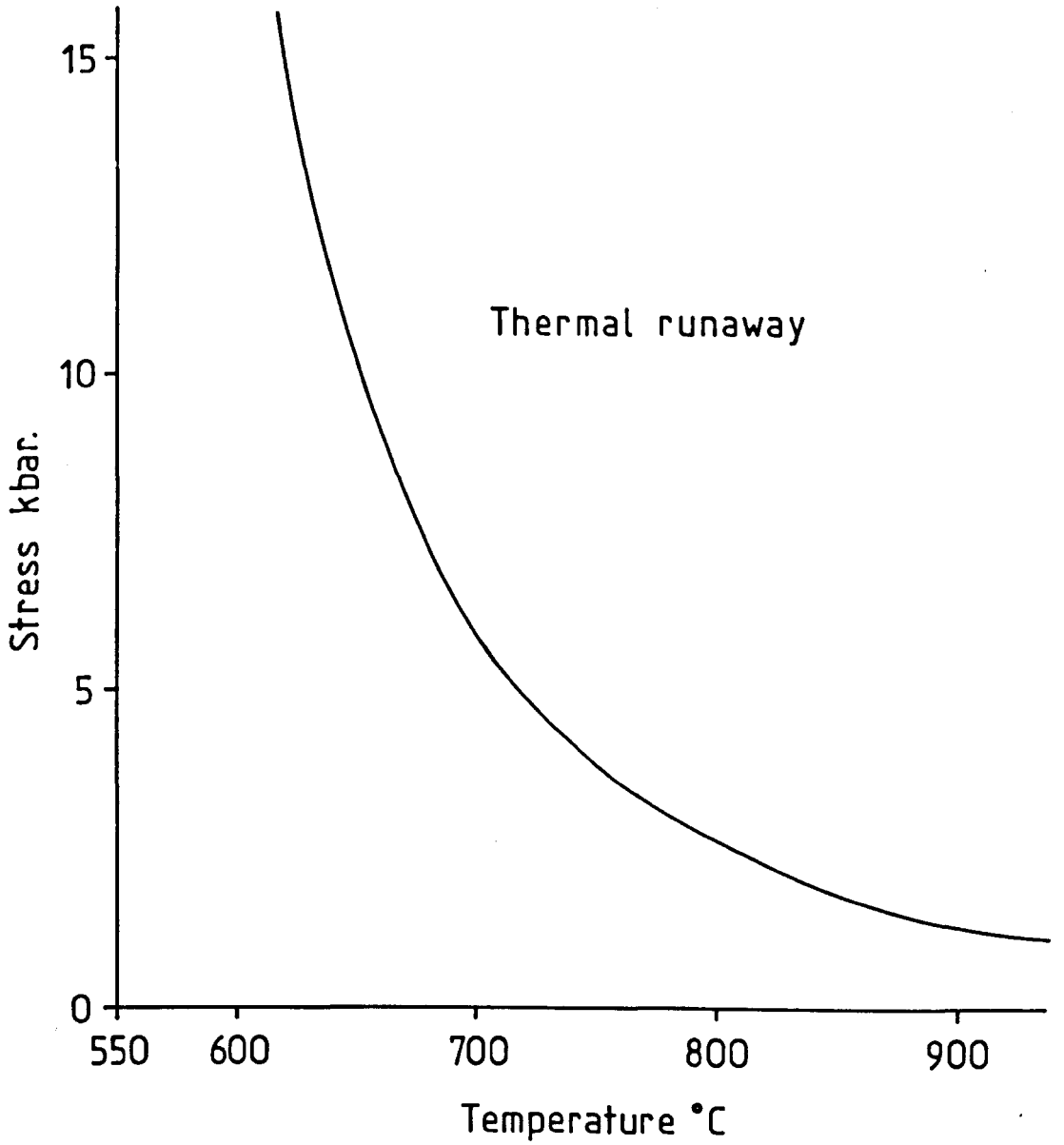

Figure 4.3.4. The temperature-stress curve for thermal runaway initiation at a fixed time of 10^5yr.

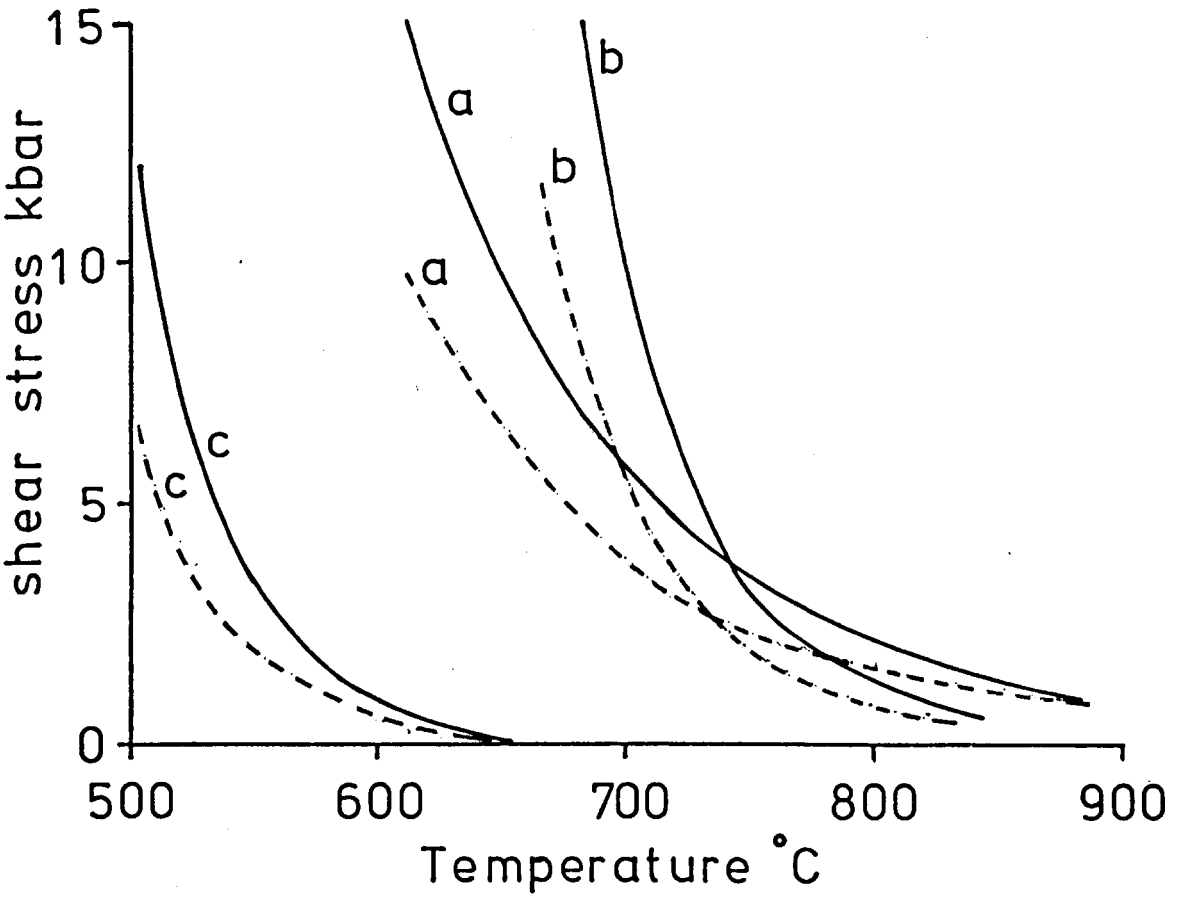

Figure 4.3.5. The temperature-stress curves for thermal runaway for various rheologies and times. Solid lines represent 10^5yr. and dashed lines 10^6yr. Profiles : a=dry olivine, b=dolerite, c=granodiorite.

includes curves for dolerite and granodiorite rheologies. The dolerite and dry olivine rheologies behave similarly but the granodiorite requires a much lower level of stress and temperature to produce thermal runaway.

The discontinuity of shear zone behaviour at the point of thermal runaway can be explained in terms of catastrophe theory. Figure 4.3.6 shows the simplest catastrophe surface (Thom 1975). The state of the system is represented by the topological surface. Moving along an axis produces a gradual change in the state except at the fold in the surface when the system changes catastrophically. Thermal runaway can be represented by such a catastrophe.

4.4 A comparison of the two models

From the previous two sections it can be seen that the constant velocity and constant stress models produce quite different shear zone structures. Constant velocity conditions produced localized zones of intense shearing which broaden with time. A corresponding thermal anomaly exists, the magnitude of which increases with time, quickly at first and then more slowly. The temperature reached by the shear zone is never high enough for melting.

Constant shear stress conditions produce shear zones with an initial uniform strain rate across them. The uniform strain rate produces constant shear heat across the model and hence a uniform temperature rise across the model. Should sufficiently high temperatures and stresses exist, large amounts of shear heating will be generated, which may develop into thermal feedback instabilities and thermal runaway.

The strain profiles produced by the two models are very different. Constant velocity models have a central high strain zone. This high strain zone slowly broadens with time as well as increasing in magnitude. Constant stress models produce a perfectly linear strain profile across

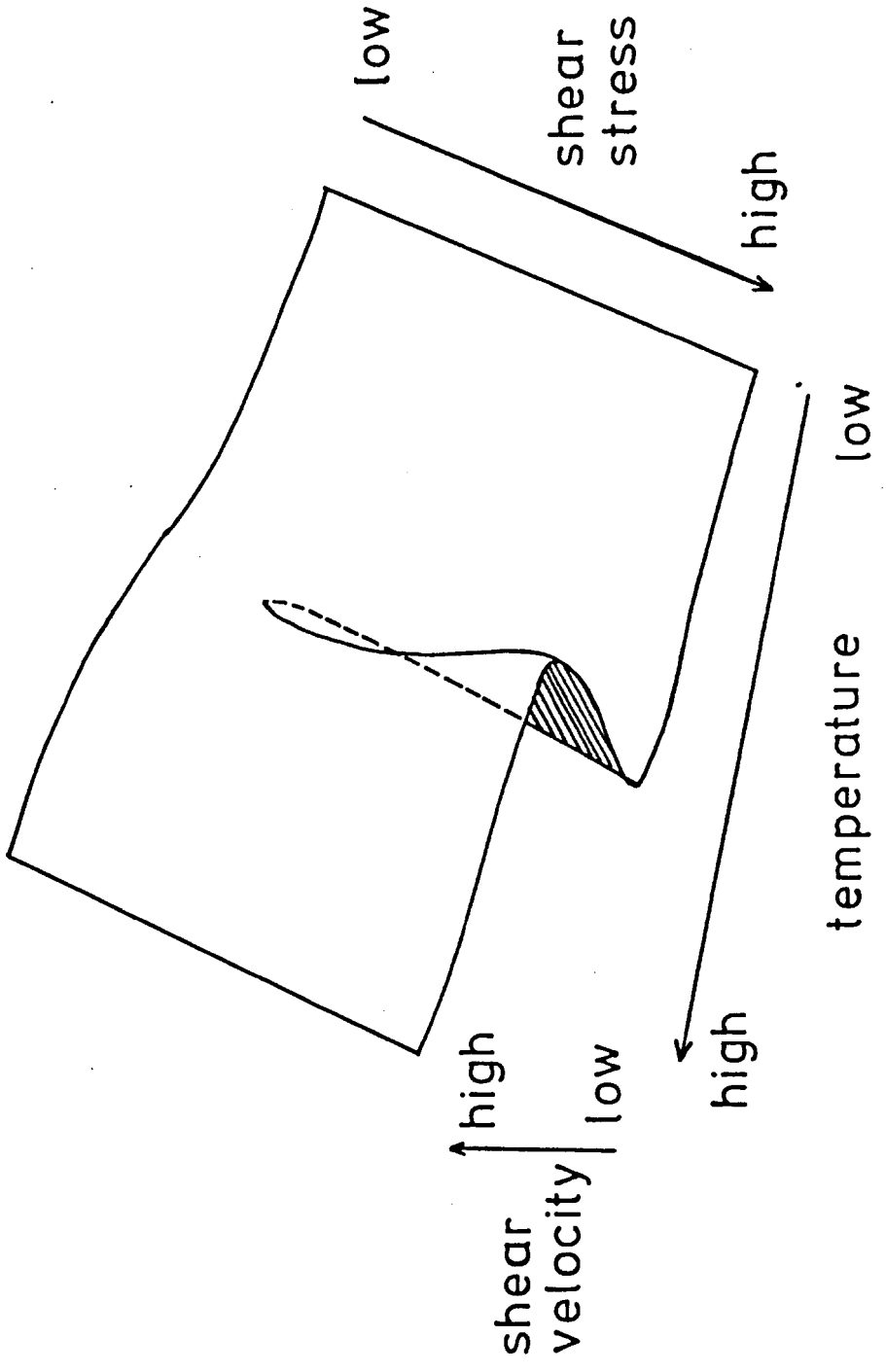

Figure 4.3.6. A simple catastophe surface representing thermal runaway(see text for explaination).

the shear zone, strain being constant at all points. Should thermal runaway occur, the strain profile is rapidly modified by the development of a central very high strain zone as a prelude to melting of the rock material. Figure 4.4.1 shows examples of the strain profiles developed by the two models.

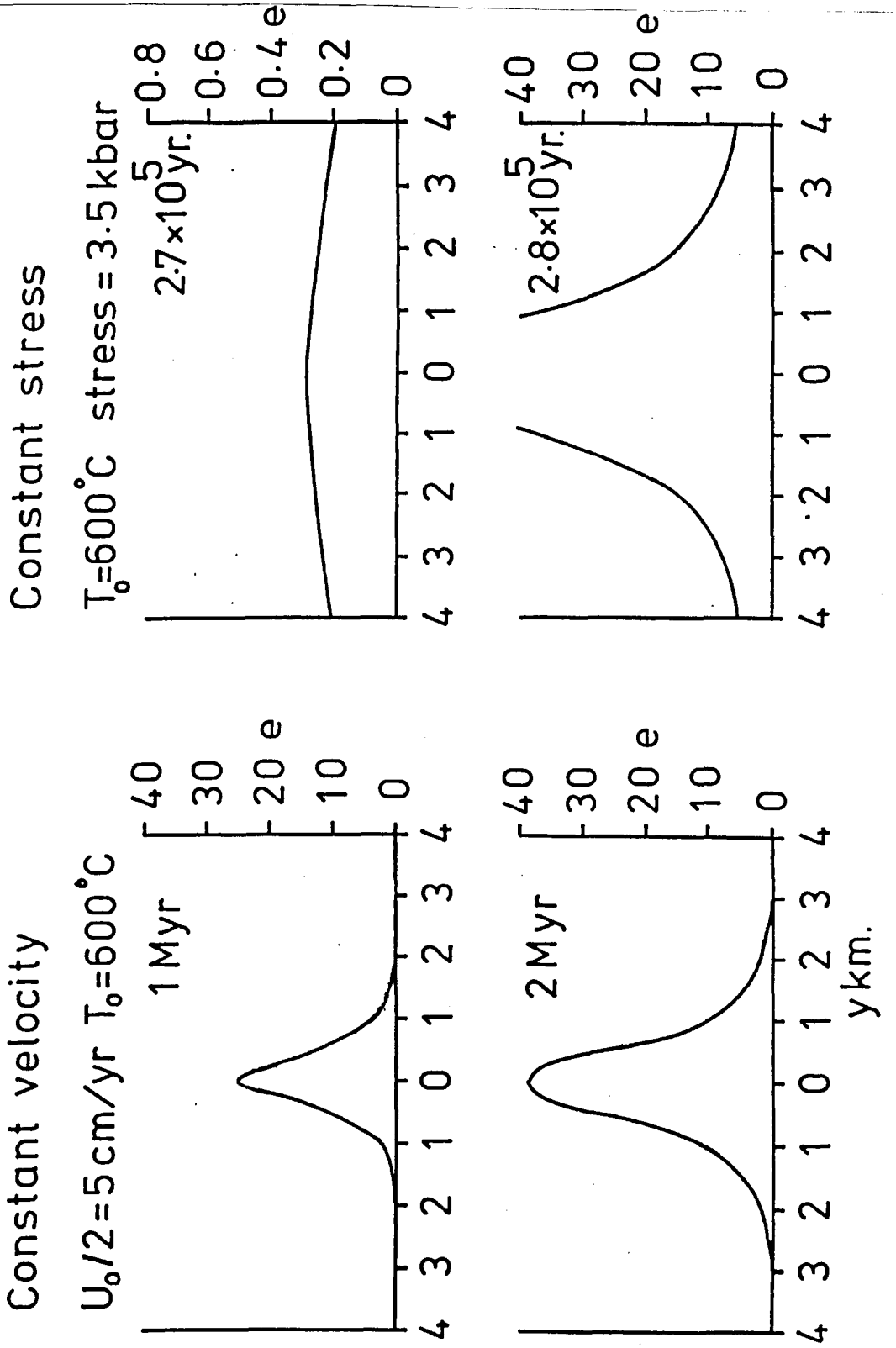

Figure 4.4.1. A comparison of the strain profiles produced by constant boundary velocity and constant shear stress models.

CHAPTER 5

Applications of Viscous Shear Zone Models

5.1 Introduction

In this chapter the implications of the viscous model on shear zone structure and behaviour will be discussed and the model extended to assess the effects of shear zone interaction and the shearing of heterogeneous materials. The majority of this chapter will deal with effects observed for constant velocity boundary conditions. Structures predicted by the constant shear stress model are generally simpler than constant velocity types and are included where appropriate.

5.2 Broadening of shear zones with depth

The behaviour of the constant velocity model was seen in section 4.2 to show a high dependence on ambient temperature. Both velocity and temperature profiles show significant changes in shape with change in ambient temperature. With increasing temperature the velocity profiles become less steep and tend towards a constant gradient, while the temperature profiles lose their high central peaks and become much wider with smaller central anomalies (see fig. 4.2.6). As the shear zone becomes broader and more diffuse with ambient temperature, it will also broaden with depth in the crust. Figure 5.2.1 shows how a shear zone broadens with ambient temperature. The ambient temperature is related to the depth in the crust by the geotherm. The shear zone is defined mechanically as being within the surface where $U = \pm 0.95\, U_o/2$, such that 95% of the deformation is accommodated within the shear zone.

Figure 5.2.1. The broadening of shear zones with depth for : (A) oceanic lithosphere, (B) continental shield lithosphere ,(C) basin and range lithosphere. Dry olivine rheology is used throughout.

A dry olivine rheology is used in the model. To determine the broadening with depth we must know the ambient temperature at a given depth. This can be done for ocean basin, continental shield and basin and range lithosphere using published geotherms (Haigh 1973, Herrin 1972, Mercier and Carter 1975).

The shear zone shows a gradual widening with depth until the ambient temperature increases to over 700°C. At these temperatures the shear zone broadens rapidly such that deformation is no longer confined to a steep vertical zone but becomes a sub-horizontal low viscosity zone. This sub-horizontal shearing is achieved at a depth of about 40 km for ocean basin, 60 km for continental shield and 23 km for basin and range lithosphere, using a dry olivine rheology.

At higher levels in the crust the viscous deformation model becomes invalid and brittle elastic deformation takes place. Seismic activity on continental transforms such as the San Andreas fault occurs at depths shallower than 10-15 km (Eaton et al. 1970). This corresponds to a change from ductile deformation to brittle seismic slip at higher levels (Sibson 1977). The broadening with depth produced by the models can also be described by the temperature anomaly of the shear zone. The resulting profiles being an order of magnitude wider than the velocity profiles.

Better estimates of shear zone broadening with depth can be achieved by using differing rheologies. The use of a dolerite rheology and an ocean basin geotherm (Haigh 1973) is shown in figure 5.2.2. On the same diagram is shown the results of using a granodiorite rheology and both continental shield and basin and range geotherms. The results for dolerite rheology are similar to those for dry olivine, the shear zone becomes horizontal at almost the same temperature but is fairly angular in shape

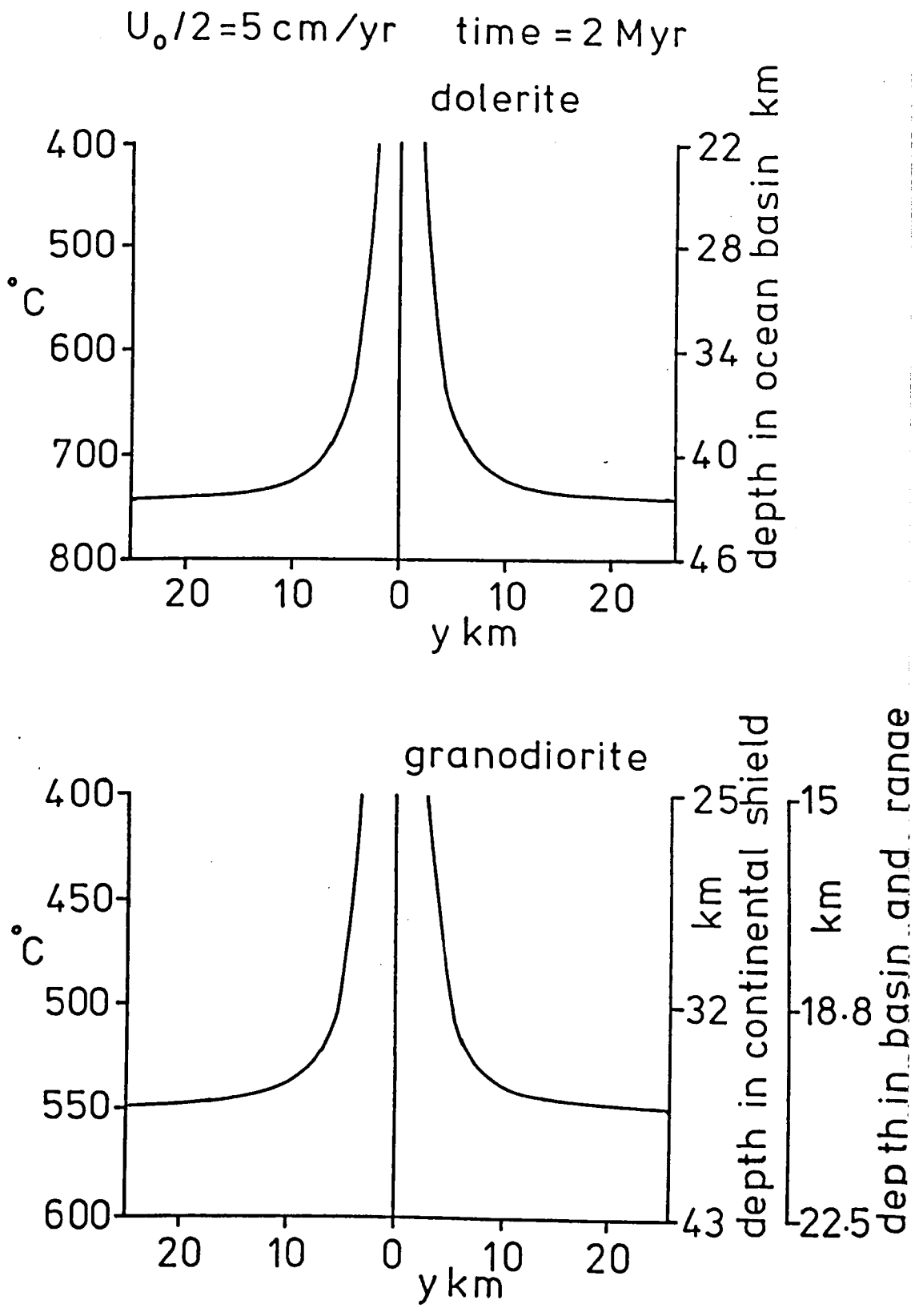

Figure 5.2.2. The broadening of shear zones with depth for (top) oceanic lithosphere using dolerite rheology and (bottom) continental shield and basin and range lithosphere using granodiorite rheology.

changing suddenly from a narrow vertical shear to a sub-horizontal shear. The granodiorite model becomes sub-horizontal at a temperature of around 550°C. This corresponds to a depth of 37 km in continental shield lithosphere and to a depth of 16 km in basin and range lithosphere.

Shear zone broadening with depth has been recorded by field workers in the Nordre Strømfjord shear belt, west Greenland. Bak et al. (1975) interpreted the shear belt as a gently eastward dipping slab of crustal material. The widening of the shear zone to the west is commensurate with an increase in metamorphic grade reflecting a deeper crustal level. The shear zone broadens from 7 to 15 km wide over an estimated vertical distance of 10 km (see fig. 5.2.3). This compares well with the broadening predicted by the granodiorite rheology over a depth range of 25-35 km for continental shield lithosphere. For basin and range lithosphere the broadening occurs over a much smaller depth range from 12 to 16 km.

The variation of shear stress with depth can also be investigated for constant velocity shear zones. The stress profiles against ambient temperature are shown in fig. 5.2.4 for dolerite, granodiorite and dry olivine rheologies. Characteristic of all three profiles is the slow decrease in shear stress with increasing temperature interupted by a sudden sharp peak. Dry olivine and dolerite rheologies produce high maximum stresses at temperatures around 700°C. Granodiorite rheology produces a lower peak stress at a much lower temperature around 540°C. The position of the peak stresses corresponds exactly to the point where the vertical narrow shear zone becomes a broader sub-horizontal structure. The temperature also corresponds to the point where the shear zone no

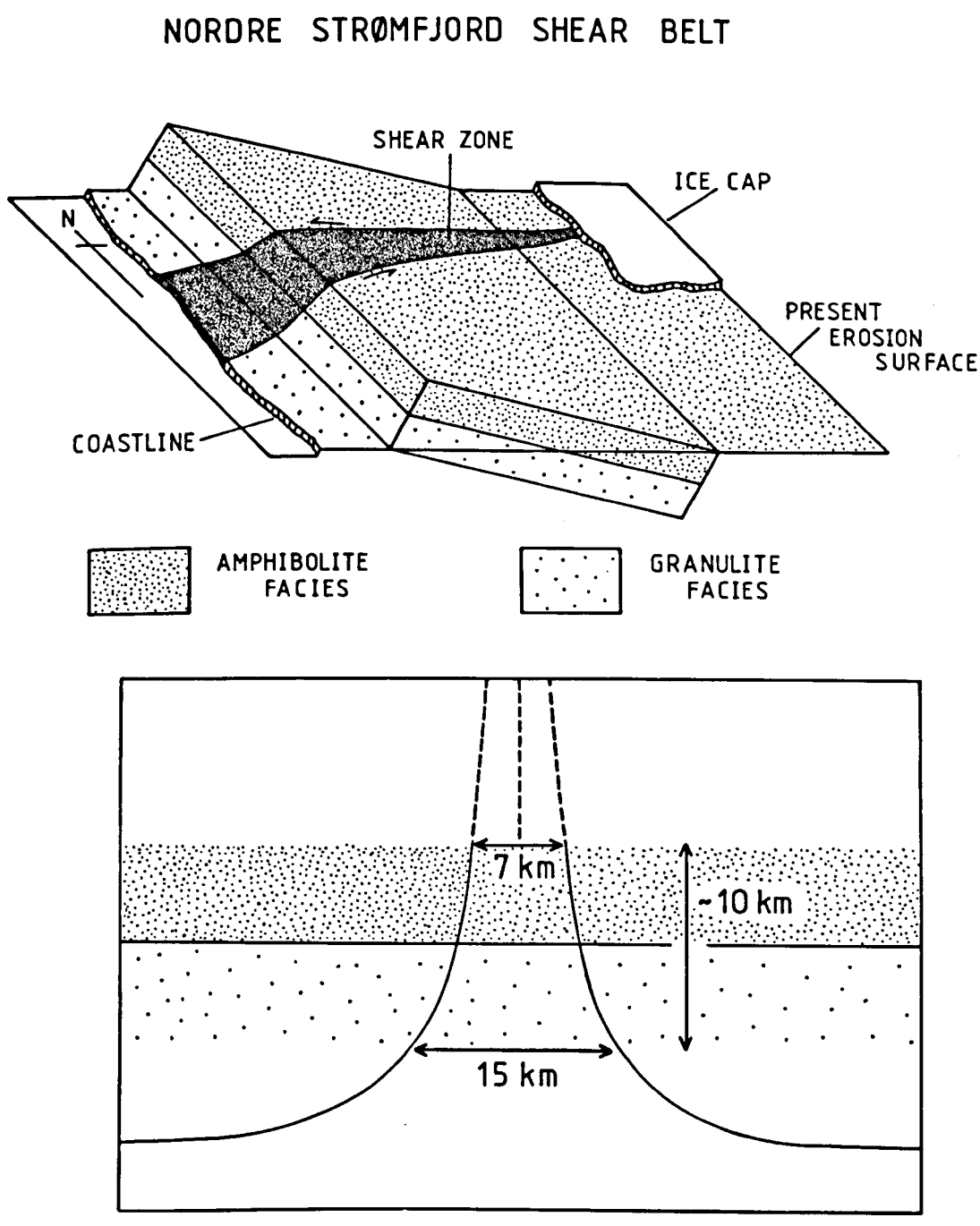

Figure 5.2.3. The structure of the Nordre Strømfjord shear belt, western Greenland (after Bak et al. 1975).

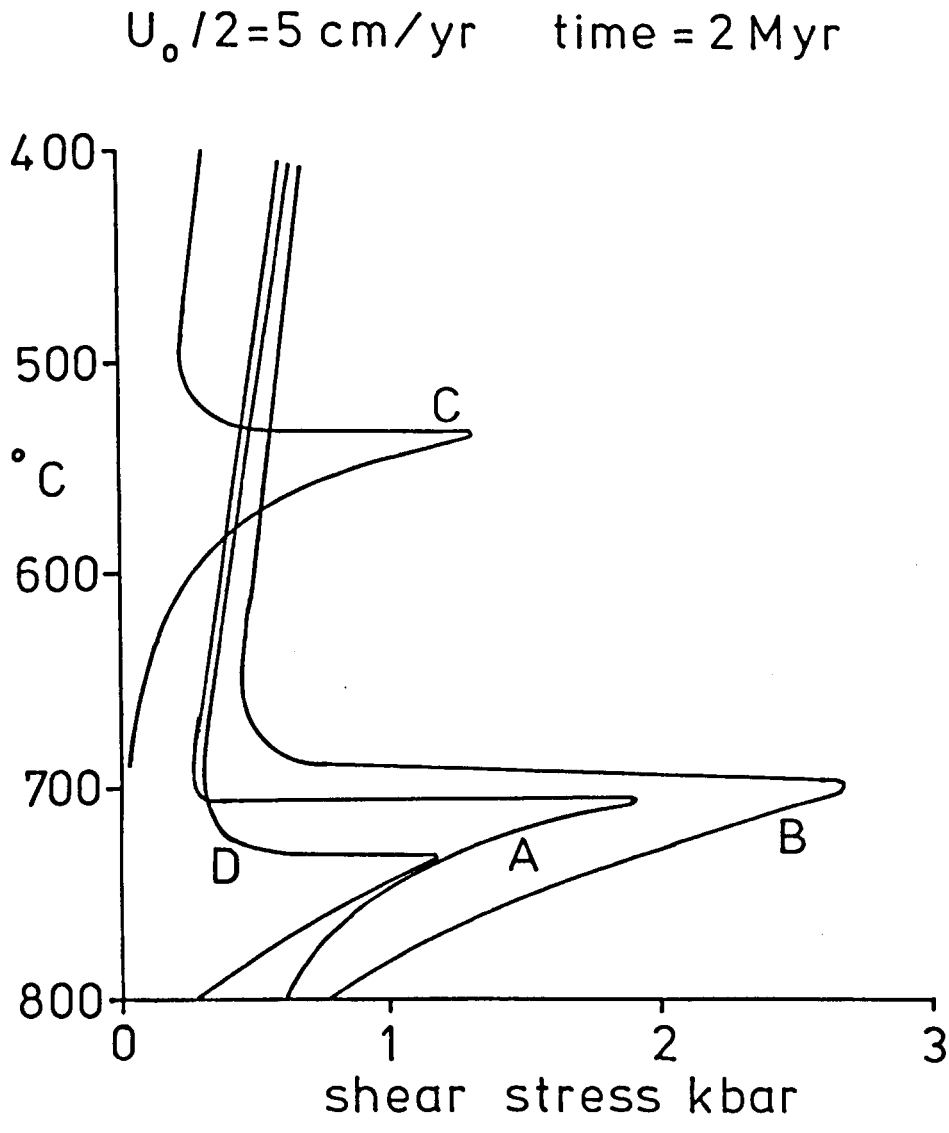

Figure 5.2.4. The variation of shear stress with ambient temperature for (A) dolerite rheology, (B) dry olivine rheology, (C) granodiorite rheology, (D) dry olivine using a temperature dependent thermal conductivity.

longer produces sharp high amplitude temperature anomalies but begins to give broader low amplitude temperature profiles.

The vertical structure of a shear zone with temperature is likely to be influenced by the values used for thermal conductivity in the model. The model was investigated using the expression derived in chapter 2 for the temperature dependence of thermal conductivity in dry olivine. The expression used is

$$k_{eff.} = 0.0109 - (4.5 \times 10^{-6}.T) \text{ cal/cm sec}^{o}\text{K}$$

the effective thermal conductivity value produced includes both thermal (phonon) conductivity and the effects of radiative heat transfer. The resulting shear zone structure is shown in fig. 5.2.5. The temperature dependent thermal conductivity tends to smooth out the transition from vertical to sub-horizontal shearing, the shear zone broadening more rapidly than the normal case. At mid and lower levels the temperature dependent conductivity causes the shear zone to be almost twice as wide. The stress profile with depth for a temperature dependent conductivity is shown in fig. 5.2.4. The peak stress is much lower and occurs at a slightly higher temperature than the plain dry olivine model.

Shear zone broadening with depth does not occur for constant shear stress boundary conditions. Referring back to fig. 4.3.2 which shows the effect of ambient temperature on a constant stress shear, it is apparent that the shear rate increases with temperature and hence depth. At temperatures which are insufficient for thermal runaway the velocity profile has a constant gradient, making the resulting velocities at the shear zone margin dependent upon the width of model. However if the stress is invariant with depth any thermal runaway will occur at the

Figure 5.2.5. The broadening of a shear zone with depth using a dry olivine rheology and a temperature dependent thermal conductivity.

deepest level of the model first.

5.3 Multiple shear zone models

Shear zone structure is determined by two effects operating against one another. Shear heat is developed by the viscous shearing which increases the temperature, lowering the viscosity. Thermal diffusion works in opposition, removing the shear heat and cooling the stabilizing anomaly. Thermo-mechanical shearing is a dynamic equilibrium between these two processes. The models considered so far assume a constant ambient temperature and that no additional heat sinks or sources exist. A possible additional heat source could take the form of another shear zone. Multiple shear zone models have been investigated to determine the conditions under which multiple shears will interact or remain as distinct entities.

For a constant shear velocity boundary condition, merging of shear zones was investigated using a dry olivine rheology at an ambient temperature of 600°C. The boundary velocity was chosen to be 5 cm yr^{-1}. Two small perturbations were introduced into the model separated by a distance of 10 km. At a time of 1 Myr the two perturbations have developed into discrete shear zones each having its own velocity and strain profile (fig. 5.3.1). The maximum temperature is, however, located centrally between the two perturbations. This central temperature maximum causes the velocity profiles to merge together into a single central shear zone. By 3 Myr the strain profile shows a large central peak the deformation being accommodated by a single shear zone. It is important to note that the strain profile peaks do not necessarily coincide with the instantaneous maximum shear velocity gradient.

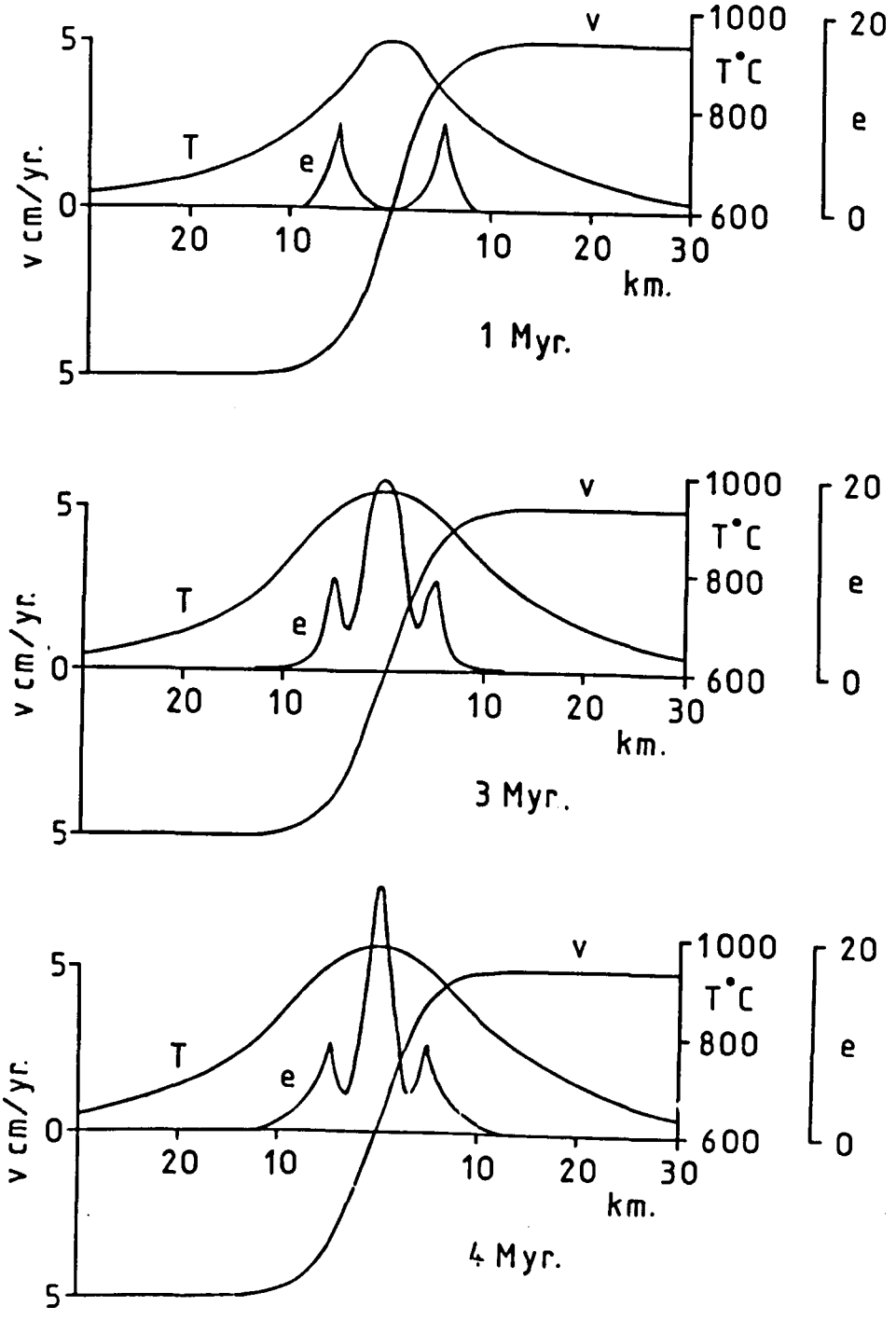

Figure 5.3.1. The velocity, temperature and strain profiles showing the convergence of a pair of shear zones, initially 10 km apart, with time. $U_o/2=5$ cm yr^{-1}, $T_o=600^{\circ}C$.

The overlapping of the two thermal anomalies is the precursor to shear zone merging. Since the thermal anomaly of a shear zone decays asymptotically to the ambient temperature with distance, then there must be a distance at which a pair of shear zones are sufficiently distant from each other to remain as distinct entities. Figure 5.3.2 shows the temperature and velocity profiles for shear pairs separated by various distances after a time of 2 Myr. A shear pair with an initial separation of 20 km shows the beginning of coalescence at 2 Myr; the temperature anomalies overlapping one another. At a distance of 50 km however the temperature midway between the pair of shears is almost the ambient temperature. For dry olivine rheology initial separations of around 50 km are required to maintain the shears as discrete entities for tens of millions of years.

Since the temperature anomaly of a shear zone broadens with time, then the minimum distance separating a pair of shears will also be time dependent. Figure 5.3.3 shows the minimum distance separating a pair of dry olivine shear zones against time. The distance is the minimum separation required to keep the shear zones as a pair, having individual velocity and strain profiles. The curves have been presented for a range of values of thermal conductivity from 0.004-0.01 $cal/cm^2\ sec^oC$. A change in the value of conductivity does not affect the shape of the curve. The minimum separation distance increases with time but the rate of increase also decreases with time. On the same diagram are shown a similar pair of curves for dolerite and granodiorite rheologies both using a thermal conductivity value of 0.006 $cal/cm^2\ sec^oC$. In all cases the shape of the curve is similar only the values varying slightly with rheology and temperature.

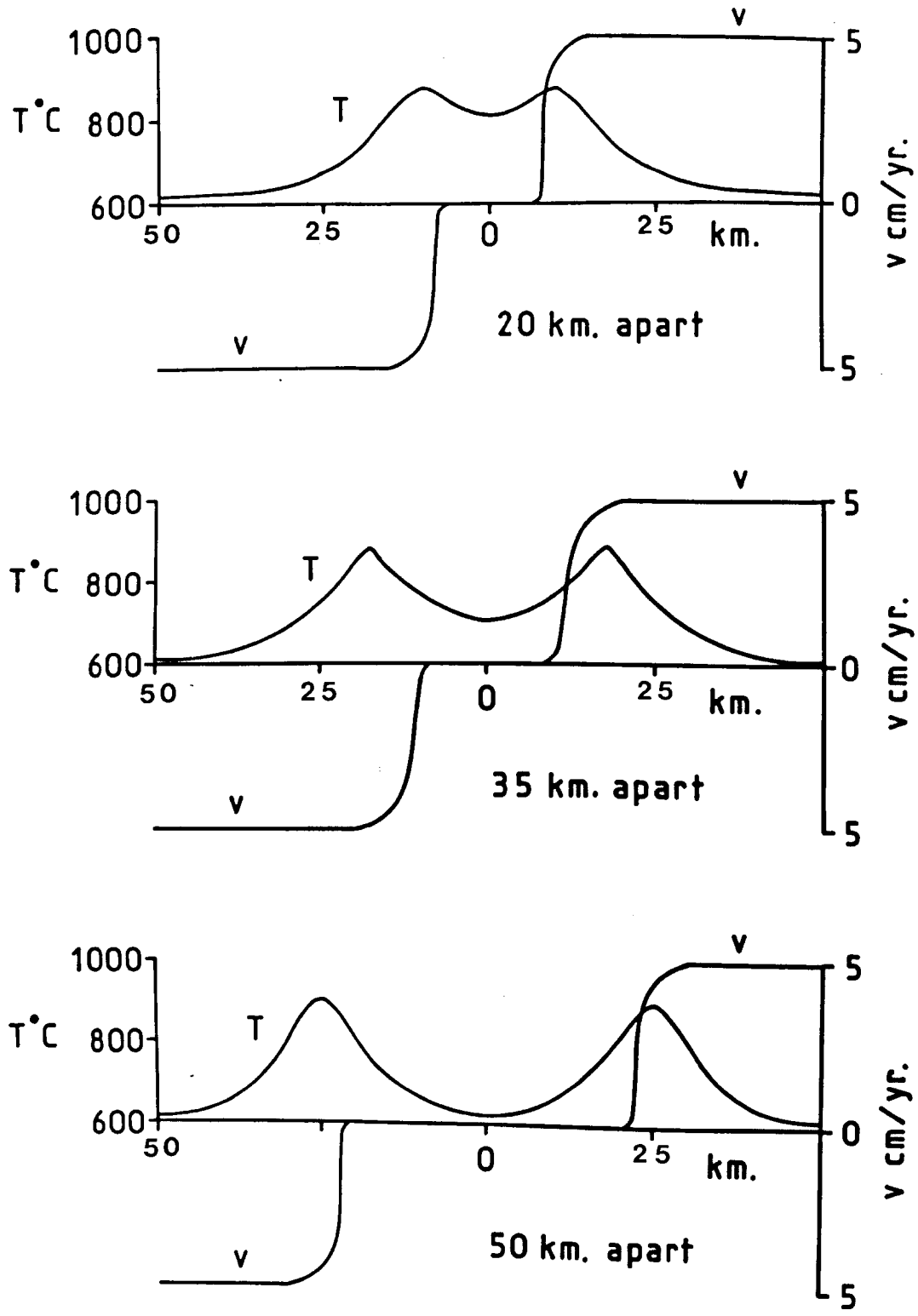

Figure 5.3.2. The velocity and temperature profiles for pairs of shear zones with various initial separations. $U_o/2$=5 cm yr^{-1}, T_o=600°C, time=2Myr.

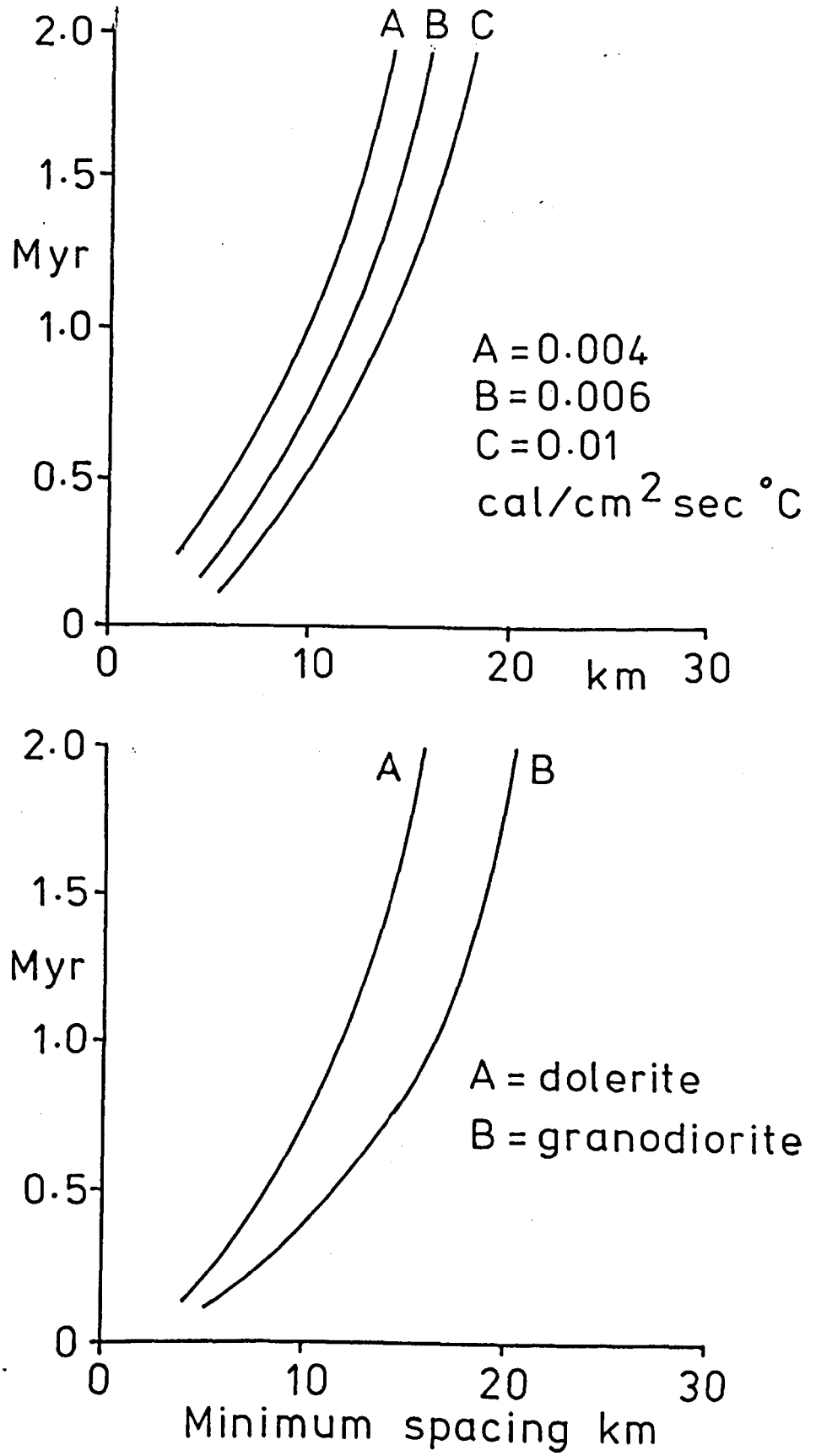

Figure 5.3.3. The minimum spacing for a pair of shears to remain discrete for a given time :(top) dry olivine rheology for various thermal conductivities T_o=600°C, $U_o/2$=5 cm yr^{-1}, and (bottom) dolerite rheology T_o=600°C and granodiorite rheology T_o=500°C.

The concept of shear zones merging with time can be extended to incorporate shear zone merging with horizontal distance. Should a pair of non-parallel shear zones initiate close to one another such that at their closest point they overlap each others temperature anomaly, then they will merge into a single shear. With time the thermal anomalies will broaden, increasing the minimum separation distance for the bifurcated end of the pair to remain discrete. Hence the pair slowly merge, the length of the original pair of shears which have merged increasing with time. Figure 5.3.4 represents the bifurcation of shears by showing the thermal anomalies of shears at various separations drawn along the length of the shear zone.

The interference and gradual merging of parallel or sub-parallel shear zones is partly controlled, as shown above, by the outward diffusion of the temperature anomalies of each shear zone. It has also been previously shown that the evolution of temperature and velocity profiles for a shear zone is highly dependent upon ambient temperature. Figure 5.3.5 shows the temperature profiles of a pair of shear zones initially 20 km apart, after 2 Myr for various ambient temepratures. With increasing ambient temperature the temperature profiles merge into a single anomaly. Since shear zone coalescence increases with ambient temperature, it is reasonable to assume that shear zones should also merge with depth.

At this point a brief discussion of the geological significance of shear interaction is appropriate. The model predicts that for any set of shear zones of the same age and shear rate there will be a minimum separation distance for the shears. Any shears initially closer

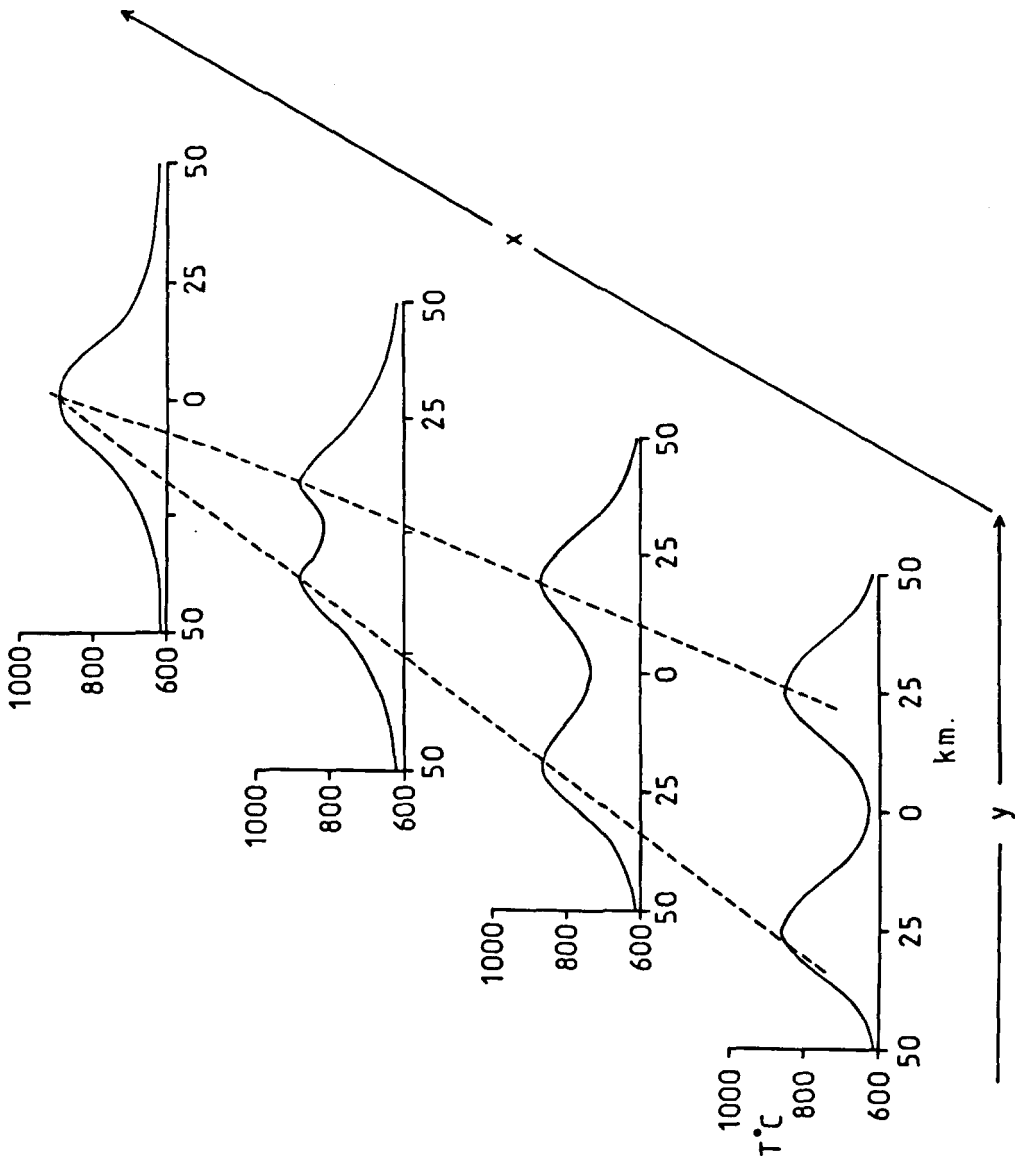

Figure 5.3.4. A schematic diagram of the temperature anomalies of a pair of shear zones merging laterally into a single zone. $U_o/2$=5 cm yr^{-1}, T_o=600°C, time =2Myr.

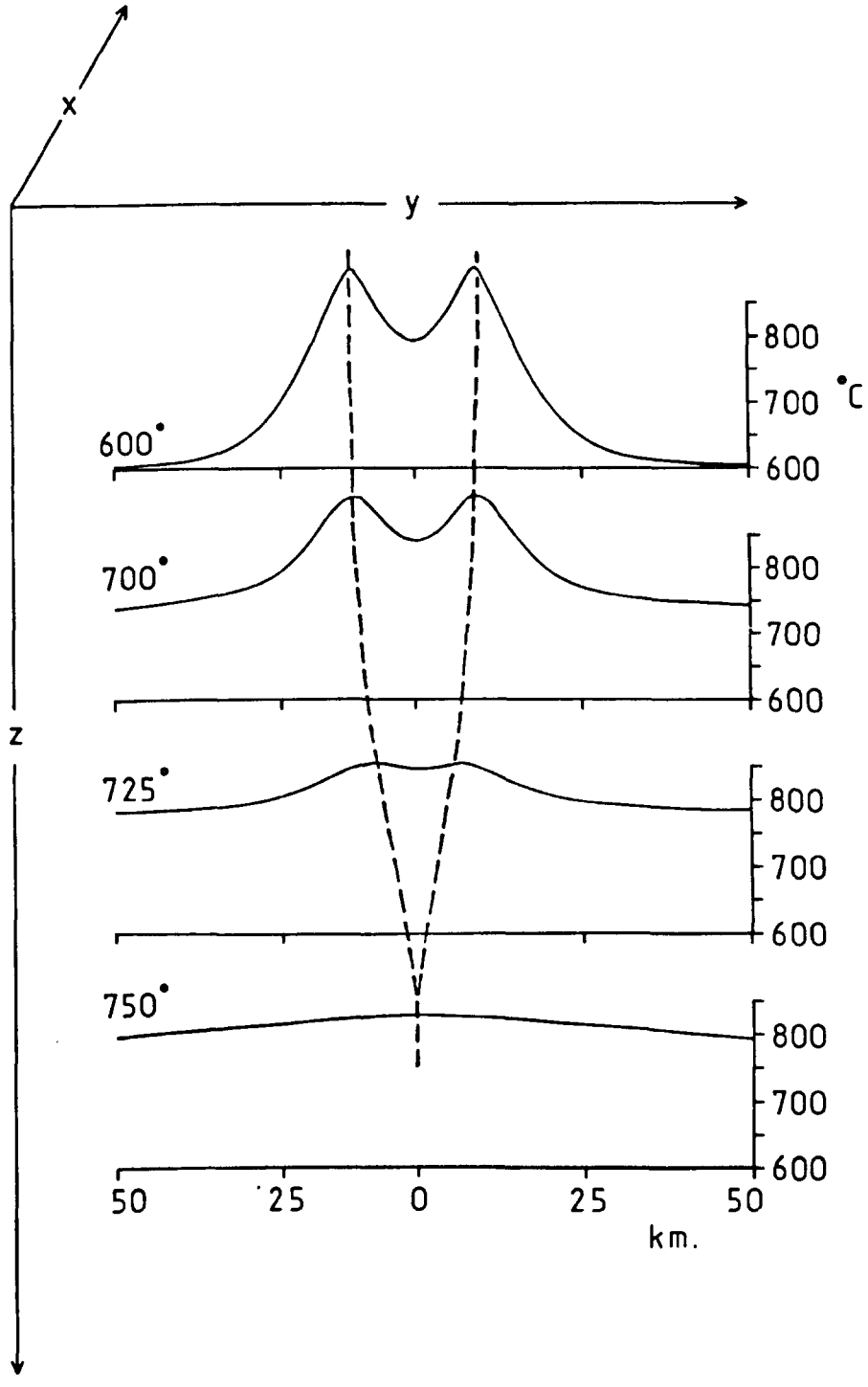

Figure 5.3.5. A schematic diagram of the temperature anomalies of a pair of shear zones merging with depth into a single zone. $U_o/2$=5 cm yr^{-1}, T_o=600°C, time =2Myr.

than the minimum distance are "swept up" by adjacent zones into a single structure. Field observations show that groups of shears can have a fairly regular spacing within a given province or area. The western Superior Province of Canada has a group of roughly parallel shear zones which have a fairly constant separation of 25-30 km (Park 1981). The shears are in a granite-greenstone terrain and the metamorphic conditions suggest ambient temperatures of around 500°C. Referring back to fig. 5.3.3, granodiorite rheology at an ambient temperature of 500°C and a shear velocity of 5 cm yr^{-1} has a minimum separation distance of 20 km at 2 Myr. The model appears to give a fair estimate of the observed shear zone separation in this case, all original shears with closer spacing being "swept up".

A more speculative case is suggested for the spacing of oceanic fracture zones. Turcotte (1974) has shown that the average length of ridge segment between fracture zones is about 100 km. Turcotte suggested a thermal contraction origin for the fracture zones but was unable to verify this. If the fracture zones become shear zones at depth, then perhaps the minimum spacing between shear zones at depth affect the spacing of fracture zones.

Shear zones at shallow depths will be geometrically localized by brittle fracture faults. This brittle fracture will modify shear zone structure at shallow levels and may inhibit or modify shear zone merging.

Constant shear stress boundary conditions behave somewhat differently. A pair of initial perturbations 10 km apart with an ambient temperature of 700°C are shown after 10^5yr in figure 5.3.6. The pair of perturbations divide up the velocity profile into three constant gradient sections. The temperature profile shows two slight peaks at

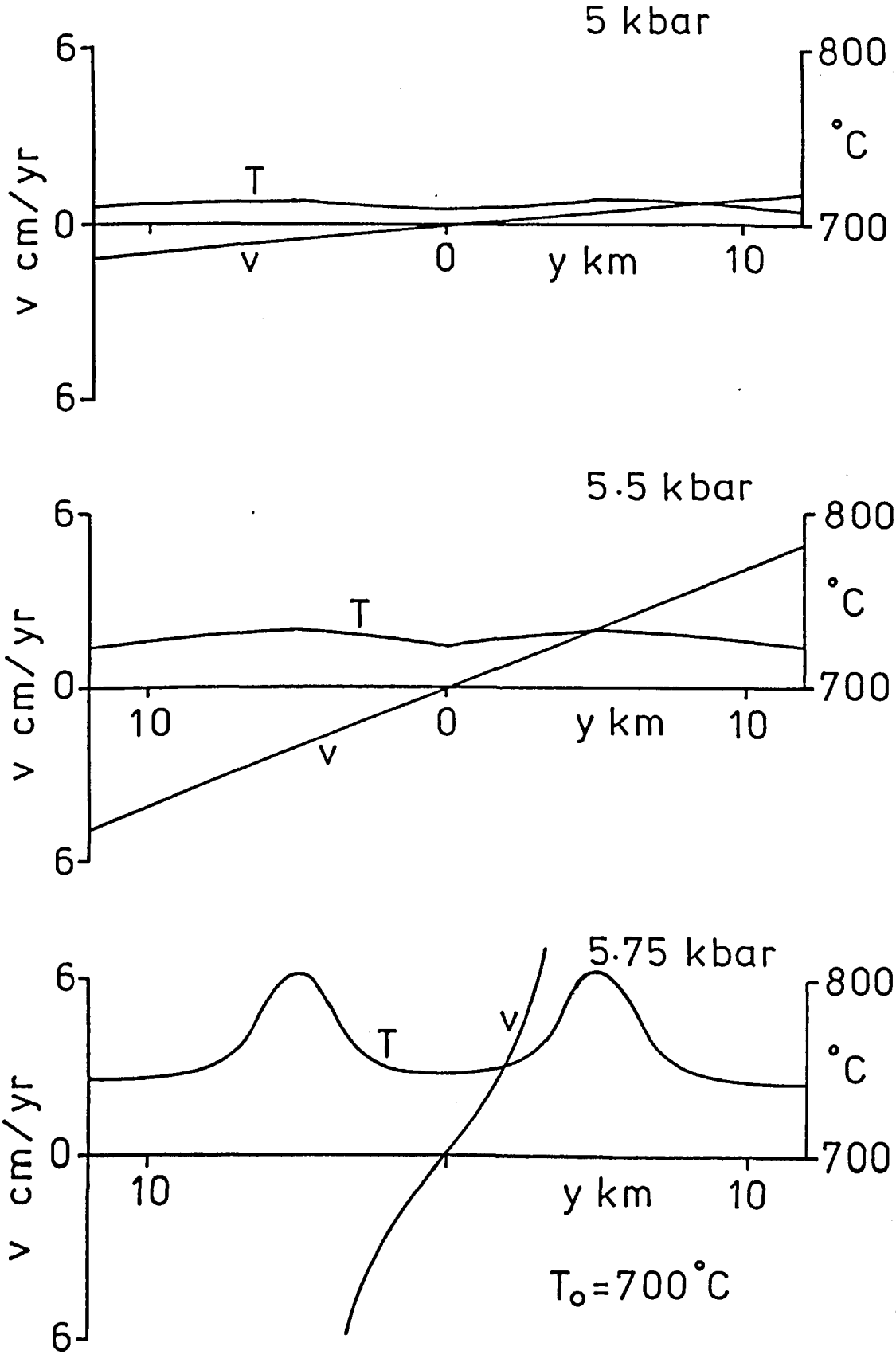

Figure 5.3.6. The velocity and temperature profiles for a pair of shear zones initially 10km apart after a time of 10^5yr for various values of shear stress.

the perturbation points. If the shear stress is sufficiently high to produce runaway then both perturbations develop into localized high strain areas and their temperature rises to the melting point. Once thermal runaway commences in the high strain zones the large amounts of shear heat generated rapidly melt the model.

5.4 Multiple material shear zone models

Multiple material shear zones were investigated using models which include both granodiorite and dolerite rheologies. The model was divided into layers of granodiorite and dolerite, the layering being parallel to the direction of shearing. Dolerite is more viscous than granodiorite for any temperature and stress condition, the viscosity ratio being 1.49×10^4:1. Initial destabilizing temperature perturbations are not required in this model since the softer granodiorite layers produce a localization of shear.

Constant velocity models were investigated using a dolerite rheology model with a soft centre of granodiorite extending 10 km either side of the shear zone axis. The development of the temperature and velocity profiles with time is shown in fig. 5.4.1 for an ambient temperature of $600^{\circ}C$ and a half shear rate of 5 cm yr^{-1}. At 0.5 Myr the velocity profile shows a constant gradient around the centre of the shear zone, the majority of the deformation being accommodated by the granodiorite. The temperature profile has a fairly broad peak value extending across most of the granodiorite region before decaying away to the edges of the shear zone. With time the shearing localizes toward the granodioritic centre producing a central temperature peak. Although the level of strain is

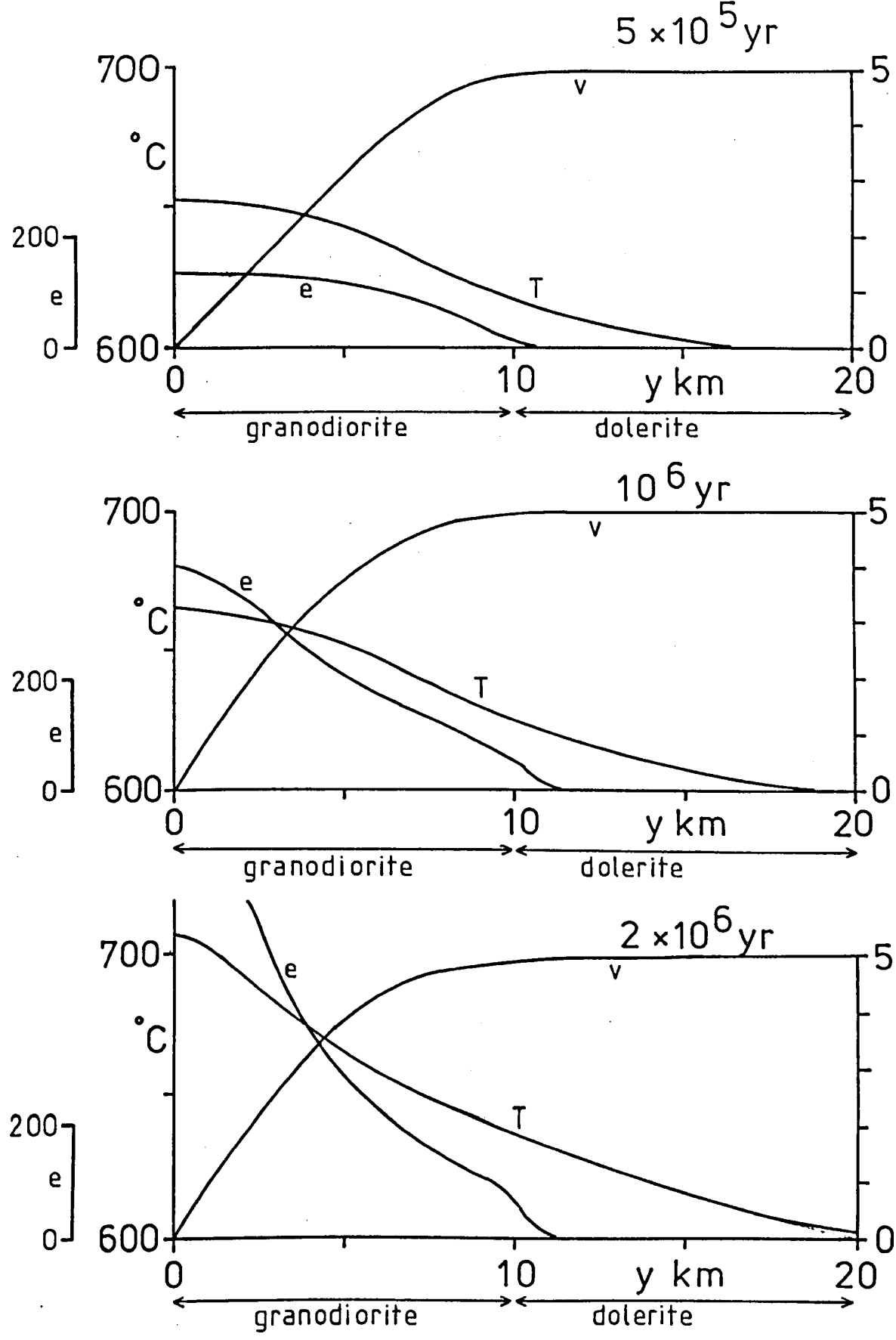

Figure 5.4.1. The velocity ,temperature and strain profiles for a dolerite model with a granodiorite centre, for various times. T_o=600°C, $U_o/2$=5 cm yr^{-1}.

very high the shape of the profile is interesting. Initially the strain profile has a flattened peak due to the even velocity gradient across the soft centre. With time the temperature anomaly begins to build up and the strain profile develops a central peak. The profile also shows a slight kink where the granodiorite forms a boundary against the dolerite. If a central temperature perturbation is introduced in the model it evolves into a normal steep shear zone.

A more elaborate model consists of a layer cake of granodiorite and dolerite. The model constructed has a wide central soft zone of granodiorite extending 4 km either side of the shear zone axis. The rest of the model consists of dolerite except two further layers of granodiorite 4 km thick, one each side of the axis, 10 km – 14 km away from the axis. This layer cake was sheared with a half velocity of 5 cm yr^{-1} at an ambient temperature of 600°C. The results for various times are shown in fig. 5.4.2. At 0.5 Myr the velocity profile shows the shearing to be localized in the granodiorite layers. The temperature profile shows shear heat peaks in the granodiorite region corresponding to high strains. With time the wider granodiorite layer in the centre of the zone begins to dominate the deformation taking up more of the deformation than the adjacent narrower granodiorite layers. At 2 Myr almost all of the deformation is being accommodated by the wider central granodiorite. It appears that although shearing initially localizes in all the weak layers, the widest weak layer takes up more deformation and slowly begins to grow at the expense of smaller layers.

Both the soft centre and the layer cake model have a geological significance. In both models shearing was localized in the weaker material. The wider layer of the layer cake model however, slowly took up all the deformation in the model. In field examples one would antici-

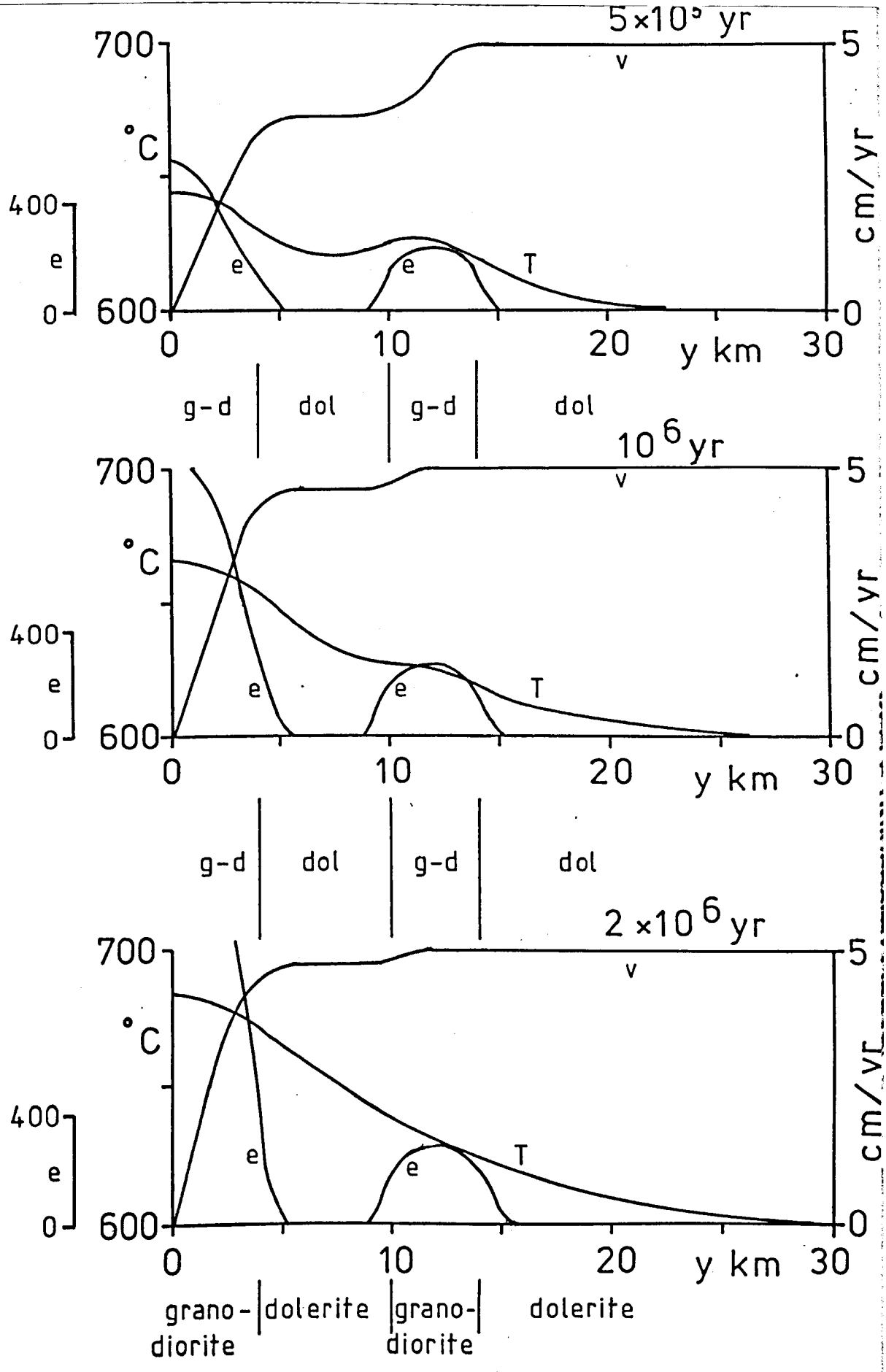

Figure 5.4.2. The velocity, temperature and strain profiles for a granodiorite-dolerite layer cake model for various times. T_o=600°C, $U_o/2$=5 cm yr^{-1}.

pate that shearing would localize in the weaker material and that progressive deformation would result in the weakest part of the shear zone developing. Where layers of the same material exist the broadest layer is the easiest to shear and hence eventually takes up all the shearing.

Multi-material shear zones under constant shear stress conditions behave very differently. The velocity profiles consist of a number of constant gradient sections. The gradient depending upon the rheology of the section in question. When thermal runaways occur, they do so in the softer material first. The softer material provides the destabilization but so much shear heating is generated that the entire model undergoes runaway. Models involving both granodiorite and dolerite rheology were investigated to determine the critical temperature and stress conditions for thermal runaway. The values obtained varied between those for a pure granodiorite model to those of a pure dolerite model; the actual values becoming closer to that of a specific material as the proportion of that material in the model is increased.

The model suggests that the thermal runaway conditions of a multi-material shear is dependent upon the relative amounts of the constituent materials, and their geometrical relationship to one another. The softer rheology produces localization of any thermal runaway, but the massive shear heating rapidly melts the entire model. This suggests that molten material should not coexist within the same shear zone with relatively undeformed unmolten rock.

Table 5.1 Summary of the behaviour of the two types of model

	Constant shear velocity model	Constant shear stress model
Velocity profile	Narrow localized shear zone	No localized shear zone
Temperature profile	Central temperature anomaly increasing with time.	Constant temperature increase across shear zone.
Strain and strain rates.	High strain area in centre of shear zone producing a shear heat maxima	Constant strain and strain rate across shear zone
Melting of shearing material	Maximum temperatures are insufficient for melting.	High stress and temperatures may result in thermal runaway with melting of the shearing material.
Temporal variation	Shear zones broaden both mechanically and thermally. Stress values decay with time to low values.	Slow increase in the gradient of linear velocity profile. Even increase in temperature across shear zone. Rapid increase of gradient and development of central shear heat maxima preceeds thermal runaway.

CHAPTER 6

Viscous Thrust Zones

6.1 Introduction

All the shear zone models so far, have considered the shear plane to be vertical. This chapter will describe the behaviour of a sub-horizontal shear zone along a thrust type structure. The thrust model represents a vertical section through the earth's crust and involves a more complicated initial temperature condition than the simple vertical shear zone.

Various authors have considered the temperature-depth profiles produced by thrusting. Oxburgh and Turcotte (1974) showed how an instantaneous thrusting of two slabs on top of each other produced an inversion in the geotherm which subsequently decayed by thermal conduction. This model was expanded by Graham and England (1976) and England (1978) to include frictional heating on the thrust plane which maintained the inversion of the geotherm. More recently Brewer (1981) has shown that frictional heating can generate a temperature inversion from a normal geothermal gradient.

The viscous model presented here assumes that the starting condition is an initial inverted geotherm. This is assumed to have occurred instantaneously allowing no thermal relaxation. To ensure that the deformation is a viscous process and not brittle failure the initial temperature on the thrust must be at least 400^{o}C, the actual value depending upon the lithology of the rocks.

6.2 The general thrust model

The model consists of a slab of uniform thickness which has been thrust upon itself causing an inversion of the geotherm (see fig. 6.2.1). This assumes that superposition of the two slabs occurs instantaneously allowing no time for thermal relaxation. Since the viscous deformation is temperature dependent, the part of an homogeneous model having the highest temperature will be the region which will undergo the maximum shearing. To localize the shear plane we must ensure that the peak temperature at the inversion is slightly higher than that at the base of the model. The model is designed to investigate how the shearing along the initial inversion behaves with time. A constant velocity or constant stress condition is applied across the model from the top of the upper slab to the base of the lower slab. The temperature at the surface has been fixed at $0^{o}C$ for all times. A temperature boundary condition is also applied at the base of the model. A point at a depth of 150 km has a fixed temperature of $1200^{o}C$. The temperature and velocity profiles are allowed to evolve between the surface and the base of the lower slab as shearing proceeds.

A one dimensional finite difference solution was used as in the vertical shear zone model. There is no difference in the mathematical formulation; both constant velocity and constant stress conditions can be applied. The initial temperature conditions are shown in figure 6.2.2.

To obtain an inversion temperature of $>400^{o}C$ we need to superimpose two slabs >30 km thick if a continental shield geotherm is used. A Basin and Range geotherm enables the slabs to be thinner $\sim$12 km but even these thicknesses prevent the model being usefully applied to ocean basin crustal thrusts.

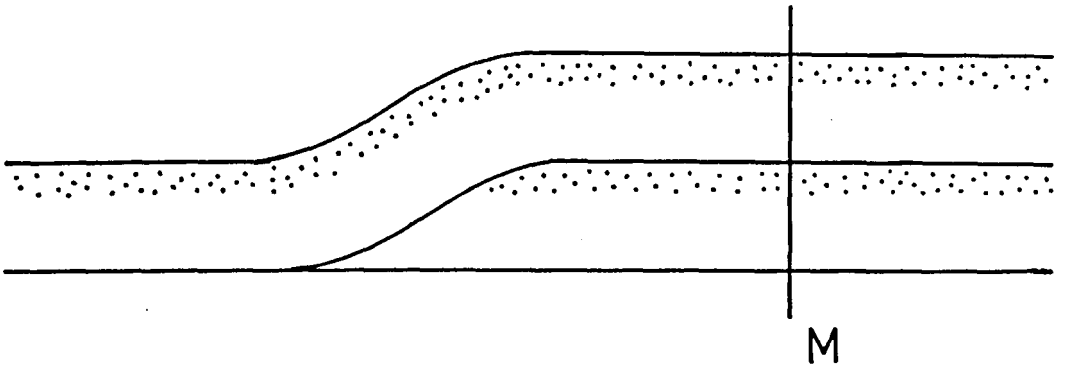

Figure 6.2.1. A diagram of a slab of uniform thickness overthrusting itself. The model is a vertical section at point M.

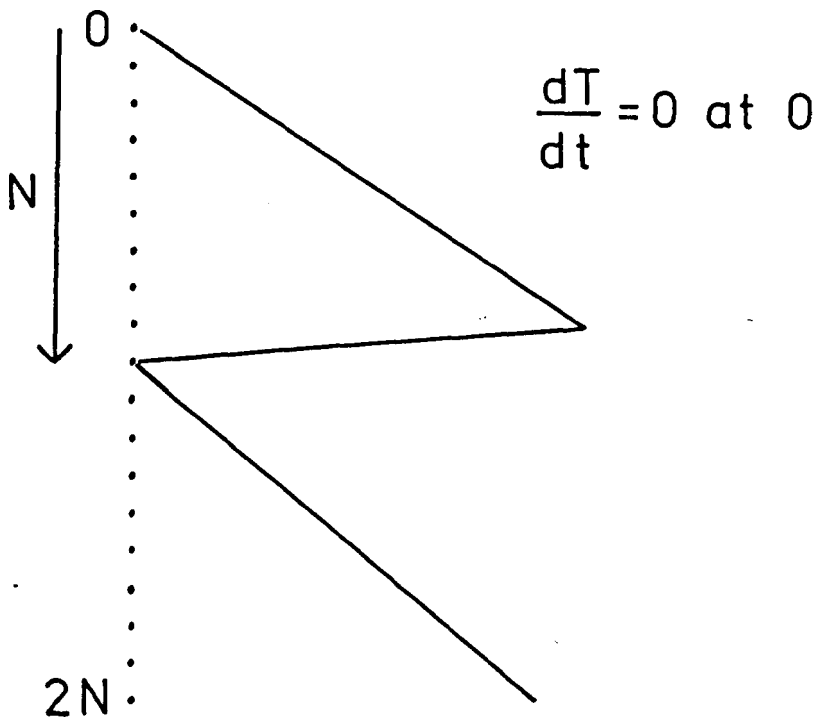

Figure 6.2.2. The initial temperature conditions of a slab of thickness N thrust upon itself. A point 150 km deep is fixed at 1200°C.

Both constant shear stress and constant boundary velocity conditions can be applied to the model. Constant velocity conditions are applicable to regimes where the overthrusting is driven by plate collision, while constant shear stress conditions are more applicable to the base of gravity driven nappes.

6.3 The constant velocity thrust model

The constant velocity model has been investigated using a continental shield and a Basin and Range geotherm. These geotherms represent the opposite extremes of thermal province found in continental regions and will encompass most possible variations in thrust behaviour due to geotherm variations.

The continental shield model assumes that two identical slabs each 35 km thick and having a granodiorite rheology are instantaneously thrust over each other. Using the continental shield geotherm of Herrin (1972) the thrust will have an initial temperature of 540^{o}C. A shear velocity of 10 cm yr^{-1} was applied between the surface and the base of the lower slab. The temporal evolution of the model is shown in figure 6.3.1. At 10^5 yr all the shearing is localized on the thrust plane. The temperature profile has evolved from the initial saw-tooth form (shown as a dashed line) to give a shear heating peak at the thrust. The lower slab heats up slowly by conduction of shear heat from the thrust and by conduction through the base of the model. With increasing time the shear heating causes the peak temperature on the thrust to increase slowly. The shearing remains localized along the thrust plane. At 2 Myr the lower slab has heated up considerably. Eventually the lower slab will heat up such that the maximum temperatures on the thrust are no longer sufficient to keep the shearing localized along the thrust plane. The deformation is then accommodated over a much wider zone, no

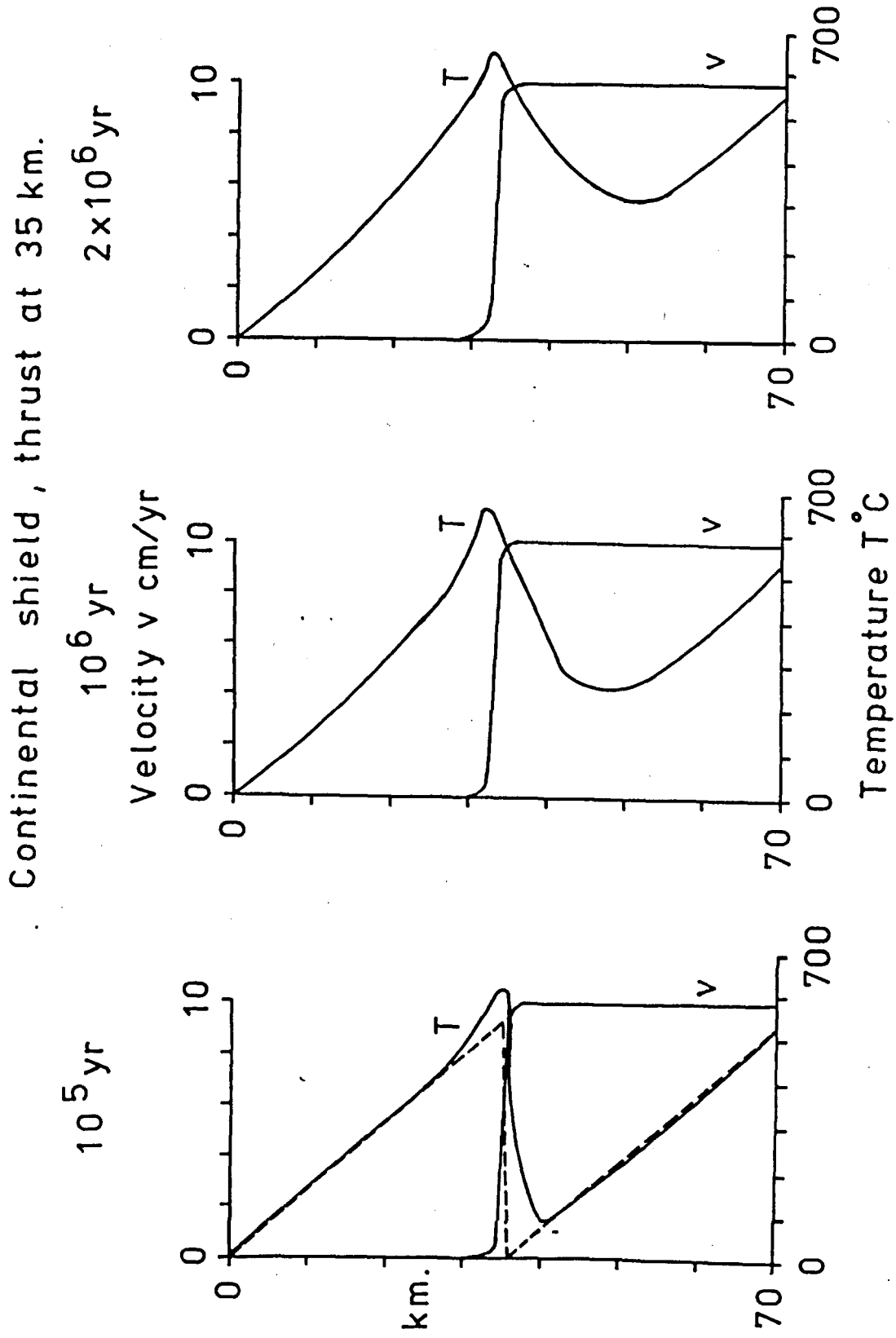

Figure 6.3.1. The velocity and temperature profiles at various times for a thrust 35 km deep in continental shield lithosphere.

real shear zone existing. At a time of 5 Myr all parts of the lower slab have been heated to over 400°C (see fig. 6.3.2).

The lower slab is heated both by shear heating and by conduction through the base of the slab. Figure 6.3.2 shows the temperature profiles for two differing temperature boundary conditions. The model with a point at 150 km depth fixed at 1200°C is compared with a model having the base of the lower slab fixed at its initial temperature. The second model with the temperature fixed at the base of the lower slab has no heat input by conduction from below and is some 20-30°C cooler as a result. The heat input into the models through the base of the lower slab has a significant effect on the heating up of the model.

Variation in the depth of the thrust has a marked effect on the maximum temperatures generated by the thrust at a given time. Figure 6.3.3 shows a plot of the maximum temperature reached versus depth of thrusting, for thrusting at 10 cm yr^{-1} for 1 Myr. The maximum temperature reached decreases with increasing depth until at a depth of just below 32 km it increases again. This increase in maximum temperature also corresponds with the temperature maximum occurring slightly shallower than the mechanical thrust. The temperature peak can be as much as 1 km shallower than the mechanical thrust.

Shear velocity is very important in the stabilization of the shearing along the thrust plane. Slow shear velocities will produce insufficient shear heating to maintain a temperature inversion along the thrust plane. Figure 6.3.4 shows the velocity and temperature profiles for a continental thrust 35 km deep using shear velocities of 5 and 6 cm yr^{-1}. The temperature and velocity profiles are shown at a time of 10^5 yr since by then any shearing will have stabilized. A shear velocity

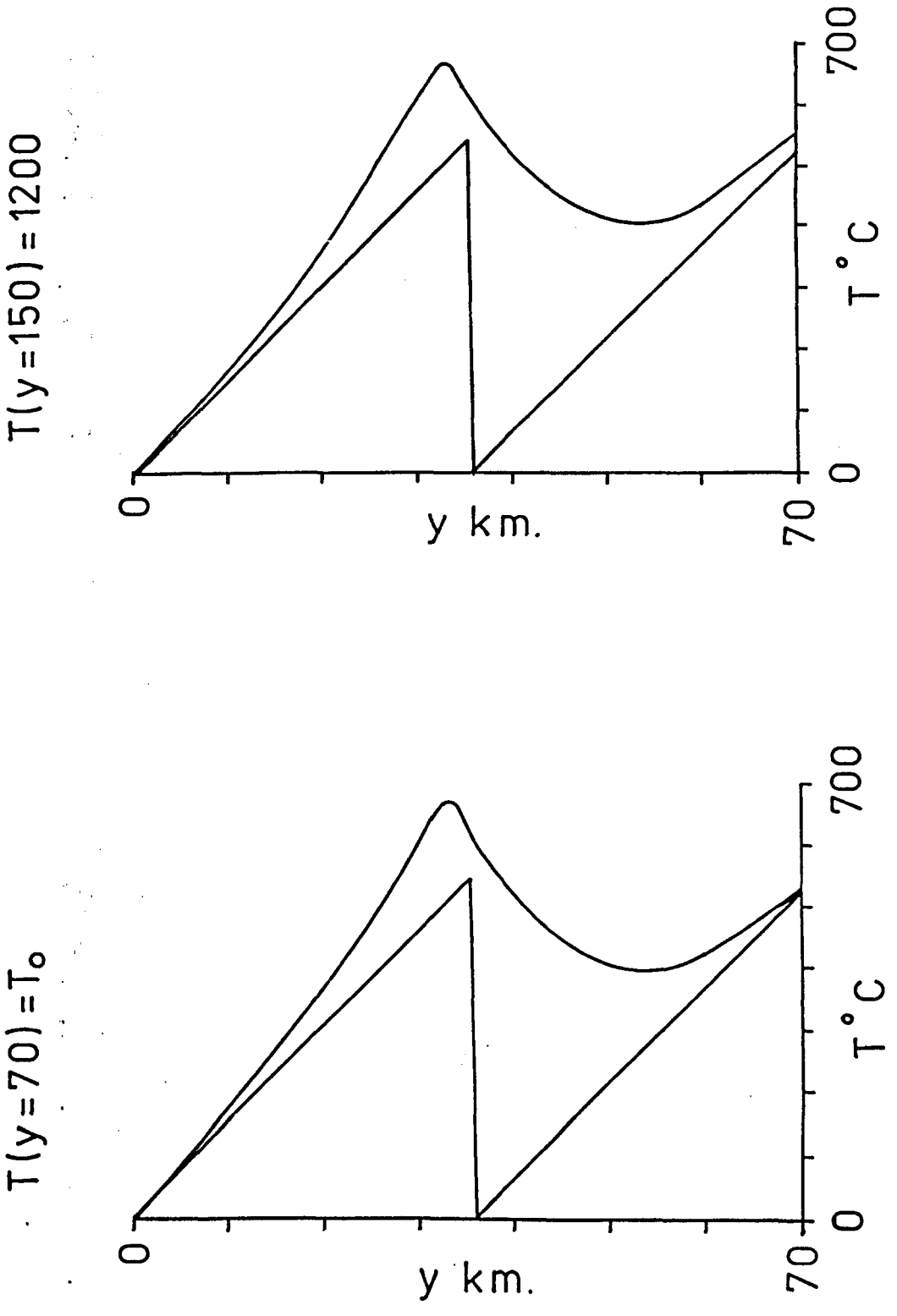

Figure 6.3.2. The velocity and temperature profiles at 5Myr for a thrust 35 km deep in continental shield lithosphere. The left hand diagram has the base of the slab fixed at its initial temperature to show the effect of heat conduction through the base of the model.

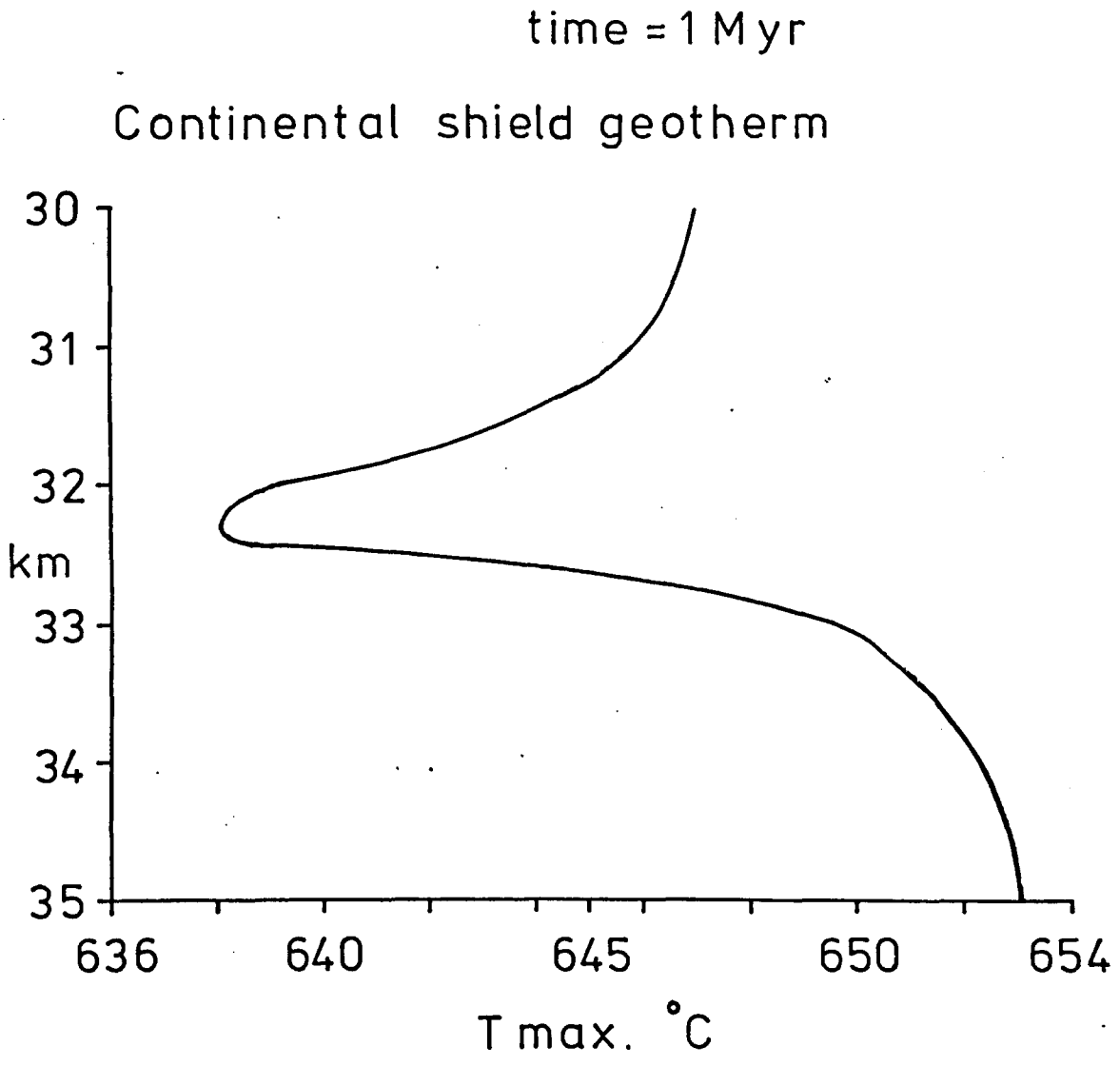

Figure 6.3.3. A plot of depth of thrust versus the maximum temperature reached at a time of 1 Myr for continental shield lithosphere.

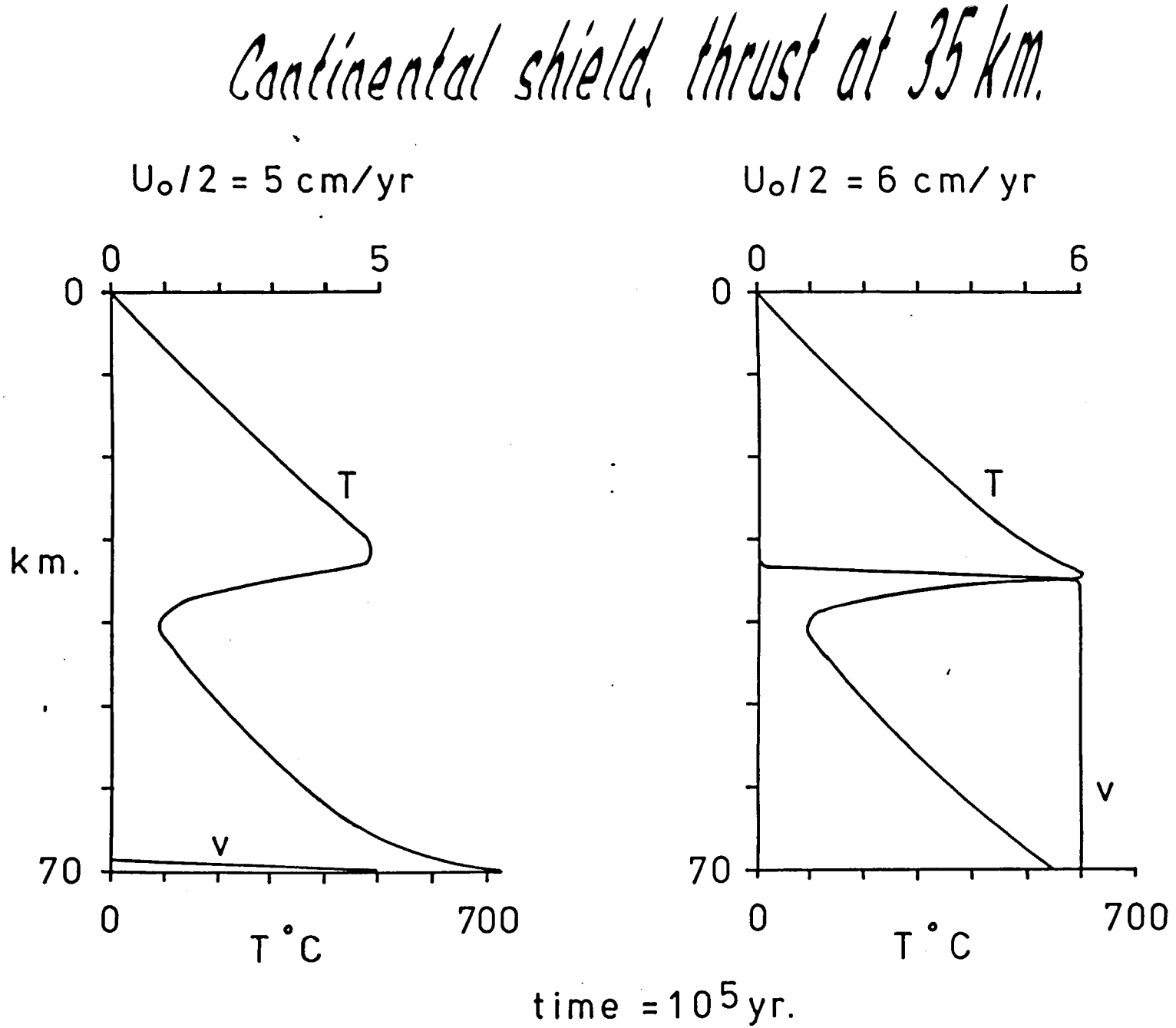

Figure 6.3.4. The velocity and temperature profiles for a thrust 35 km deep in continental shield lithosphere at 10^5 yr. For a shear velocity of 5 cm yr^{-1} no shear localization occurs.

of 6 cm yr^{-1} produces a temperature maximum and a shear localization along the thrust plane. A velocity of 5 cm yr^{-1} fails to produce a localization of shearing along the thrust, the initial temperature inversion relaxing with time. For a given geotherm a plot of the depth of the thrust versus the shear velocity required to maintain thrusting can be produced. Figure 6.3.5 shows such a plot for a continental shield geotherm. Deeper thrusts require higher shear velocities to maintain the thrusting.

The shear stress evolution with time for thrusts is shown in figure 6.3.6. Like normal shears the stress values drop rapidly from high initial values. For a thrust depth of 30 km the shear stress drops to a few kilobars in a million years. Higher shear rates produce more shear heating and causes the stress to decay more rapidly. For deeper thrusts the stress decays faster.

Zones of thrusting and décollement such as those in the Appalachians and Canadian Rockies tend to be shallower than 30-35 km (Brewer et al. 1981). To model a viscous thrust at depths of 15-20 km a higher geotherm must be used to ensure that the temperatures are high enough for dislocation creep processes. A model of thrusting in areas of high geothermal gradient was constructed using the Basin and Range geotherm of Herrin (1972). A thrust at a depth of 15 km will then have an inversion temperature of 500°C. Figure 6.3.7 shows the temperature and velocity profiles for a thrust 15 km deep moving at 5 cm yr^{-1} using a granodiorite rheology.

The behaviour of the thrust is very similar to those modelled using a continental shield geotherm. The shear velocity is localized along the thrust plane and the shear heat produces a thermal anomaly. The lower slab heats up much more rapidly than for the continental shield case, the

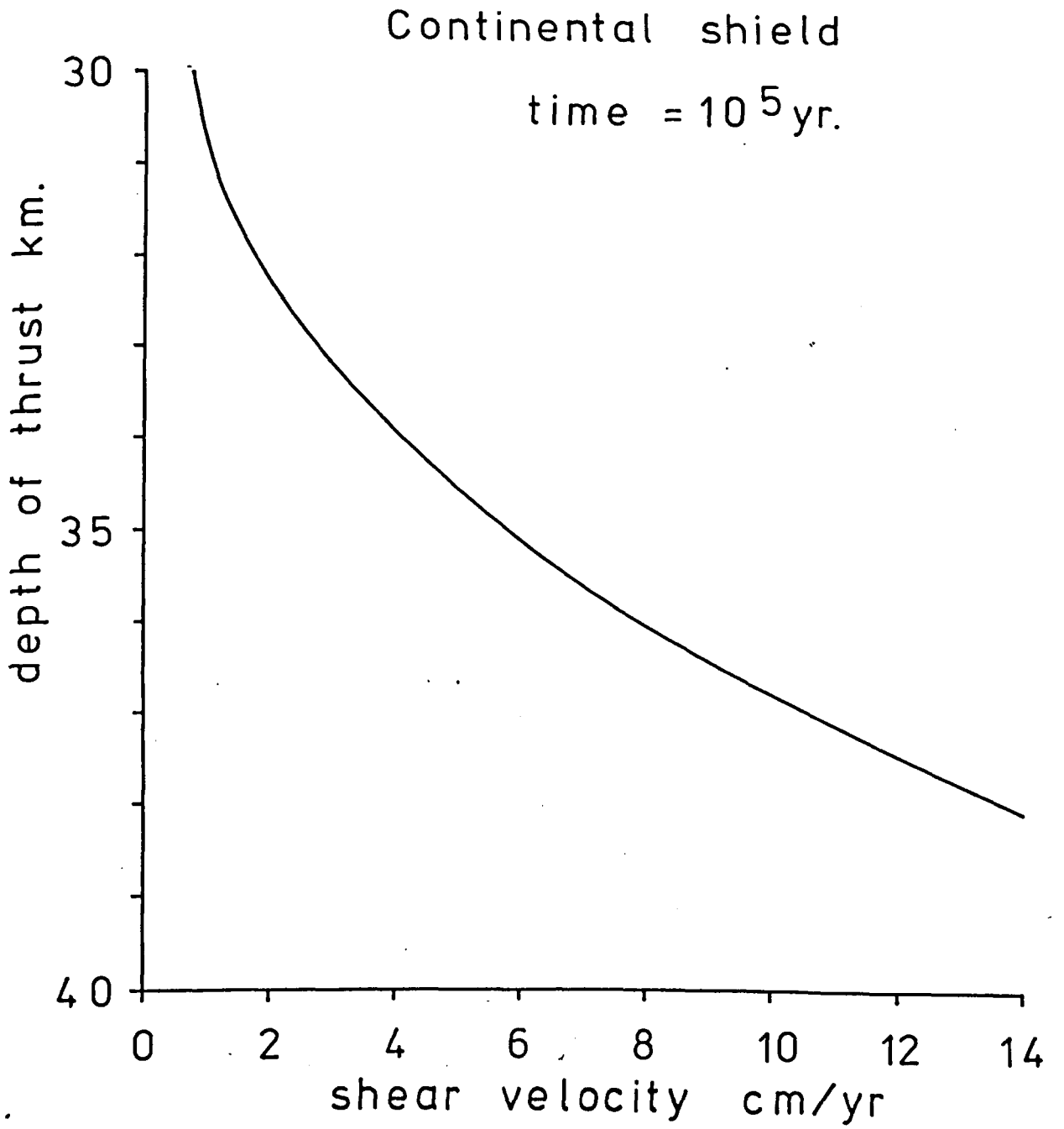

Figure 6.3.5. A plot of the depth of thrust against the critical velocity required to maintain the thrust at a time of 10^5 yr in continental shield lithosphere.

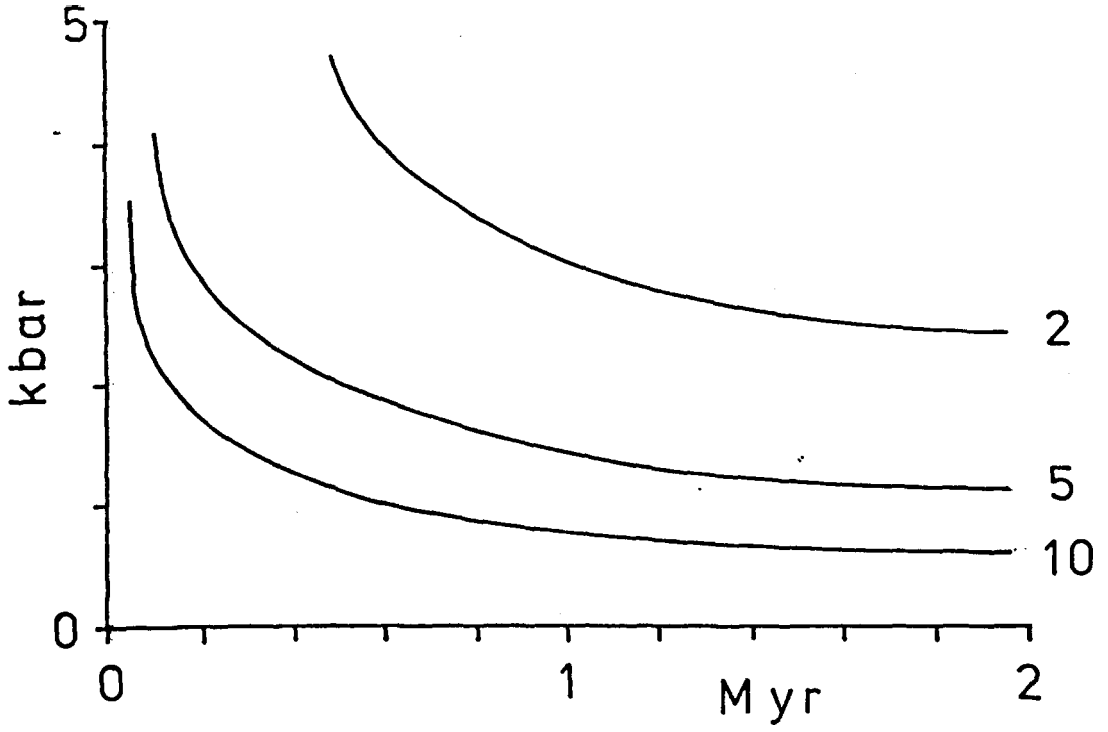

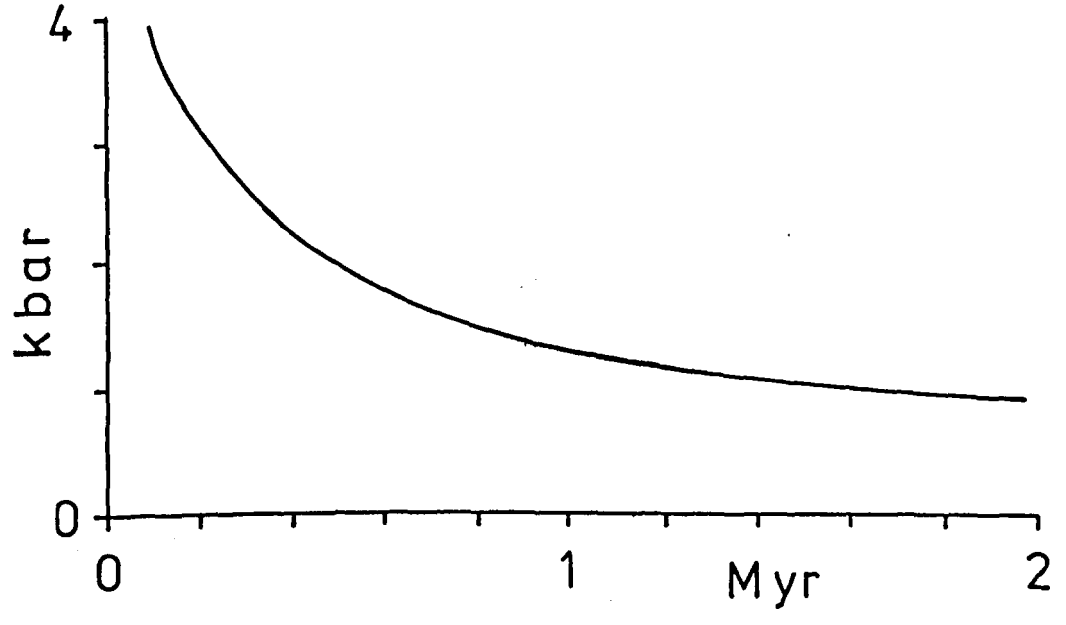

Figure 6.3.6. The temporal evolution of shear stress: (top) for a thrust 30 km deep in continental lithosphere for shear rates of 2,5,and10 cm yr^{-1} and (bottom) a thrust 15 km deep in Basin and Range lithosphere thrusting at 5 cm yr^{-1}.

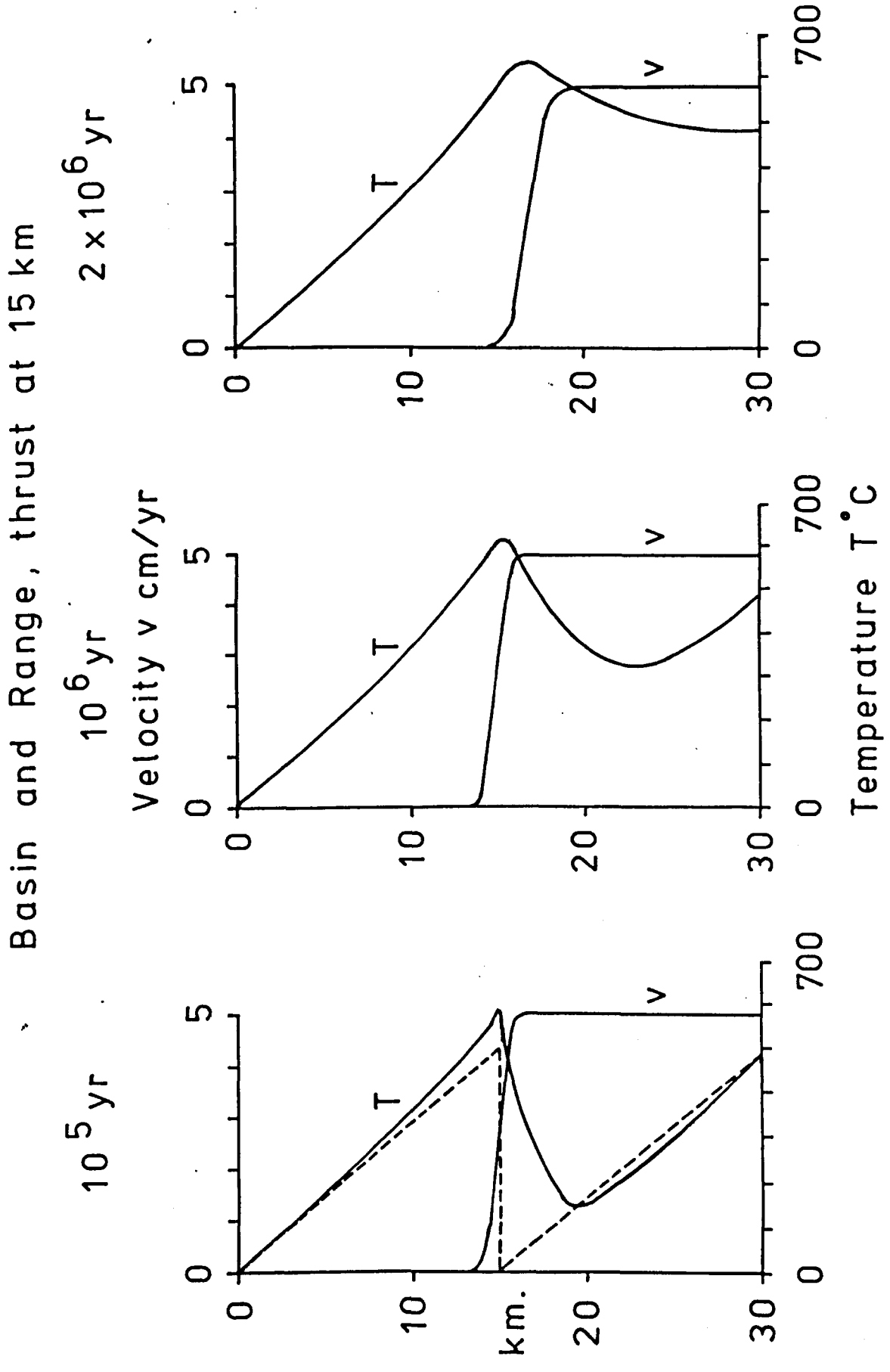

Figure 6.3.7. The temperture and velocity profiles for a thrust 15 km deep in Basin and Range lithosphere moving at 5 cm yr^{-1} for various times.

slab being thinner and more shear heat is produced. After 2 Myr the lower slab has heated up and is almost as hot as the maximum temperature on the thrust plane. Continued shearing is no longer confined to a distinct thrust plane and the deformation is accommodated over a much thicker region extending into the lower slab.

The behaviour of shear stress is similar to the continental shield geotherm model. Figure 6.3.6 shows the decay of shear stress with time for a thrust 15 km deep moving at 5 cm yr^{-1}. After a time of 2 Myr the shear stress has dropped below 1 kbar. Faster shear rates again produce lower stresses.

Generally the Basin and Range geotherm results in the lower slab heating up much more rapidly than for less steep geotherms. The thrusts do not localize the shearing for as long; the thrust becoming a less intense shear zone which progressively thickens downwards into the hot lower slab.

A critical shear velocity exists for the stabilization of shearing on the thrust plane. Figure 6.3.8 shows the critical velocity required to maintain thrusting with a Basin and Range geotherm. For thrust depths of greater than 18 km very high shear rates are required to maintain the temperature inversion on the thrust. The ambient temperature at these levels is so high that shearing occurs over a broad region, no sharp temperature peak forming except at high shear rates.

The shear heating produced by thrusting will produce a change in the surface heat flow above the thrust. Figure 6.3.9 shows heat flow profiles with time for thrusting in continental shield and Basin and Range lithosphere. When thrusting commences at levels of $\sim$30 km in continental shield lithosphere the surface heat flow increases very slowly. After 2 Myr of shearing at 5 cm yr^{-1} the heat flow begins to

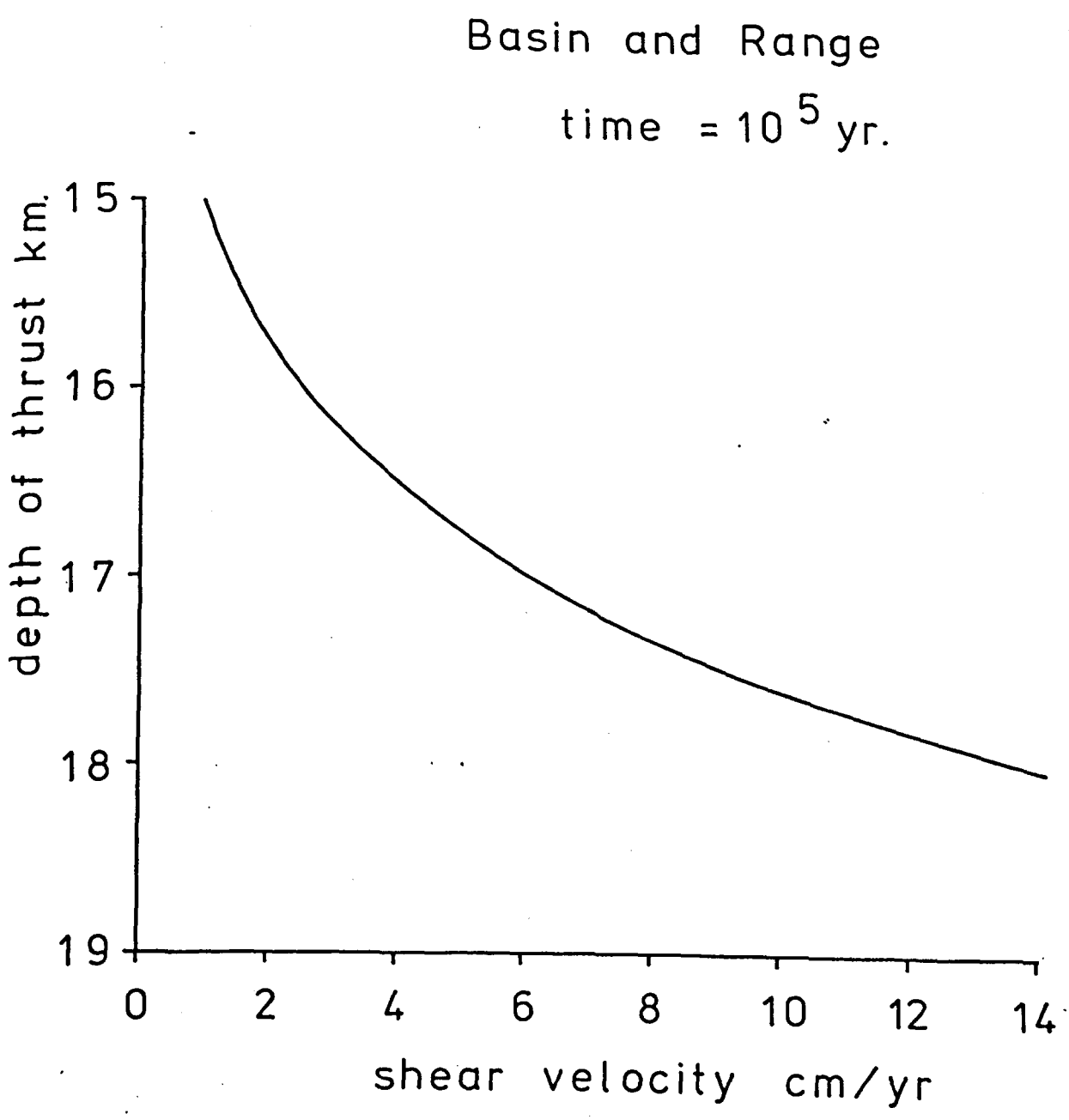

Figure 6.3.8. The depth of thrust versus the critical shear velocity required to maintain the thrust at a time of 10^5yr in Basin and Range lithosphere.

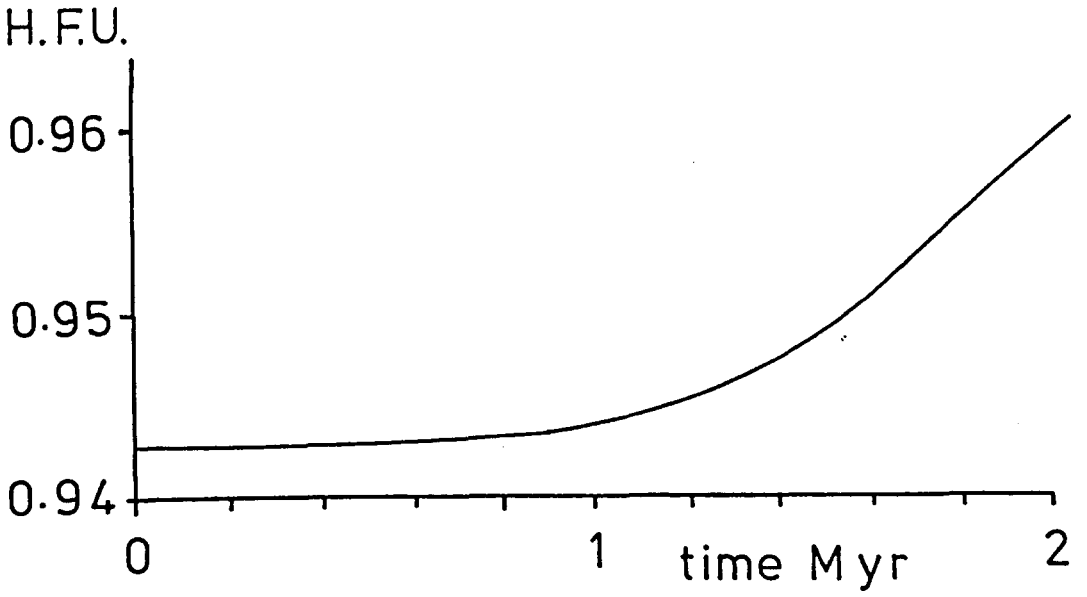

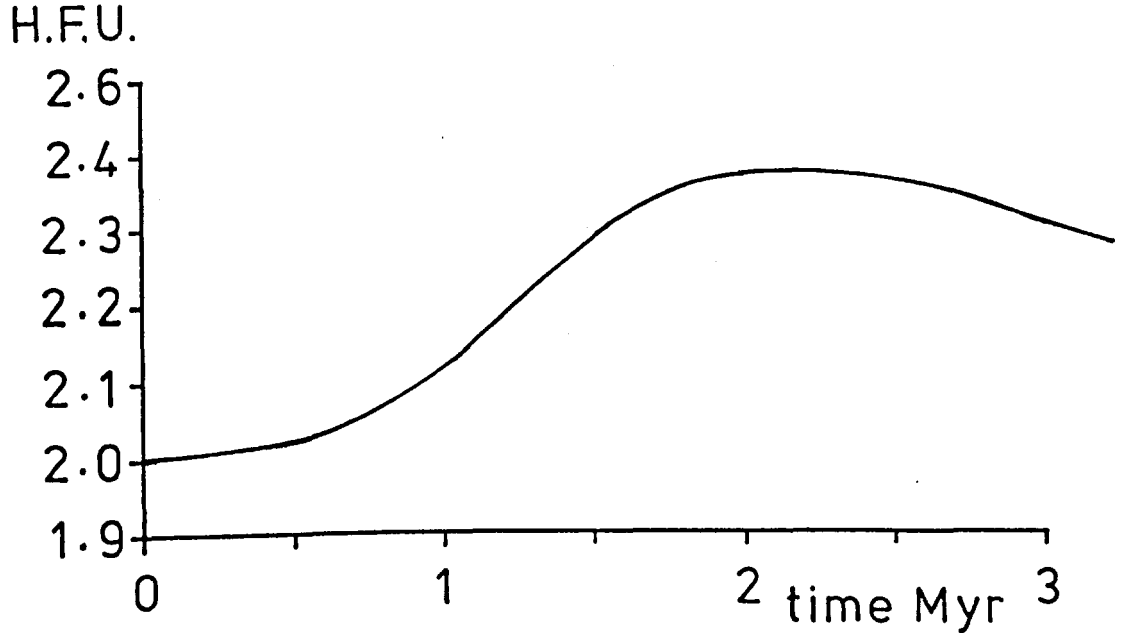

Figure 6.3.9. The temporal evolution of surface heat flow for :(top) a thrust 35 km deep moving at 10 cm yr^{-1} in continental shield lithosphere and (bottom) a thrust 15 km deep moving at 5 cm yr^{-1} in Basin and Range lithosphere.

level off at a peak value which is only 2-3% higher than the initial value. With time the lower slab of the model heats up, the thrust zone ceases to exist and the geotherm slowly returns to its equilibrium value.

For basin and range conditions the surface heat flow increases much more rapidly, the value rising from 2.00 to 2.35 H.F.U. within 2 Myr. Once the lower slab is hot the surface heat flow begins to decay to its equilibrium value.

The depth and the rate of thrusting have a small effect on the surface heat flow. Deeper thrusts produce less surface heat flow and faster thrusts produce more. The variations in heat flow due to changes in depth and thrust rate are very small when compared to the total heat flow due to the initiation of thrusting.

6.4 The constant shear stress thrust model

When constant shear stress conditions are applied to the model the behaviour is very different. Constant stress conditions are often unable to localize the thrusting at the junction of the two slabs. Low stress conditions produce very low shear velocities across the model (e.g. $<10^{-2}$ cm yr^{-1} for 35 km deep and 5 kbar). This produces very little shear heating and the temperature inversion relaxes rapidly. For both continental shield and Basin and Range geotherms a critical shear stress can be determined for a given thrust depth at which thermal runaway will occur. If the stress is high enough the thrust will move rapidly and the large amounts of shear heat will produce thermal runaway.

Figures 6.4.1 and 6.4.2 show the critical shear stress required for runaway at a given thrust depth for continental shield and Basin and Range geotherms respectively. The shallower the depth of the thrust the

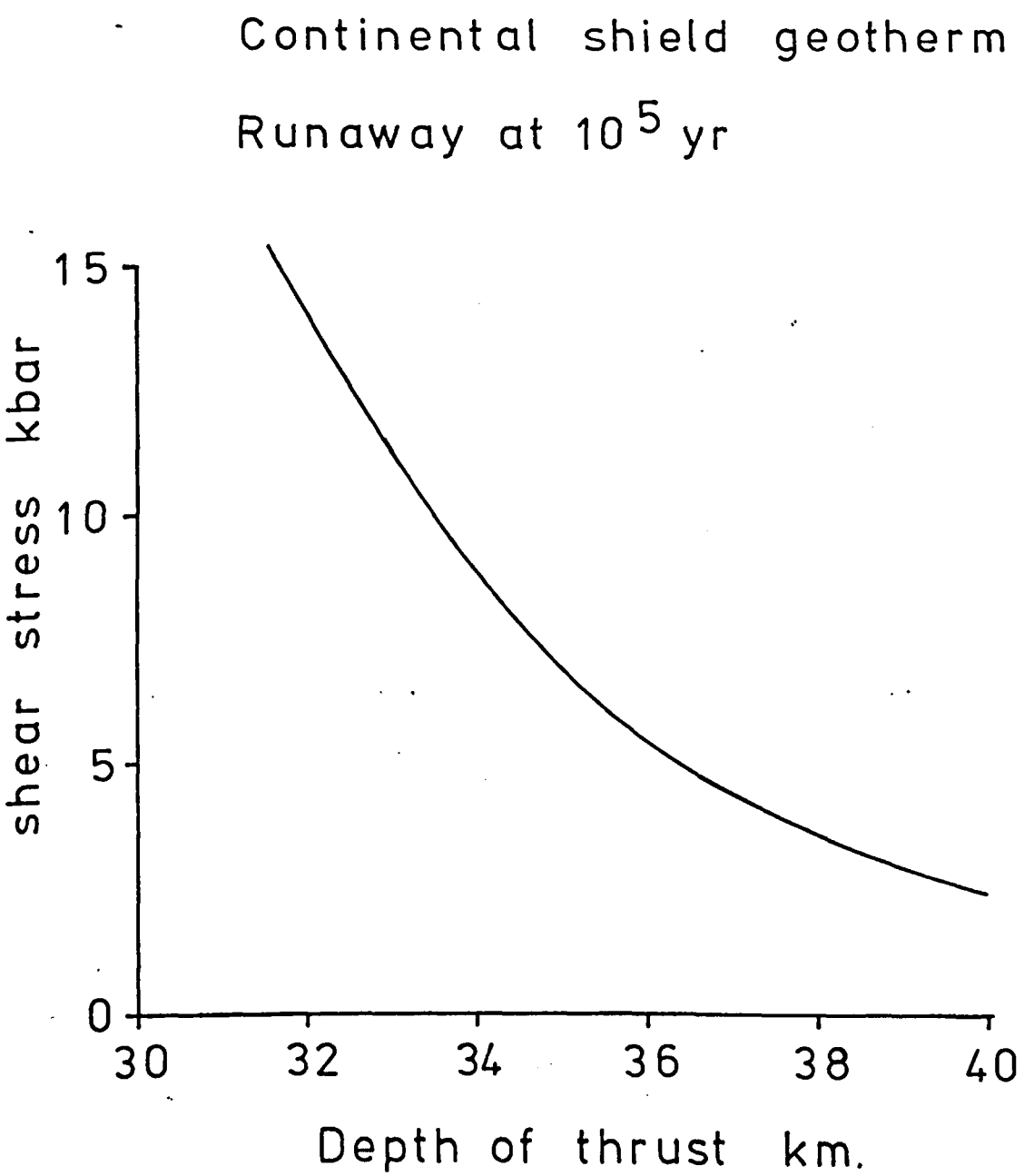

Figure 6.4.1. The critical shear stress required for thermal runaway versus depth of thrust at a time of 10^5 yr for continental shield lithosphere.

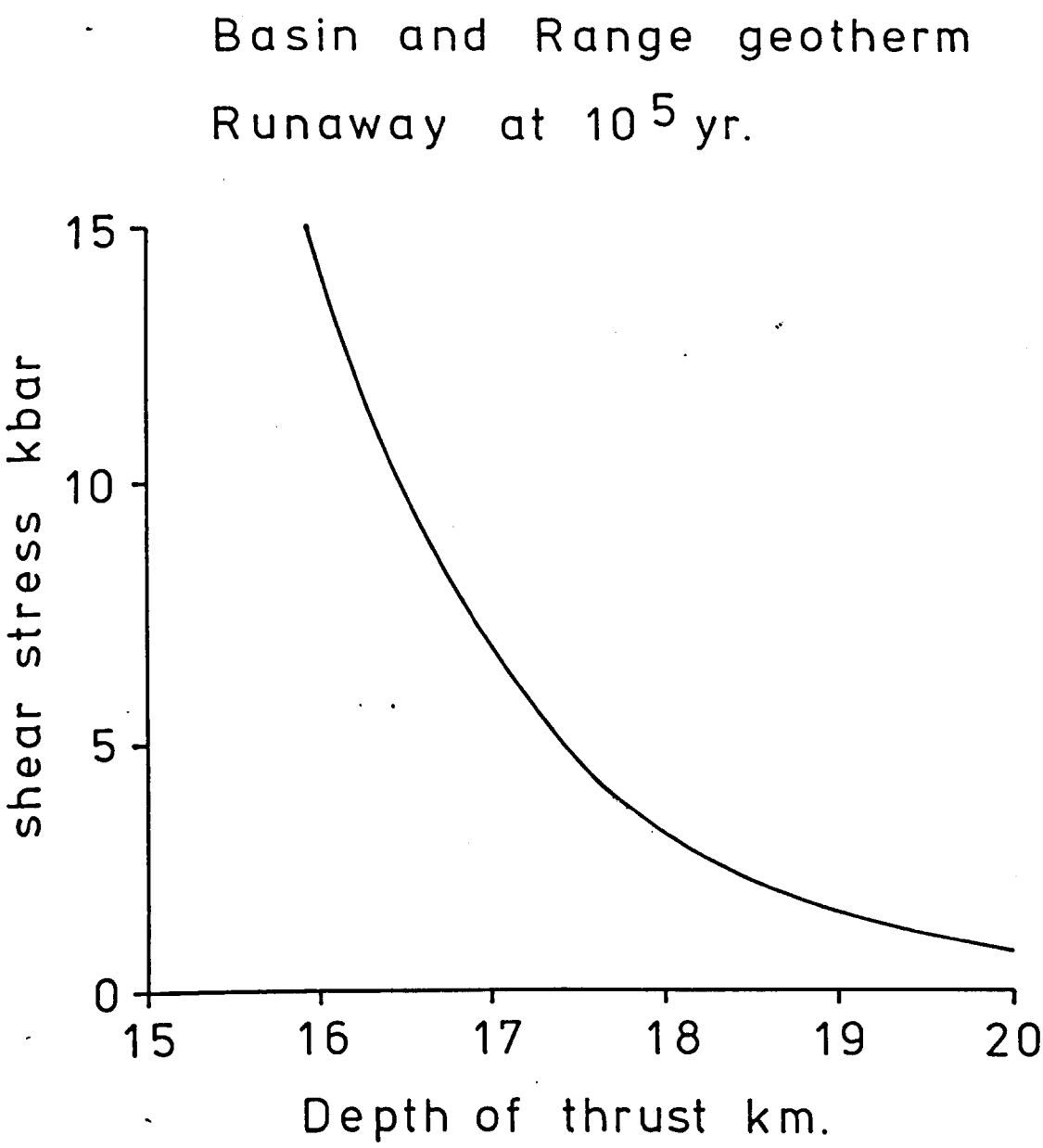

Figure 6.4.2. The critical shear stress required for thermal runaway versus depth of thrust at a time of 10^5 yr for Basin and Range lithosphere.

higher the shear stress required for runaway. This is due to the deeper thrusts having a higher ambient temperature. The stress levels required for runaway are too high to be realised except for some of the deeper thrusts.

6.5 Discussion

The constant shear velocity and constant shear stress thrust models produce very different results. Constant velocity models are applicable to overthrusts driven by collision plate movements. Constant stress conditions are best applied to the base of gravity driven nappes, the stress being due to the weight of the nappe.

All the thermo-mechanical thrust models rely upon the shear heating to maintain an inversion of the geotherm. Constant velocity models have a critical boundary velocity necessary for localization of shearing. Below this critical velocity the shear heating is insufficient to maintain the inversion of the geotherm and no localized thrust exists. With time the lower slab heats up both by shear heating from the thrust and by conduction through its base. When the lower slab has almost returned to its equilibrium temperature, the shear heating on the thrust is insufficient to maintain an inversion of the geotherm and the shearing ceases to be localized on the thrust plane. If the boundary velocity is sufficient to maintain a localized shear zone, it will only do so as long as the lower slab is relatively cool. As the lower slab heats up with time constant velocity models cease to produce localized shearing in all cases.

Deeper thrusts require higher shear velocities to maintain the temperature inversion. The deeper the thrust the higher the ambient temperature. Higher ambient temperatures produce temperature anomalies which are small in amplitude over a wide area, whereas cooler ambient

temperatures produce sharp high amplitude temperature anomalies. At high ambient temperatures high rates of thrusting are required to produce a sufficient temperature anomaly to maintain the geotherm inversion.

Constant shear stress models produce very low strain rates for lower stress values. These strain rates are too low to be of any geological significance and produce little shear heat, the geotherm inversion relaxing rapidly. A critical stress exists for any given depth of thrust at which thermal runaway and very high strain rates occur. In the case of a thrust 20 km deep in Basin and Range lithosphere, the stress required for runaway is in the order of a kilobar. These conditions are possible in the crust and thermal runaway may occur on deep thrusts.

CHAPTER 7

Viscoelastic Shear Zone Models

7.1 Introduction

A characteristic of the viscous models described in the previous chapters is the localization of a narrow shear zone and the development of a large temperature anomaly for constant velocity models. The predicted thermal anomalies across the shear zones are too large and unrealistically high stresses are associated with the initiation of motion. The temperature anomalies generated by the constant velocity model, although insufficient for partial melting, would give rise to large surface heat flow anomalies over transcurrent or transform faults which become shear zones with depth. Studies of the heat flow across the San Andreas fault (Lachenbruch and Sass 1980) have shown no measurable heat flow anomalies.

Consideration of the mathematical formulation of the viscous model suggests that the large temperature anomalies of constant velocity models are associated with the onset of motion. The stresses for the viscous model show an unrealistic near singularity at time t=o and although they decay rapidly to geologically reasonable values, the high initial values produce a large initial shear heating. The high initial shear heating may generate the large temperature anomaly of the viscous models.

The high initial stresses and the associated large temperature anomalies are in part a direct result of using a purely viscous material formulation. To overcome this a viscoelastic model has been constructed which has a more realistic initial stress condition.

The mathematical formulation of the viscoelastic model has been described in section 2.3. The temperature field differential equation

$$\frac{\partial T}{\partial t} = K\nabla^2 T + H'$$

and the force equilibrium equation for a continuum

$$F_i = \ddot{u}_i + \frac{d\sigma_{ji}}{dx_j}$$

must be solved simultaneously for a material with viscoelastic properties. The total strain in the x direction in a Maxwell viscoelastic element is given by

$$\varepsilon_x = {}^1/_E\,\sigma_x - {}^V/_E\,\sigma_y - {}^V/_E\,\sigma_z + \varepsilon_x^v$$

where V is Poisson's ratio,
and similarly for the other directions.

The viscoelastic formulation has been solved by using a coupled finite element and finite difference techniques (see section 3.5). Like viscous models, two boundary conditions can be applied to viscoelastic models,

(i) constant velocity boundary conditions

(ii) constant stress boundary conditions.

These two boundary conditions are described in turn. Conditions of plane strain are assumed throughout.

7.2 The constant velocity viscoelastic model

A rectangular finite element grid was constructed and is shown in figure 7.2.1. Boundary conditions were applied for the constant velocity condition (see section 3.5). The velocity profile produced by a visco-

Figure 7.2.1. Finite element grid showing the temperature boundary conditions.

elastic model, under constant shear velocity conditions and having a uniform initial temperature is a constant gradient. The uniform behaviour of the slab gives rise to constant shear heating across the model, the velocity profile remaining constant with time. To bring about localization of the shear zone a small positive temperature perturbation was introduced to the centre of the model. This was achieved by giving the column of finite elements, along the axis, an average temperature of $10^{o}C$ above the ambient value.

The model was investigated for various boundary velocity and ambient temperature conditions. The stress field produced by the model shows that at any given time the state of stress across the model is constant and is a pure shear. This is consistent with the conclusion in chapter 2 that $\partial\tau/\partial y = 0$. The stress is also constant along the length of the shear zone, allowing the model to be reduced to a one-dimensional problem.

The evolution of shear stress with time for various ambient temperatures is shown in fig. 7.2.2. A dry olivine rheology is used and a boundary velocity of 5 cm yr^{-1} was applied. The model has a width of 140 km and a length of 40 km. The viscoelastic stress evolution differs greatly from that of a viscous model, and shows a major change in behaviour depending upon the ambient temperature. The shear stress increases almost linearly with time until a peak value is reached and then drops to a lower value. For lower ambient temperatures this drop in stress is catastrophic occurring virtually instantaneously and reducing the stress values to effectively zero. This rapid stress drop coincides with extremely high instantaneous shear velocities. The massive amounts of shear heating produced by this rapid shearing produces localized thermal runaway and melts the model along the axis.

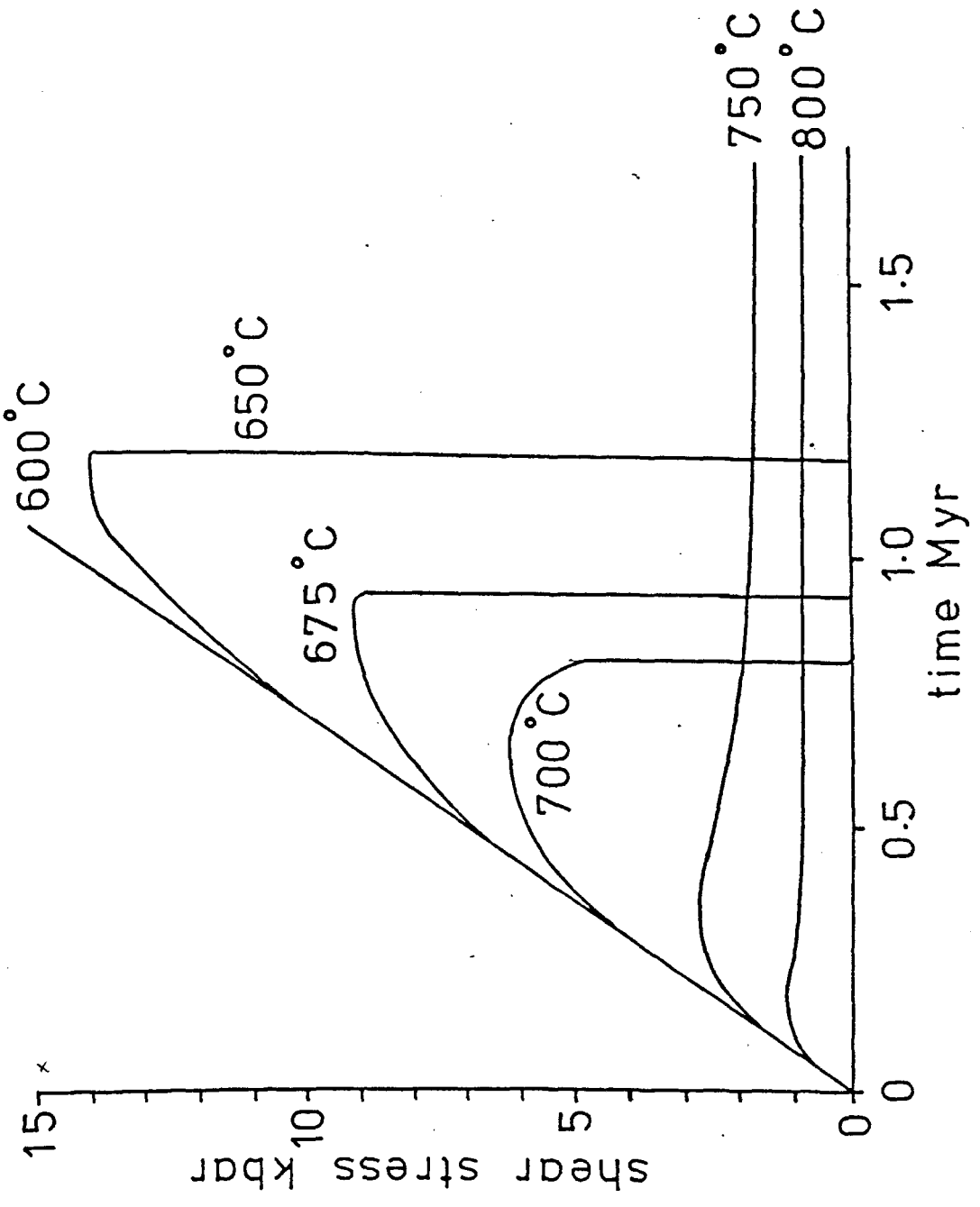

Figure 7.2.2. The temporal evolution of shear stress for various ambient temperatures. $U_o/2$ = 5 cm yr^{-1}, model width = 140 km.

At high values of ambient temperature (>750°C), the elastic energy is relaxed by slow viscous creep, the velocity profiles remaining a constant gradient with time. Small amounts of shear heating are produced, heating up the model and producing a small central temperature anomaly (see fig. 7.2.4). The shear heating produces much smaller temperature anomalies than the viscous model.

From the onset of movement the stress increases linearly with time as elastic energy is stored in the rock. When the stress reaches a maximum, the value depending upon the ambient temperature and shear rate, the stored elastic energy is released by viscous deformation. The elastic energy is relaxed either catastrophically at lower ambient temperatures or gradually at higher ambient temperatures.

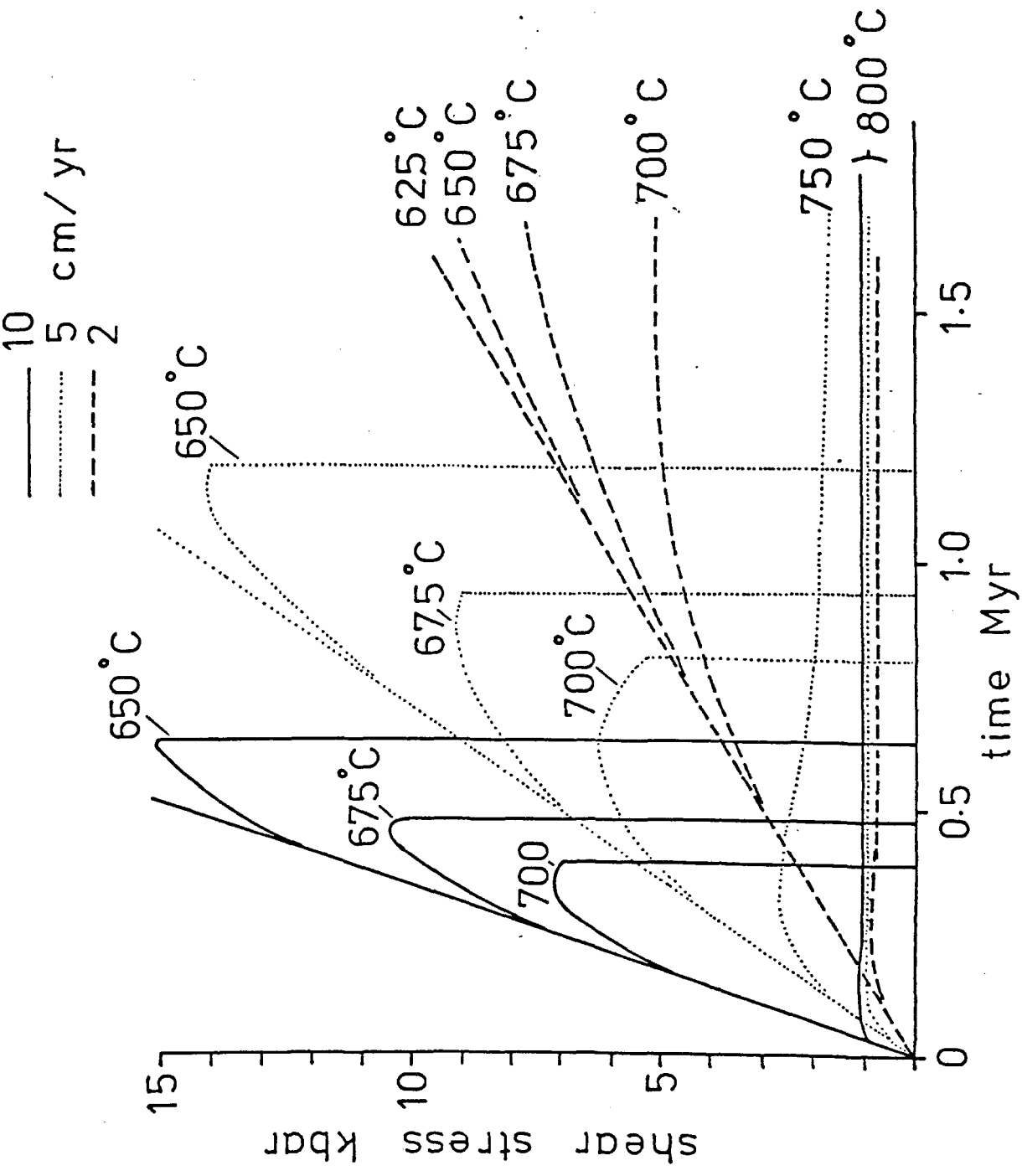

Figure 7.2.3. The temporal evolution of shear stress for various ambient temperatures and shear rates, model width = 140 km.

The velocity and temperature profiles for an ambient temperature of 750°C and shear velocity 5 cm yr^{-1} at various times are shown in fig. 7.2.4. The velocity profile remains a constant gradient with time, and shows no localization of the shearing. The temperature profile shows an even increase across the model with a slight central peak. Both the peak and flank temperatures increase slowly with time. The model heats up much more slowly than the viscous model, the peak temperature is only a few tens of degrees higher than the flank temperatures. The rapid drop in temperature at the edge of the model is due to the edge of the model being fixed at the initial ambient temperature. As the temperature variation across the shear zones is relatively small, the viscosity is fairly constant and the velocity profile remains a constant gradient. Localization of shearing does not occur at the higher temperatures, and consequently there is no catastrophic stress drop.

To bring about localization at these higher ambient temperatures a larger initial destabilizing perturbation is required. The effect of varying the size of the destabilizing perturbation is shown in fig. 7.2.5. A destabilizing perturbation of 100°C produces a small localization of the velocity profiles in the centre of the shear zone. High initial temperature perturbations are conceivable if frictional heating is generated by brittle failure before the onset of ductile deformation. Localization of the velocity profiles can also be brought about by mechanical weaknesses. At high ambient temperatures the localization of any shearing is highly dependent upon the size of any initial temperature or mechanical perturbation.

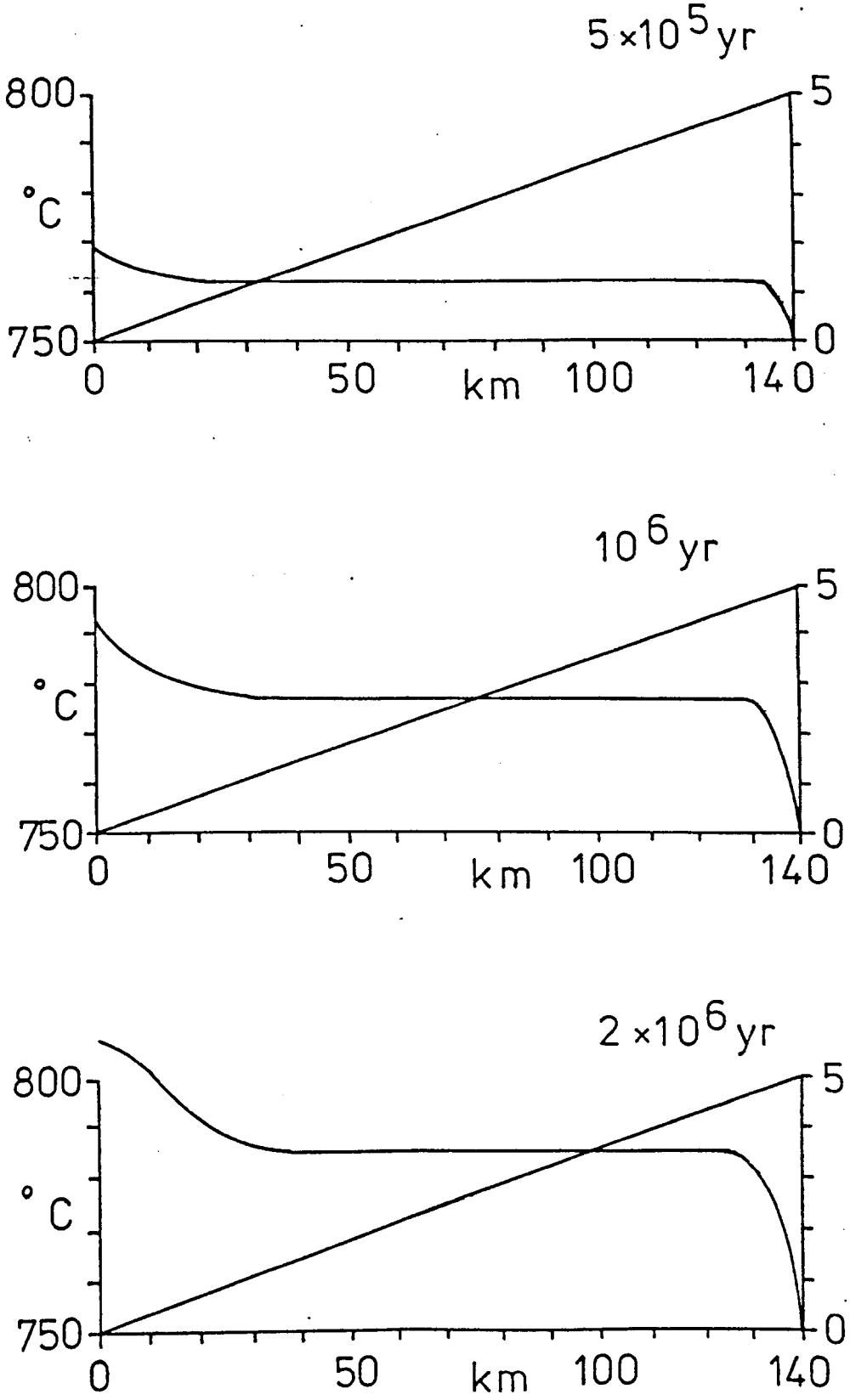

Figure 7.2.4. The velocity and temperature profiles for various times. T_o = 750°C, $U_o/2$ = 5 cm yr^{-1}, model width = 140 km.

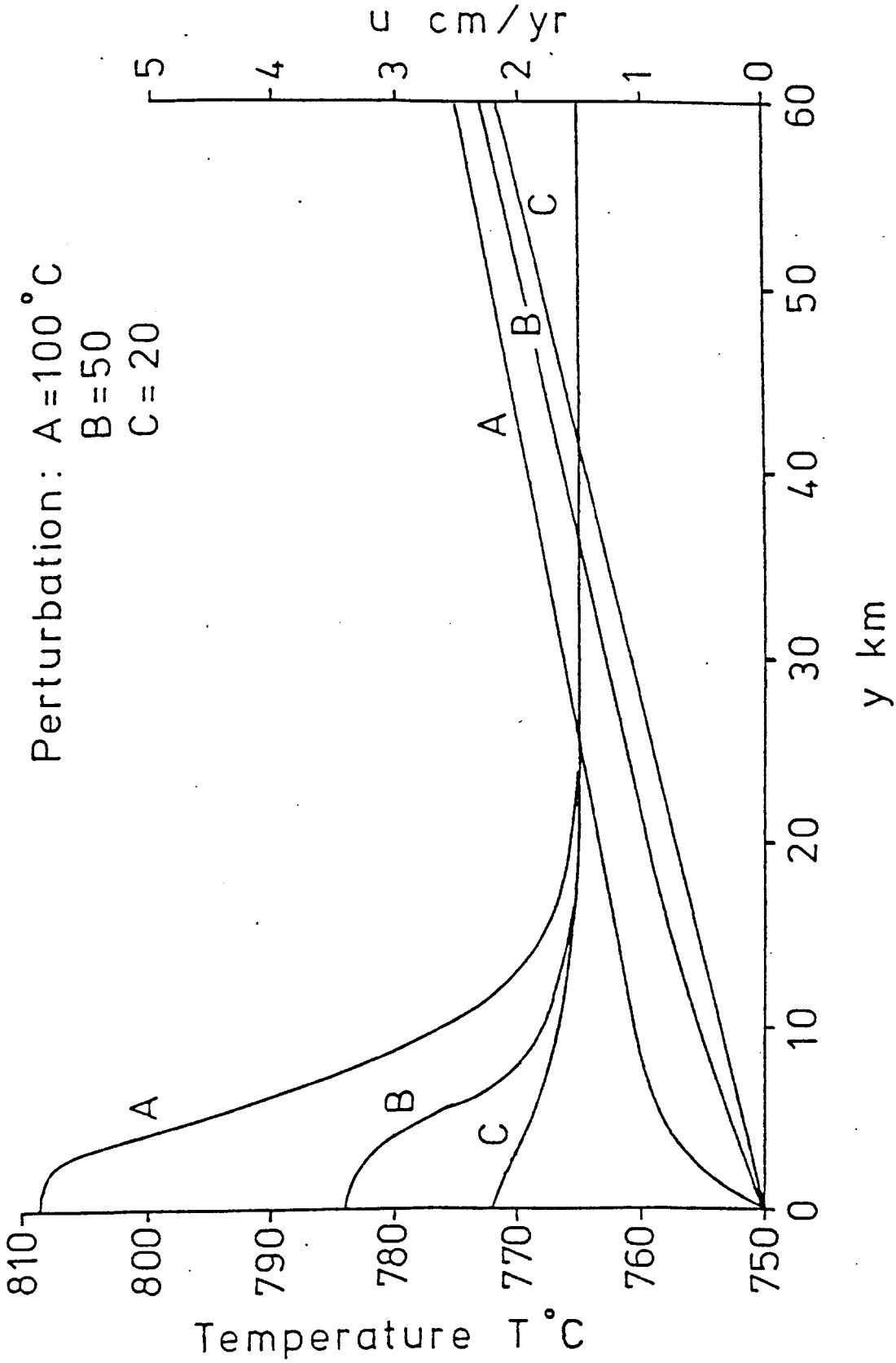

Figure 7.2.5. The velocity and temperature profiles for various destabilizing perturbations. Time = 5 x 10^5 yr, $U_o/2$ = 5 cm yr^{-1}, T_o = 750°C.

At lower ambient temperatures the catastrophic stress drop coincides with massive instantaneous shear velocities. Figure 7.2.6 shows the evolution of the velocity and temperature profiles during the stress drop and thermal runaway for an ambient temperature of 650°C and a shear rate of 5 cm yr^{-1}. The velocity and temperature profiles are shown for three successive time increments of the finite element program, the increment length being 1 second. The first iteration shows the constant gradient velocity profile just prior to the catastrophic stress drop. The temperature profile shows that some shear heating has already occurred due to the previous shearing. The second increment shows a marked increase in the temperature and the development of shear rates of the order of 10^3 cm yr^{-1}. The third iteration shows the temperature to have reached melting point in the centre of the model and the velocity is now 10^4 cm yr^{-1}.

The precise nature of this "viscoelastic rebound" is difficult to study. The stress decay occurs so rapidly that the finite element model must require a great deal of computer time. The data shown in fig. 7.2.6 used a time increment of 1 second, but increments as small as 10^{-8} second have been used. A one dimensional finite difference solution to the problem has been constructed by N.J. Kusznir to ease the problem of computation time and give greater time resolution. The viscoelastic rebound occurs in times of less than 1 second, often as rapidly as 10^{-4} second, and generates instantaneous shear velocities of the order of 10^7 cm yr^{-1}. Movement such as this could potentially be seismic in nature.

The viscoelastic rebound occurs as a result of the viscous deformation relaxing the stored elastic energy. The rebound will be affected by parameters such as shear rate, the width of the model, Young's modulus

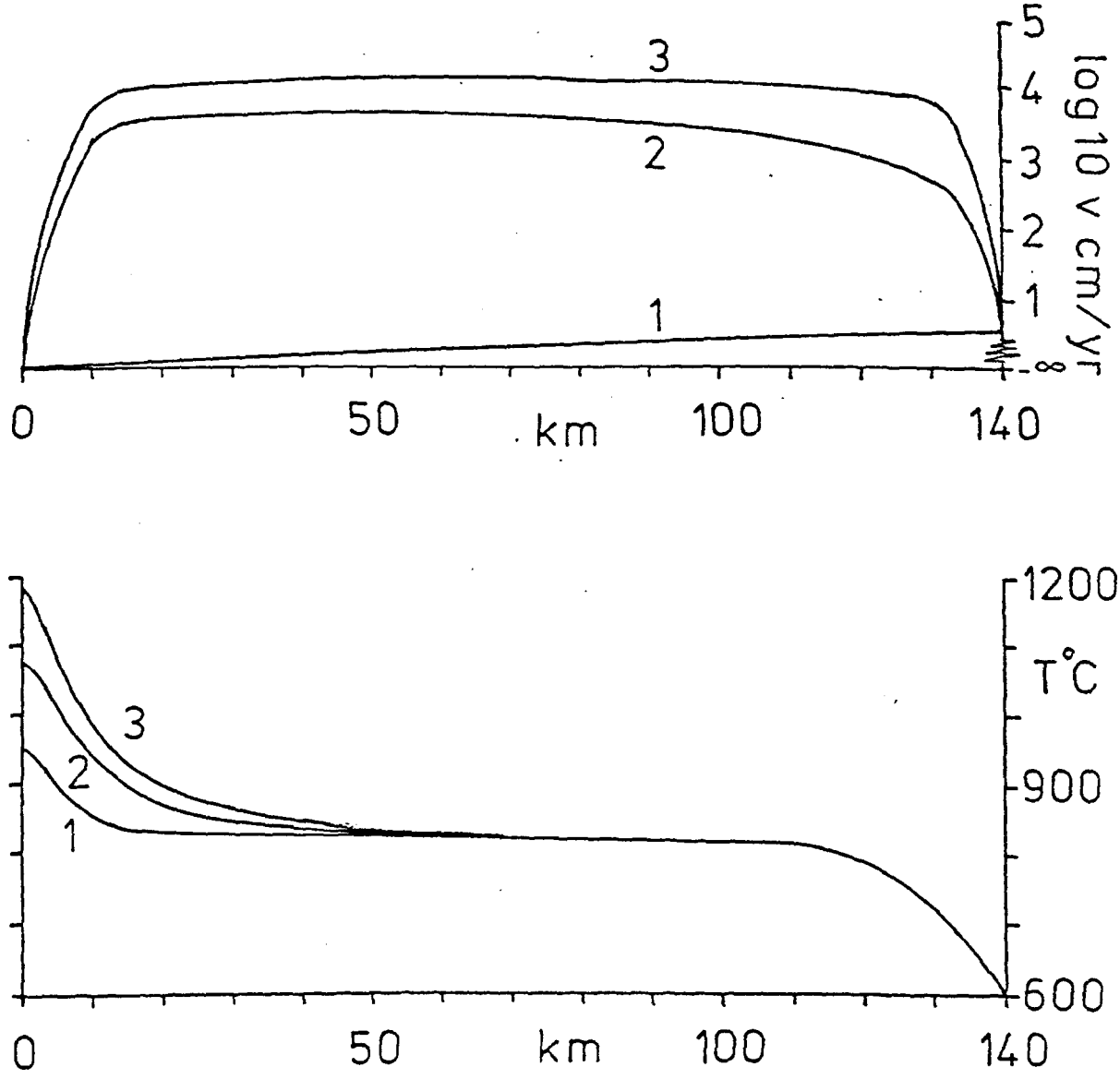

Figure 7.2.6. The velocity and temperature profiles for three successive time increments of 1 second duration at the point of viscoelastic rebound. T_o = 650°C, $U_o/2$ = 5 cm yr^{-1}. τ = 14.1 kbar, time = 1.175 Myr, W = 140 km. Note logarithmic velocity scale.

and the apparent viscosity. The narrower the model for a given shear rate, the faster the elastic energy is built up. However the narrower the model the smaller the total amount of elastic energy that can be stored. The stress evolution curves for a model with a half width of 100 km is shown in fig. 7.2.7. The data presented in this diagram is a combination of results from finite element and a one dimensional finite difference solution. The profile for an ambient temperature of 650^{o}C shows a second smaller rapid stress drop occurring some 10^{5} yr after the first. After the second stress drop, the stress builds up to a more or less steady state. These second stress drops and the build up to a steady state is not resolvable by the finite element model due to the large number of iterations required.

The maximum peak temperatures reached in a shear zone and its variation with time also reflects the rapid stress drops. For an ambient temperature of 600^{o}C the maximum temperature only increases by a few degrees until the beginning of the stress drop. At this point the maximum temperature rises very rapidly until the melting temperature of 1200^{o}C is reached (fig. 7.2.8). Once the melting temperature is reached the shear stress decays rapidly and only small amounts of shear heat are then produced. The peak temperature then decays fairly rapidly with time. An ambient temperature of 650^{o}C produces two sharp peaks in the maximum temperature profile. The second peak is smaller and does not reach the melting temperature. At the higher ambient temperature of 700^{o}C only a single peak occurs but this does not reach the melting temperature. When an ambient temperature of 800^{o}C is studied the maximum temperature increases slowly with time and does not have a sharp peak. This coincides with the absence of viscoelastic rebound at these temperatures. Even though

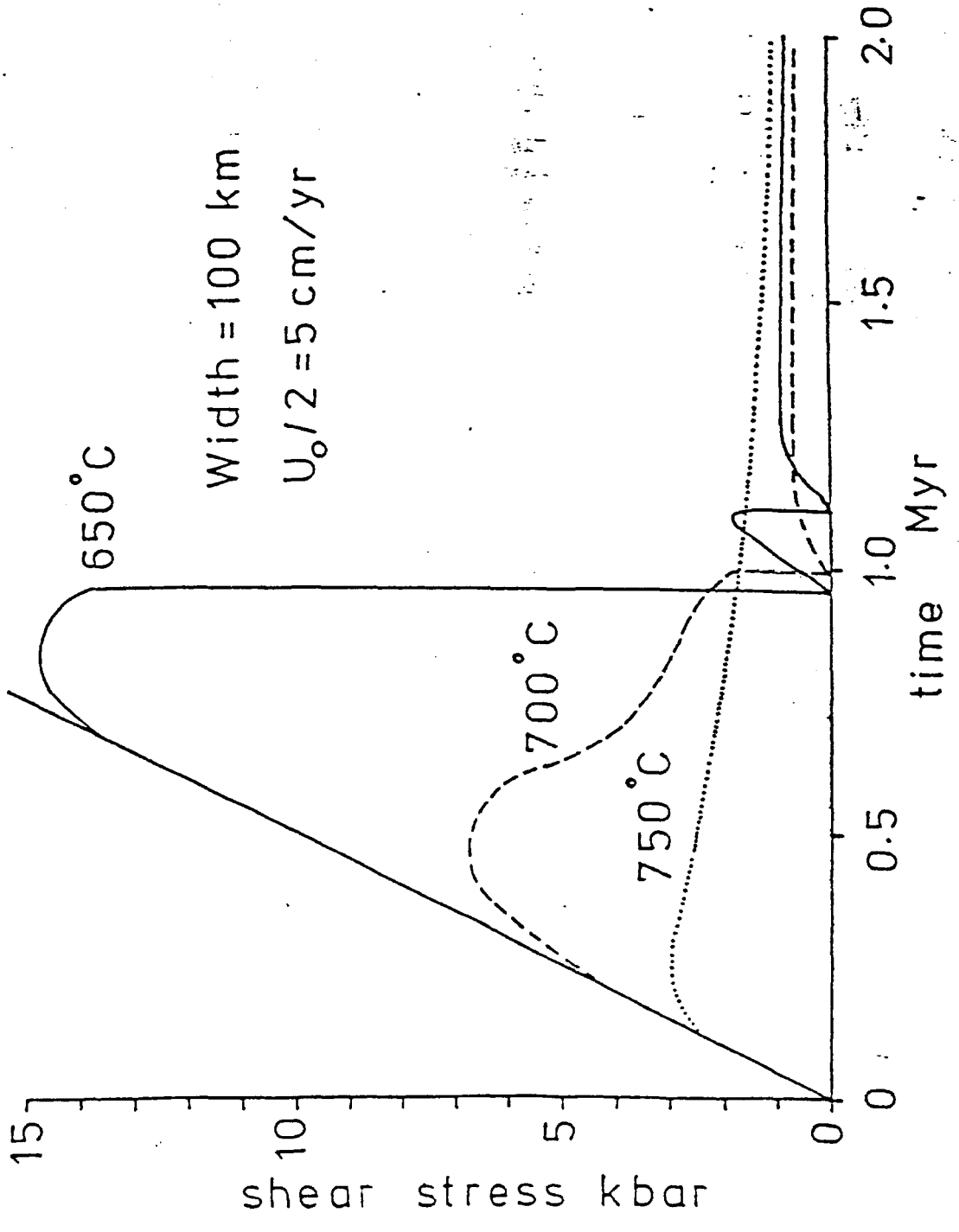

Figure 7.2.7. The temporal variation of shear stress for various ambient temperatures. $U_o/2$ = 5 cm yr^{-1}, width of model = 100 km.

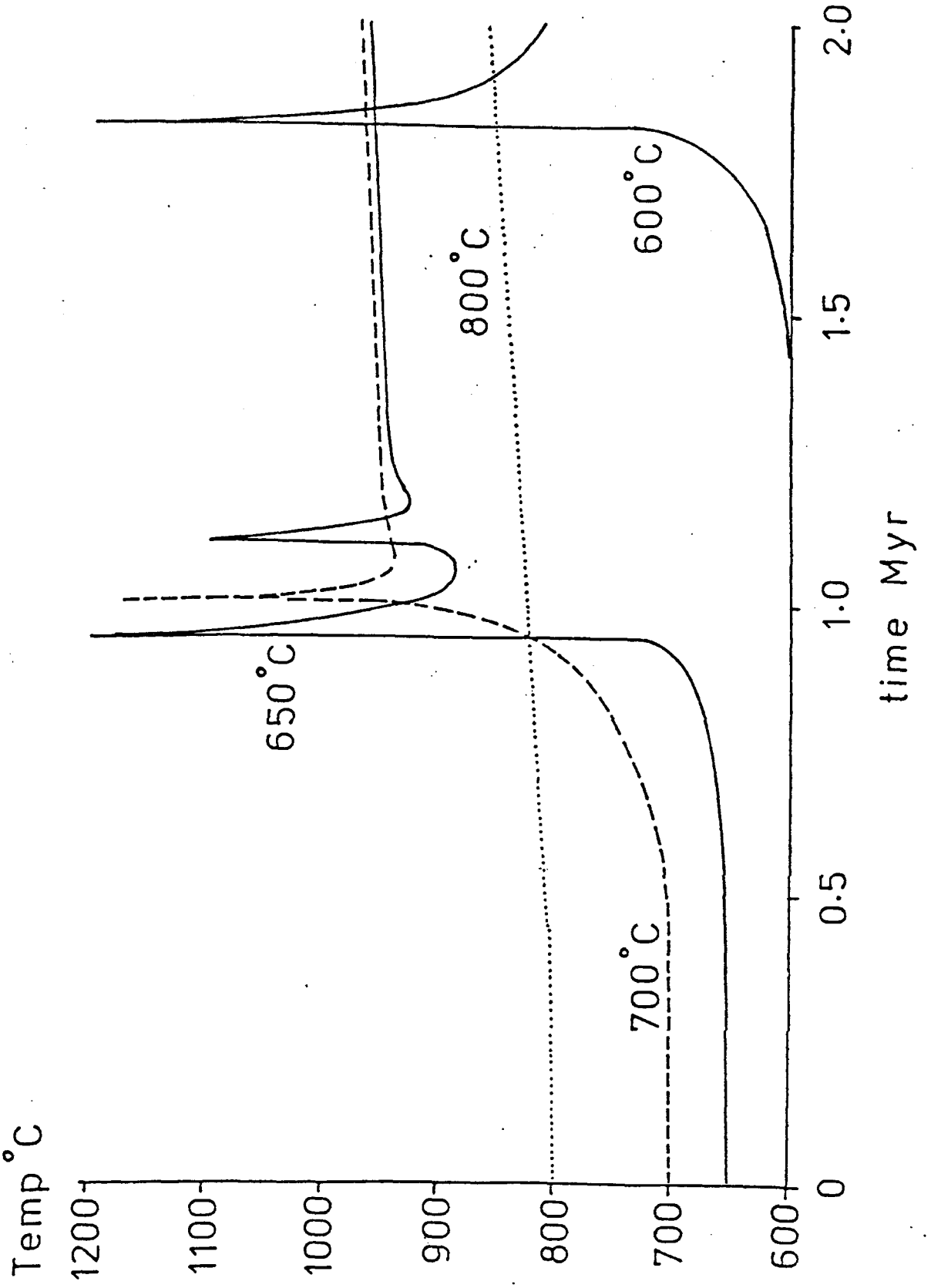

Figure 7.2.8. The variation of maximum temperature in the shear zone with time for various ambient temperatures. $U_o/2$ = 5 cm yr^{-1}. Model width = 100 km.

sharp peaks occur in the maximum temperature profiles at lower ambient temperatures, the maximum temperature increases slowly after the sharp peaks have decayed. At this point the maximum temperatures reached are very similar to those of the viscous model. Once viscoelastic rebound has occurred and the behaviour has become more gentle in variation the viscoelastic model begins to resemble the viscous model. Lockett and Kusznir (in preparation) have shown that the two models tend to converge with time.

The constant velocity viscoelastic model has two contrasting styles of behaviour. At higher ambient temperatures, the stress reaches a maximum and then decays slowly. Shear heat production is fairly uniform across the model and the velocity profile shows no localization of shearing, remaining a constant gradient with time. At lower ambient temperatures the stress rises to high values and is released catastrophically and is accompanied by viscoelastic rebound. This process may be seismic in nature. The occurrence of this viscoelastic rebound produces a possible mechanism for deep focus earthquakes. The rebound occurs at high temperatures greater than 600^{o}C but probably less than 700^{o}C. Under subduction zone conditions, creep deformation at high temperatures such as this would relax any stresses in the subducting plate before they could overcome the high confining pressure to fail by a brittle process (e.g. in accordance with a Griffith type failure criterion). The viscoelastic rebound phenomena could produce seismic events without brittle failure. This is discussed in more detail in the next chapter.

7.3 The constant shear stress viscoelastic model

By theoretical considerations alone the viscous and viscoelastic constant stress models should be very similar.

The viscoelastic shear velocity can be defined as (section 3.4)

$$\frac{du}{dy} = \frac{2(1+\nu)\dot{\tau}_{xy}}{E} + \frac{\tau_{xy}^{n}}{A \exp(BT_m/T)}$$

The shear velocity u in the x direction is therefore

$$u = \int_0^y \frac{du}{dy}\, dy'$$

$$= \int_0^y \frac{2(1+\nu)\dot{\tau}_{xy}}{E}\, dy' + \int_0^y \frac{\tau_{xy}^{n}}{A \exp(BT_m/T)}\, dy'.$$

Since at any given time the stress across the shear zone is constant

then $$\frac{\partial \tau_{xy}}{\partial y} = 0$$

So $$u = \frac{2(1+\nu)\dot{\tau}_{xy}}{E} \int_0^y dy' + \tau_{xy}^{n} \int_0^y \frac{1}{A \exp(BT_m/T)}\, dy'$$

Apart from the initial situation when $\tau_{xy} = o$, the viscoelastic velocity profiles are identical to the viscous solutions. Identical velocity profiles will produce identical temperature profiles for the two types of model.

The displacements "d" for the two models are different. The displacement for a viscoelastic material is given by

$$d = \int_o^t u \, dt'$$

So

$$d = \int_o^t \frac{2(1+\nu)}{E} \dot{\tau}_{xy} \, y \, dt + \int_o^t \int_o^y \frac{\tau_{xy}^n}{A \exp(BT_m/T)} \, dy' \, dt$$

$$= \tau_o \frac{2(1+\nu)}{E} y + \int_o^t \int_o^y \frac{\tau_{xy}^n}{A \exp(BT_m/T)} \, dy' \, dt$$

where τ_o is the initial stress.

The viscoelastic model shows the same response to variations in shear stress and ambient temperature as does the viscous model (see section 4.3). The behaviour of the constant stress model is best summarised by defining the stress-temperature conditions necessary for thermal runaway. Figure 7.3.1 shows a pair of thermal runaway curves for both and viscous and viscoelastic models under comparable conditions. The curves are identical showing that the two numerical models give good agreement. For constant stress models the viscous formulation gives a perfectly adequate representation of shear zone behaviour.

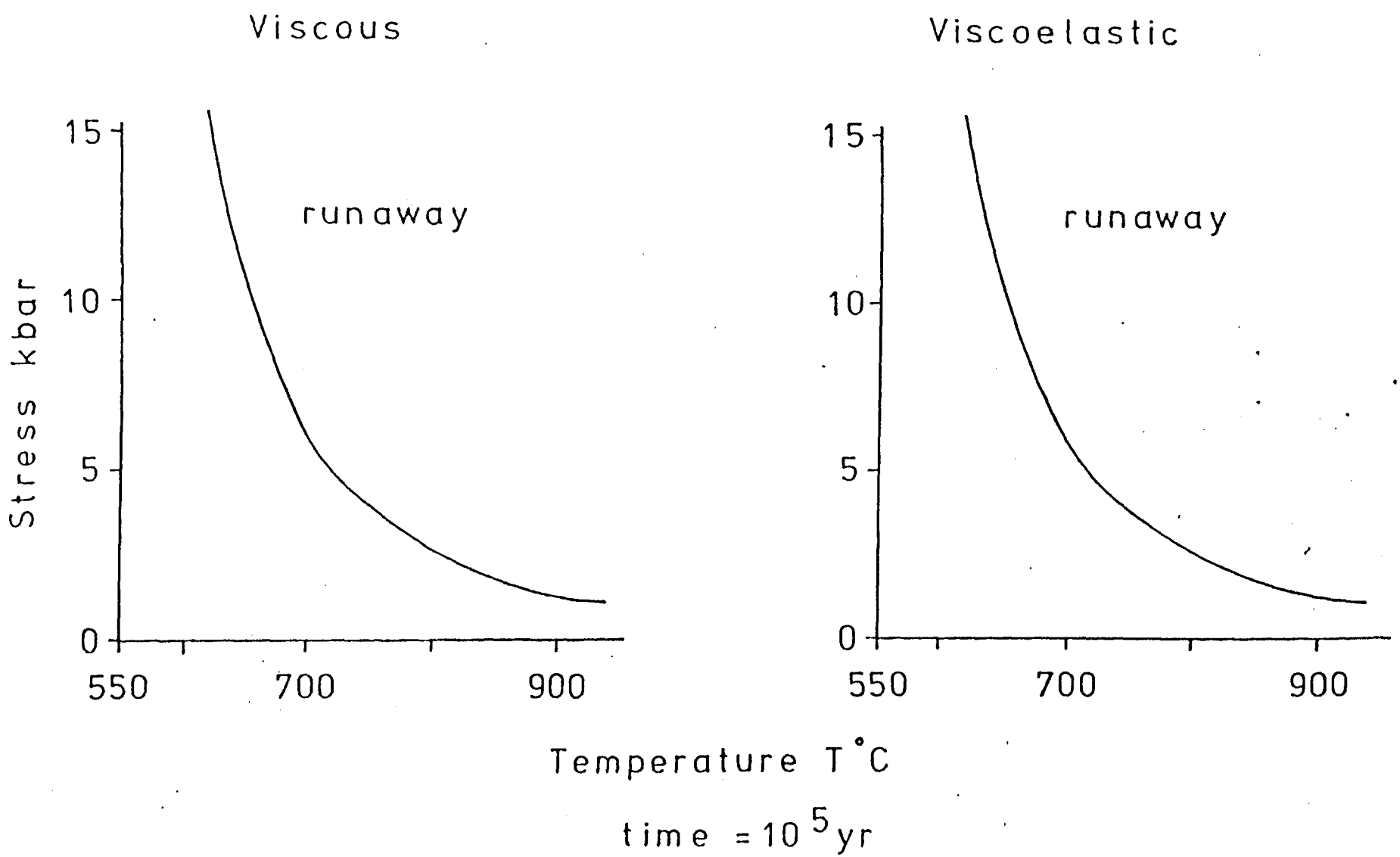

Figure 7.3.1. A comparison of the stress-temperature conditions for viscous and viscoelastic models at 10^5 yr.

CHAPTER 8

Discussion and Conclusions

8.1 General review of viscous and viscoelastic models

From the previous chapters it can be seen that the thermo-mechanical viscous ductile shear model can be used to describe the evolution of ductile shear zones and thrusts within the earth. The viscous model can be divided into constant shear velocity and constant shear stress types. The behaviour of the two models is very different.

Constant velocity conditions are characterised by narrow intense mechanical shear zones which broaden with time. A large temperature anomaly exists which is approximately an order of magnitude wider than the mechanical deformation zone. The temperature anomaly increases with time but never reaches melting temperatures. Both ambient temperature and shear rate have a marked effect on the evolution of the shear zone. Lower ambient temperatures produce narrower more intense shear zones with large temperature anomalies. At higher ambient temperatures the mechanical deformation zone and temperature anomaly become very broad and the magnitude of the temperature anomaly becomes much smaller. When ambient temperature is related to depth it can be shown that shear zones broaden with depth.

The width of the constant velocity viscous model is unimportant in most cases providing the boundary temperature conditions are sufficiently remote. The width of the model only affects the behaviour for the first 5000 yrs or so and this is rapidly swamped by later developments. If the model is constrained to be very narrow (i.e. tens of meters) very high shear rates are required to maintain a thermal anomaly and thermo-mechanical stabilization.

The stress behaviour of the viscous models shows a near singularity in the stress at time t=o. The shear stress rapidly decays from the unrealistic values to give geologically plausible values after a million years or so. This high initial stress is an effect of using a purely viscous formulation and must impair the resolution of the model during the early evolution. The viscoelastic model was developed to evaluate the effect of this high initial stress and to overcome the associated problems.

The constant stress viscous model shows a much simpler behaviour than the constant velocity model. For lower values of stress and ambient temperature very small shear velocities are generated and the initial temperature perturbation diffuses through the model. The strain rates generated at low temperatures and stresses are geologically insignificant. A critical temperature and stress level exists above which thermal feedback instability occurs. At these stress levels so much shear heating is generated that it cannot diffuse through the model fast enough, and the viscosity drops dramatically localizing all further shearing. Once this critical level is reached thermal feedback will produce thermal runaway and melting of the shearing rock. High ambient temperatures and stresses are required for thermal runaway. These stress levels could only exist in very limited environments in both space and time.

The majority of the models studied have used a dry olivine rheology. Dolerite and granodiorite rheologies behave similarly and differ from dry olivine in detail only. If models are constructed using a mixture of rock types, the deformation preferentially occurs in the softest part of the model.

The viscoelastic model was constructed to evaluate the problems associated with the high initial stresses of the ductile model. The viscoelastic model may be solved for the same boundary conditions as the

viscous model. For constant shear stress conditions the viscous and viscoelastic models are identical except for the initial elastic deformation associated with the viscoelastic model. This initial elastic deformation is small compared to the viscous deformation and very rapidly becomes insignificant. The simpler viscous model gives a perfectly good representation of the behaviour of a constant stress shear zone.

For constant velocity boundary conditions the viscoelastic model differs greatly from the viscous model. At higher ambient temperatures the velocity profiles are constant gradient and the temperature anomalies are broad and have a small amplitude. This is not too dissimilar to the viscous model. At lower ambient temperatures however, the viscoelastic model shows the phenomenon of "viscoelastic rebound". The stress evolution shows a constant increase with time as elastic energy is stored in the model. When a critical stress level is reached viscoelastic rebound occurs and the stress drops to almost zero virtually instantaneously. The velocity profile changes from a constant gradient to a very highly localized shear zone with extremely large instantaneous velocities. These very high velocities are associated with rapid shearing and produce large amounts of shear heating and bring about thermal runaway and melting in the centre of the shear zone. As the stress drops very rapidly the shear heating is short lived and the rock very rapidly cools down as the model returns to a more even phase of development.

Once the viscoelastic rebound has occurred and the stored elastic energy has been released the temperature and stress profiles show a much more gentle evolution with time. The values of stress and temperature at these times is very similar to those predicted by the viscous model. It has been shown by Lockett and Kusznir (in preparation) that the constant velocity solutions of the viscous and viscoelastic models converge with

increasing time. The main difference between the two models is the high initial stresses of the viscous model compared with the stresses of the viscoelastic model. The size of the initial destabilizing perturbation is much more important in the viscoelastic model where it is not masked by the massive shear heating of the viscous model.

8.2 Viscoelastic rebound as a potential seismic source

The high velocities associated with "viscoelastic rebound" must be considered as being possibly seismic in nature. The stress drop associated with "viscoelastic rebound" occurs very rapidly (in fractions of a second) and could generate seismic waves. The mathematical formulation of shear zone model as it stands assumes that any inertial terms are negligable. This is valid for the normal shear zone behaviour, however any detailed study of the viscoelastic rebound will require modification of the model to include the inertial term. The normal perturbation applied to the finite element model consists of increasing the average temperature of the central column of elements. Tests have shown that viscoelastic rebound will occur from a single node perturbation located at any point within the finite element grid. The rebound, when it occurs, takes place over the entire grid almost simultaneously, (certainly in less than 10^{-4} second).

The rebound occurs for relatively high ambient temperatures (greater than $600^{\circ}C$). At these high temperatures, stresses are rapidly relaxed by viscous deformation before they can accumulate to the sufficiently large levels, to bring about brittle failure. "Viscoelastic rebound" provides a potential mechanism for seismic events occurring by ductile deformation in cases where brittle failure seems implausible owing to great depth and confining pressure. Consequently "viscoelastic rebound"

may provide a possible mechanism for deep focus earthquakes.

8.3 Future developments

The viscoelastic model provides an explanation of many of the structures seen in ductile shear zones. The viscoelastic model provides a better resolution of the short term evolution of shear zones than does the viscous model. The viscoelastic model however does have shortcomings. At lower ambient temperature ($\sim 600^{o}C$) the model still generates high stresses and too much shear heating. Any further development must include a failure criterion to limit the development of high stresses. Any failure criteria should include an estimate of the frictional heating. The model should include the inertial term in the calculations as this will be significant when brittle failure or viscoelastic rebound occurs.

The thermo-mechanical models discussed in this thesis have all used a dislocation creep mechanism. Recent work by Goetze (1978) has suggested that a diffusional creep mechanism may be more applicable at low ambient temperatures. The high stresses and shear heating at low ambient temperatures may be alleviated by a change in the deformation mechanism.

These future models can be constructed using either the finite element or the finite difference technique. The finite difference technique can be used to solve a simple one dimensional model but the finite element technique is required where complex material properties and geometries are required.

REFERENCES

Aoki, H., 1973. Stability of transform faults as inferred from viscous flow in the upper mantle, J. Phys. Earth, 21, 97-118.

Badham, J.P.N., 1976. General discussion on Proterozoic tectonics, Phil. Trans. R. Soc. Lond., A280, 661-662.

Bak. J., Sørensen, K., Grocott, J., Korstgård, J.A., Nash, D., & Watterson, J., 1975. Tectonic implications of Precambrian shear belts in western Greenland, Nature, 254, 5501, 566-569.

Barton, C.M. & England, P.C., 1979. Shear heating at the Olympos (Greece) thrust and the deformation properties of carbonates at geological strain rates, Bull. geol. Soc. Am., 90, 483-492.

Beach, A., 1976. The interrelations of fluid transport, deformation, geochemistry and heat flow in early Proterozoic shear zones in the Lewisian complex, Phil. Trans. R. Soc. Lond., A280, 569-604.

Bickel, M.J., Hawkesworth, C.J., England, P.C. & Athey, D., 1975. A preliminary thermal model for regional metamorphism in the eastern Alps, Earth. planet. Sci. Lett., 26, 13-28.

Bird, P., 1978. Initiation of intracontinental subduction in the Himalaya, J. geophys. Res., 83, 4975-4987.

Blake, M.C., Irwin, W.P. & Coleman, R.G., 1967. Upside-down metamorphic zonation, blueschist-facies, along a regional thrust in California and Oregon, U.S. Geol. Surv. Prof. Pap., 575-C, C1-C9.

Brewer, J., 1981. Thermal effects of thrust faulting, Earth. planet. Sci. Lett., 56, 233-244.

Brewer, J.A., Cook, F.A., Brown, L.D., Oliver, J.E., Kaufman, S., & Albaugh, D.S., 1981. COCORP seismic reflection profiling across thrust faults, in Thrust and Nappe Tectonics, The Geological Society of London.

Briegel, U. & Goetze, C., 1978. Estimates of differential stress recorded in the dislocation structure of Lochseiten limestone (Switzerland), Tectonophysics, 48, 61-76.

Brun, J.P. & Cobbold, P.R., 1980. Strain heating and thermal softening in continental shear zones: a review, J. struct. Geol., 2, 149-158.

Bryant, B., 1967. The occurrence of green iron-rich muscovite and oxidation during regional metamorphism in the Grandfather Mountain window, northwestern North Carolina, U.S. Geol. Surv. Prof. Pap., 575-C, C10-C16.

Burg, J.P. & Laurent, Ph., 1978. Strain analysis of a shear zone in a granodiorite, Tectonophysics, 47, 15-42.

Carslaw, H.S. & Jaeger, J.C., 1959. Conduction of heat in solids, Oxford University Press.

CDC FORTRAN Extended Reference Manual, publication no. 60497800. Control Data Corporation.

Chappel, W.M., 1978. Mechanics of thin-skinned fold-and-thrust belts, Bull. geol. Soc. Am., 89, 1189-1198.

Clark, S.P., 1966. Handbook of physical constants, Geol. Soc. Am. Memoir, 97.

Clark, S.P. & Ringwood, A.E., 1964. Density distribution and constitution of the mantle, Rev. Geophys., 2, 35-88.

Clark, G.K.C., Nitsan, U., & Paterson, W.S.B., 1977. Strain heating and creep instability in glaciers and ice sheets, Rev. Geophys. Space. Phys., 15, 235-247.

Coward, M.P., 1973. Heterogeneous deformation in the development of the Laxfordian complex of South Uist, Outer Hebrides, J. geol. Soc. Lond., 129, 139-160.

Cull, J.P., 1975. Pressure and temperature dependence of thermal conductivity within the Earth, unpublished Ph.D. thesis, University of Oxford.

Davies, F.B., 1975. Evolution of Proterozoic basement patterns in the Lewisian complex, Nature 256, 568-570.

Davies, F.B., 1978. Progressive simple shear deformation on the Laxford Shear Zone, Sutherland, Proc. Geol. Ass., 89, 177-196.

Davies, F.B. & Windley, B.F., 1976. Significance of major Proterozoic high-grade linear belts in continental evolution, Nature, 263, 383-385.

Eaton, J.P., Lee, W.H.K., & Pakiser, L.C., 1970. Use of microearthquakes in the study of the mechanics of earthquake generation along the San Andreas Fault in Central California, Tectonophysics, 9, 259-282.

Elliott, D., 1976. The motion of thrust sheets, J. geophys. Res., 81, 949-963.

England, P.C., 1978. Some thermal considerations of Alpine metamorphism - past, present and future, Tectonophysics, 46, 21-40.

Etheridge, M.A. & Wilkie, J.C., 1979. The geometry and microstructure of a range of QP-mylonite zones - A field test of the recrystallized grain size palaeopiezometer, Analysis of actual fault zones in bedrock, Open file report, 79-1239, pp. 448-504, U.S. Geol. Surv., Menlo Park, Calif.

Fleitout, L. & Froidevaux, C., 1980. Thermal and mechanical evolution of shear zones, J. struct. Geol., 2, 159-164.

Fung, V.C., 1965. Foundations of solid mechanics. Prentice Hall, 525 pp.

GHOST Graphical Output system manual (NWD6), North West Universities Computer Services.

Goetze, C., 1978 see end.

Graham, R.H., 1980. The role of shear belts in the structural evolution of the South Harris igneous complex, J. struct. Geol., 2, 29-37.

Graham, C.M. & England, P.C., 1976. Thermal regimes and regional metamorphism in the vacinity of overthrust faults: An example of shear heating and inverted metamorphic zonation from southern California, Earth. planet. Sci. Lett., 31, 142-152.

Grocott, J., 1977. The relationship between Precambrian shear belts and modern fault systems, J. geol. Soc. Lond., 133, 257-262.

Grocott, J. & Watterson, J., 1980. Strain profile of a boundary within a large ductile shear zone, J. struct. Geol., 2, 111-117.

Gruntfest, I.J., 1963. Thermal feedback in liquid flow; plane shear at constant stress, Trans. Soc. Rheol., 7, 195-207.

Haigh, B.I.R., 1973. Crustal and upper mantle structures in oceanic regions, unpublished Ph.D. thesis, University of Durham.

Herrin, E., 1972. A comparative study of upper mantle models: Canadian Shield and Basin and Range Provinces, in The Nature of the Solid Earth, ed. Robertson, E.C., McGraw-Hill, New York.

Herve et al., 1979 see end.

Hopper, M.J., 1973. Harwell subroutine library, H.M.S.O..

Hsü, K.J., 1969. Role of cohesive strength in the mechanics of overthrust faulting and of landsliding, Bull. geol. Soc. Am., 80, 927-952.

Hubbert, M.K. & Rubey, W.W., 1959. Role of fluid pressure in mechanics of overthrust faulting, Bull. geol. Soc. Am., 70, 115-166.

Jaeger, J.C. & Cook, N.G.W., 1969. Fundamentals of rock mechanics, Chapman and Hall, London.

Jégouzo, P., 1980. The South Amorican shear zone, J. struct. Geol., 2, 39-47.

Jischke, M.C., 1975. On the dynamics of descending lithospheric plates and slip zones, J. geophys. Res., 80, 4809-4813.

Kohlstedt, D.L. & Goetze, C., 1974. Low stress high temperature creep in olivine single crystals, J. geophys. Res., 79, 2045-2051.

Kohlstedt, D.L., Cooper, R.F., Weathers, M.S., & Bird, J.M., 1979. Paleostress analysis of deformation-induced microstructures: Moine thrust zone and Ikertoq shear zone, Analysis of actual fault zones in bedrock, Open file report, 79-1239, pp 394-425, U.S. Geol. Surv., Menlo Park, Calif.

Kohlstedt, D.L. & Weathers, M.S., 1980. Deformation-induced microstructures, paleopiezometers, and differential stresses in deeply eroded fault zones, J. geophys. Res., 85, 6269-6285.

Lachenbruch, A.H. & Sass, J.H., 1980. Heat flow and energetics of the San Andreas Fault Zone, J. geophys. Res., 85, 6185-6222.

LeFort , P., 1975. Himalayas: The collided range. Present knowledge of the continental arc, Amer. J. Sci., 275-A, 1-44.

Lee, E.H., Radok, J.R.M., & Woodward, W.B., 1959. Stress analysis for linear viscoelastic materials, Trans. Soc. Rheol., 3, 41-59.

Lockett, J.M. & Kusznir, N.J., 1982. Ductile shear zones: some aspects of constant slip velocity and constant shear stress models, Geophys. J. R. astr. Soc., 69, 477-494.

Melosh, H.J., 1976. Plate motion and thermal instability in the asthenosphere, Tectonophysics, 35, 363-390.

Mercier, J.-C. & Carter, N.L., 1975. Pyroxene geotherms, J. geophys. Res., 80, 3349-3362.

Miyashiro, A., 1961. Evolution of metamorphic belts, J. Petrol., 2, 277-311.

Murrell, S.A.F. & Chakravarty , S., 1973. Some new rheological experiments on igneous rocks at temperatures up to 1120°C, Geophys. J. R. astr. Soc., 34, 211-250.

Neugebauer , H.J. & Breitmayer, G., 1975. Dominant creep mechanism and the descending lithosphere, Geophys. J. R. astr. Soc., 43, 873-895.

Nicolas , A., Bouchez, J.L., Blaise, J., & Poirier, J.P., 1977. Geological aspects of deformation in continental shear zones, Tectonophysics, 42, 55-73.

Nicolas , A., 1979. Oceanic lithosphere thrust in trench environment (abstract), International Conference on Shear Zones in Rocks, ICG, IUGG, Barcelona.

Nicolas , A. & Le Pichon, X., 1980. Thrusting of young lithosphere in subduction zones with special reference to structures in ophiolitic peridotites, Earth. planet, Sci. Lett., 46, 397-406.

Oxburgh, E.R. & Turcotte, D.L., 1970. Thermal structure of island arcs, Bull. Geol. Soc. Am., 81, 1665-1688.

Oxburgh, E.R. & Turcotte, D.L., 1974. Thermal gradients and regional metamorphism in overthrust terrains with special reference to the eastern Alps, Schweiz. Mineral. Petrogr. Mitt., 54, 641-662.

Park, R.G., 1981. Shear zone deformation and bulk strain in granite-greenstone terrain of the Western Superior Province, Canada, Precambrian Res., 14, 31-47.

Platt, J.P., 1975. Metamorphic and deformational processes in the Franciscan complex, California: Some insights from the Catalina schist terrane, Bull. Geol. Soc. Am., 86, 1337-1347.

Poirier, J.P., 1980. Shear localization and shear instability in materials in the ductile field, J. struct. Geol., 2, 135-142.

Poirier, J.P., Bouchez, J.L., & Jonas, J.J., 1979. A dynamic model for aseismic ductile shear zones, Earth. planet. Sci. Lett., 43, 441-453.

Ramsay, J.G. & Graham, R.H., 1970. Strain variation in shear belts, Can. J. Earth Sci., 7, 786-813.

Reid, I. & MacDonald, K., 1973. Microearthquake study of the Mid-Atlantic Ridge near 37°N using sonobouys, Nature, 246, 88-90.

Schatz, J.F. & Simmons, G., 1972. Thermal conductivity of earth materials at high temperatures, J. geophys. Res., 77, 6966-6983.

Schmid, S.M., 1975. The Glarus overthrust: Field evidence and mechanical model, Eclogae geol. Helv., 68, 247-280.

Schmid, S.M., Boland, J.N. & Paterson, M.S., 1977. Superplastic flow in fine-grained limestone, Tectonophysics, 43, 257-291.

Scholz, C.H., 1980. Shear heating and the state of stress on faults, J. geophys. Res., 85, 6174-6184.

Scholz, C.H., Beavan, J., & Hanks, T.C., 1979. Frictional metamorphism, argon depletion, and tectonic stress on the Alpine fault, New Zealand, J. geophys. Res., 84, 6770-6782.

Schubert, G. & Yuen, D.A., 1978. Shear heating instability in the earths upper mantle, Tectonophysics, 50, 197-205.

Schubert, G., Yuen, D.A., Froidevaux, C., Fleitout, L., & Souriau, M., 1978. Mantle circulation with partial shallow return flow: Effects on stresses in oceanic plates and topography of the sea floor, J. geophys. Res., 83, 745-758.

Sibson, R.H., 1977. Fault rocks and fault mechanisms, J. geol. Soc. Lond., 133, 191-213.

Sokolnikoff, I.S., 1956. Mathematical theory of elasticity, McGraw-Hill, New York.

Stocker, R.L. & Ashby, M.F., 1973. On the rheology of the upper mantle, Rev. Geophys. Space. Phys., 11, 391-426.

Sukanek, P.C. & Laurence, R.L., 1974. An experimental investigation of viscous heating in some simple shear flows, A.I.Ch.E.Jl., 20, 474-484.

Sutton, J. & Watson, J.V., 1974. Tectonic evolution of continents in early Proterozoic times, Nature, 247, 433-435.

Suwa, K., 1961. Petrological and geological studies of the Ryoke metamorphic belt, J. Earth Sci. Nagoya Univ., 9, 224-303.

Thom, R., 1975. Structural stability and morphogenesis: An outline of a general theory of models, Reading, Benjamin.

Thon, A., 1980. Steep shear zones in the basement and associated deformation of the cover sequence on Karmøy, S.W. Norwegian Caledonides, J. struct. Geol., 2, 75-80.

Turcotte, D.L., 1974. Are transform faults thermal contraction cracks?, J. geophys. Res., 79, 2573-2577.

Turcotte, D.L. & Oxburgh, E.R., 1968. A fluid theory for the deep structure of dip-slip fault zones, Phys. Earth. planet. Inter., 1, 381-386.

Turcotte, D.L. & Schubert, G., 1973. Frictional heating of the descending lithosphere, J. geophys. Res., 78, 5876-5886.

Twiss, R.J., 1977. Theory and applicability of recrystallized grain size paleopiezometer, Pure Appl. Geophys, 11, 227-244.

Watson, J.V., 1973. Effects of reworking on high grade gneiss complexes, Phil. Trans. R. Soc. Lond., A273, 443-455.

Weathers, M.S., Bird, J.M., Cooper, R.F., & Kohlstedt, D.L., 1979. Differential stress determined from deformation induced microstructures on the Moine thrust zone, J. geophys. Res., 84, 7495-7509.

Weertman, J., 1970. The creep strength of the earth's mantle, Rev. Geophys. Spece. Phys., 8, 145-168

Williams, H. & Smyth, W.R., 1973. Metamorphic aureoles beneath ophiolite suites and alpine peridotites: Tectonic implications with west Newfoundland examples, Amer. J. Sci., 273, 594-621.

Windley, B.F., 1978. The evolving continents, Wiley and Sons.

Woodward, D.J., 1976. Visco-elastic finite element analysis of subduction zones, unpublished Ph.D. thesis, University of Durham.

Yuen, D.A., Fleitout, L., Schubert, G., & Froidevaux, C., 1978. Shear deformation zones along major transform faults and subducting slabs, Geophys. J. R. astr. Soc., 54, 93-119.

Yuen, D.A. & Schubert, G., 1977. Asthenospheric shear flow: thermally stable or unstable?, Geophys. Res. Lett., 4, 503-506.

Yuen, D.A. & Schubert, G., 1979. On the stability of frictionally heated shear flows in the asthenosphere, Geophys. J. R. astr. Soc., 57, 189-207.

Yuen, D.A., Tovish, A., & Schubert, G., 1978. Shear flow beneath oceanic plates; local nonsimilarity boundary layers for olivine rheology, J. Geophys. Res., 83, 759-765.

Zienkiewicz, O.C., 1977. The finite element method, McGraw-Hill, London.

Goetze, C., 1978. The mechanisms of creep in olivine, Phil. Trans. R. Soc. Lond., A288, 99-119.

Herve, F.A., Araya, E.F., Fuenzalida, J.I. & Solano, A.R., 1979. Edades radiometricas y tectonica neogena en el sector costero de chileo continental, Xa region, Segundo Congr. Geol. Chileno, F1-F18, Inst. Invest. Geol., Arica, Chile.

APPENDICES

APPENDIX 1

Finite Difference Viscous Shear Zone Model

The finite difference program is written in Extended BASIC and was run on a GEC 4082 series machine at Keele. The model dimensions are input in kilometers, temperature in degrees centigrade, shear velocity in cms yr^{-1} and time in years. A dry olivine rheology is used in the code listing.

Temperature, velocity and viscosity profiles are output by the model. Simple modification allows strain profiles to be added. Thermal runaway conditions are flagged.

The main internal parameters and physical constants are :

Melting temperature	$1200^{o}C$
Rock density	3 gm cm^{-3}
Thermal conductivity	0.006 cal/cm sec^{-1}
Specific heat capacity	0.26 cal/$cm^{-3}{}^{o}C$

Internally the program uses c.g.s. units throughout, all scaling is done at output. Thermal runaway is defined as a velocity gradient of 1 cm/km.

VISCOUS SHEAR ZONE MODEL - PROGRAM LISTING

```
0001 REM SHEAR ZONE MODEL ********************************
0002 FILES #3,'SINK'
0005 DIM Q(1001),T(1001),V(1001)
0006 DIM Z(101) ,E(101)
0010 PRINT "NUMBER OF SPACE STEPS="
0011 INPUT N
0015 PRINT "MODEL HALF WIDTH="
0016 INPUT L
0018 K5=2
0019 K9=(L/N*1.0E5)^2*0.26*3/0.006/2
0020 K9=K9/K5
0025 PRINT "TIME="
0026 INPUT T6
0027 T6=T6*24*3600*365
0031 J1=5000
0032 PRINT "TEMPERATURE BACKGROUND="
0033 INPUT T0
0034 PRINT "FOR CONSTANT TAU CONDITION TYPE 1, FOR CONST. U0 TYPE 0"
0035 INPUT F
0036 IF F=1 GOTO 41
0037 PRINT "HALF VELOCITY="
0038 INPUT U0
0039 U0=U0/(24*60*60*365)
0040 GOTO 90
0041 PRINT"STRESS VALUE IN KBARS="
0042 INPUT S1
0043 S1=S1*1.0E9
0090 PRINT "ZERO POINT PERTUBATION="
0091 INPUT T9
0100 REM INITIALIZE VALUES OF T************************
0110 FOR I=0 TO N
0115 T(I)=T0
0120 Q(I)=T0
0122 E(I)=0
0125 NEXT I
0126 T(0)=T(0)+T9
0128 Q(0)=T(0)
0129 T5=0
0130 V(0)=0
0132 IF F=1 GOTO 500
0133 FOR I=1 TO N
0134 V(I)=U0*(I/N)
0135 NEXT I
0500 FOR P=1 TO J1
0600 GOSUB 1000
0700 GOSUB 2000
0750 NEXT P
0755 GOTO 762
0760 PRINT "THERMAL RUNAWAY"
0761 PRINT #3,"THERMAL RUNAWAY"
0762 PRINT "TIME IN YEARS=";T5/(24*3600*365)
0763 PRINT #3,"TIME IN YEARS=";T5/(24*3600*365)
0780 PRINT "NUMBER OF ITERATIONS=";P
```

```
0789 PRINT #3,"NUMBER OF ITERATIONS=";P
0790 PRINT #3,"Y-COORD","TEMP","VELOCITY","VISC"
0800 PRINT "Y-COORD","TEMP","VELOCITY","VISCOSITY"
0801 FOR I=0 TO N
0802 PRINT L*I/N,T(I),V(I)*24*3600*365*(S1^5),Z(I)*(S1^(-4)),E(I)
0803 PRINT #3,L*I/N,T(I),V(I)*24*3600*365*(S1^5),Z(I)*(S1^(-4))
0804 NEXT I
0805 PRINT "STRESS=",S1*1.0E-9
0806 PRINT #3,"STRESS=",S1*1.0E-9
0900 GOTO 3000
1000 REM VELOCITY INTEGRATION **********************************
1050 A=1.0E36
1051 I0=LOG(1.0E40)
1090 B=40*(273+1200)/(273+T(0))
1091 IF B > I0 THEN B=I0
1092 Z(0)=A*EXP(B)
1100 FOR I=1 TO N
1151 D=(40*(273+1200)/(273+T(I)))
1156 IF D>I0 THEN D=I0
1168 Z(I)=A*EXP(D)
1171 U1=(1/Z(I)+1/Z(I-1))/2
1190 V(I)=V(I-1)+U1*L/N*1.0E5
1200 NEXT I
1290 IF F=1 GOTO 1350
1300 S1=U0/V(N)
1301 S1=S1^(1/5)
1350 V6=V(N)*24*3600*365*(S1^5)
1351 IF V6 > 1.0 GOTO 760
1352 RETURN
2000 REM TEMPERATURE ROUTINE*********************
2005 K1=10
2006 H1=0
2050 Q2=1/(L/N*1.0E5)^2*0.006/0.26/3
2051 FOR I=0 TO N-1
2052 IF I=0 GOTO 2055
2053 Q1=Q(I-1)+Q(I+1)-Q(I)*2
2054 GOTO 2057
2055 Q1=2*Q(1)-2*Q(0)
2057 Q1=Q1*Q2
2100 C1=Z(I)
2101 S2=S1^6
2102 H=S2/C1/3/0.26/1.0E7/4.2
2105 IF H<1.0E-50 THEN H=1.0E-50
2106 IF H > H1 THEN H1=H
2107 Q1=Q1+H
2108 T(I)=Q1
2110 NEXT I
2112 T1=K1/H1/K5
2113 IF T1 > K9 THEN T1=K9
2124 FOR I=0 TO N-1
2125 T(I)=Q(I)+T(I)*T1
2126 IF T(I) > 1200 THEN T(I)=1200
2127 Q(I)=T(I)
2128 NEXT I
2300 T5=T5+T1
2400 FOR I=0 TO N-1
2410 E1=Z(I)*(S1^(-4))
```

```
2420 E2=S1/(E1*3)
2425 E2=E2*T1
2430 E(I)=E(I)+E2
2435 NEXT I
2440 IF T5 > T6 GOTO 755
2500 RETURN
3000 PRINT #3,"NUMBER OF SPACE STEPS=";N
3001 PRINT #3,"MODEL HALF WIDTH=";L
3002 PRINT #3,"TIME STEP =";T6/(24*3600*365)
3003 PRINT #3,"HALF VELOCITY=";U0*24*60*60*365
3005 IF T>0 GOTO 3007
3006 GOTO 3010
3007PRINT #3,"ZERO POINT TEMP. PERT=";T9
3010 IF F=1 GOTO 3012
3011 GOTO 9998
3012 PRINT #3,"CONSTANT TAU CONDITIONS,VALUE IN KBARS=";S1*1.0E-9
9998 STOP
9999 END
```

APPENDIX 2

Finite Element Visco-elastic Shear Zone Program

The finite element programs discribed in this appendix have been written in CDC Extended FORTRAN 4 and were run on the ICL 1906A/CDC 7600 Joint System at UMRCC. During the Spring of 1982 the system was being upgraded resulting in many minor changes to protocols and compilers. Some modification may be necessary to run the programs at the time of reading.

The plotting program utilises subroutines of the GHOST graphics library and may substantial translation for use with another graphics system. The bibliography contains the references to the appropriate system manuals.

The finite element package is divided into three separate programs :

1. **PROGRAM LDGRID** generates the finite element mesh and assigns the elastic and viscous properties to the model.

2. **PROGRAM LOADFIN** accomplishes a finite element analysis of the model generated by **LDGRID**.

3. **PROGRAM PLOT** produces line printer and plotter graphics of the analysis from **LOADFIN**.

PROGRAM LDGRID

This program generates a rectangular finite element grid consisting of simple triangular elements. Co-ordinates are assigned to each node and the material properties of each element determined. The grid data is output onto files for transfer to **PROGRAM LOADFIN**. The most significant variables are :

TS scaler for initial nodal forces

NN number of nodes in y-direction.

NE number of elements in y-direction.

STEP distance between nodes.

NREP number of columns of elements

AB minimum node spacing in cm^{-1}

P Poissons ratio

E elastic modulus

IVISC flag indicating rheological properties

S0 inherent shear strength

VALMU coefficient of friction

BVEL boundary velocity

All values are in c.g.s. system of units excepting co-ordinates which are in kilometres.

```
      PROGRAM LDGRID(INFILE,INPUT,OUTPUT,FF6,
     1 TAPE5=INFILE,TAPE6=FF6,TAPE3=INPUT,TAPE4=OUTPUT)
C******PROGRAM GRID - GENERATES F.E. GRID*******************
      DIMENSION X(500),Y(500),NODEL(1000,3),ISTBC(256),
     1 E(1000),P(1000),FORST(1000),TEMP(1000),VALMU(500),S0(500),
     2 NS(50,3),XS(50),YS(50),IBREF(500),IVISC(500)
C*****TO GENERATE THE LITHOSPHERE GRID*****************************
C ****** TO GENERATE THE F.E. GRID *****************
C       NN=NO. OF COLUMNS OF NODES *********************
C       NE=NO. OF COLUMNS OF ELEMENTS ********************
C       SET FORCE SCALER TS  *************
      TS=0.0E9
      NN=21
      NE=20
      NE2=NE*2
      STEP=4.0
      NREP=10
C****** NUMERATION OF NODES **********************
      K=1
      L=2
      N1=1
      N2=NN+1
      N3=2
      N4=NN+2
      DO 5 I=1,NE
      NS(K,1)=N1+I-1
      NS(K,2)=N2+I-1
      NS(K,3)=N3+I-1
      NS(L,1)=N2+I-1
      NS(L,2)=N3+I-1
      NS(L,3)=N4+I-1
      K=K+2
      L=L+2
    5 CONTINUE
C ***** SET UP NODAL COORDINATES ***********************
      DO 10 I=1,16
      XS(I)=0.0
   10 CONTINUE
      IJI=0
      DO 20 I=1,6
      YS(I)=IJI
   20 IJI=IJI+1
      YS(7)=10.0
      YS(8)=15.0
      YKI=20.0
      DO 21 I=9,21
      YS(I)=YKI
   21 YKI=YKI+10.0
      DO 11 I=1,21
      X(I)=XS(I)
   11 Y(I)=YS(I)
      K=NN
      HIT=STEP
      L=0
      DO 1 I=1,NREP
      DO 2 J=1,NN
      K=K+1
      X(K)=XS(J)+HIT
    2 Y(K)=YS(J)
      STEP=4.0
```

```
      HIT=HIT+STEP
      DO 3 J=1,NE2
      L=L+1
      DO 4 M=1,3
    4 NODEL(L,M)=NS(J,M)+(I-1)*NN
    3 CONTINUE
    1 CONTINUE
      NNOD=K
      NEL=L
      NOST=NN
C ***** LOAD ANY INITIAL NODAL FORCES **********************
      A=Y(2)-Y(3)
      B=Y(NN-1)-Y(NN)
      A=A*TS*1.0E5/2.0
      B=B*TS*1.0E5/2.0
      FORST(2*2-1)=A
      FORST(2*NN-1)=B
      S=A+B
      NN1=NN-1
      DO 991 I=3,NN1
      A=Y(I-1)-Y(I+1)
      A=A*TS*1.0E5/2.0
      S=S+A
  991 FORST(2*I-1)=A
C ***** AB = MINIMUM NODE SPACING IN CM-1  ************
      AB=1.0E5
C***** INITIALIZE TEMPERATURE BOUNDARY CONDITIONS **********
      DO 60 I=1,NNOD
      ISTBC(I)=0
   60 CONTINUE
      NREP1=NREP+1
      NN=NOST
      DO 61 I=1,NREP1
      J=I*NOST
      ISTBC(J)=1
   61 CONTINUE
C*****SET UP TEMPERATURE CONDITIONS *******
      DO 50 I=1,NNOD
      TEMP(I)=750.0
   50 CONTINUE
      NK=1
      NE1=NE+1
      DO 51 I=1,NE1
      TEMP(NK)=760.0
      NKR=NK+1
      TEMP(NKR)=700.0
      NK=(NN*I)+1
   51 CONTINUE
      NELCOL=(NOST-1)*2
      NREP3=NREP+3
      I=1
      IJI=0
      DO 52 J=1,NREP3
      JI=J-1
      DO 52 IJ=1,NOST
      IAA=((IJ-1)*2)+(JI*NELCOL)
      IBREF(I)=IAA
      I=I+1
   52 CONTINUE
```

```
C ****** ASSIGN ELASTIC CONSTANTS ,VISCOSITIES ETC. ***********
      DO 7001 I=1,NEL
      X0=(X(NODEL(I,1))+X(NODEL(I,2))+X(NODEL(I,3)))/3.0
      Y0=(Y(NODEL(I,1))+Y(NODEL(I,2))+Y(NODEL(I,3)))/3.0
      P(I)=0.25
      IVISC(I)=1
      E(I)=1.0E11
      S0(I)=3.79E6
      VALMU(I)=0.66
 7001 CONTINUE
C ***** READ BOUNDARY VELOCITY *********************************
      READ(3,106)BVEL
  106 FORMAT(10X,F10.3)
      ST=4.0E9
      D=0.0
C ***** WRITE GRID DATA TO FILES ******************
      WRITE(6,100) NNOD,NEL,NN,ST,D
      WRITE(6,101) (I,X(I),Y(I),FORST(2*I-1),FORST(2*I),I=1,NNOD)
      WRITE(6,102) (I,(NODEL(I,J),J=1,3),E(I),P(I),
     1 IVISC(I),I=1,NEL)
      WRITE(6,120)(VALMU(I),S0(I),I=1,NEL)
  120 FORMAT(E10.4,2X,E10.4)
      WRITE(6,103)(I,TEMP(I),I=1,NNOD)
      WRITE(6,105) BVEL,AB
      WRITE(6,110)(ISTBC(I),I=1,NNOD)
      WRITE(6,107)(IBREF(I),I=1,NNOD)
  107 FORMAT(I5)
  110 FORMAT(I2)
  105 FORMAT(2F10.3)
  103 FORMAT(I10,E10.3)
  100 FORMAT(3I10,E10.3,F10.3)
  101 FORMAT(I10,2F10.3,2E10.3)
  102 FORMAT(4I10,E10.3,F10.3,I3)
      STOP
      END
```

PROGRAM LOADFIN

This program is the finite element analysis of the model. A flow diagram of the algorithm is given with the program listing. Input variables are :

NNOD number of nodes in grid

NEL number of elements in grid

NOST number of nodes in y-direction

K node number

X(K) y-coordinate of that node

Y(K) y-coordinate of that node

FORST(2*K-1) force on node in x-direction

FORST(2*K) force on node in y-direction

NODEL(K,3) node numbers for element K

E elemental elastic modulus

P elemental poissons ratio

IVISC viscosity flag for element

VALMU coefficient of friction of element

S0 inherent shear strength of element

TEMP temperature at node

ISTBC flag for temperature boundary condition

IBREF flag for node at edge of grid

BVEL boundary velocity

AB minimum node separation

TMF duration of model run

RSM stress scaler

ISTRAIN flag for plane stress or strain

ISP flag for displacement boundary condition

PDIS prescribed displacement

NARR1 must be = NNOD+NOST

NARR2 must be = NEL+((NOST-1)*2)

Output Data

The program calculates and outputs to various channels the following data.

1. All input data specifying grid,boundary conditions and initial temperature and stress condition.
2. The variation of maximum shear stress with time.
3. The displacement field for the grid.
4. Stress state, viscosity, temperature and shear heating for each element.
5. Flags indicating failure of any elements.
6. The velocity field at the end of the run.

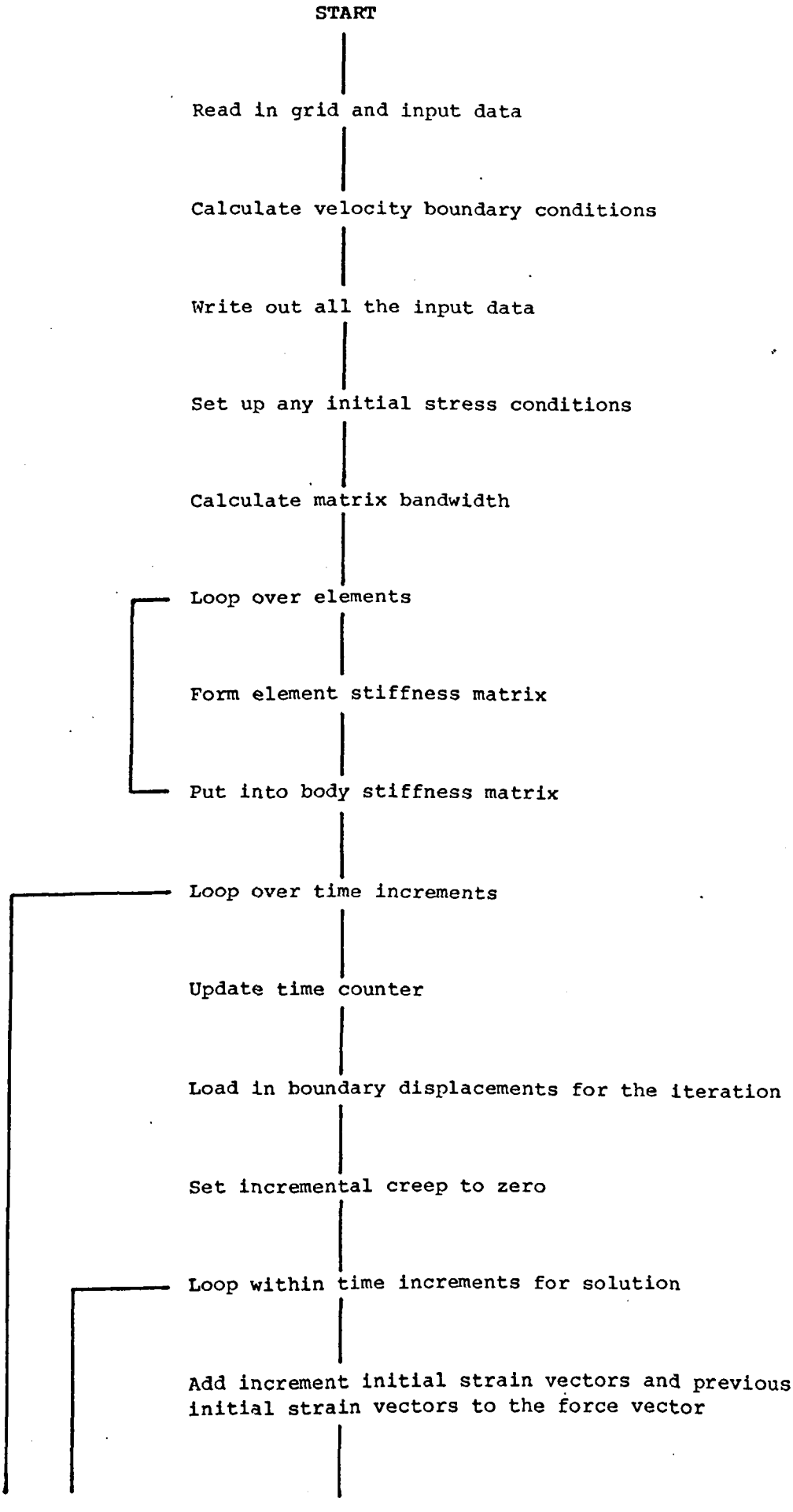
START
Read in grid and input data
Calculate velocity boundary conditions
Write out all the input data
Set up any initial stress conditions
Calculate matrix bandwidth
Loop over elements
Form element stiffness matrix
Put into body stiffness matrix
Loop over time increments
Update time counter
Load in boundary displacements for the iteration
Set incremental creep to zero
Loop within time increments for solution
Add increment initial strain vectors and previous initial strain vectors to the force vector

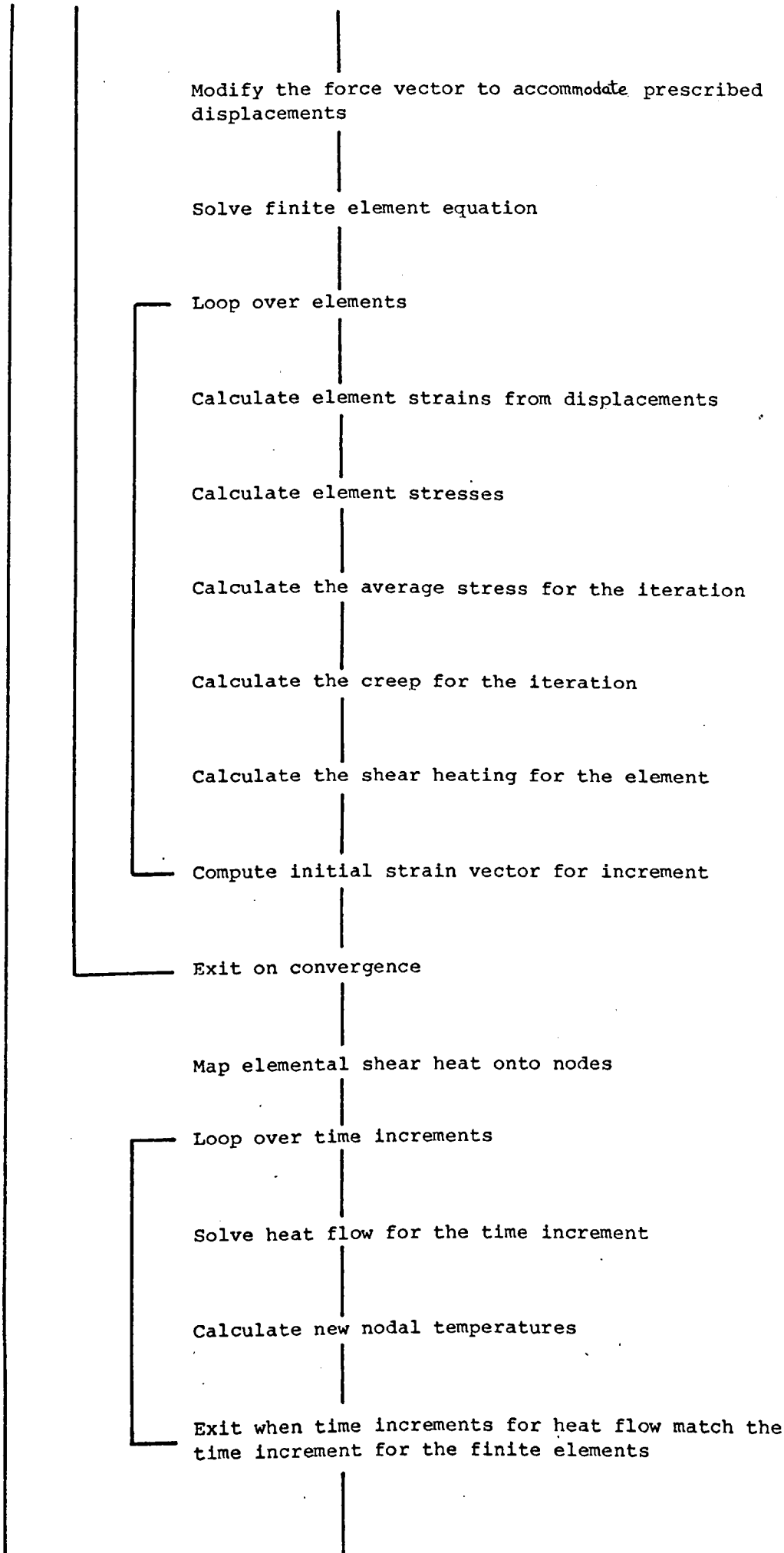
Modify the force vector to accommodate prescribed displacements
Solve finite element equation
Loop over elements
Calculate element strains from displacements
Calculate element stresses
Calculate the average stress for the iteration
Calculate the creep for the iteration
Calculate the shear heating for the element
Compute initial strain vector for increment
Exit on convergence
Map elemental shear heat onto nodes
Loop over time increments
Solve heat flow for the time increment
Calculate new nodal temperatures
Exit when time increments for heat flow match the time increment for the finite elements

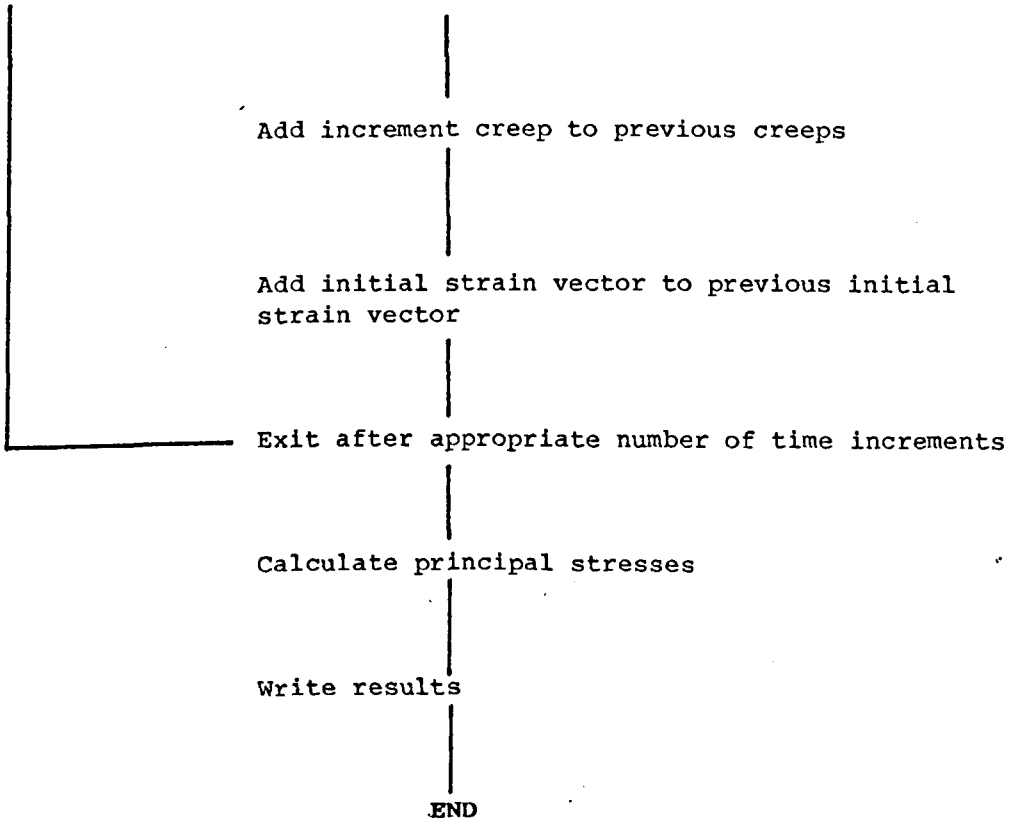
Add increment creep to previous creeps
Add initial strain vector to previous initial strain vector
Exit after appropriate number of time increments
Calculate principal stresses
Write results
END

The flow diagram shows how the algorithm has been constructed for simultaneous finite element stress and finite difference heat flow analysis. Using this , the code and the following description of the Subroutine functions the reader should be able to use and modify the programs.

SUBROUTINE GMPRD

Multiplies two matrices to form a third. This Subroutine is adapted from an I.B.M. scientific subroutine package.

SUBROUTINE GMTRA

Performs the transposition of any matrix. Adapted from an I.B.M. package as above.

SUBROUTINE MATSOL

Solves matrix equation by Gaussian elimanation. Taken from Harwell Subroutine library(Hooper 1973).

SUBROUTINE MATHEL

Called from Subroutine MATSOL.

SUBROUTINE TIME

Calculates maximum time increment iteration period for both visco-elastic and thermal analysis.

SUBROUTINE DMATR

Called from Subroutine SMATR. Calculates element elasticity matrix.

SUBROUTINE HEAT

Solves the two dimensional finite difference heat flow and shear heating for the grid.

SUBROUTINE FAIL

Calculates rock failure using Coulomb-Navier failure criterion.

SUBROUTINE CENTRE

Calculates average value of a parameter at element centre from nodal values.

SUBROUTINE BMATR

Called from Subroutine SMATR. Calculates element B matrix.

SUBROUTINE SMATR

Assembles all matrices for finite element analysis and calculates body stiffness matrix.

SUBROUTINE WARMTH

Called from Subroutine HEAT. Calculates heat flow in the grid.

SUBROUTINE RHEO

Calculates the viscosity of an element.

SUBROUTINE AXIAL

Calculates principal stresses from stress data.

SUBROUTINE SHAPE

Called from Subroutine HEAT. Maps the elemental shear heating data onto nodes for incorporation into finite difference heat flow calculations.

```
      PROGRAM LOADFIN(OUTPUT,INPUT,TAPE3=INPUT,F5,F6,F1,F8,
     1 TAPE1=F1,TAPE4=OUTPUT,TAPE5=F5,TAPE6=OUTPUT,TAPE8=F8)
C***** VISCO-ELASTIC F.E. PROGRAM*************************************
C******MAIN PROGRAM*********************************************************
      COMMON /K/ AT,BLIB,DELIB,DLIB
C*****DIMENSION STATEMENTS*************************************************
      DIMENSION
     1 X(256),Y(256),NODEL(450,3),E(450),P(450),
     2 NK(100),PRES(100),YFINC(100),TEMP(450),ATEMP(450),
     3 LD(100),ISP(100,2),PDIS1(100,2),PDIS(100,2),IBREF(231),
     4 FORST(462),FIST(462),ISTBC(256),VALMU(400),S0(400),
     5 IFAIL(400),CSTIN(462,4),STIN(462,4),
     6 T(36),D(9),B(18),V(6),F(18),H(18),VISCOS(512),
     7 W(3),QQ(3),CC(3),STRAY(462,4),IVISC(450),
     8 CREEP(4),DISEL(6),STRESS(4),STRAIN(4),STEL(4),DISP(462)
     9 ,DF(9),EF(3),AT(462,132),TRAY(600,4),EDISP(231)
     1 ,DLIB(9,600),BLIB(18,600),DELIB(600)
     2 ,DFS(50),WD(450),NODELD(256),SHEAT(256),VEL(231)
      LEVEL 2,AT,BLIB,DLIB,DELIB
      TIMTOT=0.0
C
C*****READ IN INPUT DATA**************************************************
C*****READ NUMBER OF NODES AND ELEMENTS,STRESS SCALER AND OUTPUT MARKER
      READ(5,800) NNOD,NEL,NOST,STMAX,DEV
      NNOD2=NNOD*2
  800 FORMAT(3I10,E10.3,F10.3)
      DO 850 I=1,NNOD
  850 READ(5,801) K,X(K),Y(K),FORST(2*K-1),FORST(2*K)
  801 FORMAT(I10,2F10.3,2E10.3)
      DO 851 I=1,NEL
  851 READ(5,802) K,(NODEL(K,J),J=1,3),E(K),P(K)
     1 ,IVISC(K)
  802 FORMAT(4I10,E10.3,2F10.3,I3)
      READ(5,1792)(VALMU(I),S0(I),I=1,NEL)
 1792 FORMAT(E10.4,2X,E10.4)
C*****READ IN  TEMPERATURE DATA*******
      DO 2890 I=1,NNOD
 2890 READ(5,2891)K,TEMP(K)
 2891 FORMAT(I10,E10.3)
C***** READ IN VELOCITY STRUCTURE ******************
      READ(5,8080)BVEL,AB
 8080 FORMAT(2F10.3)
      READ(5,8076)(ISTBC(I),I=1,NNOD)
 8076 FORMAT(I2)
      READ(5,8077)(IBREF(I),I=1,NNOD)
 8077 FORMAT(I5)
C*****READ NUMBER OF TIME INCREMENTS AND STEP LENGTH******************
      READ(3,803) TMF
  803 FORMAT(E10.3)
      READ(3,1803) RSM
 1804 FORMAT(3I10)
 1803 FORMAT(F10.3)
C*****READ PLANE STRESS OR STRAIN MARKER**************
C****** 1,PLANE STRESS ,2,PLANE STRAIN ****************
      READ(3,1805) ISTRAIN
 1805 FORMAT(I10)
C***** READ BOUNDARY CONDITIONS*****************************************
      READ(5,808) ND
      DO 853 I=1,ND
  853 READ(5,809) K,FORST(2*K-1),FORST(2*K)
```

```
  809 FORMAT(I10,2E10.3)
C*****READ SPECIFIED DISPLACEMENTS************************************
      READ(5,808) ND
  808 FORMAT(I10)
      DO 854 I=1,ND
  854 READ(5,807) LD(I),(ISP(I,J),PDIS(I,J),J=1,2)
  807 FORMAT(I10,2(I10,F10.3))
      DO 8555 I=1,ND
      DO 8555 J=1,2
 8555 PDIS(I,J)=PDIS(I,J)*BVEL
      NARR1=256
      NARR2=450
C
C*****WRITE OUT INPUT DATA*************************************************
      WRITE(4,150) NNOD,NEL,STMAX,DEV
  150 FORMAT(2X,'NUMBER OF NODES =',I4,10X,'NUMBER OF ELEMENTS =',I4,
     1 5X,E10.3,F4.1)
      WRITE(6,199)
  199 FORMAT('0')
      WRITE(6,98)
   98 FORMAT(14X,'NODE',22X,'X-COORDINATE',10X,'Y-COORDINATE',11X,'FORCE
     1-X',3X,'FORCE-Y')
      WRITE(6,199)
      DO 100 I=1,NNOD
  100 WRITE(6,152) I,X(I),Y(I),FORST(2*I-1),FORST(2*I)
  152 FORMAT(13X,I5,24X,F10.3,12X,F10.3,10X,2E10.3)
      WRITE(6,199)
      WRITE(6,99)
   99 FORMAT(11X,'ELEMENT',30X,'NODE NUMBERS',10X,'ELASTICITY',2X,'P-
     1RATIO')
      WRITE(6,199)
      DO 101 I=1,NEL
  101 WRITE(6,154) I,(NODEL(I,J),J=1,3),E(I),P(I)
  154 FORMAT(14X,I4,18X,I4,12X,I4,12X,I4,D10.3,F6.3)
      WRITE(6,199)
      WRITE(6,199)
      WRITE(6,7501)
 7501 FORMAT(17X,'NODE',9X,'TEMPERATURE')
      WRITE(6,199)
       DO 7502 I=1,NNOD
 7502 WRITE(6,7503)I,TEMP(I)
 7503 FORMAT(10X,I10,F10.3)
      WRITE(6,199)
      WRITE(6,199)
      WRITE(6,198)
  198 FORMAT(26X,'NODE',15X,'X-FIXED',12X,'X-STRAIN',15X,'Y-FIXED',12X,'
     1Y-STRAIN')
      WRITE(6,199)
      DO 105 I=1,ND
  105 WRITE(6,169) LD(I),((ISP(I,J),PDIS(I,J)),J=1,2)
  169 FORMAT(20X,I10,12X,I10,10X,F10.3,10X,I10,10X,F10.3)
C****** SCALE DIMENSIONS FROM KM TO CM*********************************
 1762 DO 3576 I=1,NNOD
      FORST(2*I)=FORST(2*I)*RSM
      FORST(2*I-1)=FORST(2*I-1)*RSM
      X(I)=X(I)*1.0E5
      Y(I)=Y(I)*1.0E5
 3576 CONTINUE
```

```
C*****TO CALC THE PARAM NBW*********************************************
      PT=1.0
      NBW=0
      DO 9182 I=1,NEL
      KB1=IABS(NODEL(I,1)-NODEL(I,2))
      KB2=IABS(NODEL(I,2)-NODEL(I,3))
      KB3=IABS(NODEL(I,3)-NODEL(I,1))
 9182 NBW=AMAX0(KB1,KB2,KB3,NBW)
      NBW=2*NBW+2
      NBW=2*NBW-1
      WRITE(6,199)
      WRITE(4,9187) NBW
 9187 FORMAT(2X,'MATRIX BANDWIDTH=',I10)
C***** SET UP ALL THE MATRICES ****************************
C
C
      CALL SMATR(NEL,NNOD,E,P,D,B,DLIB,AT,DELIB,
     1 BLIB,X,Y,ISTRAIN,NBW,NODEL,NARR1,NARR2)
C
      DO 1793 I=1,NEL
 1793 IFAIL(I)=0
      VIKMIN=1.0E20
C***** START ITERATIONS FOR TIME INCREMENTS ***********************
      DO 201 IN=1,10000
      VL=1.0E30
      TIMTOT=TIMTOT+TIMY
      TIMC=TIMY*365.25*24.0*3600.0
C***** INTRODUCE PRESCRIBED DISPLACEMENTS*******************************
      DO 30 II=1,ND
      DO 31 J=1,2
      PDIS1(II,J)=PDIS(II,J)*TIMTOT
      LIK=ISP(II,J)
      IF(LIK.EQ.0) GO TO 31
      I=LD(II)
      N=2*I+J-2
      FORST(N)=PDIS1(II,J)*1.0D 24
      LOC=0.5*(NBW+1)
      AT(N,LOC)=1.0D 24
   31 CONTINUE
   30 CONTINUE
C
C*****TO PUT BODY FORCES AND INITIAL STRESS INTO FORCE VECTOR**********
C*****TO INCORPORATE BODY FORCES******
      DO 4 I=1,NEL
      I1=NODEL(I,1)
      I2=NODEL(I,2)
      I3=NODEL(I,3)
      DELTA=Y(I3)*X(I2)
     1      -Y(I2)*X(I3)
     2      -X(I1)*Y(I3)
     3      +X(I1)*Y(I2)
     4      +Y(I1)*X(I3)
     5      -Y(I1)*X(I2)
      DELTA=ABS(DELTA)
      A=DELTA/6.0
      K1=2*I1
      K2=2*I2
      K3=2*I3
      L1=K1-1
      L2=K2-1
```

```
      L3=K3-1
      FORST(K1)=FORST(K1)+A
      FORST(K2)=FORST(K2)+A
      FORST(K3)=FORST(K3)+A
    4 CONTINUE
C*****SET INCREMENTAL CREEP TO ZERO************************************
 1624 DO 24 J=1,NNOD2
      FIST(J)=0.0
      DO 24 IJ=1,4
   24 CSTIN(J,IJ)=0.0
      DO 1841 I=1,NNOD
      IJ=(2*I)-1
      EDISP(I)=DISP(IJ)
 1841 CONTINUE
C
C*****START SOLUTION ITERATIONS WITHIN TIME STEP************************
C
C
      DO 204 J=1,3
      DIFSTR=0.0
C*****ADD FIST TO FORST TO GIVE FORCE VECTOR*****************************
      DO 205 K=1,NNOD2
  205 DISP(K)=FIST(K)+FORST(K)
C*****TO SET FORCE VECTOR TO ZERO FOR PRESCRIBED DISPLACEMENTS*********
      DO 35 KOD=1,ND
      DO 36 LOD=1,2
      MOD=ISP(KOD,LOD)
      IF(MOD.EQ.0) GO TO 36
      NID=LD(KOD)
      MID=2*NID+LOD-2
      KID=2*NNOD*(MID-1)+MID
      DISP(MID)=PDIS1(KOD,LOD)*1.0D 24
   36 CONTINUE
   35 CONTINUE
C
C*****TO SOLVE THE EQUATION   AT*DISP=DISP******************************
C*****CALL SOLUTION SUBROUTINE HARWELL LIBRARY GAUSSIAN ELIMINATION****
      NUM=NNOD2
      CALL MATSOL(AT,DISP,NUM,NNOD2,NBW,PT)
      PT=0.0
C*****RESET FIST TO ZERO*************************************************
      DO 208 LI=1,NNOD2
  208 FIST(LI)=0.0
C*****WE NOW HAVE DISPLACEMENTS*****************************************
C*****TO OBTAIN STRAINS FROM DISPLACEMENTS******************************
      DO 20 I=1,NEL
      I1=NODEL(I,1)
      I2=NODEL(I,2)
      I3=NODEL(I,3)
      XD=X(I1)+X(I2)+X(I3)
      XD=XD/3.0/1.0E5
      ZD=Y(I1)+Y(I2)+Y(I3)
      ZD=ZD/3.0/1.0E5
      DO 9403 KK=1,18
 9403 B(KK)=BLIB(KK,I)
      DO 9404 KK=1,9
 9404 D(KK)=DLIB(KK,I)
      DELTA=DELIB(I)
      J1=2*I1
      K1=J1-1
```

```
      J2=2*I2
      K2=J2-1
      J3=2*I3
      K3=J3-1
      DISEL(1)=DISP(K1)
      DISEL(2)=DISP(J1)
      DISEL(3)=DISP(K2)
      DISEL(4)=DISP(J2)
      DISEL(5)=DISP(K3)
      DISEL(6)=DISP(J3)
C*****MULT B BY DISEL TO GIVE STRAINS IN STRAIN*****
      N=3
      M=6
      L=1
      CALL GMPRD(B,DISEL,STRAIN,N,M,L)
C*****TO OBTAIN STRESSES FROM STRAINS**********************************
C*****TO MULT D BY STRAINS TO GET STRESS ******************************
C***** SUBTRACT INITIAL STRAIN TO GIVE ELASTIC STRAIN******************
      IF(ISTRAIN.EQ.2) STRAIN(4)=0.0
      DO 1007 IK=1,4
 1007 STEL(IK)=STRAIN(IK)-STIN(I,IK)-CSTIN(I,IK)
      N=3
      M=3
      L=1
      CALL GMPRD(D,STEL,STRESS,N,M,L)
C***** AMEND STRESS TO ALLOW FOR CREEP*********************************
      ELC=E(I)/((1.0+P(I))*(1.0-2.0*P(I)))
      STRESS(1)=STRESS(1)+ELC*P(I)*STEL(4)
      STRESS(2)=STRESS(2)+ELC*P(I)*STEL(4)
      STRESS(4)=ELC*P(I)*(STEL(1)+STEL(2))+ELC*(1.0-P(I))*STEL(4)
C***** ADD INITIAL STRESS TO CALC STRESS*******************************
      IF(J.GT.1) GO TO 526
C PUT STRESSES INTO TRAY*****************************************************
      DO 1000 IK=1,4
 1000 TRAY(I,IK)=STRESS(IK)
  526 CONTINUE
      AS=STRESS(1)-TRAY(I,1)
      BS=STRESS(2)-TRAY(I,2)
      CS=STRESS(3)-TRAY(I,3)
      DS=STRESS(4)-TRAY(I,4)
      ZAS=ABS(AS)
      ZBS=ABS(BS)
      ZCS=ABS(CS)
      DIFSTR=AMAX1(ZAS,ZBS,ZCS,DIFSTR)
      AS1=AS/2.0
      BS1=BS/2.0
      CS1=CS/2.0
      DS1=DS/2.0
      STRAY(I,1)=STRESS(1)
      STRAY(I,2)=STRESS(2)
      STRAY(I,3)=STRESS(3)
      STRAY(I,4)=STRESS(4)
      AS=TRAY(I,1)+AS/2.0
      BS=TRAY(I,2)+BS/2.0
      CS=TRAY(I,3)+CS/2.0
      DS=TRAY(I,4)+DS/2.0
C*****TO OBTAIN VALUE OF CREEP FROM STRESS AND STRAIN******************
      STRM=(AS+BS+DS)/3.0
      S1=AS-STRM
      S2=BS-STRM
```

```
      S3=CS
      S4=DS-STRM
      CALL AXIAL(AS,BS,CS,DS,AX1,AX2,THETA)
      SIG1=AMAX1(AX1,AX2,AX3)
      SIG2=AMIN1(AX1,AX2,AX3)
      TAU=(SIG1-SIG2)/2.0
      RS=1.0
      CALL FAIL(S0,VALMU,NEL,I,IFAIL,SIG1,SIG2)
      CALL RHEO(TAU,VIK,TEMP,I,NODEL,X,Y,IVISC,NARR2,NARR1,VIKMIN)
      CREEP(1)=RS*S1*TIMC/(VIK*2.0)
      CREEP(2)=RS*S2*TIMC/(VIK*2.0)
      CREEP(3)=RS*S3*TIMC/(VIK)
      CREEP(4)=RS*S4*TIMC/(VIK*2.0)
      VL=AMIN1(VL,VIK)
      VISCOS(I)=VIK
C***** AMEND MATRIX W FOR CREEP*****************************************
      AW1=ELC*P(I)*CREEP(4)
C*****PUT ELEMENT CREEP INTO CSTIN**************************************
      DO 207 NIL=1,4
  207 CSTIN(I,NIL)=CREEP(NIL)
C*****TO INCORPERATE INITIAL  CREEP BY EXPRESSING AS INITIAL STRAIN****
C*****TO MULTIPLY D BY CREEP*******************************************
      N=3
      M=3
      L=1
      CALL GMPRD(D,CREEP,W,N,M,L)
      W(1)=W(1)+AW1
      W(2)=W(2)+AW1
C*****TO TRANSPOSE B TO F**********************************************
      N=3
      M=6
      CALL GMTRA(B,F,N,M)
C*****TO MULTIPLY F BY W***********************************************
      N=6
      M=3
      L=1
      CALL GMPRD(F,W,V,N,M,L)
      DO 831 NERG=1,6
  831 V(NERG)=V(NERG)*DELTA/2.0
C*****TO MAKE FIST*****************************************************
      FIST(J1)=FIST(J1)+V(2)
      FIST(K1)=FIST(K1)+V(1)
      FIST(J2)=FIST(J2)+V(4)
      FIST(K2)=FIST(K2)+V(3)
      FIST(J3)=FIST(J3)+V(6)
      FIST(K3)=FIST(K3)+V(5)
      IF(J.LT.3) GO TO 20
C*****CALCULATE SHEAR HEAT FOR EACH NODE *************
C
C*****CALCULATE WORK DONE FOR EACH ELEMENT******************
      CALL AXIAL(CREEP(1),CREEP(2),CREEP(3),CREEP(4),AAX1,AAX2,THETA)
      AAX3=CREEP(4)
      AAX1=AAX1*AX1
      AAX2=AAX2*AX2
      AAX3=AAX3*AX3
      AAX1=(AAX1+AAX2+AAX3)
      WD(I)=AAX1
```

```
C*****CALCULATE NODAL TEMPERATURE RISE FROM ELEMENT VALUES *******
      IF(I.LT.NEL) GO TO 20
      CALL HEAT(NNOD,NOST,NEL,NODEL,WD,X,Y,SHEAT,IBREF,NARR1,
     + NARR2,ATEMP,TIMC,TEMP,ISTBC,INCRT,THEAT)
C***** THERMAL RUNAWAY TEST ************************
      DO 1090 ILAP=1,NEL
 1090 IF(ATEMP(ILAP).EQ.1200.0) GO TO 9898
   20 CONTINUE
C
C*****TO TEST FOR CONVERGENCE*********************************************
      WRITE(4,8520) DIFSTR
 8520 FORMAT(2X,'DIFSTR=',E10.3)
  204 CONTINUE
  293 CONTINUE
C***** ADD CSTIN TO STIN*************************************************
      DO 28 IJ=1,NEL
      DO 28 IK=1,4
      STIN(IJ,IK)=STIN(IJ,IK)+CSTIN(IJ,IK)
   28 CONTINUE
C***** ADD FIST TO FORST*************************************************
      DO 27 IJ=1,NNOD2
   27 FORST(IJ)=FORST(IJ)+FIST(IJ)
C*****UPDATE TEMPERATURE VALUES ******************************
      DO 1101 IJ=1,NNOD
      TEMP(IJ)=ATEMP(IJ)
 1101 CONTINUE
      CALL TIME(VL,AB,ABC,TMF,TIMTOT,TIMY,IN,VIKMIN,INCRT,THEAT)
      STRMAX=0.0
      WRITE(6,1815) TIMY,ABC
 1815 FORMAT(E10.4,2X,E10.4)
      DO 4281 I=1,NEL
      CALL AXIAL(STRAY(I,1),STRAY(I,2),STRAY(I,3),STRAY(I,4),
     1 PR1,PR2,PR3)
      PR4=(ABS(PR1)+ABS(PR2))/2.0
      STRMAX=AMAX1(STRMAX,PR4)
 4281 CONTINUE
      WRITE(6,1673)STRMAX
 1673 FORMAT(2X,'MAX SHEAR STRESS=',E10.4)
      DO 1910 I=1,NNOD
      IJ=(2*I)-1
      VEL(I)=(DISP(IJ)-EDISP(I))/TIMY
 1910 CONTINUE
      IF(TIMTOT.GE.TMF) GO TO 1297
  201 CONTINUE
C***** WRITE RESULTS FOR FINAL STATE ***********************
 1297 CONTINUE
      GO TO 9889
 9898 WRITE(6,9899)TIMTOT
 9899 FORMAT(2X,'THERMAL RUNAWAY AT',E10.3)
 9889 CONTINUE
      WRITE(4,250) IN,J,TIMTOT,TIMY
  250 FORMAT(2X,'TIME INCREMENT=',I6,2X,'NUMBER OF ITERATIONS=',I4
     1 ,5X,'MINIMUM TOTAL YRS.=',E10.3,5X,'LAST ITERATION PERIOD YRS.',
     2 E10.3)
      WRITE(1,1798) NNOD,NEL
 1798 FORMAT (2I10)
      WRITE(6,199)
      WRITE(6,1817)
 1817 FORMAT(6X,'NODE',3X,'DISP(X)',3X,'DISP(Y)')
      WRITE(6,199)
```

```
      DO 209 I=1,NNOD
      IJ=2*I
      IK=IJ-1
      WRITE(6,162)I,DISP(IK),DISP(IJ)
  209 WRITE(1,162) I,DISP(IK),DISP(IJ)
  162 FORMAT(I10,2E10.3)
      WRITE(1,6161) ISTRAIN
      WRITE(1,6161)NOST
 6161 FORMAT(I10)
      WRITE(8,1520)TIMTOT,ISTRAIN,MARK,BVEL,NNOD,NEL
 1520 FORMAT(E10.4,2(2X,I2),2X,F10.4,2(2X,I4))
      WRITE(8,1521)(X(I),Y(I),I=1,NNOD)
 1521 FORMAT (E12.4,2X,E12.4)
      DO 1903 I=1,NEL
 1903 WRITE(8,1522)(NODEL(I,J),J=1,3)
 1522 FORMAT(3(2X,I4))
      WRITE(6,199)
      WRITE(6,6176)
 6176 FORMAT(30X,'FINITE ELEMENT ANALYSIS VISCO-ELASTIC MODEL')
      WRITE(6,199)
      IF(ISTRAIN.EQ.1) WRITE(6,1808)
 1808 FORMAT(37X,'PLANE STRESS SOLUTION')
      IF(ISTRAIN.EQ.2) WRITE(6,1809)
 1809 FORMAT(37X,'PLAIN STRAIN SOLUTION')
      WRITE(6,199)
      IF(MARK.EQ.1)WRITE(6,1810)
      IF(MARK.EQ.2)WRITE(6,1811)
 1810 FORMAT(30X,'CONSTANT VELOCITY BOUNDARY CONDITIONS')
 1811 FORMAT(30X,'CONSTANT STRESS BOUNDARY CONDITIONS')
      WRITE(6,199)
      WRITE(6,1104)
 1104 FORMAT(10X,'STRESSES AND VISCOSITY IN CGS, ROTATION IN DEGREES
     1 COORDINATES IN KM')
      WRITE(6,199)
      WRITE(4,163)
  163  FORMAT(3X,'ELEMENT',2X,'X-STRESS',2X,'Y-STRESS',2X,'ROTATION',2X
     1,'Z-STRESS',1X,'X-COORD',1X,'Y-COORD',1X,'VISCOSITY',1X,'TEMPERATU
     2RE',2X,10X,'TAUMAX',6X,'TAUXY')
      WRITE(6,199)
C
C***** TO CALCULATE THE PRINCIPAL STRESSES*****************************
      KAV=1
      DO 210 I=1,NEL,KAV
      IP=I+KAV-1
      SC1=(STRAY(I,1)+STRAY(IP,1))/2.0
      SC2=(STRAY(I,2)+STRAY(IP,2))/2.0
      SC3=(STRAY(I,3)+STRAY(IP,3))/2.0
      SC4=(STRAY(I,4)+STRAY(IP,4))/2.0
      VIK=(VISCOS(I)+VISCOS(IP))/2.0
      CALL AXIAL(SC1,SC2,SC3,SC4,ANZA,ANZB,THETA)
      THET=THETA
      BXB=X(NODEL(I,1))+X(NODEL(I,2))+X(NODEL(I,3))
      BYB=Y(NODEL(I,1))+Y(NODEL(I,2))+Y(NODEL(I,3))
      BXP=X(NODEL(IP,1))+X(NODEL(IP,2))+X(NODEL(IP,3))
      BYP=Y(NODEL(IP,1))+Y(NODEL(IP,2))+Y(NODEL(IP,3))
      BXB=(BXB+BXP)/6.0*1.0E-5
      BYB=(BYB+BYP)/6.0*1.0E-5
```

```
C***** EVALUATE SHEAR STRESSES FOR ELEMENTS*************
      TAUMAX=AMAX1(ANZA,ANZB,SC4)
       TAUMIN=AMIN1(ANZA,ANZB,SC4)
      TAUMAX=(TAUMAX-TAUMIN)/2
      TAUXY=(ABS(ANZA)+ABS(ANZB))/2
C*****CALCULATE TEMP AT ELEMENT CENTRE ***********
      CALL CENTRE(NODEL,X,Y,TEMP,BXB,BYB,I,ELTEMP,NARR2,NARR1)
      WRITE(4,164) I,ANZA,ANZB,THET,SC4,BXB,BYB,VIK,ELTEMP,WD(I)
     1 ,TAUMAX,TAUXY
      WRITE(1,164) I,ANZA,ANZB,THET,SC4,BXB,BYB,VIK,ELTEMP,WD(I)
     1 ,TAUMAX,TAUXY
      WRITE(8,1523) ANZA,ANZB,THET,SC4,BXB,BYB,ELTEMP
 1523 FORMAT(4(E10.4,2X),3(2F10.4,2X))
      STRAY(I,1)=ANZA
      STRAY(I,2)=ANZB
      STRAY(I,3)=THET
  210 CONTINUE
  164 FORMAT(I10,4E10.3,2F8.3,E10.3,E10.4,E10.3,2E10.3)
      WRITE(6,199)
      WRITE(6,1784)
 1784 FORMAT(2X,'FAILED ELEMENTS')
      DO 1785 I=1,NEL
 1785 WRITE(6,1786)IFAIL(I)
 1786 FORMAT(2X,I3)
      WRITE(6,1833)
      WRITE(1,1842)BVEL
 1842 FORMAT(F10.3)
 1833 FORMAT(25X,'VELOCITY STRUCTURE')
      DO 1832 I=1,NNOD
      WRITE(1,1831) VEL(I)
      WRITE(8,1524) VEL(I)
 1524 FORMAT(F10.4,2X)
 1832 WRITE(6,1831) VEL(I)
 1831 FORMAT(10X,E10.4)
      STOP
      END
C
C
C
C***** SUBROUTINE MATRIX MULTIPLICATION*********************************
      SUBROUTINE GMPRD(A,B,R,N,M,L)
      DIMENSION A(1),B(1),R(1)
      IR=0
      IK=-M
      DO 10 K=1,L
      IK=IK+M
      DO 10 J=1,N
      IR=IR+1
      JI=J-N
      IB=IK
      R(IR)=0
      DO 10 I=1,M
      JI=JI+N
      IB=IB+1
   10 R(IR)=R(IR)+A(JI)*B(IB)
      RETURN
      END
```

```
C*****  SUBROUTINE MATRIX TRANSPOSITION*********************************
      SUBROUTINE GMTRA(A,R,N,M)
      DIMENSION A(1),R(1)
      IR=0
      DO 10 I=1,N
      IJ=I-N
      DO 10 J=1,M
      IJ=IJ+N
      IR=IR+1
   10 R(IR)=A(IJ)
      RETURN
      END
C
C
C
      SUBROUTINE MATSOL(A,B,IA,N,NW,PT)
      DIMENSION  A(IA,1),B(N)
      EQUIVALENCE (IP,I,NEX,KIB,NCO),(NR12,NS,J,LBO),
     1(AMAXT,TBEST,TEMP)
      LEVEL 2,A
      DATA LP/6/
      NR=(NW-1)/2
      NR1=NR+1
      NR2=NR1+NR
      NR32=NR2+NR1
      IF(PT.EQ.0.)GO TO 99
      DO 4 ISET=1,N
      NR12=MIN0(NR2+1,N-ISET+NR1+1)
      DO 4 JSET=NR12,NR32
   4  A(ISET,JSET)=0.0
      DO 22 K=1,N
      IP=K
      NS=NR1
      BEST=ABS(A(IP,NS))
      DO 7 NFT=1,NR
      IPT=K+NFT
      IF(IPT.GT.N)GO TO 7
      NT=NR1-NFT
      TBEST=ABS(A(IPT,NT))
      IF(BEST.GE.TBEST)GO TO 7
      BEST=TBEST
      NS=NT
      IP=IPT
   7  CONTINUE
      IF(K.EQ.1)PT=BEST
      PT=AMIN1(BEST,PT)
      IF(BEST.NE.0.)GO TO 5
      WRITE(LP,6)
   6  FORMAT(///' ZERO PIVOT FOUND IN MATSOL.  ATTEMPT TO SOLVE THE
SYSTE
     1M OF EQUATIONS ABANDONED.'///)
      RETURN
   5   A(K,NR32)=IP
      IF(IP.EQ.K)GO TO 3
      DO 8 NV=1,NR2
      TEMP=A(K,NR+NV)
      A(K,NR+NV)=A(IP,NS+NV-1)
   8  A(IP,NS+NV-1)=TEMP
```

```
C       ELIMINATION AND COEFF. STORAGE
    3   IF(K+NR.LE.N)GO TO 15
        NL=N-K
        IF(NL)22,22,16
   15   NL=NR
   16   CONTINUE
        CALL MATHEL (A,NL,K,NR,IA)
   22   CONTINUE
C       NOW B IS PROCESSED
   99   DO 17 KB=1,N
        NEX= A(KB,NR32)
        IF(NEX.EQ.KB)GO TO 20
        TEMP=B(KB)
        B(KB)=B(NEX)
        B(NEX)=TEMP
   20   DO 17 IB=1,NR
        KIB=KB+IB
        IF(KIB.GT.N)GO TO 17
        B(KIB)=B(KIB)-B(KB)*A(KB,IB)
   17   CONTINUE
C       BACK SUBSTITUTE
        DO 25 NBACK=1,N
        NCO=N+1-NBACK
        BNCO=B(NCO)
        L2=MIN0(NR2,NBACK)
        IF(L2.EQ.1)GO TO 25
        DO 31 LCO=2,L2
   31   BNCO=BNCO-B(LCO+NCO-1)*A(NCO,LCO+NR)
   25   B(NCO)=BNCO/A(NCO,NR1)
        RETURN
        END
C
C
C
        SUBROUTINE MATHEL(A,NL,K,NR,IA)
        DIMENSION A(1)
        LEVEL 2,A
        NR1=NR+1
        NR3=3*NR
        J4=K+NR*IA
        PIVT=A(J4)
        DO 9 IK=1,NL
        I=IK+K
        J1=I+(NR-IK)*IA
        TEMP=-A(J1)/PIVT
        A(K+(IK-1)*IA)=-TEMP
        J2=I+(NR3-IK)*IA
        J3 = J4
        DO 9 J=J1,J2,IA
        A(J)=A(J)+A(J3)*TEMP
        J3 = J3 + IA
    9   CONTINUE
        RETURN
        END
C
C
C
        SUBROUTINE TIME(VL,AB,ABC,TMF,TIMTOT,TIMY,IN,VIKMIN,INCRT,THEAT)
        RHO=3.0
        SIGMA=0.26
```

```
      COND=0.006
      IF(TMF.GT.1.0E5) LONGT=1
      TIMY=(VL/1.0E11)/(3600*365.25*24)
      ABC=((AB**2)*RHO*SIGMA/(2*COND))/(3600*365.25*24)
      TIMY=AMIN1(TIMY,ABC)
      IF(IN.EQ.1) TIMY=10.0
      IF(TIMY.GT.10000.0) TIMY=10000.0
      IF(LONGT.EQ.1) GOTO 2
      GO TO 3
    2 IF(TIMTOT.GT.1.0E5)TIMY=0.05*TIMTOT
      VIKMIN=(3600*365.25*24)*1.0E11*TIMY
      INCRT=(TIMY/ABC)+0.5
      IF(INCRT.LT.1) INCRT=1
      THEAT=TIMY/INCRT
      THEAT=THEAT*(3600*365.25*24)
    3 RETURN
      END
C
C
C
      SUBROUTINE DMATR(E,P,D,ISTRAIN,I,NARR2)
      DIMENSION E(NARR2),P(NARR2),D(9)
      IF(ISTRAIN.EQ.2) GO TO 5
C********* PLANE STRESS MATRIX ******************************
      A=E(I)/(1.0-2*P(I))
      Q=(1.0-P(I))/2.0
      D(1)=A
      D(2)=A*P(I)
      D(3)=0.0
      D(4)=A*P(I)
      D(5)=A
      D(6)=0.0
      D(7)=0.0
      D(8)=0.0
      D(9)=A*Q
      GO TO 10
C********** PLANE STRAIN MATRIX *
    5 A=E(I)*(1.0-P(I))/((1.0+P(I))*(1.0-2*P(I)))
      Q=P(I)/(1.0-P(I))
      D(1)=A
      D(2)=A*Q
      D(3)=0.0
      D(4)=A*Q
      D(5)=A
      D(6)=0.0
      D(7)=0.0
      D(8)=0.0
      D(9)=A*(1.0-Q)/2.0
   10 CONTINUE
      RETURN
      END
C
C
C
      SUBROUTINE HEAT(NNOD,NOST,NEL,NODEL,WD,X,Y,SHEAT,IBREF,NARR1,
     + NARR2,ATEMP,TIMC,TEMP,ISTBC,INCRT,THEAT)
      DIMENSION NODEL(NARR2,3),WD(NARR2),X(NARR1),Y(NARR1),NODELC(400)
     +,IBREF(NNOD),ATEMP(NARR2),TEMP(NARR2),ISTBC(NARR1),SHEAT(NARR2)
      CALL SHAPE(NNOD,NOST,NEL,NODEL,WD,X,Y,SHEAT,IBREF,NARR1,NARR2)
      DO 30 I=1,NNOD
```

```
   30  NODELC(I)=0
       IF(INCRT.GT.1) GO TO 5
       GO TO 10
   5   TIMC=THEAT
       DO 15 IJ=1,NNOD
   15  SHEAT(IJ)=SHEAT(IJ)/INCRT
       DO 20 JI=1,INCRT
       CALL WARMTH(X,Y,NODEL,ATEMP,NODELC,NNOD,NOST,NEL,TIMC,SHEAT,
      + TEMP,ISTBC,NARR1,NARR2)
       DO 25 J=1,NNOD
   25  NODELC(J)=0
   20  CONTINUE
       GO TO 35
   10  CALL WARMTH(X,Y,NODEL,ATEMP,NODELC,NNOD,NOST,NEL,TIMC,SHEAT,
      + TEMP,ISTBC,NARR1,NARR2)
   35  CONTINUE
       RETURN
       END
C
C
C
       SUBROUTINE FAIL(S0,VALMU,NEL,I,IFAIL,SIG1,SIG2)
C ****** COULOMB-NAVIER FAILURE CRITERION *************
       DIMENSION S0(NEL),VALMU(NEL),IFAIL(NEL)
       SUM=SQRT((VALMU(I)*2)+1)
       SUM1=(SUM-VALMU(I))*SIG1
       SUM2=(SUM+VALMU(I))*SIG2
       SVAL=SUM1-SUM2
       FCOND=2*S0(I)
       IF(SVAL.GE.FCOND) IFAIL(I)=1
       RETURN
       END
C
C
C
       SUBROUTINE CENTRE(NODEL,X,Y,TEMP,XCENT,YCENT,I,ANS,NARR2,NARR1)
       DIMENSION NODEL(NARR2,3),X(NARR1),Y(NARR1),TEMP(NARR2)
       DIS1=((X(NODEL(I,1))-XCENT)**2)+((Y(NODEL(I,1))-YCENT)**2)
       DIS1=SQRT(ABS(DIS1))
       DIS2=((X(NODEL(I,2))-XCENT)**2)+((Y(NODEL(I,2))-YCENT)**2)
       DIS2=SQRT(ABS(DIS2))
       DIS3=((X(NODEL(I,3))-XCENT)**2)+((Y(NODEL(I,3))-YCENT)**2)
       DIS3=SQRT(ABS(DIS3))
       SUM=(1/DIS1)+(1/DIS2)+(1/DIS3)
       F1=TEMP(NODEL(I,1))/DIS1
       F2=TEMP(NODEL(I,2))/DIS2
       F3=TEMP(NODEL(I,3))/DIS3
       ANS=(F1+F2+F3)/SUM
       RETURN
       END
C
C
C
       SUBROUTINE BMATR(NODEL,I,DLIB,BLIB,DELIB,X,Y,
      1 D,B,DELTA,NARR1,NARR2)
       DIMENSION NODEL(NARR2,3),B(18),CC(3),QQ(3),X(NARR1),Y(NARR1)
      1 ,DLIB(9,600),BLIB(18,600),DELIB(600),D(9)
       LEVEL 2,DLIB,BLIB,DELIB
       I1=NODEL(I,1)
       I2=NODEL(I,2)
```

```
      I3=NODEL(I,3)
      DELTA=Y(I3)*X(I2)
     1      -Y(I2)*X(I3)
     2      -X(I1)*Y(I3)
     3      +X(I1)*Y(I2)
     4      +Y(I1)*X(I3)
     5      -Y(I1)*X(I2)
      QQ(1)=(Y(I2)-Y(I3))/DELTA
      CC(1)=(X(I3)-X(I2))/DELTA
      QQ(2)=(Y(I3)-Y(I1))/DELTA
      CC(2)=(X(I1)-X(I3))/DELTA
      QQ(3)=(Y(I1)-Y(I2))/DELTA
      CC(3)=(X(I2)-X(I1))/DELTA
      B(1)=QQ(1)
      B(2)=0.0
      B(3)=CC(1)
      B(4)=0.0
      B(5)=CC(1)
      B(6)=QQ(1)
      B(7)=QQ(2)
      B(8)=0.0
      B(9)=CC(2)
      B(10)=0.0
      B(11)=CC(2)
      B(12)=QQ(2)
      B(13)=QQ(3)
      B(14)=0.0
      B(15)=CC(3)
      B(16)=0.0
      B(17)=CC(3)
      B(18)=QQ(3)
      DELTA=ABS(DELTA)
      DO 10 K=1,18
   10 BLIB(K,I)=B(K)
      DELIB(I)=DELTA
      DO 15 K=1,9
   15 DLIB(K,I)=D(K)
      RETURN
      END
C
C
C
      SUBROUTINE SMATR(NEL,NNOD,E,P,D,B,DLIB,AT,DELIB,BLIB,X,Y,
     1 ISTRAIN,NBW,NODEL,NARR1,NARR2)
      DIMENSION E(NARR2),P(NARR2),D(9),B(18),DELIB(600),DLIB(9,600)
     1 ,BLIB(18,600),X(NARR1),Y(NARR1),T(36),H(18),F(18)
     2 ,AT(462,132),NODEL(NARR2,3)
      LEVEL 2, AT,BLIB,DLIB,DELIB
      DATA LP/6/
C**** FORM ELEMENT STIFFNESS MATRIX ****************************
      DO 5 I=1,NEL
C**** SET H AND T TO ZERO ***************************************
      DO 10 LIT=1,36
   10 T(LIT)=0.0
      DO 15 LIT=1,18
   15 H(LIT)=0.0
C**** FORM D MATRIX *********************************************
      CALL DMATR(E,P,D,ISTRAIN,I,NARR2)
```

```
C**** FORM B MATRIX ********************************************
      CALL BMATR(NODEL,I,DLIB,BLIB,DELIB,X,Y,
     1 D,B,DELTA,NARR1,NARR2)
      N=3
      M=6
      CALL GMTRA(B,F,N,M)
C**** B IS TRANSPOSED TO F *************************************
C**** MULTIPLY D BY B TO GIVE H *********************************
      N=3
      M=3
      L=6
      CALL GMPRD(D,B,H,N,M,L)
C**** MULTIPLY F BY H TO GIVE T *********************************
      N=6
      M=3
      L=6
      CALL GMPRD(F,H,T,N,M,L)
C**** TO MULTIPLY BY DELTA/2 ************************************
      DO 20 NI=1,36
  20  T(NI)=T(NI)*DELTA/2.0
C**** WE NOW HAVE ELEMENT STIFFNESS MATRIX **********************
C**** TO PUT T INTO BODY STIFFNESS MATRIX ***********************
      K=1
      DO 25 MS=1,3
      DO 25 NS=1,2
      DO 25 KS=1,3
      DO 25 LS=1,2
      JX=NODEL(I,MS)
      JX=2*JX-2+NS
      IY=NODEL(I,KS)
      IY=2*IY-2+LS
      LOC=JX-IY+0.5*(NBW+1)
      IF(LOC.LT.1) GO TO 25
      IF(LOC.GT.NBW) GO TO 25
      AT(IY,LOC)=AT(IY,LOC)+T(K)
   25 K=K+1
  5   CONTINUE
      WRITE(LP,100)
 100  FORMAT(2X,'TOTAL STIFFNESS FORMED')
      RETURN
      END
C
C
C
      SUBROUTINE WARMTH(X,Y,NODEL,ATEMP,NODELC,NNOD,NOST,NEL,TIMC,
     1 SHEAT,TEMP,ISTBC,NARR1,NARR2)
      DIMENSION X(NARR1),Y(NARR1),NODEL(NARR2,3),SHEAT(NARR1),
     1 NODELC(NARR2),ATEMP(NARR2) ,TEMP(NARR2),ISTBC(NARR1)
      RHO=3.0
      SIGMA=0.26
      COND=0.006
      TMELT=1200.0
       NREP=NNOD/NOST
      DO 5 I=1,NEL
      DO 10 J=1,3
      NODEN=NODEL(I,J)
      IF(NODELC(NODEN).EQ.1) GO TO 10
      T0=TEMP(NODEN)
      X0=X(NODEN)
      Y0=Y(NODEN)
```

```
      IF((NODEN-NOST).LT.1) GO TO 21
      T1=TEMP(NODEN-NOST)
      X1=X(NODEN-NOST)
 21   IF((NODEN+NOST).GT.NNOD) GO TO 22
      T2=TEMP(NODEN+NOST)
      X2=X(NODEN+NOST)
 22   IF((NODEN-1).LT.1) GO TO 23
      T3=TEMP(NODEN-1)
      Y3=Y(NODEN-1)
 23   IF((NODEN+1).GT.NNOD) GO TO 24
      T4=TEMP(NODEN+1)
      Y4=Y(NODEN+1)
   24 IF(NODEN.LE.NOST) X1=2*X0-X2
      IF(NODEN.LE.NOST) T1=T2
      IF(NODEN.GT.(NNOD-NOST)) X2=2*X0-X1
      IF(NODEN.GT.(NNOD-NOST)) T2=T1
      DO 11 II=1,NREP
      IF(NODEN.EQ.((NOST*(II-1))+1)) Y3=2*Y0-Y4
   11 IF(NODEN.EQ.((NOST*(II-1))+1)) T3=T4
      DO 12 IJ=1,NREP
      IF(NODEN.EQ.(NOST*IJ)) Y4=2*Y0-Y3
      IF(NODEN.EQ.(NOST*IJ)) T4=T3
 12   CONTINUE
      GRADX=((T1-T0)/(X1-X0))-((T0-T2)/(X0-X2))
      GRADX=GRADX/((X1-X2)/2)
      GRADY=((T3-T0)/(Y3-Y0))-((T0-T4)/(Y0-Y4))
      GRADY=GRADY/((Y3-Y4)/2)
      GRAD=GRADX+GRADY
      FLOW=GRAD*COND*TIMC/(RHO*SIGMA)
      ATEMP(NODEN)=TEMP(NODEN)+FLOW+(SHEAT(NODEN)/(RHO*SIGMA*4.2E7))
      IF(ATEMP(NODEN).GT.TMELT) ATEMP(NODEN)=TMELT
      IF(ISTBC(NODEN).EQ.1) ATEMP(NODEN)=TEMP(NODEN)
      NODELC(NODEN)=1
 10   CONTINUE
   5  CONTINUE
      RETURN
      END
C
C
C
       SUBROUTINE RHEO(TAU,VIK,TEMP,I,NODEL,X,Y,IVISC,NARR2,NARR1
     1 ,VIKMIN)
      DIMENSION NODEL(NARR2,3),TEMP(NARR2),X(NARR1),Y(NARR1),
     1 IVISC(NARR2)
       RN=-2.0
      TM=1200.0
      A=2.1E17
      XCENT=X(NODEL(I,1))+X(NODEL(I,2))+X(NODEL(I,3))
      XCENT=XCENT/3.0
      YCENT=Y(NODEL(I,1))+Y(NODEL(I,2))+Y(NODEL(I,3))
      YCENT=YCENT/3.0
      CALL CENTRE(NODEL,X,Y,TEMP,XCENT,YCENT,I,B,NARR2,NARR1)
      IF(IVISC(I).EQ.2) GO TO 10
      IF(IVISC(I).EQ.3) GO TO 20
C
C
C *******   DRY OLIVINE RHEOLOGY *****************
      ARG=40.0*(TM+273.00)/(B+273.00)
      IF(ARG.GT.200.0) ARG=200.0
      IF(ARG.LT.40.0) ARG=40.0
```

```
      VIK=A*EXP(ARG)*TAU**RN
      GO TO 15
C
C
C ****** DOLERITE RHEOLOGY ****************
  10  RN=-1.5
      TM=1120.0
      A=1.5E3
      ARG=53.0*(TM+273.00)/(B+273.00)
      IF(ARG.GT.200.0) ARG=200.0
      IF(ARG.LT.53.0) ARG=53.0
      VIK=A*EXP(ARG)*TAU**RN
      GO TO 15
C
C
C ******   GRANODIORITE RHEOLOGY **********************
   20 RN=-1.5
      TM=1120.0
      A=6.0E3
      ARG=42*(TM+273.00)/(B+273.00)
      IF(ARG.GT.200.00) ARG=200.0
      IF(ARG.LT.42.0) ARG=42.0
      VIK=A*EXP(ARG)*TAU**RN
  15  IF(VIK.LT.VIKMIN) VIK=VIKMIN
      IF(VIK.GT.1.0E40) VIK=1.0E40
      RETURN
      END
C
C
C
      SUBROUTINE AXIAL(A,B,C,D,AX1,AX2,THETA)
      IF(A.EQ.B) GO TO 5
      THET=2.0*C/(A-B)
      GO TO 6
    5 THET=0.0
    6 THET=ATAN(THET)
      THET=THET/2.0
      THET=57.29*THET
      IF(THET.GT.0.0) GO TO 10
      THET=THET+90.0
 10   CONTINUE
      ALPHA=THET/57.29
      AX1=(A*(COS(ALPHA))**2)+
     1 (B*(SIN(ALPHA))**2)+
     2 (C*(SIN(2.0*ALPHA)))
      AX2=A+B-AX1
      THETA=THET
      RETURN
      END
C
C
C
      SUBROUTINE SHAPE(NNOD,NOST,NEL,NODEL,WD,X,Y,SHEAT,IBREF,NARR1,
     1 NARR2)
      DIMENSION NODELD(256),NODEL(NARR2,3),WD(NARR2),X(NARR1),
     1 Y(NARR1),SHEAT(NNOD),IBREF(NNOD)
      INTEGER B,B1,B2,A1,A2,A3
      DO 5 ISH=1,NNOD
      NODELD(ISH)=0
 5    CONTINUE
```

```
      NREP=NNOD/NOST
      NELCOL1=(NOST-1)*2
      DO 20 I=1,NEL
      DO 20 J=1,3
      NODELD1=NODEL(I,J)
      IF(NODELD(NODELD1).EQ.1) GO TO 20
      B=IBREF(NODELD1)
      B1=B-1
      B2=B+1
      A1=B-NELCOL1
      A2=A1+1
      A3=A2+1
      IF(NODELD1.LE.NOST) A2=B
      IF(NODELD1.LE.NOST) A1=B1
      IF(NODELD1.LE.NOST) A3=B2
      IF(NODELD1.GE.((NREP-1)*NOST)) B1=A1
      IF(NODELD1.GE.((NREP-1)*NOST)) B=A2
      IF(NODELD1.GE.((NREP-1)*NOST)) B2=A3
      DO 11 II=1,NREP
      IF(NODELD1.EQ.((NOST*(II-1))+1)) A1=A2
      IF(NODELD1.EQ.((NOST*(II-1))+1)) B=B2
      IF(NODELD1.EQ.((NOST*(II-1))+1)) B1=B2
11    CONTINUE
      DO 12 IJ=1,NREP
      IF(NODELD1.EQ.(NOST*IJ)) B2=B
      IF(NODELD1.EQ.(NOST*IJ)) A2=A1
      IF(NODELD1.EQ.(NOST*IJ)) A3=A1
12    CONTINUE
      IF(A1.EQ.0) A1=1
      IF(A2.EQ.0) A2=1
      BXB1=(X(NODEL(B,1))+X(NODEL(B,2))+X(NODEL(B,3)))/3.0
      BYB1=(Y(NODEL(B,1))+Y(NODEL(B,2))+Y(NODEL(B,3)))/3.0
      BXB2=(X(NODEL(B1,1))+X(NODEL(B1,2))+X(NODEL(B1,3)))/3.0
      BYB2=(Y(NODEL(B1,1))+Y(NODEL(B1,2))+Y(NODEL(B1,3)))/3.0
      BXB3=(X(NODEL(B2,1))+X(NODEL(B2,2))+X(NODEL(B2,3)))/3.0
      BYB3=(Y(NODEL(B2,1))+Y(NODEL(B2,2))+Y(NODEL(B2,3)))/3.0
      BXB4=(X(NODEL(A1,1))+X(NODEL(A1,2))+X(NODEL(A1,3)))/3.0
      BYB4=(Y(NODEL(A1,1))+Y(NODEL(A1,2))+Y(NODEL(A1,3)))/3.0
      BXB5=(X(NODEL(A2,1))+X(NODEL(A2,2))+X(NODEL(A2,3)))/3.0
      BYB5=(Y(NODEL(A2,1))+Y(NODEL(A2,2))+Y(NODEL(A2,3)))/3.0
      BXB6=(X(NODEL(A3,1))+X(NODEL(A3,2))+X(NODEL(A3,3)))/3.0
      BYB6=(Y(NODEL(A3,1))+Y(NODEL(A3,2))+Y(NODEL(A3,3)))/3.0
      S1=((X(NODEL(I,J))-BXB1)**2)+((Y(NODEL(I,J))-BYB1)**2)
      S1=SQRT(ABS(S1))
      S2=((X(NODEL(I,J))-BXB2)**2)+((Y(NODEL(I,J))-BYB2)**2)
      S2=SQRT(ABS(S2))
      S3=((X(NODEL(I,J))-BXB3)**2)+((Y(NODEL(I,J))-BYB3)**2)
      S3=SQRT(ABS(S3))
      S4=((X(NODEL(I,J))-BXB4)**2)+((Y(NODEL(I,J))-BYB4)**2)
      S4=SQRT(ABS(S4))
      S5=((X(NODEL(I,J))-BXB5)**2)+((Y(NODEL(I,J))-BYB5)**2)
       S5=SQRT(ABS(S5))
      S6=((X(NODEL(I,J))-BXB6)**2)+((Y(NODEL(I,J))-BYB6)**2)
      S6=SQRT(ABS(S6))
       SUM=(1/S1+1/S2+1/S3+1/S4+1/S5+1/S6)
      TOP1=WD(B)/S1
      TOP2=WD(B1)/S2
      TOP3=WD(B2)/S3
      TOP4=WD(A1)/S4
      TOP5=WD(A2)/S5
```

```
      TOP6=WD(A3)/S6
      SHEAT(NODELD1)=(TOP1+TOP2+TOP3+TOP4+TOP5+TOP6)/SUM
      NODELD(NODELD1)=1
20    CONTINUE
      RETURN
      END
```

PROGRAM PLOT

This program uses the **GHOST** graphical output system to produce plots of displacement, temperature and the state of stress. The data is read in directly from program **LDFIN**. The only other input data required is the limits of the plotting field in the x and y directions and scaling factors for the size of plot. The output consists of 4 graph frames.

Frame 1
This is the finite element grid.

Frame 2
This shows the state of stress in the model. Both principal stress directions and the magnitudes are shown.

Frame 3
This frame shows the nodal displacements for the grid.

Frame 4
This frame shows the finite element grid with the average element temperatures plotted at the element centroids.

```
C       FINITE ELEMENT PLOTTING PROGRAM
        PROGRAM PLOT(F1,F5,INPUT,TAPE1=F1,TAPE5=F5,TAPE3=INPUT,
       1 OUTPUT,TAPE6=OUTPUT)
        DIMENSION
       1 X(500),Y(500),NODEL(600,3),STRAY(600,4),YGR(50),H(20)
       2 ,TRAY(600,4),DISP(500,2),DINIT(500),A(50,20),XGR(50)
       3 ,XC(600),VIK(500),ELTEMP(500),YC(600),VEL(600)
C ***** READ IN MAXIMUM AND MINIMUM PLOT COORDINATES ***************
        READ(3,16) XL,XH,YL,YH
        READ(3,15) STMAX,K,KIK
        R=(XH-XL)/(YH-YL)
C ***** READ IN DATA FROM FILES ****************
        READ(5,10) NNOD,NEL
        DO 50 I=1,NNOD
   50 READ(5,11) X(I),Y(I)
        DO 51 I=1,NEL
   51 READ(5,12) NODEL(I,1),NODEL(I,2),NODEL(I,3)
        READ(1,10)NULL,NUL1
        DO 60 I=1,NNOD
   60 READ(1,13) DISP(I,1),DISP(I,2)
        READ(1,17) ISTRAIN
        READ(1,17) NOST
        DO 61 I=1,NEL,K
   61 READ(1,14) (STRAY(I,J),J=1,4),VIK(I),ELTEMP(I)
        READ(1,18)BVEL
        READ(1,19)(VEL(I),I=1,NNOD)
   10 FORMAT(2I10)
   11 FORMAT(10X,2F10.3)
   12 FORMAT(10X,3I10)
   13 FORMAT(10X,2E10.3)
   14 FORMAT(10X,4E10.3,16X,E10.3,E10.3)
   15 FORMAT(E10.3,2I10)
   16 FORMAT(4F10.3)
   17 FORMAT(I10)
  18  FORMAT(F10.3)
  19  FORMAT(10X,E10.4)
        SCALER=1.0E10
C*****TO FIND MAXIMUM DISPLACEMENT*************************************
        DISMAX=0.0
        DO 5013 I=1,NNOD
        CMAX=DISP(I,1)
        EMAX=DISP(I,2)
        CMAX=ABS(CMAX)
        EMAX=ABS(EMAX)
 5013 DISMAX=AMAX1(DISMAX,CMAX,EMAX)
        DISMAX=DISMAX*50.0/(YH-YL)
C ***** SET UP FIRST GRAPH FRAME *********************************
        CALL PAPER(1)
        CALL MAP(XL,XH,YL,YH)
        CALL SCALES
        CALL BORDER
C ***** CALCULATE CENTRIOD COORDINATES FOR ELEMENTS *****************
        DO 200 I=1,NEL
        X1=X(NODEL(I,1))
        Y1=Y(NODEL(I,1))
        X2=X(NODEL(I,2))
        Y2=Y(NODEL(I,2))
        X3=X(NODEL(I,3))
        Y3=Y(NODEL(I,3))
        XC(I)=(X1+X2+X3)/3.0
```

```
      YC(I)=(Y1+Y2+Y3)/3.0
C ***** DRAW FINITE ELEMENT GRID *************************
      CALL POSITN(X1,Y1)
      CALL JOIN(X2,Y2)
      CALL JOIN(X3,Y3)
      CALL JOIN(X1,Y1)
  200 CONTINUE
C    PLOT PRINCIPAL STRESSES OR DEV STRESSES**************************
C ***** TENSILE STRESSES ARE POSITIVE ***************
      CALL FRAME
      CALL SCALES
      CALL BORDER
      YH1=YH-1.0
      YL1=YL+1.0
      IF(ISTRAIN.EQ.1) CALL PLOTCS(XOR,YH1,22H PLANE STRESS SOLUTION,22)
      IF(ISTRAIN.EQ.2) CALL PLOTCS(XOR,YH1,22H PLANE STRAIN SOLUTION,22)
      XLOC=XL+((XH-XL)/2)
      CALL PLOTCS(XLOC,YL1,23H DISTANCE IN KILOMETRES,23)
      SCALIN=SCALER/STMAX
      CALL POSITN(XOR,YL1)
      CALL JOIN(SCALIN,YL1)
      CALL PLOTCS(SCALIN,YL1,17H  1.0E9 DYNES/CM2,17)
      CALL CTRMAG(10)
      DO 501 I=1,NEL,K
      X1=X(NODEL(I,1))
      Y1=Y(NODEL(I,1))
      X2=X(NODEL(I,2))
      Y2=Y(NODEL(I,2))
      X3=X(NODEL(I,3))
      Y3=Y(NODEL(I,3))
 5017 CONTINUE
      AVER=(STRAY(I,1)+STRAY(I,2)+STRAY(I,3))/3.0
      IF (IDEV.EQ.2) AVER=0.0
      XXC=(X1+X2+X3)/3.0
      YYC=(Y1+Y2+Y3)/3.0
      ST1=STRAY(I,1)-AVER
      ST2=STRAY(I,2)-AVER
      ST4=STRAY(I,4)-AVER
      TA=COS(STRAY(I,3)/57.29)*ST1/STMAX
      TB=SIN(STRAY(I,3)/57.29)*ST1/STMAX
      TX=COS(STRAY(I,3)/57.29)*ST2/STMAX
      TY=SIN(STRAY(I,3)/57.29)*ST2/STMAX
      TA=TA*R
      TY=TY*R
   20 XN1=XXC+TA
      XN2=XXC-TA
      YN1=YYC+TB
      YN2=YYC-TB
      XS1=XXC-TY
      XS2=XXC+TY
      YS1=YYC+TX
      YS2=YYC-TX
      CALL POSITN(XN1,YN1)
      CALL JOIN(XN2,YN2)
      CALL POSITN(XS1,YS1)
      CALL JOIN(XS2,YS2)
      TA=ST1
      TX=ST2
      QUAD=(STRAY(I,3)/90.0)-1.0
      IF(TA.LT.0.0) QUAD=QUAD+2.0
```

```
      IF(TA.LT.0.0) GO TO 9331
      CALL CTRORI(QUAD)
      CALL PLOTNC(XN1,YN1,54)
      QUAD=QUAD+2.0
      CALL CTRORI(QUAD)
      CALL PLOTNC(XN2,YN2,54)
 9331 CONTINUE
      IF(TX.LT.0.0) GO TO 9332
      QUAD=QUAD-1.0
      CALL CTRORI(QUAD)
      CALL PLOTNC(XS1,YS1,54)
      QUAD=QUAD+2.0
      CALL CTRORI(QUAD)
      CALL PLOTNC(XS2,YS2,54)
 9332 CONTINUE
  501 CONTINUE
      CALL CTRORI(0.0)
C***** PLOT NODAL DISPLACEMENTS*****************************************
      CALL FRAME
      CALL SCALES
      CALL BORDER
      CALL CTRMAG(8)
      CALL PLOTCS(XOR,YH1,20H NODAL DISPLACEMENTS,20)
      CALL PLOTCS(XLOC,YL1,23H DISTANCE IN KILOMETRES,23)
      DO 506 I=1,NNOD
      XXC=X(I)
      YYC=Y(I)
      CALL POINT(XXC,YYC)
      XD=XXC+DISP(I,1)/DISMAX*R
      YD=YYC+DISP(I,2)/DISMAX
      CALL JOIN(XD,YD)
  506 CONTINUE
C***** PLOT TEMPERATURES ***********************
      CALL FRAME
      CALL SCALES
      CALL BORDER
      CALL PLOTCS(XOR,YH1,21H ELEMENT TEMPERATURES,21)
      CALL PLOTCS(XLOC,YL1,23H DISTANCE IN KILOMETRES,23)
      DO 510 I=1,NEL
      X1=X(NODEL(I,1))
      Y1=Y(NODEL(I,1))
      X2=X(NODEL(I,2))
      Y2=Y(NODEL(I,2))
      X3=X(NODEL(I,3))
      Y3=Y(NODEL(I,3))
      CALL POSITN(X1,Y1)
      CALL JOIN (X2,Y2)
      CALL JOIN (X3,Y3)
      CALL JOIN (X1,Y1)
      CALL PLOTNF(XC(I),YC(I),ELTEMP(I),2)
 510  CONTINUE
      CALL GREND
      STOP
      END
```

APPENDIX 3

Test of Finite Difference Heat Flow for Visco-elastic Program

The numerical formulation was tested against the analytical solution of a heat flow problem in a rectangle (Carslaw and Jaeger, 1980). The analytical solution for heat flow at the corner of a rectangle having a unit initial temperature is given as a map of isothermals. The two dimensional finite difference grid was set up such that the grid was at an initial temperature of $100^{o}C$. Heat was lost from corner of the rectangle such that $x>0, y>0$. The edges of the model remote from this corner were constrained such that $dT/dx = 0$ and $dT/dy = 0$. The edges losing heat were set at an initial temperature of $0^{o}C$. The model now represents heat loss from a free corner of an infinite rectangle.

The grid was set up to model a rectangular sheet of copper metal of size X=4m. and Y=2m. Finite difference point spacing represented 2cm. The material properties for copper used were in c.g.s. units :

Density	8.94
Specific heat	0.0914
Thermal conductivity	0.93
Thermal diffusivity	1.14

The model was run for a period of 0.375 seconds represented by 150 iterations of 0.0025 seconds. Isothermals are plotted as the ratio of final temperature to initial temperature and scaled along the axes by the ratio $x/2\sqrt{(kt)}$ where k is the diffusivity and t is time. Figure A3.1 shows the isotherms produced by contouring of the difference point values using the GHOST graphical system. Comparison of this diagram with the published solution shows a good numerical solution.

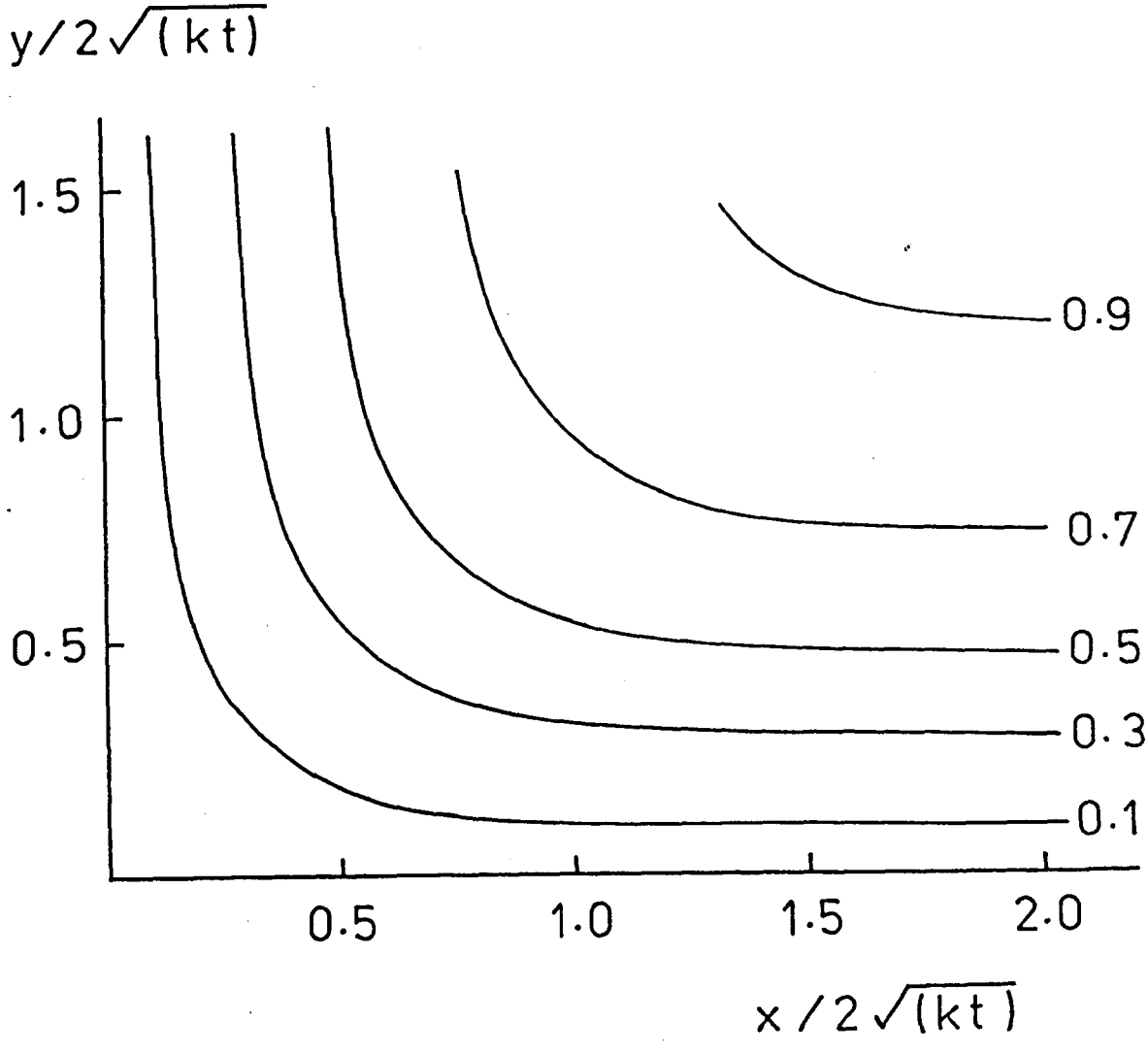

Figure A3.1 Isotherms for finite difference heat flow test.

APPENDIX 4

Test of Finite Element Visco-elastic Stress Analysis Program

The numerical formulation was tested against an analytical solution for stress transfer from the inside of a visco-elastic cylinder to an outside reinforcement (Lee, Radok and Woodward 1959).

A finite element grid for a cylinder was set up as in figure A4.1. Only one quadrant was used due to axial symmetry. Plane strain was assumed throughout and the constraint of zero tangential displacement was placed on the radial boundaries of the grid. An internal pressure F_o was applied to the inside of the model. The inner material was concrete and behaves as a visco-elastic material reinforced by a steel sleeve. Dimensions of the model are :

Bore diameter 'a'	2 inches
Concrete sleeve diameter 'b'	4 inches
Thickness of steel jacket 'h'	4/33 inch

These dimensions give a Maxwell relaxation time of 1 second to the visco-elastic body. This relaxation time is equal to 8/3 of the elemental time period, so the iteration period used was 3/8 x 0.01 =1/270 second.

Material properties used were :

	Visco-elastic	Steel
E	10^5 p.s.i.	3×10^7 p.s.i.
v	1/3	$1/\sqrt{11}$
n	$3/8 \times10^5$ p.s.i.	10^{60} p.s.i.

Figure A4.2 shows the tranference of stress from the inside of the cylinder ,normalised as σ_θ/F_o against the distance from the centre of the cylinder, normalised as r/b. The solid lines represent the analytical solution for various relaxation times T and the dots are the numerical solutions showing a good approximation.

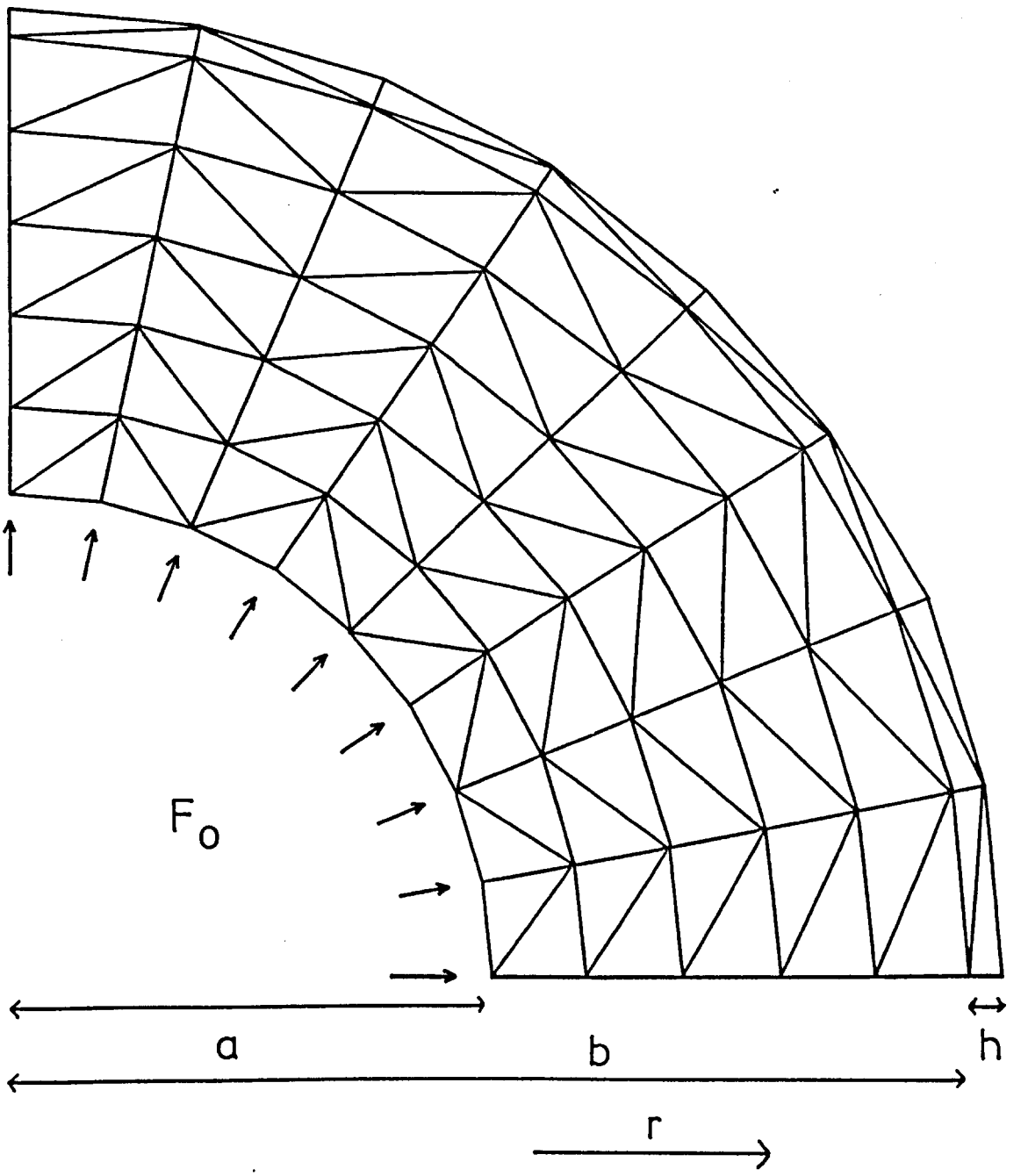

Figure A4.1 Grid for test of visco-elastic finite element program.

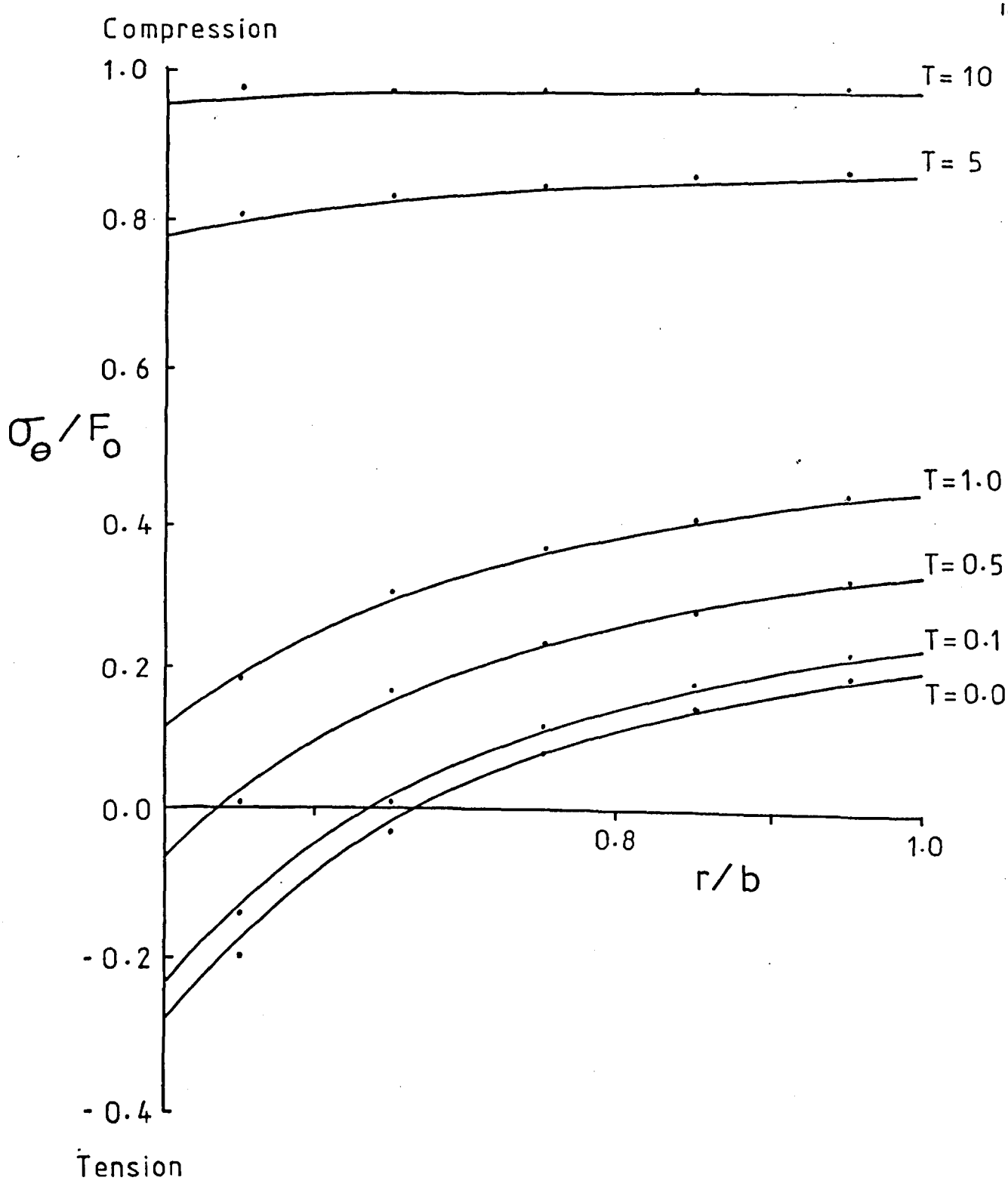

Figure A4.2 Visco-elastic finite element solution (dots) compared with the analytical solution for an internally pressurised cylinder.